Fall 12-2009

Preparation and Characterization of Thiol Based Polymeric Materials

Junghwan Shin
University of Southern Mississippi

The University of Southern Mississippi

PREPARATION AND CHARACTERIZATION OF THIOL BASED POLYMERIC MATERIALS

by

Junghwan Shin

A Dissertation
Submitted to the Graduate School
of The University of Southern Mississippi
in Partial Fulfillment of the Requirements
for the Degree of Doctor of Philosophy

Approved:

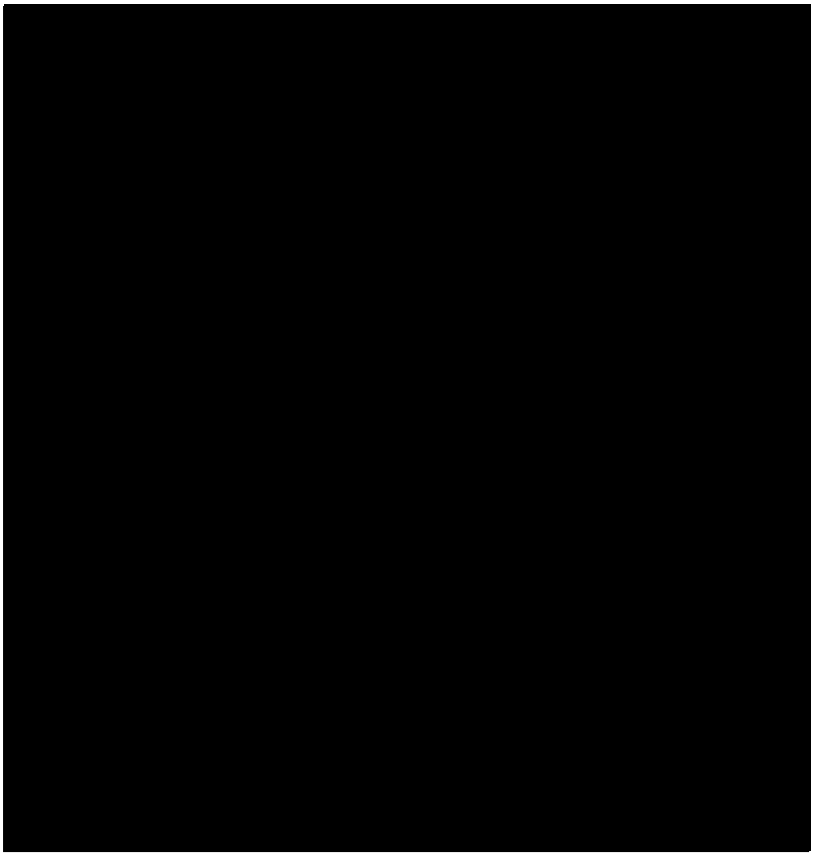

December 2009

The University of Southern Mississippi

PREPARATION AND CHARACTERIZATION OF THIOL BASED POLYMERIC MATERIALS

by

Junghwan Shin

Abstract of a Dissertation
Submitted to the Graduate School
of The University of Southern Mississippi
in Partial Fulfillment of the Requirements
for the Degree of Doctor of Philosophy

December 2009

ABSTRACT

PREPARATION AND CHARACTERIZATION OF THIOL BASED POLYMERIC MATERIALS

by Junghwan Shin

December 2009

The thiol click-type reaction is one of the most efficient chemical processes that can undergo at room temperature in the benign organic solvent providing excellent opportunity in the fabrication of new materials as well as development of new manufacturing processes. Moreover, the versatility of thiol click-type reactions with many different functional groups such as ene, yne, epoxy, isocyanate, and alkyl halide is the important aspect that should be differentiated from the classic azide-alkyne click chemistry. Although, there are tremendous studies on many areas using thiol click-type reactions, the efficiency and utilities for the material applications have been barely explored. Especially, the combination of different types of thiol click reactions can provide new synthetic methodologies for the preparation of thiol based materials and much more choice in designing chemical structures and thus tenability of physical and mechanical properties. In addition to the advantages of thiol click-type reactions in the chemical reaction point of view, the uniform and homogeneous network structure resulting from the unique reaction mechanism presents an excellent platform to investigate the effects of the fundamental molecular parameters on physical and mechanical properties of thiol based networks. Thus, in this dissertation, three major thiol click-type reactions, i.e. thiol-electron rich double bonds by free radical, thiol-electron poor double bonds by nucleophile catalyzed hetero-Michael addition, and

tertiary amine catalyzed thiol-isocyanate nucleophilic coupling reactions, were studied in terms of the efficiency of thiol click-type reactions for the fabrication of materials and their physical / mechanical properties. Also, sub-T_g aging of thiol-ene photopolymerized network films monitored by enthalpy relaxation was investigated in terms of fundamental molecular parameters such as network density, rigidity, uniformity, and polar / non-polar side chains.

In Chapter III, highly elastic segmented polythiourethanes linear polymers were synthesized through sequential thiol click-type reactions involving the phosphine catalyzed thiol-acrylate hetero-Michael addition and triethylamine catalyzed thiol-isocyanate nucleophilic coupling reactions. Real-time FTIR and NMR showed that both the thiol-acrylate hetero-Michael addition and the thiol-isocyanate coupling reactions are very fast and efficient with no side products. Physical and mechanical properties investigated by DSC, DMA, and tensile strength measurements showed that polythiourethanes are highly elastic materials due to the micro-phase separated soft and hard segments.

In Chapter IV, thiol-ene-isocyanate ternary networks were studied as a new approach to modify classic thiol-ene networks by incorporating thiourethane linkages through sequential and simultaneous two thiol click-type reactions. The thiol-isocyanate coupling reaction providing strong hydrogen bonding in thiol-ene networks was triggered thermally and photolytically in order to control the sequence with the thiol-ene photo-polymerization. The kinetics of the ternary networks was investigated for both sequential and simultaneous processes. The relationships between the chemical composition and physical/mechanical properties of thiourethane-thiolene hybrid networks were also

established. The identical thermal properties that are independent of the reaction sequence were obtained, indicating that highly uniform and dense network structure of thiol based networks was not affected by the reaction sequence change.

In Chapter V~VIII, sub-T_g aging behavior of thiol-ene networks measured by the extent of enthalpy relaxation was extensively investigated. The fundamental enthalpy relaxation study on thiol-ene networks was accomplished in Chapter V. The highly dense and uniform network structure of the thiol-ene networks, exhibiting narrow glass transition temperature ranges, showed characteristic temperature and time dependency relationships for enthalpy relaxation. The extent of enthalpy relaxation was correlated with thiol-ene network density and chemical group rigidity. Mechanical property measured by pendulum hardness values for a selected thiol-ene film showed a clear change in hardness upon aging indicating sub-T_g mechanical relaxation, consistent with the related enthalpy relaxation process.

In Chapter VI, the effect of chemical modification of thiol-ene networks on enthalpy relaxation was investigated as an unprecedented methodology to control sub-T_g aging process. Flexible alkyl side chains and hydrogen bonding were incorporated into thiol-ene networks without sacrificing network uniformity using the phosphine catalyzed Michael addition reaction. Overall both the rate and extent of enthalpy relaxation slightly decreased as a function of the flexible n-alkyl chain length, while hydrogen bonding resulted in enhanced enthalpy relaxation. A trifunctional acrylate (TMPTA), being capable of homopolymerization as well as thiol-acrylate copolymerization, was incorporated into a thiol-ene network structure, to investigate the effect of network uniformity on enthalpy relaxation. Inhomogeneous TMPTA homopolymer domains

disrupted the uniformity of thiol-ene networks, thereby, glass transition temperature and enthalpy relaxation were significantly affected. In all cases, the clear relationships between the extent of enthalpy relaxation and chemical structural effects were established.

In Chapter VII, as an extended study of the modification of thiol-ene networks in order to control sub-T_g aging process described in Chapter VI, the degree of restriction effect of the rigid TMPTA homopolymer domains and gold nanoparticles on thiol-ene networks was quantitatively determined by calculating the apparent activation energy (Δh^*) for enthalpy relaxation. The incorporation of TMPTA homopolymer and gold nanoparticles into the thiol-ene network increased T_g and decreased the extent of enthalpy relaxation due to molecular mobility restrictions. In addition, the apparent activation energy for enthalpy relaxation (Δh^*) obtained by the differential cooling rate experiments on DSC clearly indicated significant restriction effects of the TMPTA hard domains and gold nanoparticles on the molecular mobility in the thiol-ene network.

Finally, in Chapter VIII, 10- and 32-layered thiol-ene based films with different components were fabricated to investigate sub-T_g aging of multi-layered thiol-ene network films. The distinctive glass transition temperatures of each component were observed at corresponding transition regions of each bulk sample. Enthalpy relaxation of each layer component occurred independently and showed overlapped unsymmetrical bell shaped enthalpy relaxation distribution having peak maximum at T_g-10 °C of each layer component, resulting in wide distribution of enthalpy relaxation over wide temperature range. Enthalpy relaxation of each layer component in the multi-layered thiol-ene films was significantly accelerated compared to that of bulk thiol-ene networks.

DEDICATION

This dissertation is dedicated to the late Dr. Hoyle who was the best person I have ever met. He was not just a professor and an advisor to me. I will pursue my scientific goals as I have learned from him. I still can feel him in every corner of this building. He will be remembered in my heart forever.

This dissertation is also dedicated to my family and especially my dear wife, Jiyoung Kim, for encouraging me to start Ph.D. studies and being along with me all the time. I regret that she spent the hardest time in her life by herself during my Ph.D. studies. Now, I swear that I will be where she is and will be.

ACKNOWLEDGEMENTS

I would like to acknowledge my advisor, the late Dr. Hoyle, for guiding me with his endless excitement on science. He was the most enthusiastic person whom I have ever met in my life. It was never possible for me to work harder than he did. I pray for the repose of his soul. His great personality will be my goal that I pursue to achieve in my life along with academic knowledge.

I would like to specially thank Dr. Nazarenko for his great physical chemistry class and insightful discussion on the enthalpy relaxation project. His comments always pointed out precisely what I missed and had to know.

I would also like to extend my heartfelt gratitude to the following persons who have made the completion of my Ph.D. possible:

My committee members, Dr. Janice P. Phillips, Dr. Jeffery S. Wiggins, and Dr. Derek L. Patton, for their help and support leading to the successful completion of my dissertation;

Drs. Trent E. Gould and Scott G. Piland in Human Performance and Sports Materials for their help to accomplish the projects on energy damping materials. It was great experience for me to learn sports applications using polymeric materials;

Past and present Hoyle Research Group members for their assistance and valuable discussion. I especially thank Justin Chan, who always sang in the lab, "Junghwan Shin is my friend, I'm so happy, happy, happy~," for his help to not only complete my Ph.D. work but learn many non-scientific things that made my life more enjoyable;

My dear classmates for helping me to survive in the first year course work. I am especially grateful to Joel D. Flores for useful academic discussion.

I also acknowledge Perstorp, Bruno Bock, Ciba Specialty Chemicals, and Bayer Materials Science for materials and Fusion UV Systems for the light source.

TABLE OF CONTENTS

LIST OF TABLES

Table

LIST OF CHARTS AND SCHEMES

Chart

Scheme

LIST OF ILLUSTRATIONS

Figure

CHAPTER I

INTRODUCTION

Thiols and thiol click chemistry

The chemical structure of thiols (-SH) is analogous to that of alcohols (-OH) except for the oxygen atom instead of sulfur which has lower electronegativity than oxygen. Thus, bonds to S atoms are longer and weaker than those to O. In addition, the bond angle about the sulfur atom, for example, in methanethiol (100.3°) is different with oxygen (109.5°) in ethanol due to more *p* character to the bonding orbital of divalent sulfur than there is to oxygen (Figure 1.1).[1,2]

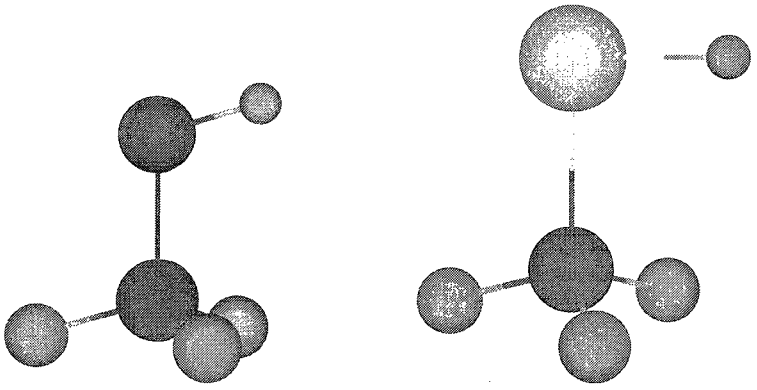

CH_3OH CH_3SH

Figure 1.1. Molecular structures of ethanol and ethanethiol.

Thiols also exhibit many differentiated physical and chemical properties compared to alcohols. For instance, hydrogen bonding is much weaker in thiols than in alcohols resulting in lower boiling points and less polarity as shown in Table 1.1.[1,2] In addition to the dipole moment difference, the lower electronegativity of sulfur atoms provides

important chemical characteristics to thiols. A hydrogen atom attached to a sulfur atom is essentially much more abstractable than one attached to an oxygen atom.

Table 1.1. Boiling points of alcohols and thiols

Thiols		Alcohols	
Methanethiol	6 °C	Methanol	65 °C
Ethanthiol	35 °C	Ethanol	78 °C
1-Butanethiol	98 °C	1-Butanol	117 °C

In other words, thiols are much more acidic than comparable alcohols, e.g. CH_3SH (pK_a = 10.3) vs. CH_3OH (pK_a = 15.5).[1-3] As a result, thiols are also much more nucleophilic than comparable alcohols in the presence of a base catalyst that abstracts proton from thiols generating thiolate anions. In a similar way, thiols readily produce thiyl radical by the photo or thermal initiating process.

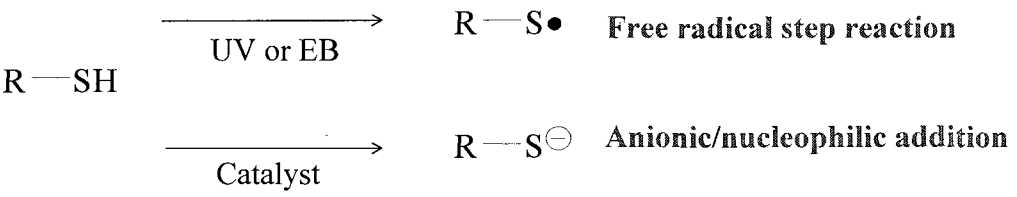

Scheme 1.1. Generation of thiyl radicals and thiolate anions from thiols.

Both thiyl radicals and thiolate anions are essential highly reactive chemical species that are involved in many chemical reactions with various chemical functional groups as shown in Scheme 1.2. It has been reported that thiol based reactions described in Scheme 1.2 satisfy many characteristics for 'Click' reactions.[4-28] High yields (near 100%

conversion) are obtained in a matter of seconds or minutes at room temperature without generating offensive side products. It should be noted that thiol click type reactions can be differentiated from the conventional azide-alkyne click reaction by the versatility of the functional groups that react with thiols. Reaction conditions are basically dependent on the reaction types determined by functional groups that coupled with thiols.

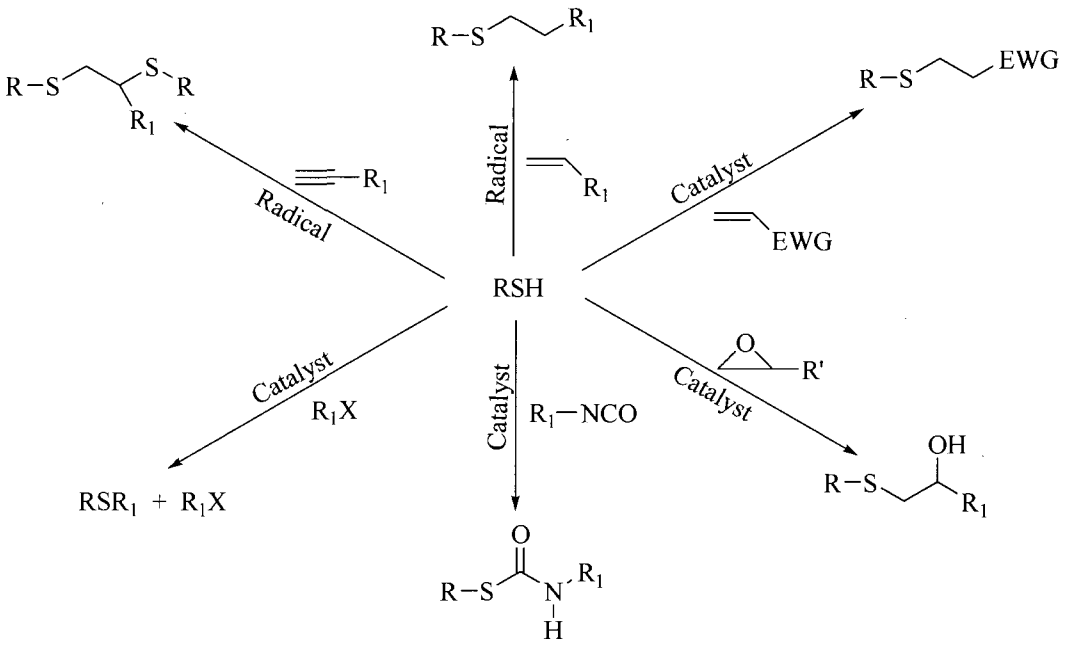

Scheme 1.2. Versatility of thiol reactions with different functional groups.

The most common thiol click-type reactions are the thiol radical-medicated and base / nucleophilic catalyzed thio-Michael addition reactions, which depend upon the electron density of the carbon double bonds, i.e. free-radical for electron rich[4-6,21-27] and hetero-Michael addition for electron poor double bonds.[20-26] Recently, thiol-unsaturated carbon triple bond (alkyne) reactions by light induced free-radical step mechanism which is analogous to the thiol-ene photopolymerization has been reported.[22,23,28] Each alkyne

functional group is capable of consecutive reactions with two thiol functional groups involving the sequential propagation of a thiyl radical with either an yne or ene functional group followed by chain transfer of the intermediate radical to another thiol. A base catalyzed nucleophilic addition reactions of thiols across isocyanates or epoxies are also well known to be fast and efficient click-type reactions.[17,29] Finally, it has been also reported that thiols are involve in SN_2 substitution reactions.[30-33] This dissertation will focus on the three major thiol click-type reactions, i.e. thiol-electron rich carbon double bond by free-radical, thiol-electron poor carbon double bond by hetero-Michael addition, and finally thiol-isocyanate nucleophilic addition reactions in the presence of a tertiary amine catalyst.

Thiol-electron rich carbon double bond free-radical reaction

While classical photo-induced (meth)acrylates homopolymerization follows a free-radical chain growth mechanism, the photopolymerization of thiol-ene systems occur by a free-radical chain mechanism involving two steps of propagation process.[34,35] As shown in Scheme 1.3, the thiol-ene free-radical reaction is an essentially stoichiometric equal molar reaction if the carbon double bonds are electron rich such as allyl ether, vinyl ether, and vinyl ester. Since thiyl radicals are produced through photolysis with or without initiator, the addition of thiyl groups across ene double bonds producing carbon centered radicals (Propagation 1) and subsequent regeneration of thiyl radicals by carbon centered radicals abstracting protons from thiols (Propagation 2) are consecutively occurred. It has been reported that photo-induced thiol-ene free-radical step reactions can

be classified as click type reactions due to the simplicity in kinetics, robustness, and high conversion with no side products.[4-6,21,22,26,27]

Initiation

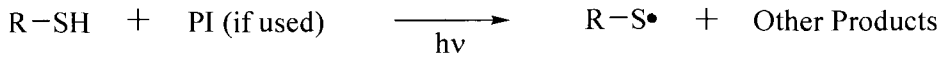

Propagation

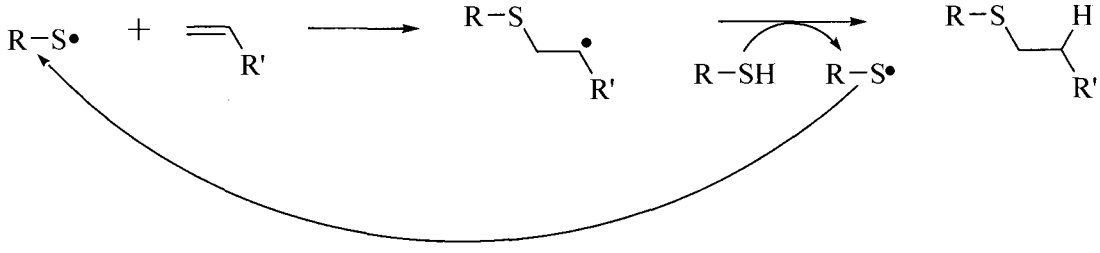

Termination Coupling of radicals

Scheme 1.3. Free-radical step growth mechanism of thiol-ene photopolymerization.

The free-radical step growth reaction mechanism of thiol-ene systems exhibits completely different kinetic and viscosity profiles compared to the traditional acrylate homopolymerization following free-radical chain growth mechanism resulting in reduced shrinkage / stress and high conversion.[35-40] In the case of multi-functional thiols and enes, essentially highly dense and uniform network structure is formed providing tremendous advantages over traditional cross-linked polymer systems.[35-46] Thus, thiol-ene photopolymerization effectively combines the benefits of click-type reactions and

advantages of the photo-induced process that are one of the powerful methodologies for fabricating polymeric materials.

Thiol-electron poor carbon double bond hetero-Michael addition reaction

The thiol-electron poor carbon double bond reaction by free-radical results in both thiol-ene coupling and ene homopolymerization, which is an overall non-quantitative reaction.[35,41-43] However, it is well known that a base catalyzed conjugate addition of thiols to electron deficient carbon double bonds is a stoichiometric equal molar reaction and affords relatively high yield as described in the literatures.[20,24,25] In addition to the base catalyzed reaction, a nucleophile catalyzed thiol-electron poor carbon double bond hetero-Michael addition reaction was also reported.[22,29] Interestingly, the nucleophile catalyzed thiol-ene hetero-Michael addition reaction exhibits more rapid and efficient kinetic profiles than a base catalyzed system resulting in near 100 % yields at room temperature with no side product formation, which is an attribute synonymous with the click nature of free-radical mediated thiol-electron rich carbon double bond click-type reaction. In Scheme 1.4, a proposed mechanism of tertiary phosphine, which is an efficient nucleophilic catalyst, catalyzed thiol-acrylate hetero-Michael addition reaction is shown. A tertiary phosphine catalyst initiates the thiol-ene hetero-Michael addition by the formation of a thiolate anion followed by the addition of the thiolate anion across electron deficient carbon double bond and re-generating the thiolate anion by the abstraction of a proton from another thiol. It has been reported that nucleophilic catalysts show enhanced activity over bases with comparable or lower pK_a values because the addition of a nucleophilic catalyst initiates the reaction by forming an electronically

unfavorable, i.e. very reactive, enolate anion that readily abstracts a proton from a thiol. Thus, the nucleophile catalyzed thiol-electron poor carbon double bond hetero-Michael addition reaction exhibits exceptionally fast kinetic profiles and quantitative conversion in a short period of time (minutes) at room temperature.

Initiation

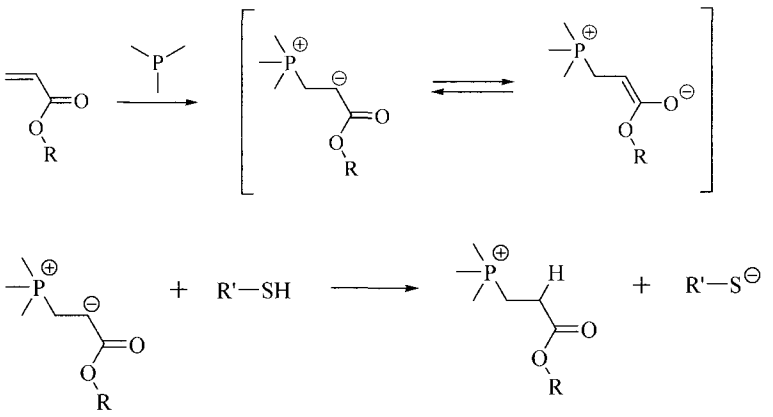

Propagation

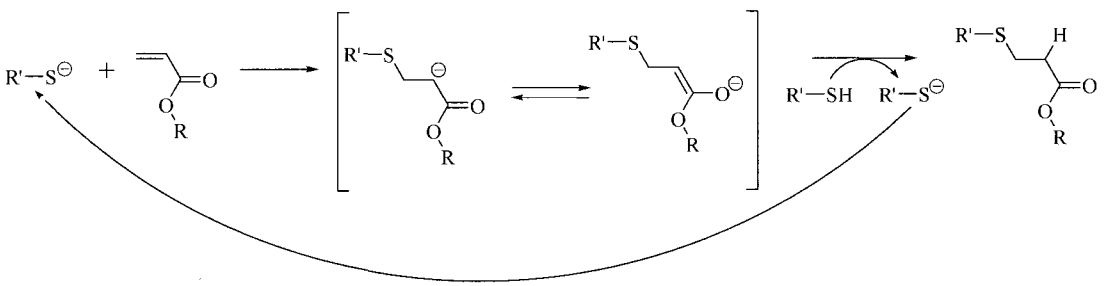

Scheme 1.4. A phosphine catalyzed thiol-acrylate hetero-Michael addition reaction mechanism.

Thiol-isocyanate nucleophilic coupling reaction

Thiol-isocyanate nucleophilic coupling reaction is analogous to the classical reaction of an alcohol with an isocyanate. The nucleophilic addition mechanism involves the addition of the electro negative oxygen or sulfur to the partial positive carbon of the isocyanate functional group (NCO) and subsequent proton transfer.[47-49] It is well known that organo-metallic catalysts such as dibutyltin dilaurate (DBTDL) are the common and efficient catalysts for the nucleophilic addition reaction of alcohols to isocyanates by increasing the partial positive charge of carbon in the isocyanate functional group.[48,49] In the case of a thiol, due to the significantly lower electronegativity of a sulfur atom compared to oxygen, DBTDL associated with the isocyanate does not accelerate the addition reaction of the thiol to the isocyanate. However, thiols readily form thiolate anions which are very strong nucleophiles in the presence of a base catalyst leading the fast and efficient thiol-isocyanate nucleophilic coupling reaction. In Scheme 1.5, a proposed reaction mechanism of the tertiary amine catalyzed nucleophilic coupling reaction of the thiol and isocyanate is shown. The reaction is initiated by the abstraction of proton from a thiol by a tertiary amine base producing a thiolate anion, followed by consecutive addition of the thiolate anion to an isocyanate functional group and abstraction of a proton from another thiol re-generating the thiolate anion. Thus, it should be noted that a base catalyzed thiol-isocyanate nucleophilic coupling reaction essentially follows an anionic chain process involving both initiation and propagation steps, which are completely different chemical process from the classical nucleophilic addition reaction of alcohols to isocyanates. In the 1960s, Dyer et al. reported that the tertiary amine catalyzed thiol-isocyanate reaction is very rapid, proceeds to 100%

conversion with no side product formation such as allphonates that are commonly formed in alcohol-isocyanate reaction and has many attributes of click reactions, i.e. the selectivity and no requirement for product clean up.[11,50] According to the original criteria defining click chemistry, the amine-isocyanate reaction was classified as a click-type reaction.[51] The base catalyzed thiol-isocyanate reaction is very closely related to the amine-isocyanate reaction in that both are selective and rapid resulting in high yields with no by products.

Initiation

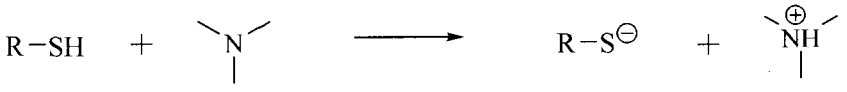

Propagation

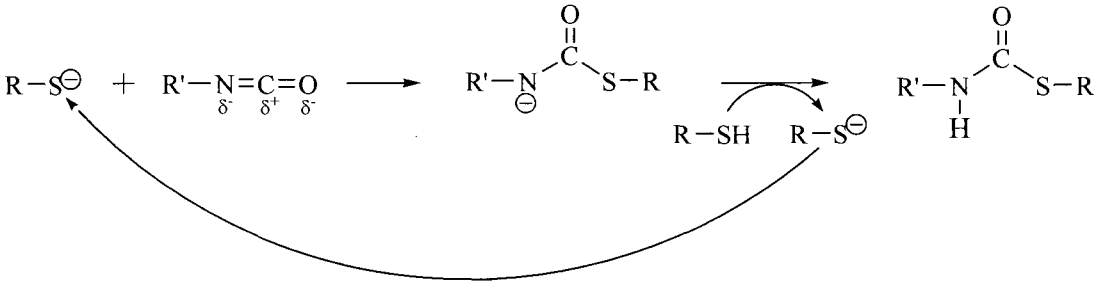

Scheme 1.5. A tertiary amine catalyzed thiol-isocyanate nucleophilic coupling reaction mechanism.

Chemical structure of thiol based networks. Since thiols participate in click-type reactions with many functional groups, the reactions of multi-functional thiols and other multi-functional monomers produce highly uniform and homogeneous network structures.

For instance, the simplified photo-polymerized trithiol-triene network and triacrylate homopolymer are shown in Figure 1.2. While thiol-ene network forms highly dense and uniform network structure by the typical photopolymerization (Figure 1.2 (a)), a broad distribution of molecular weight between cross-links and many dangling chain ends resulting in the inhomogeneous cross-linked structure are formed by multi-functional acrylate homopolymerization (Figure 1.2 (b)).

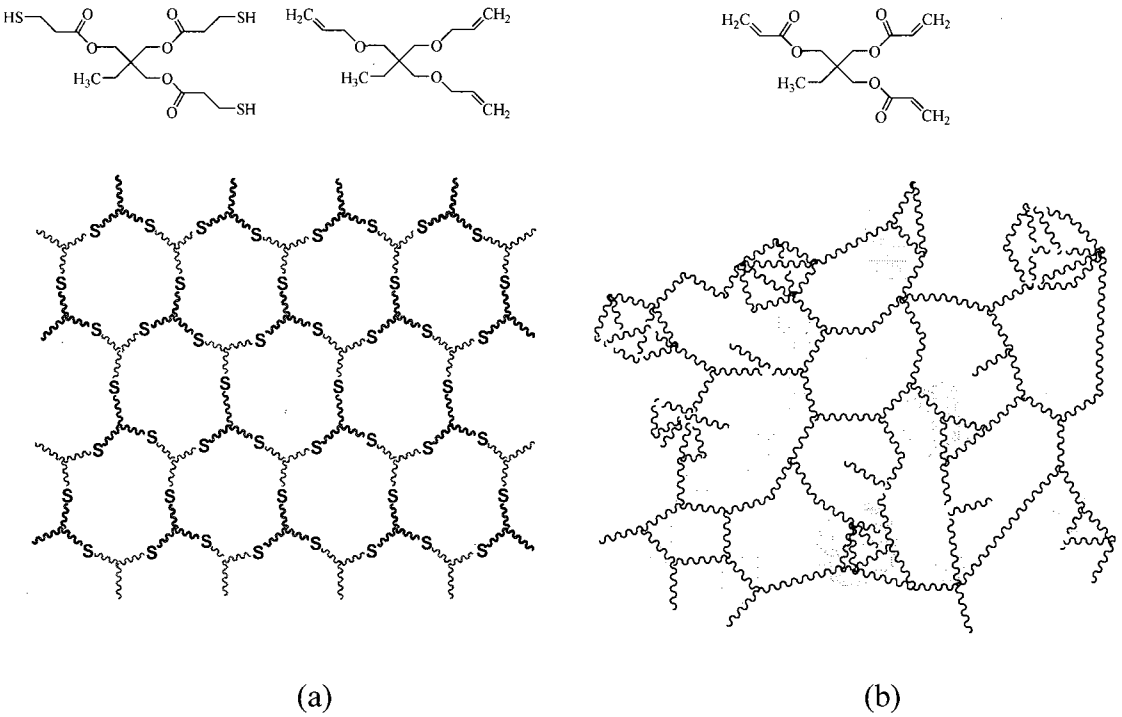

(a) (b)

Figure 1.2. Chemical structures of photo-polymerized (a) trithiol-triene network and (b) cross-linked triacrylate homopolymer.

The uniformity of thiol-ene networks is best illustrated by the narrow glass transition regions ranging 10 ~ 20 °C compared to multi-functional acrylate homopolymer exhibiting significantly extended T_g over 200 °C.[35,41,42,52,53] Uniform network structures of thiol based networks have a tremendous advantage over traditional cross-linked

systems that are plagued by the heterogeneity of chemical structure as well as physical and mechanical properties. It has been reported that holographic polymer dispersed liquid crystals (HPDLCs) based on photo-polymerized thiol-ene systems yield superior phase separation behavior and uniform spherical liquid crystal droplets compared to conventional acrylate systems.[46,54-56] Also, the uniform chemical structure accompanying the step-growth reaction mechanism and lower shrinkage during polymerization satisfy the requirements for photolithography and microdevice fabrication. The ability to maintain the original dimensions of shapes after polymerization due to the low shrinkage of thiol based materials leads to high fidelity in the reproduction of micro- and nano-scaled patterns.[57,58] The exceptional uniformity of chemical structure resulting in narrow glass transition regions imparts highly desirable mechanical behaviors such as excellent energy damping performance at a specific temperature or frequency region. It has been reported that photopolymerized thiol-ene and urethane modified thiol-ene networks exhibit good impact damping properties (~90 %) which are directly related to tan δ results.[41,59]

Physical aging and enthalpy / volume relaxation

Since the concept of physical aging was defined by Struik in the 1950's, enthalpy or volume relaxation of amorphous polymers has been extensively studied.[60,61] When amorphous polymers in the melt state are cooled at a certain cooling rate below their corresponding glass transition temperatures, polymer chains lose the ability to undergo long range cooperative segmental motions since the timescale for these molecular motions becomes comparable or longer than the time scale of the experiment as defined

by the cooling rate. As a result, the polymeric melt behavior deviates from equilibrium resulting in the formation of the glassy state exhibiting an excess of enthalpy and free volume (Figure 1.3A). The process of vitrifying the melt occurs over a distinct temperature interval with the T_g defined as the point of inflection of either the heat capacity or the thermal expansion coefficient measured as a function of temperature upon cooling or heating. If reheated immediately without annealing, enthalpy and volume increase along the same path as they decreased upon cooling (Figure 1.3B, curve a), and the heat capacity measured at constant pressure by DSC exhibits a characteristic change or jump, ΔC_p, at T_g. (Figure 1.3C, curve a).

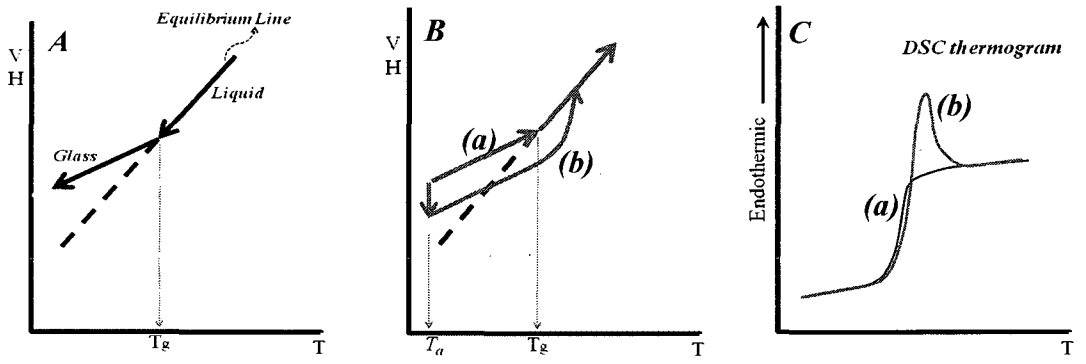

Figure 1.3. Diagram of physical aging process (A:cooling, B:heating) and the resultant enthalpy relaxation peak in a DSC scan (C) (curves (a) are heating w/o annealing, and curves (b) are w/ annealing).

However, if the sample is annealed below, but still in close proximity to the glass transition temperature, enthalpy and/or volume will relax with time and approach the values defined at equilibrium. This sub-T_g annealing involves a slow reorganization of

chains through a combination of long-range segmental and short-range local motions producing a material that is closer to thermodynamic equilibrium. Sub-T_g annealing results in densification, lengthening of viscoelastic relaxation times, and corresponding changes in physical/mechanical properties.[61,62] When the sub-T_g aged sample is reheated, the difference in the enthalpy or volume between the aged and un-aged states is subsequently recovered above the glass transition (Figure 1.3B, curve b). When heat capacity is measured by DSC, the aged sample displays an enthalpy relaxation peak (Figure 1.3C, curve b) at a temperature just above T_g. The process of physical aging is entirely reversible, i.e. it can be repeated after the sample's thermal history is fully erased at temperatures above T_g.[61-64] This is in contrast to irreversible chemical or thermal aging involving chemical reactions.

The heat capacity at constant pressure, C_p, which is defined thermodynamically as $(\partial H/\partial T)_p=T(\partial S/\partial T)_p$, in the glassy state of a polymer, is primarily determined by the vibrational degrees of freedom, characteristic of solid-like behavior, while above the glass transition, in the melt state, the heat capacity is determined by the translational degrees of freedom, which is a characteristic of liquid-like behavior, as well as vibrational degrees of freedom. Naturally, $C_{p,liquid} > C_{p,glass}$, leads to positive values of the heat capacity jump at T_g, thus $\Delta C_p = C_{p,liquid} - C_{p,glass}$. The heat capacity jump, ΔC_p, at T_g varies from polymer to polymer and determines the maximum amount of excess enthalpy for aging. The enthalpic departure from equilibrium, ΔH_∞, is often defined as the product of ΔC_p and ΔT which is the difference in the aging temperature, T_a, and T_g, i. e., $\Delta T = T_g - T_a$. This is demonstrated pictorially in Figure 1.4 by plotting the enthalpy versus temperature for three systems with progressively larger changes in heat capacity upon

transition from the glassy to the rubbery/liquid state. Taking the slopes (heat capacities) in the glassy state to be approximately constant, the ΔC_ps for the three systems are primarily determined by the differences in the heat capacities in the rubbery/liquid state. Moreover, for a given ΔT, the difference in the actual enthalpy of the glass with no aging and the thermodynamic equilibrium enthalpy can be depicted by extending the line of the enthalpy versus temperature plot above the T_g to temperatures below the T_g (shown as the dotted lines in Figure 1.4).

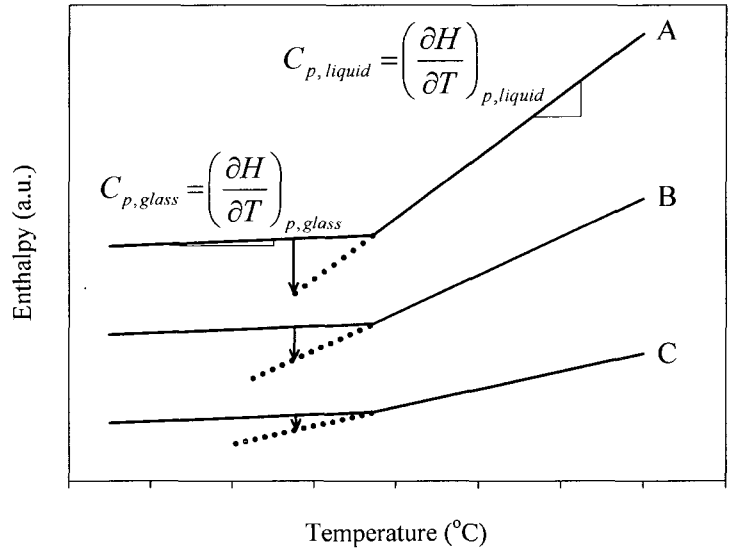

Figure 1.4. Diagram of enthalpy vs. temperature with different heat capacities ($\Delta C_{p,A} > \Delta C_{p,B} > \Delta C_{p,C}$).

The enthalpy differences at a given temperature are depicted in Figure 1.4 by the three arrows between the actual and projected enthalpy versus temperature lines. As shown, the enthalpy differences represented by the three arrows are essentially the possible enthalpy relaxations that can occur for each system assuming that a long enough time is

allowed for each enthalpy relaxation process to be completed. Of course this picture is somewhat oversimplified as the corresponding slopes of enthalpy, the heat capacities, below and above T_g, are temperature dependent.

A critical and potential problem of the highly uniform network structure of thiol based materials is propensity for sub-T_g aging. Compared to conventional crosslinked polymers, thiol based networks have a highly uniform dense structure accompanied by inherently narrow glass transition and probably characteristic relaxation times.[35,36,41,59] Considering the relationships between molecular dynamics and sub-T_g aging, it is expected that thiol based networks might be very sensitive to annealing temperature and time. This suggests that a large amount of enthalpy or volume relaxation would occur in a short period of time under specific physical aging conditions (temperature, pressure). In practice, it has been observed (but without strict documentation) that one of the disadvantages of thiol-ene networks is that physical properties change on a short time scale. In some cases, remarkable changes occur within a month. This is coincident with the expected result of the uniform network structure of thiol-enes as discussed above. Thus, it is essential to study the sub-T_g aging of thiol-ene networks and its relationship to physical and mechanical properties.

Summary

In this dissertation, thiol click-type reactions with several different functional groups such as electron rich carbon double bonds, electron poor carbon double bonds, and isocyanates were discussed in terms of the efficiency of the reaction for the fabrication of materials and uniqueness of resultant chemical structures, i.e. well

controlled segmented linear block copolymers and highly dense, uniform networks. Highly elastic polythiourethanes were synthesized using sequential thiol-acrylate hetero-Michael addition and thiol-isocyanate nucleophilic coupling reactions, that are essentially fast and robust satisfying the requirements of classic click reactions. The segmented structure comprising hard and soft segments was systematically controlled providing the tunability in physical and mechanical properties over wide ranges. Thiol-isocyanate-ene ternary networks were prepared by both sequential and simultaneous thiol click-type reactions, i.e. a base catalyzed thiol-isocyanate coupling reaction and a thiol-ene free-radical step reaction. The sequence of two reactions was controlled by triggering the thiol-isocyanate coupling reaction using thermally and photolytically activated base catalysts. The incorporation of thiourethane groups in the classic thiol-ene networks offers numerous advantages such as enhanced physical and mechanical properties due to extensive hydrogen bonding. The relationships between the chemical composition and physical/mechanical properties of thiol-isocyanate-ene based ternary networks were also established that are indicative of a wide range of properties achievable with thiol-isocyanate-ene based ternary networks.

The near perfect network structure of photopolymerized thiol-ene systems presents a good opportunity to evaluate sub-T_g aging in terms of fundamental molecular parameters such as network density and chemical structure of monomers. Accordingly, the aging of photo-polymerized thiol-ene networks was investigated by measuring the extent of enthalpy relaxation as a function of monomer functionality and rigidity. Additionally, sub-T_g aging of thiol-ene networks was intentionally controlled by manipulating network structures, i.e. incorporation of polar and non-polar side chains

without sacrificing network uniformity and control of network uniformity by incorporating inhomogeneous multi-functional acrylate homopolymer domains. Thus, the relationships between fundamental molecular parameters and sub-T_g aging were established. Finally, multi-layered thiol-ene photo-polymerized films were prepared and evaluated in terms of sub-T_g aging monitored by enthalpy relaxation. The extent and rate of enthalpy relaxation of multi-layered thiol-ene thin films networks were compared with thick films to investigate the effect of thickness and interaction of each layer on sub-T_g aging.

References

1. Solomons, T. W. G. *Organic Chemistry*, 6th Ed, John Wiley & Sons, Inc., New York, **1996**.
2. Patai, S. *The Chemistry of the Thiol Group: Part 1*, John Wiley & Sons, Inc., New York, **1974**.
3. Serjeant, E. P.; Dempsey, B. *Ionisation Constants of Organic Acids in Aqueous Solution*, Pergamon Press, New York, **1979**.
4. Hoyle, C. E.; Bowman, C. N. *Angew. Chem. Internat. Edit.* **2009**, in preparation.
5. Lowe, A. B.; Hoyle, C. E.; Bowman, C. N. *J. Mater. Chem.* **2009**, submitted.
6. Dondoni, A. *Angew. Chem. Int. Ed.* **2008**, 47, 8995.
7. Becer, C. R.; Hoogenboom, R.; Schubert, U. S. *Angew. Chem. Int. Ed.* **2009**, 48, 2.
8. van Dijk, M.; Rijkers, D. T. S.; Liskamp, R. M. J.; van Nostrum, C. F.; Hennick, W. E.; *Bioconjugate Chem.* **2009**, in press (ASAP).
9. Dietliker, K.; Husler, R.; Birbaum, J. -L.; Ilg, S.; Villeneuve, S.; Studer, K.; Jung, T.; Benkhoff, J.; Kura, H.; Matsumoto, A.; Oda, H. *Prog. Org. Coat.* **2007**, 58, 146.
10. Yuan, Y. C.; Rong, M. Z.; Zhang, M. Q.; Chen, J.; Yang, G. C.; Li, X. M.; *Macromolecules* **2008**, 41, 5197.
11. Dyer, E.; Glenn, J. F.; Lendrat, E. G. *J. Org. Chem.* **1960**, 26, 2919.
12. Movassagh, B.; Soleiman-Beigi, M. *Monat. Fur Chem.*, **2008**, 139, 137.
13. Klemm, E.; Stockl, C. *Makromol. Chem.* **1991**, 153.
14. Kosaka, M.; Kageyma, Y. US Patent 5,744, 568.
15. Droger, N.; Primel, O.; Halary, J. L. *J. Appl. Polym. Sci.* **2008**, 107, 455.
16. Nakayama, N.; Hayashi, T. *Prog. Org. Coat.* **2008**, 62, 274.

17. Li, H.; Yu, B.; Matsushima, H.; Hoyle, C. E.; Lowe, A. B. *Macromolecules* **2009**, 42, 6537.

18. Charles, D.; Gershbein, H.; Gershbein, L. *J. Am. Chem. Soc.* **1947**, 69, 2328.

19. Brian, D.; Viswanathan, M. K.; Miller, K. M.; Long, T. E. *Prog. Polym. Sci.* **2006**, 31, 487.

20. Chan, J. W.; Yu, B.; Hoyle, C. E.; Lowe, A. B. *Chem. Commun.* **2008**, 4959.

21. Chan, J. W.; Yu, B.; Hoyle, C. E.; Lowe, A. B. *Polymer* **2009**, 50, 3158.

22. Chan, J. W.; Hoyle, C. E.; Lowe, A. B. *J. Am. Chem. Soc.* **2009**, 131, 5751.

23. Chan, J. W.; Zhou, H.; Hoyle, C. E.; Lowe, A. B. *Chem. Mater.* **2009**, *21*, 1579.

24. Yu, B.; Chan, J. W.; Hoyle, C. E.; Lowe, A. B. *J. Polym. Sci., Part A: Polym. Chem.* **2009**, 47, 3544.

25. Yu, B.; Chan, J. W.; Hoyle, C. E.; Lowe, A. B. *J. Polym. Sci., Part A: Polym. Chem.* **2009**, 47, 3577.

26. Kloxin, C.J.; Scott, T.; Bowman, C.N. *Macromolecules,* **2009**, 42, 2551.

27. Campos, L. M.; Killops, K. L.; Sakai, R.; Paulusse, J. M. J.; Damiron, D.; Drockenmuller, D. E.; Messmore, B. M.; Hawker, C. J. *Macromolecules*, **2008**, 41, 7063.

28. Fairbanks, B. D.; Scott, T. F.; Kloxin, C. J.; Anseth, K. S.; Bowman, C. N. *Macromolecules* **2009**, 42, 211.

29. Shin, J.; Matsushima, H.; Chan, J. W.; Hoyle, C. E. *Macromolecules* **2009**, 42, 3294.

30. Rosen, B. M.; Lligadas, G.; Hahn, C.; Percec, V. *J. Polym. Sci.: Part A: Polym. Chem.* **2009**, 47, 3931.

31. Rosen, B. M.; Lligadas, G.; Hahn, C.; Percec, V. *J. Polym. Sci.: Part A: Polym. Chem.* **2009**, 47, 3940.

32. Samaroo, D.; Vinodu, M.; Chen, X.; Drain, C. M. *J. Comb. Chem.* **2007**, 9, 998.

33. Becer, C. R.; Babiuch, K.; Pilz, D.; Hornig, S.; Heinze, T.; Gottschaldt, M.; Schubert, U. S. *Macromolecules*, **2009**, 42, 2387.

34. Jacobine, A. F. In *Radiation Curing in Polymer Science and Technology III*, J. D. Fouassier; J. F. Rabek Eds.; Elsevier: London, **1993**; Chapter 7, 219-268.

35. Hoyle, C. E.; Lee, T. Y.; Roper, T. *J. Polym. Sci. Part A: Polym. Chem.* **2004**, 42, 5301.

36. Roper, T. M.; Rhudy, K. L.; Chandler, C. M.; Hoyle, C. E.; Guymon, C. A. *RadTech NA Tech Conf Proc.* **2002**, 697.

37. Roper, T. M.; Guymon, C. A.; Hoyle, C. E. *Polymer* **2004**, 45, 2921.

38. Cramer, N. B.; Bowman, C. N. *J. Polym. Sci., Part A: Polym. Chem.* **2001**, 39, 3311.

39. Cramer, N. B.; Reddy, S. K; Cole, M.; Hoyle, C. E.; Bowman, C. N. *J. Polym. Sci., Part A: Polym. Chem.* **2004**, 42, 5817.

40. Khire, V. S.; Harant, A. W.; Watkins, A. W.; Anseth, K. S.; Bowman, C. N. *Macromolecules* **2006**, *39,* 5081.

41. Senyurt, A. F.; Hoyle, C. E.; Wei, H.; Piland, S. G.; Gould, T. E. *Macromolecules* **2007**, 40, 3174.

42. Wei, H.; Senyurt, A. F.; Jönsson, S.; Hoyle, C. E. *J. Polym. Sci., Part A: Polym. Chem.* **2007**, 45, 822.

43. Lee, T. Y.; Roper, T. M.; Jönsson, E. S.; Guymon, C. A.; Hoyle, C. E. *Macromolecules* **2004**, 37, 3606.

44. Li, Q.; Zhou, H.; Wicks, D. A.; Hoyle, C. E. *J. Polym. Sci., Part A: Polym. Chem.* **2007**, 45, 5103.

45. Wei, H.; Li, Q.; Ojelade, M.; Madbouly, S.; Otaigbe, J. U.; Hoyle, C. E. *Macromolecules* **2007**, 40, 8788.

46. Senyurt, A. F.; Warren, G.; Whitehead, J. B.; Hoyle, C. E. *Polymer* **2006**, 47, 2741.

47. Odian, G. *Principle of Polymerization* 4th Ed. John Wiley & Sons, Inc.: Hoboken, **2004**.

48. Hepburn, C. *Polyurethane Elastomers*; Elsevier: Essex, **1992**.

49. Szycher, M. *Szycher's Handbook of Polyurethanes*; CRC Press LLC: Boca Raton, FL, **1999**; Chapter 3.

50. Klemm, E.; Stockl C. *Macromol. Chem.* **1991**, 192, 153.

51. Kolb, H. C.; Finn, M. G.; Sharpless, K. B. *Angew. Chem. Int. Ed.* **2001**, 40, 2004.

52. Shin, J.; Nazarenko, S.; Hoyle, C. E. *Macromolecules* **2009**, 42, 6549.

53. Shin, J.; Philips, J. P.; Nazarenko, S.; Hoyle, C. E. "Physical and Chemical Modifications of Thiol-Ene Networks to Control Activation Energy of Enthalpy Relaxation" *Polymer*, submitted.

54. Sutherland, R. L.; Tondiglia, V. P.; Natarajan, L. V.; Lloyd, P. F.; Bunning, T. J. *J. App. Phys.* **2006**, 99. 12.

55. Natarajan, L. V.; Brown, D. P.; Wofford, J. M.; Tondiglia, V. P.; Sutherland, R. L.; Lloyd, P. F.; Bunning, T. J. *Polymer* **2006**, 47. 4411.

56. Woo, J. Y.; Kim, E. H.; Kim, B. K. *J. Polym. Sci. Part A-Polym Chem.* **2007**, 34, 527.

57. Khire, V. S.; Yi, Y.; Clark, N. A.; Bowman, C. N. *Adv. Mater.* **2008**, 20, 3308.

58. Campos, L. M.; Meinel, I.; Guino, R. G.; Schierhorn, M.; Gupta, N.; Stucky, G. D.; Hawker, C. J. *Adv. Mater.* **2008**, 20, 3728.

59. Senyurt, A. F.; Wei, H.; Hoyle, C. E.; Piland, S. G.; Gould, T. E. *Macromolecules* **2007**, 40, 4901.

60. Kovacs, J. *Journal of Polymer Science* **1958**, 30, 131.

61. Struik, L. C. E. *Physical Aging in Amorphous Polymers and Other Materials*, Elsevier Publishing Company, New York, **1978**.

62. Hutchinson, J. M. *Progress in Polymer Science* **1995**, 30, 703.

63. Wunderlich, B. *Thermal Analysis*, Academic Press, Inc, New York, **1990**.

64. Haward, R. N.; Young, R. J. *The Physics of Glassy Polymers*, Chapman & Hall, New York, **1997**.

CHAPTER II

OBJECTIVES

Thiol click-type reactions have many advantages and utilities by virtue of the unique chemical reaction mechanisms. However, systematic studies on the importance of thiol click-type reactions as a methodology for the polymer synthesis have not been reported. Also, there is an important implication of the uniform highly dense network structure of thiol based materials on the physical properties which needs to be considered. Thus, this dissertation is composed of two parts:

In the first part (Chapter III and IV), thiol click-type reactions are exploited as a new strategy for the efficient synthesis of high performance polymeric materials. In order to achieve this goal the following questions will be probed in detail:

- Can thiol-click type reactions be utilized for the fabrication of polymeric materials in a click nature, i.e. fast and robust reaction, no side products, and benign reaction conditions?
- Can multiple thiol click-type reactions be combined in a system to tailor chemical reaction profiles and physical / mechanical properties?
- Structure-property relationships of thiol based materials will be established to answer the question
    - Can thiol click-type reactions be effectively controlled to design molecular structure exhibiting a wide range of physical and mechanical properties?

Thus, the first part of this dissertation will provide new approaches for the fabrication of high performance polymers such as linear polythiourethanes (Chapter 3) and thiourethane -thiolene hybrid crosslinked networks (Chapter 4) using the benefits of thiol click-type

reactions. Also, the critical structure-property relationships for designing polymeric materials from highly elastomeric thermoplastics to strong glassy networks with a wide range of thermal and mechanical properties will also be established.

The second part (Chapter V~VIII) is focused on the significance of the uniform network structure on physical properties, especially, sub-T_g aging. The goals are specifically stated below:

- To establish the relationships between basic molecular parameters, i.e. network density and rigidity, and enthalpy relaxation of binary thiol-ene based networks
- To determine the effect of chemical modification on enthalpy relaxation of thiol-ene based networks to answer the fundamental questions
  - How do n-alkyl and hydroxyl alkyl side chains affect enthalpy relaxation of thiol-ene networks?
  - Does network uniformity affect enthalpy relaxation of thiol-ene networks?
  - Can sub-T_g aging be intentionally controlled by manipulating chemical structures of thiol-ene networks?
- To quantitatively investigate the restrictive effect of rigid amorphous region and gold nanoparticles on molecular mobility and sub-T_g aging
- To investigate sub-T_g aging of multi-layered thiol-ene based films

In the second part of this dissertation, the chemical structural effects of thiol-ene components on the uniform dense network formation and subsequent sub-T_g aging, and the relationship of physical aging to physical and mechanical properties will be investigated (Chapter V). The fundamental investigation will provide the opportunity to modify selectively the molecular structure and chemical/physical environment to control

sub-T_g aging of thiol-ene based films. The purpose of the chemical and physical modification of thiol-ene system investigation is to determine the effect of chemical functional groups, networks uniformity, and gold nanoparticles on sub-T_g aging (Chapter VI and VII). This should allow quantitative analysis of sub-T_g aging and moreover unprecedented control of enthalpy relaxation of thiol-ene based networks. In the last chapter, with the increasing realization of the importance of polymer thin films in both academic and applied venues, multi-layered thiol-ene based thin films will be evaluated (Chapter VIII). The role of layering multiple thiol-ene networks on accelerating or impeding sub-T_g aging and its effect on physical / mechanical property changes of thiol-ene based thin films with annealing time will be determined. Finally, the high uniformity of thiol-ene networks resulting from click nature of thiol based reactions, i.e. quantitative conversion with no side products, will provide a perfect platform for the investigation of sub-T_g aging as a model system.

CHAPTER III

SEGMENTED POLYTHIOURETHANE ELASTOMERS THROUGH SEQUENTIAL THIOL-ENE AND THIOL-ISOCYANATE REACTIONS

Abstract

Highly elastic polythiourethanes were synthesized through sequential thiol reactions involving 1,6-hexane dithiol (HDT), 1,4-butanediol diacrylate (BDDA) and several diisocyanates (ISO). Thiol-terminated prepolymers prepared by the phosphine catalyzed thiol Michael addition of HDT and BDDA form flexible thioether oligomers which were then incorporated as soft segments into polythiourethane main chains through a triethylamine catalyzed thiol-isocyanate reaction with HDT and ISO to give polymers with both hard and soft segments. Real-time FTIR, used to investigate the kinetic conversion profiles of both reactions, and NMR showed that both the thiol Michael addition and the thiol-isocyanate reactions are very fast and efficient, having the chemical attributes generally associated with thiol-ene radical click reactions. The effects of the soft and hard segment length, soft/hard segment weight ratio, and chemical structure of the ISO on thermal and dynamic thermal mechanical properties was characterized in terms of micro-phase separation determined by DSC and DMA. Tensile properties of the polythiourethanes were measured and correlated with the degree of micro-phase mixing between the soft and hard segments.

Introduction

Sulfur-containing polymers such as polythiourethanes, polysulfides, polythioesters, polysulfones, and polythiocarbonates are beginning to attract increased attention due to many important attributes, not the least of which are excellent optical properties and biocompatibility.[1-10] Sulfur can lead to enhancement in refractive index, increased flexibility, and enhanced crystallinity when incorporated into polymer thermosets and thermoplastics.[1,9-16] However, in order for sulfur containing polymers to be used in many applications, physical/mechanical properties such as extensibility and toughness must be tailored and optimized.

Multifunctional thiols (-SH) have been employed to form sulfur linkages in polymer backbones through reactions with unsaturated hydrocarbons (e.g. allyl ether, vinyl ether, (meth)acrylate), epoxies, or isocyanates.[17-22] Such polymers have rather limited extensibility,[17-29] i.e., they are not good elastomers. However, the inclusion of difunctional and monofunctional thiols in thiol-ene network results in low-modulus, elastomeric materials.[30]

It is well known that incorporation of urethane linkages into both linear polymers and crosslinked networks results in hydrogen bonding capabilities that imparts exceptional elastic properties. Interestingly, in the case of thiol-acrylate/ene based networks, incorporating urethane groups results into the network results in enhanced mechanical and thermal transitions with potential use in bio- and optical applications.[17,27,31] It can be projected that incorporation of a combination of sulfide linkages, which provide for the unique combination of flexibility and crystallizability,[9-16] and thiourethane groups in polymer systems would afford a distinct opportunity to

control mechanical and thermal properties. This, combined with the well known optical and mechanical (flexibility) advantages of thiourethane and sulfide groups in polymer chains, would result in significant potential for the synthesis of linear segmented polythiourethane elastomers. It has already been reported that the addition of difunctional thiols to difunctional isocyanates leads to the formation of simple non-segmented polythiourethanes,[32,33] which are classified as members of the polyurethane family with the hydrogen bonding features that typically accompany polyurethanes.[32,34,35] In addition to synthesizing polythiourethanes by thiol-isocyanate step growth polymerization processes, polythiourethanes made from cyclic dithiocarbonates by living cationic polymerization have been reported by Endo et al.[36-40] The use of these linear, non-segmented polythiourethanes, characterized by controllable molecular weights and narrow molecular weight distributions resulting from the living cationic polymerization process, is limited to applications requiring glassy materials and/or highly dense cross-linked structures.[41,42] Since sulfide linkages incorporated into aliphatic polyesters have been reported to lead to the unique combination of flexible films with low glass transitions and high degrees of crystallization,[13] it is expected that the synthesis of segmented polythiourethanes with sulfide linkages in the soft segment would open up a new potential for elastomers with a unique combination of properties. While it is possible to use a combination of short chain dithiols and oligomeric polyols to make segmented elastomeric poly(thiourethane-urethane)s,[43] incorporation of sulfide linkages in the soft segment polyol would certainly lead to both high flexibility and enhanced crystallinity.

Herein, we report the efficient synthesis and characterization of segmented polythiourethanes with elastomeric properties induced by micro-phase separation between soft and hard segments. By making thiol terminated oligomers with sulfide linkages in the oligomeric chain, followed by subsequent reaction with a combination of a diisocyanate and small molecule dithiol chain extender, the synthesis of a series of high molecular weight polythiourethanes with elevated sulfur content and excellent elastomeric properties has been accomplished. The first reaction involves the highly efficient phosphine catalyzed thiol-acrylate Michael addition reaction, which has been reported[44] as a quantitative, rapid click reaction that we project to proceed by an anionic chain process that is complete on the order of minutes or less upon mixing. This action was previously used to make star polymers in a dilute solution synthetic process.[44] While the triethylamine catalized reaction of dithiols with diacrylates has been reported,[3,45] it is noted that the reaction is very slow and requires long reaction times (i.e. 140 h at 30 ^{o}C). Herein, the phosphine catalyzed reaction previously used for the synthesis of star polymers will be used for the first time for quantitative synthesis of thiol terminated oligomers. The second reaction in the sequence will involve the reaction of the thiol-terminated oligomers and low molecular weight dithiols with diisocyanates using a triethyl amine catalyzed reaction. It has been reported that the tertiary amine catalyzed thiol-isocyanate reaction is very rapid, proceeds to 100% conversion with no allphonates[33,46] or other side products typical of traditional alcohol-isocyanate reactions, and has many of the attributes of click reactions, including selectivity and no requirement for product clean up. In the original article by Kolb, Finn and Sharpless[47] that defined click chemistry, the amine-isocyanate reaction was noted to be quite efficient; the thiol-

isocyanate reaction is very closely related to the amine-isocyanate reaction in that both are selective and rapid resulting in high yields with no by products. Thus, the sequential phosphine catalyzed thiol-acrylate and tertiary amine catalyzed thiol-isocyanate reactions are reported herein to be very effective for the general synthesis of high performance materials. The segmented polythiourethanes are shown to be high performance materials characterized by a flexible phase and a rigid hard phase with strong hydrogen bonding and crystallization, respectively. The degree of micro-phase separation between the soft and hard segments of the resulting series of polythiourethane oligomers has been systematically evaluated by thermal and dynamic mechanical analysis, and the results correlated with mechanical properties. The inclusion of sulfur in the form of sulfide linkages as well as thiourethane linkages provides a new methodology for the general synthesis of high performance elastomers. The polythiourethane synthesis by the two sequential high yield reactions in this work presents a clear guide for designing the microstructure of high performance elastic polythiourethanes with high sulfur content, and tailoring the physical properties to meet a potential wide range of applications. It effectively moves sequential thiol chemistry to the realm of an industrially viable synthetic route for fabricating elastomeric polythiourethanes. Since there is a large availability of diacrylates and dithiols available commercially, the prospect for tailoring polythiourethane elastomers to meet a specific set of property requirements for a wide range of applications is significant.

Experimental

Materials

1,6-Hexanedithiol (HDT, ≥ 97%) and 1,4-butanediol diacrylate (BDDA, 93.7% by GC), used to prepare the thiol-terminated prepolymers, diisocyanates (4,4′-methylene bis (phenyl isocyanate) (MDI, 98%), 4,4′-methylenebis (cyclohexyl isocyanate) (H_{12}MDI, ≥ 98%), tolylene-2,4-diisocyanate (2,4-TDI, ≥ 98%), isophorone diisocyanate (IPDI, 98%), and hexamethylene diisocyanate (HDI, ≥ 99%), dimethylphenyl phosphine (DMPPh) and triethylamine (TEA), used as catalysts for the thiol Michael addition and thiol-isocyanate reaction, respectively, were purchased from Aldrich. Dimethylacetamide (DMAc) anhydrous grade, tetrahydrofuran (THF), and butyl acetate (BAc) urethane grade were also obtained from Aldrich. All chemicals were used as received.

Synthesis of Thiol Terminated Prepolymers

A 250 mL, round-bottom, three-necked flask with a magnetic stirrer equipped with an ice bath was used as a reactor. First, HDT was mixed with 0.1 wt% of DMPPh and diluted with DMAc to 50 wt% solution in the flask while nitrogen purging. BDDA was dripped into the mixture for 10 min and the temperature was controlled below 30 °C with an ice bath in order to prevent BDDA from undergoing thermally initiated free-radical polymerization. After completion of adding BDDA, the mixture was further reacted for 10 ~ 20 min at room temperature until all the BDDA was consumed. Additional DMAc was added to make the solution 30 % by weight of thiol-terminated prepolymer. The complete disappearance of carbon double bonds in BDDA was confirmed by peaks at 812 cm^{-1} for FTIR, 5.71(q), 5.99(q), and 6.23(q) ppm for ^{1}H NMR,

and 128.3 and 130.5 ppm for ^{13}C NMR. The molecular weights of thiol-terminated prepolymers (length of soft segment) were controlled by stoichiometry from 1,000 to 3,000 g/mol with excess thiol and dictated by theoretical calculation using the Carothers equation.[48] M_n was measured using titration and compared with the theoretical values (Table 3.1).

Synthesis of Polythiourethane Elastomers

HDT and thiol-terminated prepolymers were mixed with 0.1 wt% of TEA and DMAc to give a 30 % solution, followed by feeding the requisite isocyanate for 10 min at room temperature. Temperature was maintained at less than 30 °C with an ice bath during feeding. The mixtures were further reacted at 60 °C for 1 h. The complete consumption of NCO was confirmed by the disappearance of the FTIR isocyanate peak at 2250 cm^{-1}. The length of the hard segment varied from 550 to 1,000 g/mol by stoichiometry. The formulations for the polythiourethane elastomer synthesized are shown in Table 3.2.

Kinetics

Kinetic profiles of the thiol Michael addition reaction of HDT and BDDA and the subsequent polythiourethane reaction were obtained using real-time infrared (RTIR) spectroscopy. A modified Bruker IFS 88 FTIR spectrometer was equipped with a horizontal sample accessory. Samples for thiol-terminated prepolymer were prepared by adding BDDA into the 40 wt% HDT solution in DMAc with 0.006 wt% of DMPPh based on the total solution weight. For polythiourethane formation, the requisite diisocyanate was dissolved in THF and added into the pre-mixed THF solution of HDT, thiol-terminated prepolymer, and 0.03 wt% of TEA based on the total solution weight. The

solid content of the final mixture was 20 wt%. Thin samples (25μm) between two salt plates sealed with silicon were placed immediately in the RTIR after mixing the samples; note that there is some delay in initiating the kinetic measurement which introduces some error into the measurement. The conversion of BDDA and HDT as a function of time was measured by monitoring the peaks of the carbon double bond and thiol at 812 and 2570 cm^{-1}, respectively, while the peak at 2250 cm^{-1} was used to measure the isocyanate conversion.

Characterization

Molecular weights (MW) of the thiol-terminated prepolymer prepared via thiol Michael addition of HDT to BDDA were determined using a thiol titration strategy.[49] In a 250 mL flask, prepolymers were dissolved in 15 mL of pyridine (99%, Aldrich) followed by the addition of 0.4 M silver nitrate aqueous solution (5 mL). This mixture was magnetically stirred for 5 minutes and 100 mL of di-H_2O was added with 6 drops of phenolphthalein indicator solution. This mixture was titrated with 0.1 M sodium hydroxide aqueous solution until a light pink color formed. The method was standardized by titration of a known amount of 6-mercapto-1-hexanol; 98.99% reliability was obtained. For the polythiourethane elastomers, molecular weights and PDI were determined using a Viscotek-TDA size exclusion chromatography (GPC) unit comprised of a 302 nm RI (633 nm), 7 mW 90° and 7° true low angle light scattering detectors and Viscotek I-Series Mixed Bed low MW and mid MW columns. A 20 mM LiBr DMF eluent at 60 °C was used at a flow rate of 1.0 mL/min controlled by an Agilent 1100 series pump. M_n, M_w, and PDI were determined using the Viscotek refractometer and OmniSec software.

^{1}H and ^{13}C NMR spectra of thiol terminated prepolymers were obtained on a Varian 500 MHz NMR in $CDCl_3$ with tetramethysilane (TMS) as the internal reference.

Thiol-terminated prepolymers and films of polythiourethanes for thermal and mechanical property measurements were prepared by casting the polythiourethane solution on a Teflon mold. After evaporation of DMAc at 80 °C for 24 h and 100 °C for 48 h, the films were further dried and kept at 25 °C under vacuum.

Thermal properties of the thiol-terminated prepolymers and polythiourethane elastomers were characterized by differential scanning calorimetry (DSC, TA Instruments Q 1000) equipped with RCS 90 (Refrigerated Cooling System). Three calibration steps (T_{zero}, enthalpy constant, and temperature calibration) were performed before the measurements. All experiments were carried out under nitrogen with a flow rate of 50 mL/min. Sample weights were 8.0 ± 1.0 mg to ensure sufficient sensitivity for heat capacity measurements. For thiol-terminated prepolymers, DSC scans were conducted over a temperature range from -90 to 100 °C using 10 °C/min heating and cooling rates. On the first heating scan, samples were equilibrated at 60 °C (higher than the T_m of the thiol-terminated prepolymer) for 10 min to erase thermal history and hysteresis of the samples, followed by cooling to -90 °C and a subsequent second heating to 100 °C. The temperature range for scanning the polythiourethane elastomers was -90 to 280 °C to ensure all thermal transitions of the soft and hard segments were observed. All samples were equilibrated at 150 °C (higher than the T_g hard segment) for 10 min before cooling to -90 °C and reheating to 280 °C. Heating and cooling rates were 10 °C/min. The second heating scans were recorded for all thiol-terminated prepolymers and polythiourethane elastomer films.

Dynamic thermal mechanical properties of thin cast films were measured using a DMTA (MK VI, Rheometrics). Measurements were conducted in the vertical tension mode with dimensions of 10 × 5.0 × 0.5 mm (L × W × T) from -110 to 250 °C at a 5 °C/min heating rate and 1 Hz frequency with 0.05 % strain.

Tensile property measurements were made with a mechanical testing machine (MTS, Alliance RT/10) according to ASTM D882 using a 100 N load cell with a specimen gauge length of 20 mm at a crosshead speed of 500 mm/min.

Results and Discussion

The highly elastomeric and tough mechanical properties of polyurethanes result from a segmented molecular structure consisting of at least two dissimilar phases along the backbone. Polythiourethanes, as a member of the polyurethane family, are characterized by high refractive index values and biocompatibility as well as strong hydrogen bonding with accompanying outstanding mechanical properties.[41-43] However, polythiourethanes as elastomers have not been reported because of the absence in availability of flexible long-chain polythiols. In this study, thiol-acrylate and thiol-isocyanate reactions which have many of the attributes of click chemistry including high efficiency, little side products, benign catalysts, and high reaction rates were used to synthesize segmented polythiourethanes; we note that in this work we used an organic solvent in which the oligomers and polymers were soluble. In order to incorporate soft segments into polythiourethanes, difunctional thiol (HDT) reacted with difunctional acrylate (BDDA) to form flexible thioether linkages by a very rapid phosphine catalyzed Michael addition reaction with no byproducts. Hard segments were formed by the

reaction of the isocyanates with difunctional thiol (HDT) using triethylamine (TEA) as the catalyst resulting in thiourethane linkages with strong hydrogen bonds. Microphase separation was systematically introduced by the difference in the polarity and chemical structures between soft and hard segments resulting in structures with highly elastic mechanical properties.

Thiol Terminated Prepolymers

The procedure for the preparation of thiol terminated prepolymers as soft segments in the polythiourethane is shown in Scheme 3.1. The target theoretical number average molecular weight values ($M_{n,theo}$) for the thiol oligomers selected to range from 1,000 to 3,000 g/mol were based upon the use of similar molecular weight diol oligomers for synthesis of high performance polyurethanes.[50-55] The phosphine catalyzed thiol (HDT)-acrylate (BDDA) reaction was performed in 50 wt% DMAc solution with only 0.1 wt% of DMPPh; the temperature was carefully controlled to prevent any extraneous free-radical acrylate homopolymerization. In Figure 3.1, the complete loss of the carbon double bonds in BDDA is shown 20 min after mixing. ^{1}H and ^{13}C NMR for an uncatalyzed mixture of HDT and BDDA and the thiol-terminated prepolymer are given in Figure 3.2 clearly showing that all of the carbon double bonds completely reacted. No side product formation was detected indicating that the reaction was quantitative requiring absolutely no clean up. Additionally, careful analysis of neat small molecule thiol-acrylate reactions using the nucleophilic DMPPh catalyst also shows that these coupling reactions are quantitative. We have already reported that DMPPh catalyzed thiol-acrylate coupling reactions in dilute solution proceeded rapidly to 100 % conversion using a combination of NMR and MALDI to confirm the product identity with no side

product formation.[33] The thiol-acrylate coupling reaction mediated by nucleophilic phosphine catalysts is a very powerful click reaction with short reaction times. The kinetic profiles of three samples obtained by RTIR with low concentration of DMPPh (0.006 wt%) in Figure 3.3 show that the phosphine catalyzed Michael addition reaction is indeed exceptionally fast and efficient with acrylate conversions of 98 %, 96 % and 94 %. The corresponding percent thiol conversions in 5 min were 65 %, 77 %, and 80 %, well within experimental error to the values of 65 %, 80 % and 82 % that are calculated via the corresponding acrylate conversions after adjusting for the SH : Acrylate ratios in Table 3.3. The conversion of thiol varies based on stoichiometric control in order to achieve $M_{n,theo}$ from 1,000 to 3,000 g/mol. The acrylate conversion reaches higher than 90 % within 200 seconds regardless of $M_{n,theo}$, eventually attaining 100 % conversion. The kinetic profiles in Figure 3.3 show the reaction in real time for the first 5 min. The NMR results in Figure 3.2 confirm that 100 % reaction has occurred by the time samples could be evaluated by NMR, i.e., a few minutes. In order to extend the NMR and IR results and provide an assessment of the molecular weight of the thiol terminated prepolymers, a method based on end group analysis by silver nitrate titration was used to assess the number average molecular weight of all of the samples. In Table 3.1, titration results for the five thiol-terminated prepolymers prepared using the thiol Michael addition reaction of HDT with BDDA are given. The M_n values obtained by titration are in good agreement with the theoretical molecular weights calculated by the Carothers equation. It is apparent that the molecular weight of the thiol-terminated prepolymers was effectively controlled by the component stoichiometry and the efficient thiol Michael addition reaction. DSC was used to characterize the thermal properties of the thiol-

terminated oligomers as a function of molecular weight. As shown in Figure 3.4 and Table 3.1, T_g, T_m, and the heat of fusion (ΔH_f) increase with increasing molecular weight, typical of the effect of molecular weight on the thermal transitions of linear crystalline polymers.

Polythiourethane Elastomers

Segmented polythiourethane elastomers were next synthesized by using a triethyl amine (TEA) catalyzed thiol-isocyanate reaction in DMAc as shown in Scheme 3.2. It is well known that segment length, overall composition (soft/hard segment ratio), and the chemical structure of each segment affects the micro-phase separation process leads to the highly elastic and tough mechanical properties of polyurethanes. In addition to the variation of soft segment length, i.e., the molecular weight of dithiol oligomers described above, the length of the hard segments was also controlled from 550 to 1,000 g/mol by varying the molar ratio of HDT to MDI at a fixed soft segment molecular weight (2,000 g/mol). The effect of isocyanate chemical structure was also investigated for a fixed length of the soft (2,000 g/mol) and hard (1,000 g/mol) segments as shown in Table 3.2. The ratios of thiol:isocyanate and dithiol:thiol oligomer were selected based upon the use of similar molecular weight diols and polyol oligomers for synthesis of high performance polyurethanes.[50-55] GPC results in Table 3.4 show that $M_{n,GPC}$ of the polythiourethanes is 21,000 ~ 56,000 g/mol with reasonably low PDI values, indicating that the thiol-terminated prepolymers were successfully incorporated into polythiourethane backbones, and that hard segments consisting of HDT and diisocyanates were formed based on the stoichiometry.

The rate of the reaction in Scheme 3.2 was evaluated using real-time IR spectroscopy. In order to obtain real-time kinetic plots as a demonstration of the efficiency of the segmented polyurethane formation, low concentrations of the base catalyst TEA (0.03 wt%) were used since the reaction was completed in very short times with the concentrations actually employed for the synthesis such that real-time analysis could not be performed, i.e., it was not possible to begin the real-time IR analysis before significant conversion had taken place. It is well known that a thiol is less nucleophilic than an alcohol due to the low electronegativity of sulfur compared to oxygen.[56] Therefore, the thiol-isocyanate reaction is much slower than the corresponding alcohol-isocyanate reaction in the absence of a catalyst. However, base catalysts readily abstract protons from the more acidic thiols resulting in the formation of thiolate anions which are strong nucleophiles.[56] In Figure 3.5 (a), kinetic profiles of the TEA catalyzed MDI-based polythiourethane reactions (Scheme 3.2) obtained by monitoring the NCO peak as a function of time show that conversion of the isocyanate reaches 95 % within 10 min. This kinetic plot is representative of the reaction between the thiol-terminated oligomers, dithiol extender (HDT) and diisocyanate (MDI). As already stated, for the preparation of the materials used for physical and mechanical analysis, a higher concentration of TEA (0.1 wt%) was used to ensure higher conversions. For comparison, kinetic profiles of the reactions between HDT and MDI using a 0.03 wt% TEA catalyst are shown in Figure 3.5 (b). The reaction comprising MDI, HDT, and thiol-terminated oligomers (soft segment) is a little slower than the reaction of HDT and MDI due to the lower concentration of functional groups and viscosity restricted chain mobility of the higher molecular weight polythiourethanes. Nevertheless, it is clear that the TEA catalyzed thiol-isocyanate

reaction is exceptionally fast and efficient even when high molecular weight thiol-terminated prepolymers are used. Focusing attention again on the results in Figure 3.5, we note that the reaction attains 100 % conversion (no detectable side products) using the 0.03 % TEA catalyst without the necessity of using highly anhydrous conditions, i.e., the catalyzed thiol-isocyanate reaction exhibits most of the aspects of a click reaction, provided that one begins with pure thiols and isocyanates. It has been previously reported that tertiary amine calaylzed thiol-isocyanate reactions give a single thiocarbamate product with no side products.[32,33]

Micro-Phase Separation Behavior

As already mentioned, the highly elastic properties of polyurethane type materials result from the micro-phase separation between the soft and hard segments. The micro-phase behavior of segmented polythiourethane prepared by sequential thiol reactions was investigated in terms of the length of each segment, the segment weight ratio, and the structure of the hard segments. The thermal properties of the polythiourethanes obtained by DSC are shown in Figure 3.6 and Table 3.4. The glass transitions were observed at two distinctively separated temperatures for all of the MDI based polythiourethanes (Figure 3.6 (a) and (b)). The lower T_g was observed from -57 to -23 °C while the higher T_g appeared at about 130 °C, clearly confirming that this set of polythiourethanes consist of two distinctive separate phases with concomitant T_gs that are correspondent to the glass transition temperature of the soft (HDT + BDDA) and hard segments (HDT + MDI), respectively. In Figure 3.6 (a), it is seen that the T_g of the soft segment increases as the length of the soft segment decreases from 3,000 (M1030) to 1,000 g/mole (M1010), with the hard segment T_g in each case around 130 °C. The higher hard segment content and

consequential decreased segmental mobility of the soft segments result in increased physical crosslinking density and higher T_g of the soft segment. The soft segment melting points (T_m) are observed only for M1025 (18.3 °C) and M1030 (27.5 °C) since these two samples have longer flexible chains and reduced hard segment content, which is conducive to crystallization of the soft segment. The T_ms of the hard segments are observed at about 220 °C regardless of the soft segment length because the length of the hard segment is fixed at 1,000 g/mole. However, the area of the endothermic melting peaks (Figure 3.6 (a)) increases from M1030 to M1010 due to an increase of the hard segment content as shown in Table 3.2. Figure 3.6 (b) shows the effect of the hard segment length with fixed soft segment length on the thermal properties. As the length and content of the hard segment decreases from 1,000 (M1020) to 550 g/mole (M0520), the T_g of the soft segment only decreases slightly and the T_m of the hard segment also changes very little. The endothermic melting peak of the soft segment for M0520 reflects the higher degree of phase separation between the soft and hard segments resulting in more mobile and flexible soft segments capable of crystallizing. Apparently, the soft segments of samples M0720 and M1020 which have larger hard segment content cannot crystallize due to restricted chain mobility prohibiting more extensive phase separation. The effect of hard segment structure on thermal properties of segmented polythiourethane elastomers with the fixed soft and hard segment lengths of 2,000 and 1,000 g/mol, respectively, is shown in Figure 3.6 (c). As discussed above, the T_g of the soft segment depends on the degree of phase separation (or mixing) between the soft and hard segments when the length of the soft segment is fixed. IPDI (IP1020) and 2,4-TDI (T1020) based polythiourethanes have a higher single T_g than HDI (H1020), MDI

(M1020), or H_{12}MDI (HM1020) based polythiourethanes indicating the higher degree of phase mixing between soft and hard segments due to the asymmetric structure of IPDI and 2,4-TDI. This prevents hard segment domain formation and crystallization of soft segments resulting in pronounced phase mixed micro structure. In other words, it can be concluded that coarsely formed hard segments are dissolved into soft segment matrix rather than forming rigid hard phase separated domains. The lowest soft segment T_g at -57 °C and the largest endothermic melting peak are observed for H1020. It seems that the similarity in chemical structure between HDT and HDI with the same number of hydrocarbon (6) causes the formation of the larger crystalline hard segment domain resulting in more pronounced phase separation. However, the lower melting point observed at 185.8 °C for H1020 compared to 221.2 °C for M1020 is due to the weaker hydrogen bonding of thiourethane linkages formed from aliphatic diisocyanates than from aromatic diisocyanate. The hydrogenated MDI (H_{12}MDI) based polythiourethane (HM1020) also has a lower T_m and smaller endothermic peak at 130.8 °C than M1020.

The micro-phase behavior of segmented polythiourethane elastomers would be expected to have a significant influence on dynamic mechanical properties (Figures 7 ~ 9). For the series with different soft segment length (Figure 3.7), the T_g of the soft segment, defined by the tan δ peak maximum or E′ inflection point, increases along with the rubbery modulus with decreasing soft segment length from $M_{n,theo}$ = 3,000 (M1030) to $M_{n,theo}$ = 1,000 g/mol (M1030). The increase in hard segment content with the decrease in soft segment length results in a material with higher physical crosslink density. This leads to an increase in the rubbery modulus (G_N°) commensurate with the ideal rubber theory according to Equation 1[57]

$$G_N^\circ = \frac{\rho RT}{M_C} \qquad \text{Equation 1}$$

where ρ, R, and T are the density, ideal gas constant, and absolute temperature, and M_c represents the molecular weight between crosslinks. In Figure 3.8, the effect of hard segment length on the micro-phase behavior of polythiourethanes results in obvious differences in the DMTA scans. The T_g of the soft segment increases with increasing hard segment length at a constant soft segment length (2,000 g/mole), i.e. from M0520 to M1020, owing to phase mixing, which is consistent with the DSC results. In addition, increasing the hard segment content from M0520 to M1020 gives rise to a notable increase in the rubbery modulus which is, as discussed above in the context of Equation 1, due to an increase in physical crosslink density. Also, a significant increase of the melt flow temperature occurs with increased hard segment content, i.e. melt flow for M1020 occurs at the highest temperature. Finally, the E′ versus temperature plot in Figure 3.8 shows a distinct drop in modulus for the M0520 sample corresponding to melting of the soft segment noted by the DSC scan in Figure 3.6 (b) for the M0520 sample only. Figure 3.9 shows the effect of hard segment structure on the tan δ and E′ of each of the different types of the segmented polythiourethane elastomers. IP1020 and T1020 prepared with the asymmetric diisocyanates IPDI and 2,4-TDI have much lower rubbery modulus than any of the other samples with melt flow starting at very low temperatures around 100 °C. As discussed already, the asymmetric structures of IPDI and 2,4-TDI hinder hard segment crystallization and formation of rigid domains that induce phase mixing between the soft and hard segments resulting in only a single low T_g. The lowest soft segment T_g at -40 °C for H1020 (Figure 3.9) and melt flow temperatures corresponding to T_m of hard

segments at 130, 180, and 210 °C for HM1020, H1020, and M1020, respectively, are all consistent with the DSC results. Finally, it can be concluded from the DSC results in Figure 3.6 and Table 3.4 and the DMTA results in Figures 7-9 that the length of the soft and hard segment has a significant impact on the degree of phase separation. In addition, the structure of the diisocyanate also plays a crucial role in influencing micro-phase behavior as well as thermal and mechanical transitions.

Mechanical Properties

The tensile properties of the segmented polythiourethane elastomers are shown in Figure 3.10. It is well known that Young's modulus, in accordance with the results for the rubbery modulus obtained by E′ of DMA at room temperature (measurement temperature of tensile property), should be directly related to the amount of hard segment content in an elastomer. In Figure 3.10 (a) and (b) it is observed that Young's modulus as well as the tensile stress at break increase as a function of increasing hard segment content from M1030 to M1010 and from M0520 to M1020. On the other hand, the elongation at break decreases from M1020 to M1010 as well as from M1020 to M1030 in Figure 3.10 (a) implying that an optimum hard segment content or degree of phase separation exists for optimum elongation. Figure 3.10 (b) shows that the elongation at break increases with increasing hard segment length from 550 to 1,000 g/mole. The essential difference in tensile properties for segmented polythiourethane elastomers synthesized with the structurally different diisocyanates shown in Figure 3.10 (c) is dictated by the different degrees of micro-phase separation. The symmetric structure of the diisocyanates and stronger hydrogen bonding of the corresponding thiourethane linkages derived from MDI and HDT units produce more pronounced hard segment

domains which act as physical cross-links or reinforcing fillers, resulting in superior mechanical properties. H1020, which has the biggest hard segment endotherm melting peak by DSC (Figure 3.6), has the highest Young's modulus. However, the tensile behavior of the micro-phase mixed systems, i.e. IP1020 and T1020, exhibit very low modulus and tensile strength but very large elongations at break (~ 1,000 %), typically observed for un-crosslinked rubbery materials. HM1020 prepared from the hydrogenated MDI (cyclo-aliphatic diisocyanate) shows almost the same elongation at break as MDI (aromatic diisocyanate) based M1020, but Young's modulus and yield stress is less than half due to the weaker hydrogen bonding in the hard segment. Summarizing, the mechanical properties of segmented polythiourethane elastomers can be systematically controlled by the length of soft or hard segment, ratio of soft-hard segment, and chemical structure of the hard segment governing micro-phase separation.

Conclusions

This study represents a new and highly efficient procedure for the rapid synthesis of highly elastic segmented polythiourethanes, and provides a clear rationale for designing and controlling micro-phase separation and thermal/mechanical properties. The sequential thiol-acrylate phosphine catalyzed and tertiary amine catalyzed thiol-isocyanate reactions used to synthesize the segmented polythiourethanes under the conditions described herein bear the salient attributes of click type reactions as identified by kinetics and product analysis; we do note that the reactions were conducted in an organic solvent to ensure that all components were molecularly dissolved. Thermal and dynamic thermal mechanical property measurements showed that the soft and hard

phases could be separated and the degree of phase mixing controlled by varying the length of each segment, the ratio of two phases, and the chemical structure of the hard segment. The tensile property results represented materials with a very wide spectrum of Young's modulus, tensile strength, and elongation at break governed by micro-phase separation behavior. The efficient synthesis of segmented polythiourethanes reported herein opens up a totally new materials platform since the thiol oligomers can be readily synthesized in high yields with no side products in a matter of seconds. Since there is an extensive range of commercially available acrylates and thiols, there is significant opportunity to literally tune the polythiourethane elastomer over a wide range of physical and mechanical properties. Finally, it is expected that the sequential reaction process demonstrated herein, due to the extremely efficient and rapid nature of the reactions with essentially no appreciable byproducts, can be extended to efficient bulk reactions that can be used for the production of segmented thermoplastic polythiourethanes by in situ formation of hard and soft segments using melt processing. The ability of thiol-isocyanate reactions to proceed in more rigorous environments where other reactive components are present is currently being conducted to provide define any competitive reaction pathways that might limit the utility of the chemistry.

References

1. Marianucci, E.; Berti, F.; Pilati, F.; Manaresi, P. *Polymer* **1994**, 35, 1564.
2. Huang, Y.; Paul, D. R. *Macromolecules* **2006**, 39, 1554-1559
3. Tomasi, S.; Bizzarri, R.; Solaro, R.; Chiellini, E. *J. Bioact. Comp. Polym.* **2002**, 17, 3.
4. Lamba, N. M. K.; Woodhouse, K. A.; Cooper, S. L. *Polyurethanes in Biomedical Applications* CRC Press LLC: Boca Raton, **1998**.
5. Rydholm, A. E.; Reddy, S. K.; Anseth, K. S.; Bowman, C. N. *Biomacromolecules* **2006**, 7, 2827.
6. Rydholm, A. E.; Bowman, C. N.; Anseth, K. S. *Biomaterials* **2005**, 26, 4495.
7. Rydholm, A. E.; Held, N. L.; Bowman, C. N.; Anseth, K. S. *Macromolecules* **2006**, 39, 7882.
8. Santerre, J. P.; Brash, J. L. *Macromolecules* **1991**, 24, 5497.
9. Tanaka, M.; Kuma, S.; Funaya, M.; Kobayashi, S. U.S. Patent 7,396,900 B2, 2008.
10. Lu, C; Cui, Z.; Wang, Y.; Li, Z.; Guan, C.; Yang, B.; Shen, J. *J. Mater. Chem.* **2003**, 13, 2189.
11. Kakayama, N.; Hayashi, T. *Prog. Org. Coat.* **2008**, 62, 274.
12. Berti, C.; Celli, A.; Marianucci, E. M. *Eur. Polym. J.* **2002**, 38, 1281.
13. Berti, C.; Celli, A.; Marianucci, E.; Vannini, M. *Eur. Polym. J.* **2006**, 42, 2562.
14. Lotti, N.; Siracusa, V.; Finelli, L.; Marchese, P.; Munari, A. *Eur. Polym. J.* **2006**, 42, 3374.
15. Berti, C.; Celli, A.; Marianucci, E.; Vannini, M. *Eur. Polym. J.* **2007**, 43, 2453.

16. Berti, C.; Celli, A.; Marchese, P.; Marianucci, E.; Marega, C.; Causin, V.; Marigo, A. *Polymer* **2007**, 48, 174.

17. Hoyle, C. E.; Lee, T. Y.; Roper, T. *J. Polym. Sci.: Part A: Polym. Chem.* **2004**, 42, 5301.

18. Jacobine, A. F. *In Radiation Curing in Polymer Science and Technology III*; Fouassier, J. D.; Rabek, J. F., Eds; Elsevier: London, **1993**; Chapter 7.

19. Reddy, S. K.; Cramer, N. B.; Bowman, C. N. *Macromolecules* **2006**, 39, 3673.

20. Lee, T. Y.; Smith, Z.; Reddy, S. K.; Cramer, N. B.; Bowman, C. N. *Macromolecules* **2007**, 40, 1466.

21. Sato, E.; Yokozawa, T.; Endo, T. J. *Polym. Sci.: Part A: Polym. Chem.* **1996**, 34, 669.

22. Carioscia, J. A.; Stansbury, J. W.; Bowman, C. N. *Polymer* **2007**, 48, 1526.

23. Yoshida, H.; Takenoshita, Y. Japan Kokai Tokkyo Koho 11, 1988.

24. Kawaki, T.; Kobayashi, M.; Aoki, O.; Yamazaki, Y.; Iwai, T. Japan Kokai Tokkyo Koho 4, 1989.

25. Toh, H. K.; Bateman, I. R.; Diggins, D. R.; Cielinski, B. G. U.S. Patent 5,977,276, 1999.

26. Bateman, I. R.; Toh, H. K.; Diggins, D. R.; Kloubek, H. U.S. Patent 6,391,983, 2002.

27. Norland 65 or a related thiol-ene system from Norland Optical Adhesives, Inc.

28. Diggins, D. R.; Toh, H. K. European Patent AU PL 5865, 1992.

29. Toh, H. K.; Fang, C. WO 00/64956, 2000.

30. Good, B. T.; Reddy, S.; Davis, R. H.; Bowman, C. N. *Sensors & Actuators, B: Chemical* **2007**, 473, 480.

31. Li, Q.; Zhou, H.; Wicks, D. A.; Hoyle, C. E. *J. Polym. Sci.: Part A: Polym. Chem.* **2007**, 45, 5103.

32. Dyer, E.; Osborne, D. W. *J. Polym. Sci.* **1960**, 47, 361.

33. Klemm, E.; Stockl C. *Macromol. Chem.* **1991**, 192, 153.

34. Ghatge, N. D.; Murphy, R. A. N. *J. App. Polym. Sci.* **1982**, 27, 1557.

35. Li, Q.; Zhou, H.; Wicks, D. A.; Hoyle, C. E. Magers, D.; McAlexander, H. R. *Macromolecules* **2009**, 42, 1824.

36. Morigucci, T.; Endo, T. *Macromolecules* **1995**, 28, 5386.

37. Nagai, A.; Ochiai, B.; Endo, T. *Macromoleculaes* **2004**, 37, 7538.

38. Nagai, D.; Sato, M.; Ochiai, B.; Endo, T. *Macromoleculaes* **2004**, 37, 3523.

39. Nagai, D.; Ochiai, B.; Endo, T. *Macromoleculaes* **2004**, 37, 4417.

40. Nagai, A.; Hamaguchi, T.; Kikukawa, K.; Kawamoto, E.; Endo, T. *Macromolecules* **2007**, 40, 6454.

41. Soule, E. R.; Jaffrennou, B.; Mechin, F.; Pascault, J. P.; Borrajo, J.; Williams, J. J. *J. Polym. Sci.: Part A: Polym. Chem.* **2006**, 44, 2821.

42. Droger, N.; Primel, O.; Halary, J. L. *J. App. Polym. Sci.* **2008**, 107, 455.

43. Kultys, A.; Rogulska, M.; Pinkus, S. *J. Polym. Sci.: Part A: Polym. Chem.* **2008**, 46, 1770.

44. Chan, J. W.; Yu, B.; Hoyle, C. E.; Lowe, A. B. *Chem.Commun.* **2008**, 4959.

45. Mather, B.; Viswanathan, K.; Miller, K. M.; Long, T. E. *Prog. Polym. Sci.* **2006**, 31, 487.

46. Dyer, E.; Glenn, J. F.; Lendrat, E. G. *J. Org. Chem.* **1961**, 26, 2919.

47. Kolb, H. C.; Finn, M. G.; Sharpless, K. B. *Angew. Chem. Int. Ed.* **2001**, 40, 2004.

48. Odian, G. *Principle of Polymerization* 4th Ed. John Wiley & Sons, Inc.: Hoboken, **2004**.

49. Salville, B. *Analyst* **1961**, 86, 29.

50. Lin, Y-H.; Chou, N-K.; Chen, K-F.; Ho, G-H.; Chang, C-H.; Wang, S-S.; Chu, S-H.; Hsieh, K-H. *Polym. Inter.* **2007**, 56, 1415.

51. Chen, S.; Hu, J.; Liu, Y.; Liem, H.; Zhu, Y.; Liu, Y. *J. Polym. Sci., Part B: Polym. Phy.* **2007**, 45, 444.

52. Gisselfaelt, K.; Helgee, B. *Macro. Mat. Eng.* **2003**, 288, 265.

53. Urakawa, R.; Mochizuki, A.; Takahashi, M. J. Soc. Rheo., Japan **2002**, 30, 141.

54. Lee, Y. M.; Lee, J. C.; Kim, B. K. *Polymer* **1994**, 35, 1095.

55. Petrovic, Z. S.; Javni, I.; Soda-So. *J. Polym. Sci., Part B: Polym. Phy.* **1989**, 27, 545.

56. Dyer, E.; Glenn, J. F.; Lendrat, E. G. *J. Org. Chem.* **1961**, 26, 2919.

57. Park, S. H.; Kim, J. W.; Lee, S. H.; Kim, B. K. *J. Macromol. Sci., Part B-Phy.* **2004**, B43, 447.

Table 3.1. Titration and DSC results of thiol-terminated prepolymers

SH:Acrylate	$M_{n,theo}$ (g/mol)	$M_{n,Titration}$ (g/mol)	T_g (°C)	T_m (°C)	ΔH_f (J/g)
1.515 : 1	1,000	1,017	-79	25	35.5
1.296 : 1	1,500	1,450	-74	29	41.5
1.207 : 1	2,000	1,858	-74	33	45.5
1.160 : 1	2,500	2,590	-73	44	59.0
1.130 : 1	3,000	2,811	-73	47	61.4

Table 3.2. Formulation of segmented polythiourethane elastomers

Run #	$M_{n,theo}$* of Hard Segment	$M_{n,theo}$* of Soft Segment	wt % of Hard Segment	Isocyanate
M0520	550		21.6	
M0720	750	2000	27.3	
M1020	1000		33.3	
M1010		1000	50.0	MDI
M1015		1500	33.3	
M1020	1000	2000	25.0	
M1025		2500	20.0	
M1030		3000	16.7	
M1020				MDI
H1020				HDI
HM1020	1000	2000	33.3	H_{12}MDI
IP1020				IPDI
T1020				2,4-TDI

* theoretical molecular weight (length) of segment

Table 3.3. Conversion of 1,6-HDT and 1,4-BDDA by RTIR

$M_{n,theo}$ (g/mol)	$Conversion_{C=C}$ (%)	$Conversion_{thiol}$ (%)
1,000	98	65 (65)*
2,000	96	77 (80)
3,000	94	80 (82)

*Parenthesis is the theoretical conversion of thiols at the actual conversion of acrylate.

Table 3.4. GPC and DSC results of segmented polythiourethane elastomers

Run #	$M_{n,GPC}$ (g/mol)	PDI	Hard Segment		Soft Segment	
			T_g	T_m	T_g	T_m
M0520	40,624	2.1	131	236	-52	23
M0720	39,646	2.6	130	220	-51	n/d
M1020	56,071	1.9	131	221	-45	n/d
M1010	36,271	2.4	132	223	-23	n/d
M1015	44,978	2.1	132	220	-41	n/d
M1020	56,071	1.9	131	221	-45	n/d
M1025	34,944	2.3	131	222	-50	18
M1030	50,523	1.5	133	219	-57	28
M1020	56,071	1.9	131	221	-45	n/d
H1020	Insoluble*	Insoluble*	n/d	186	-57	n/d
HM1020	38,720	2.2	n/d	131	-44	n/d
IP1020	25,440	2.6	n/d	n/d	-26	n/d
T1020	21,004	1.5	n/d	n/d	-40	n/d

* insoluble in DMF at room temperature

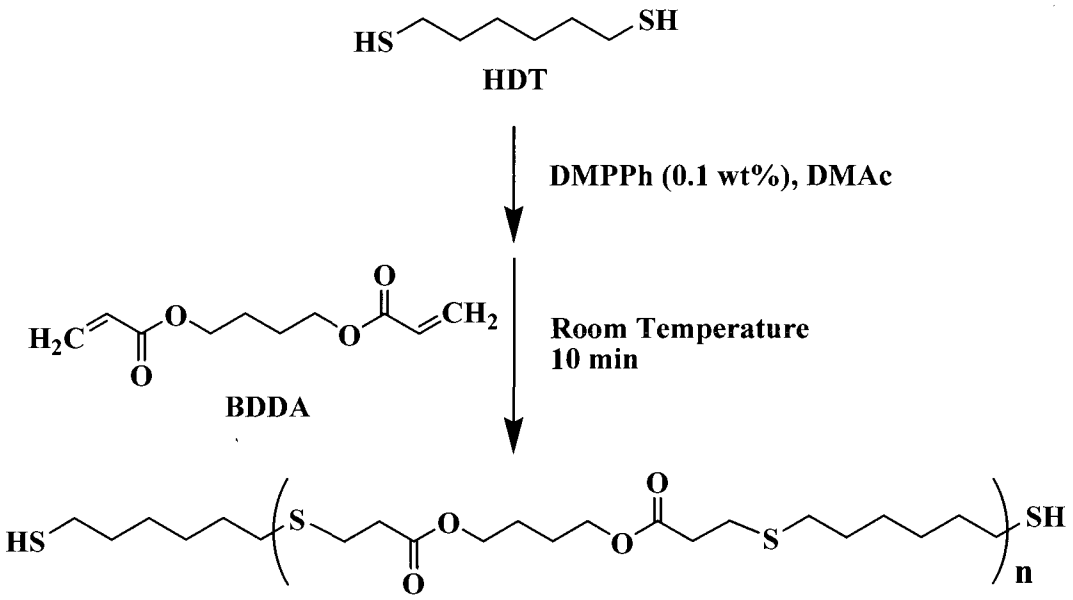

Thiol-terminated Prepolymers

$M_{n,theo}$ = 1000 g/mol ⟶ HDT : BDDA = 1.515 mol : 1 mol
$M_{n,theo}$ = 2000 g/mol ⟶ HDT : BDDA = 1.207 mol : 1 mol
$M_{n,theo}$ = 3000 g/mol ⟶ HDT : BDDA = 1.130 mol : 1 mol

Scheme 3.1. Synthetic procedure for the thiol-terminated prepolymers.

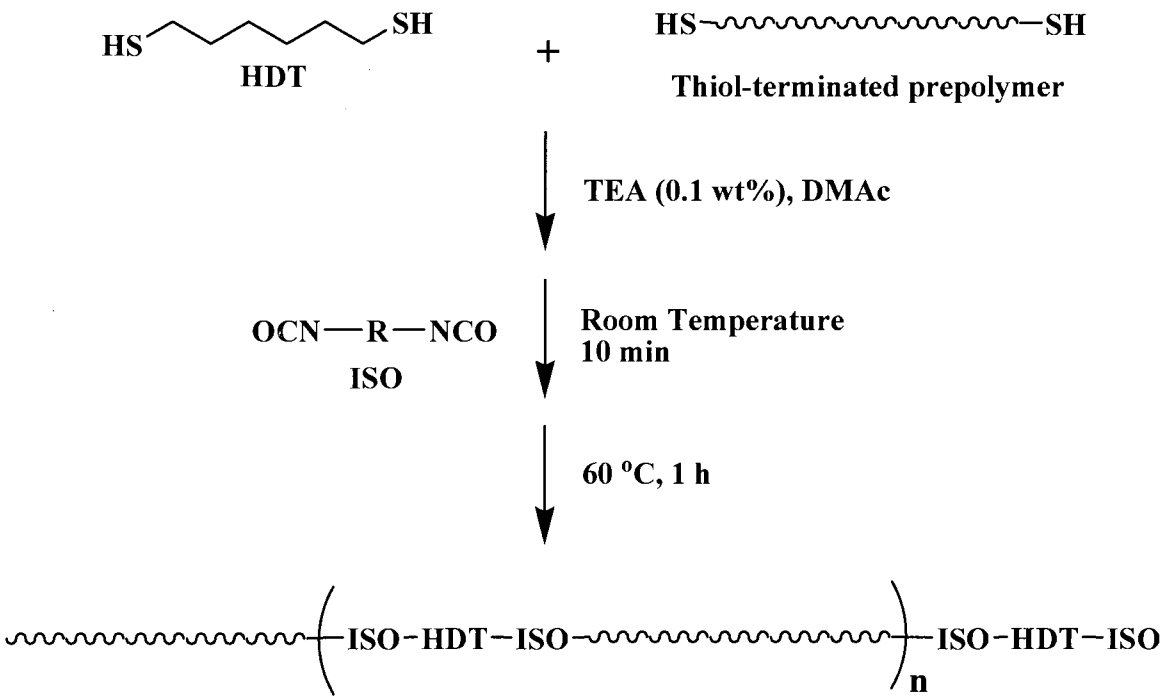

Segmented Polythiourethane Elastomers

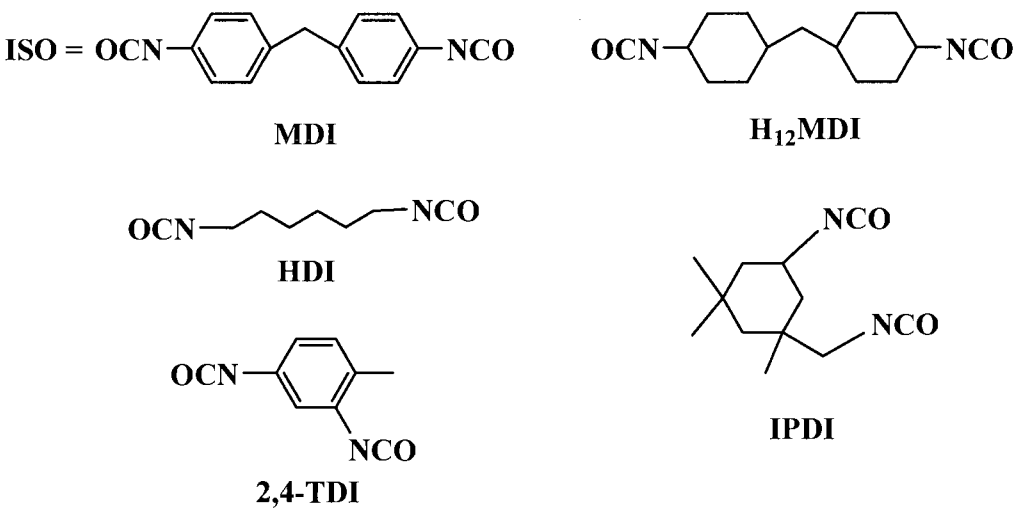

Scheme 3.2. Synthetic procedure for segmented polythiourethane elastomers and the structure of diisocyanates.

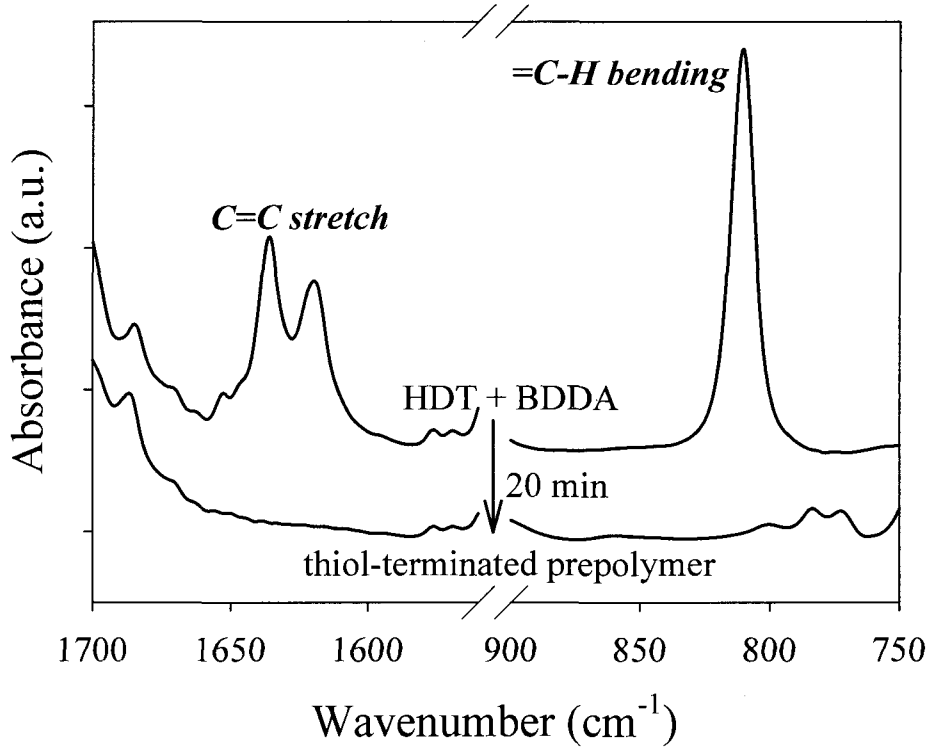

Figure 3.1. FTIR spectrum of the HDT and BDDA mixture and thiol-terminated prepolymer after the completion of thiol Michael addition reaction.

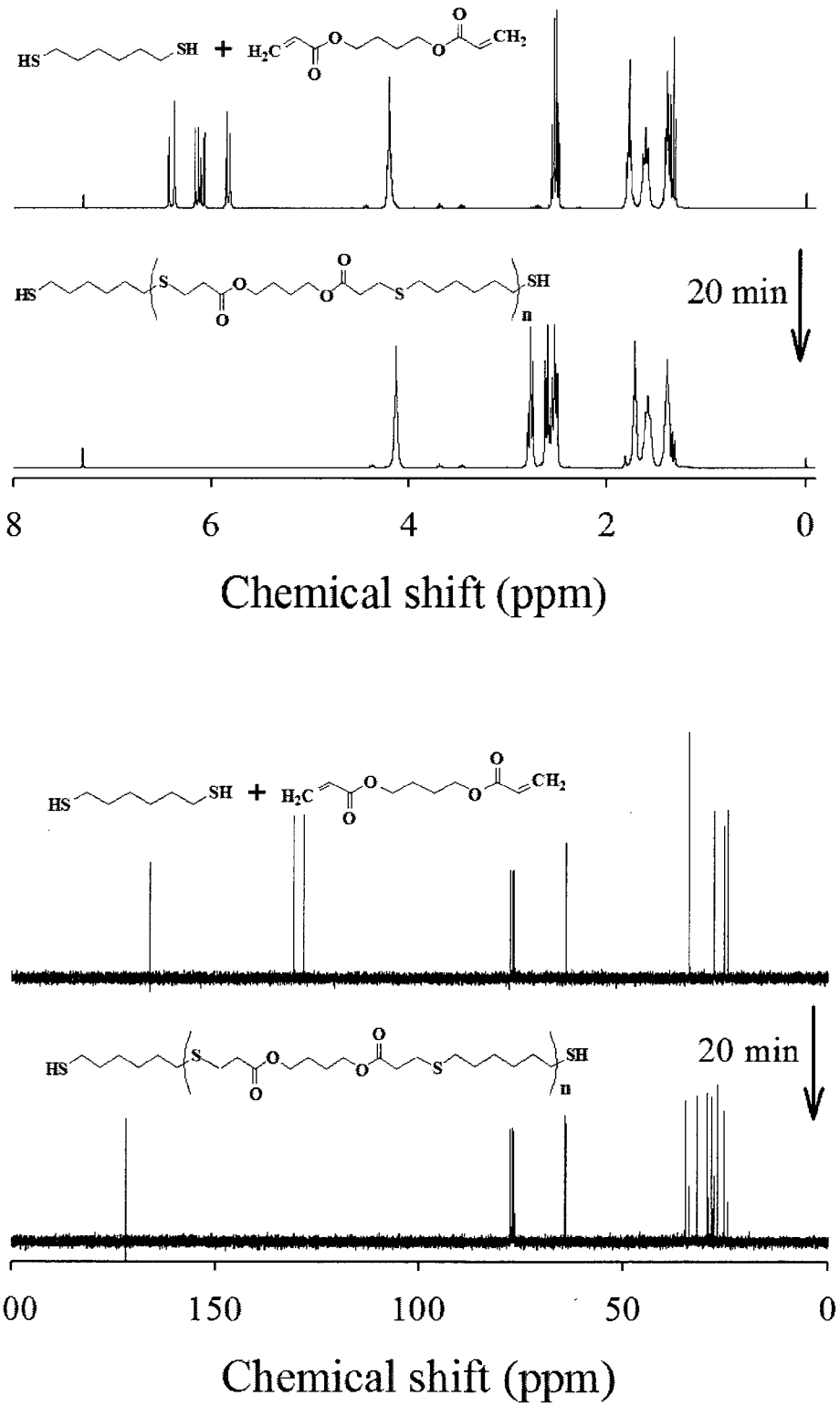

Figure 3.2. ^{1}H and ^{13}C NMR spectrum of the HDT + BDDA mixture and thiol-terminated prepolymer after the completion of thiol Michael addition reaction.

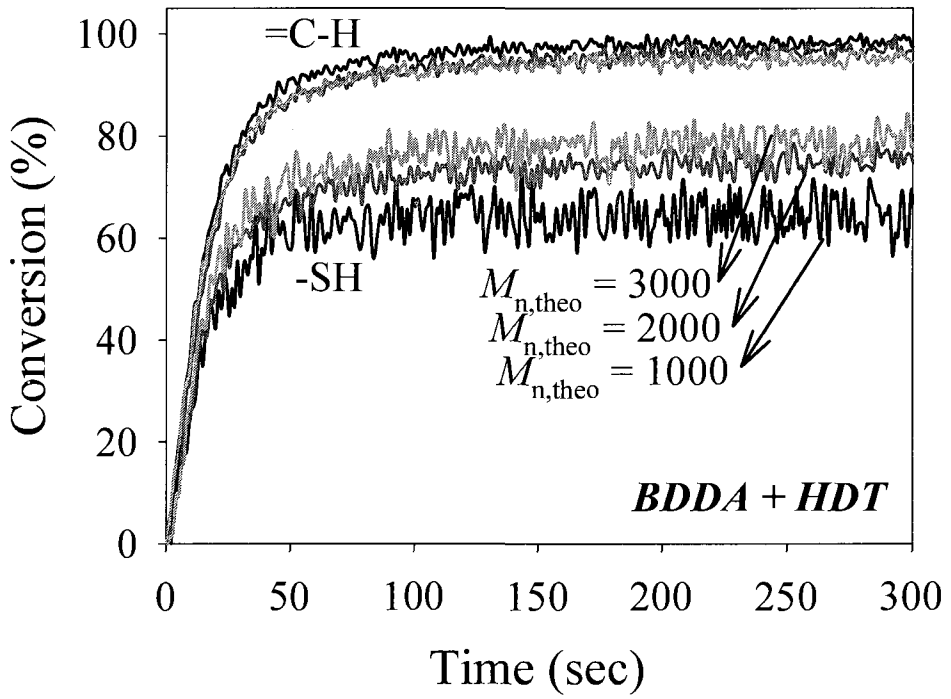

Figure 3.3. Kinetic profiles of thiol Michael addition reaction with HDT and BDDA as a function of time.

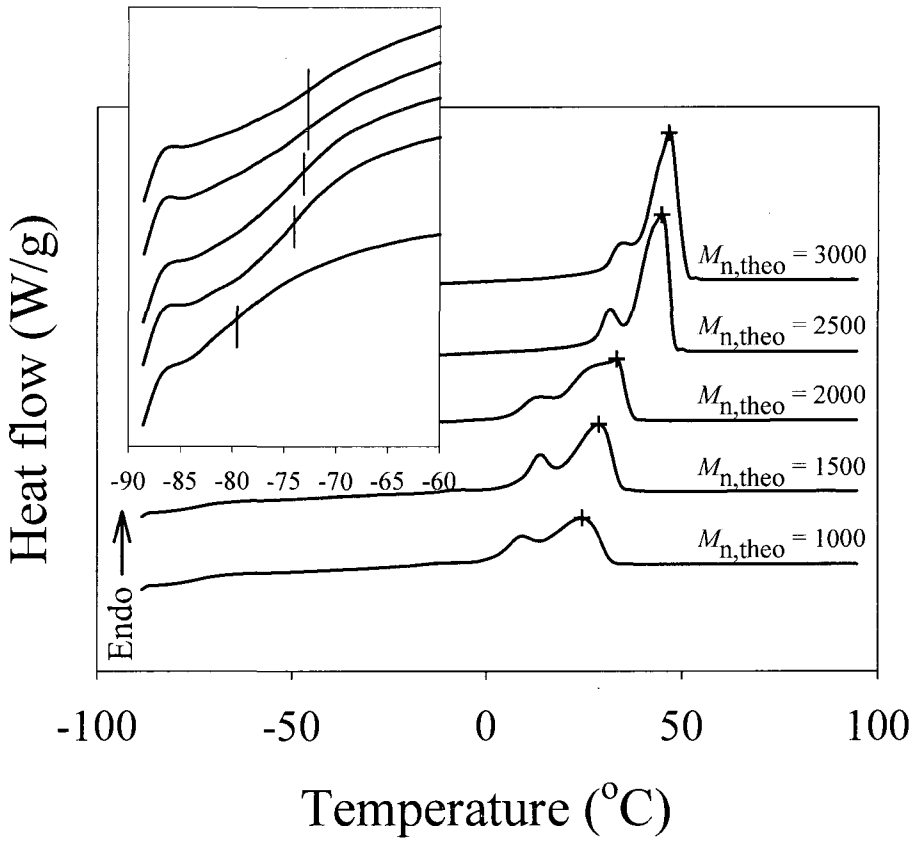

Figure 3.4. DSC heating scans of thiol-terminated prepolymers.

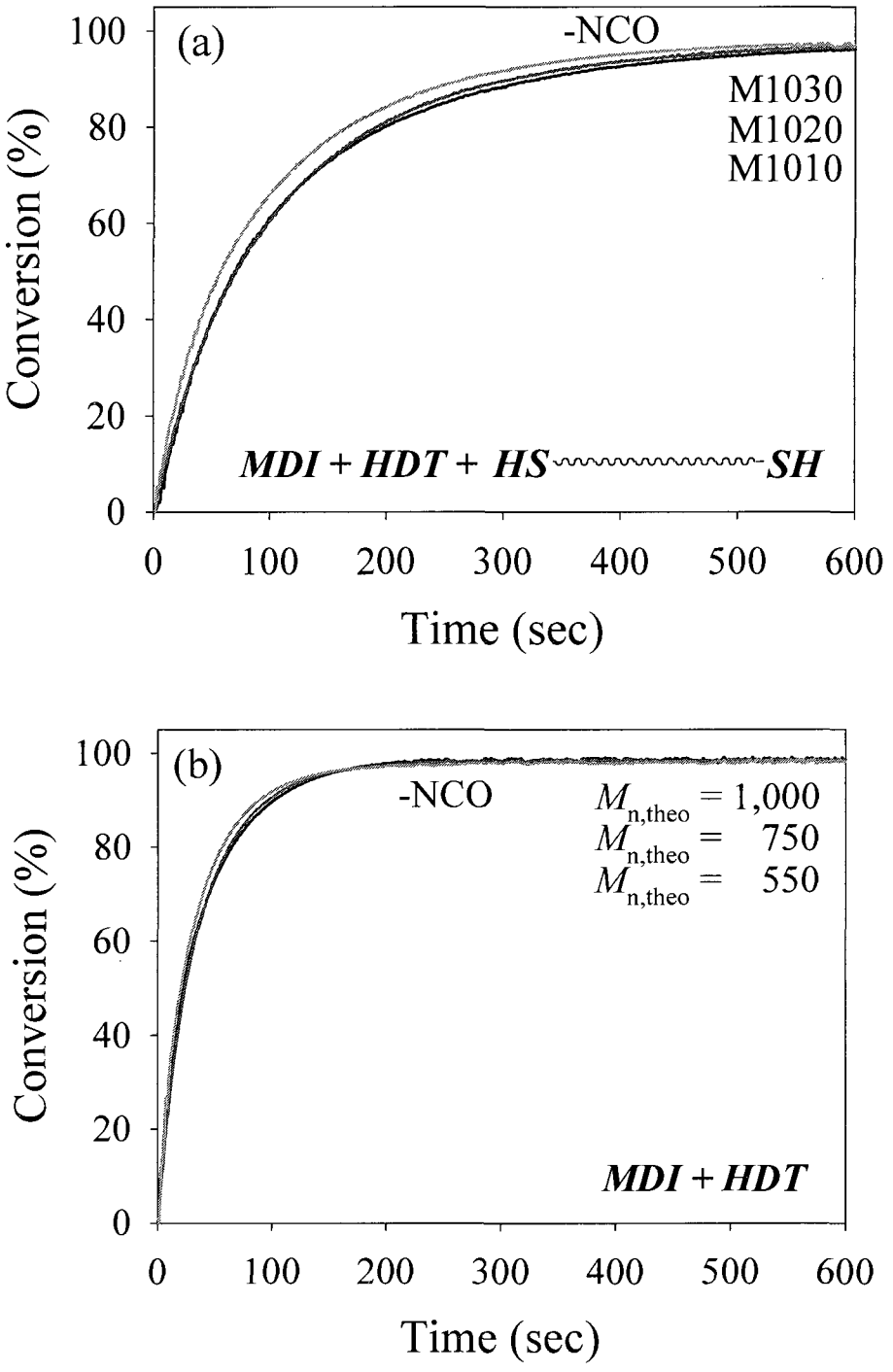

Figure 3.5. Kinetic profiles of polythiourethane (a) and hard segment formation (b) as a function of time using TEA catalyst concentrations of 0.03 wt%.

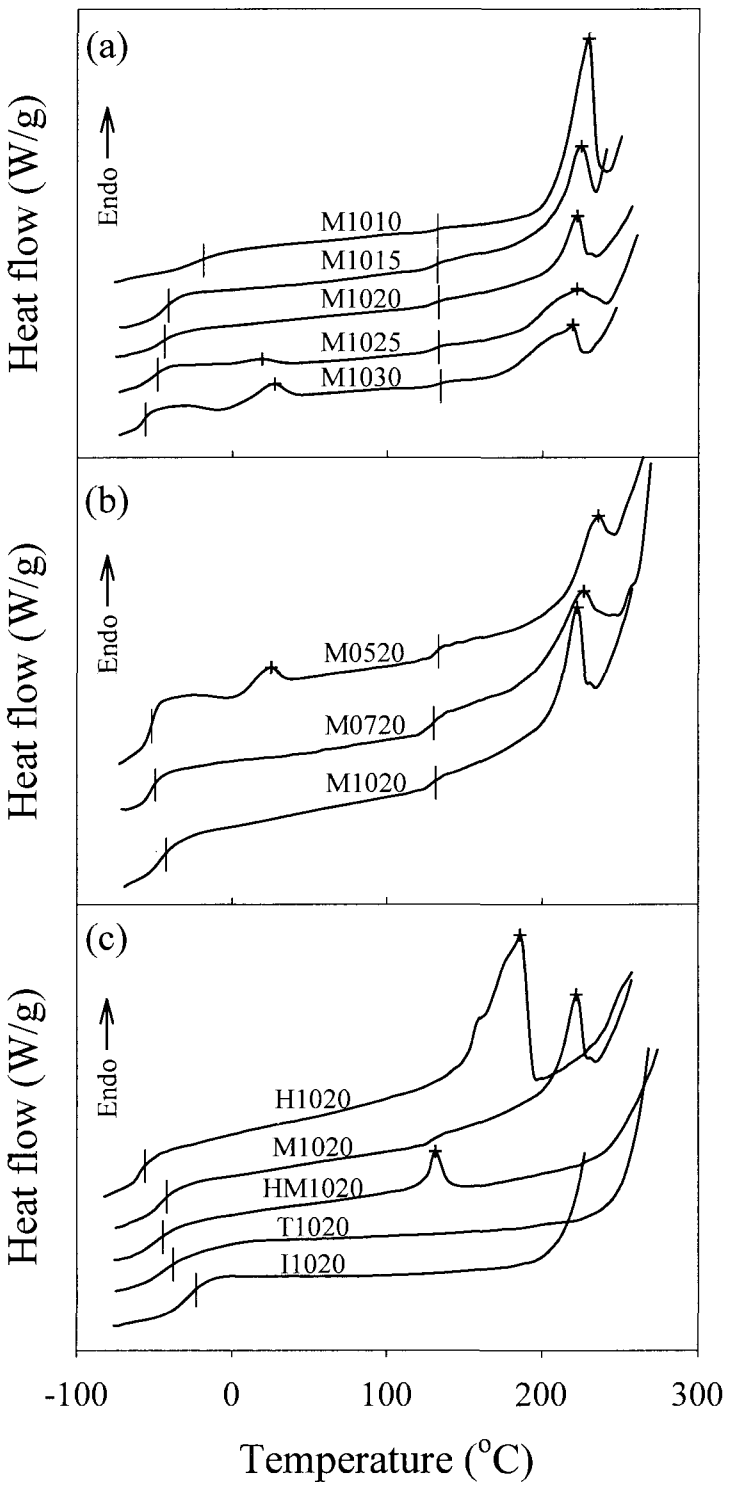

Figure 3.6. DSC heating scans of segmented polythiourethane elastomers.

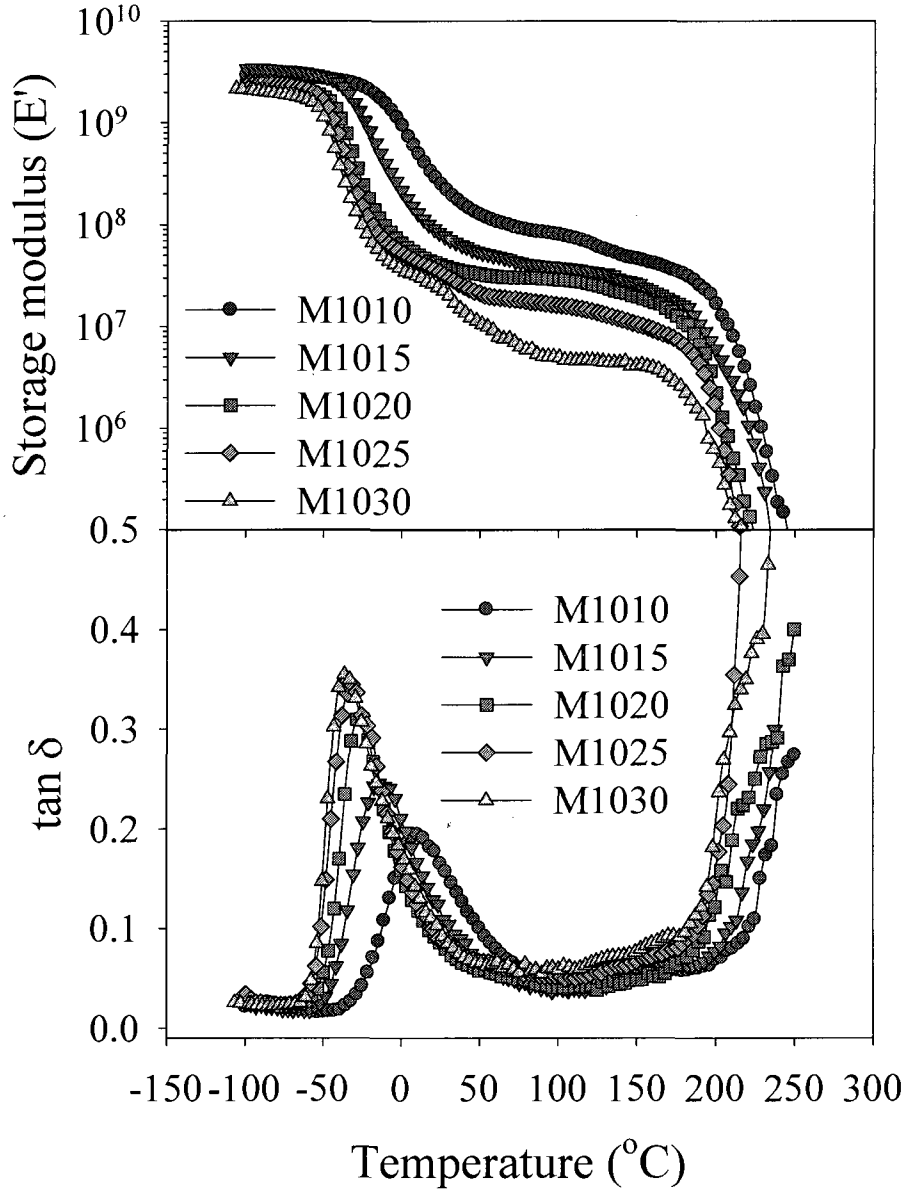

Figure 3.7. Dynamic mechanical properties of segmented polythiourethane elastomers with variation of soft segment length.

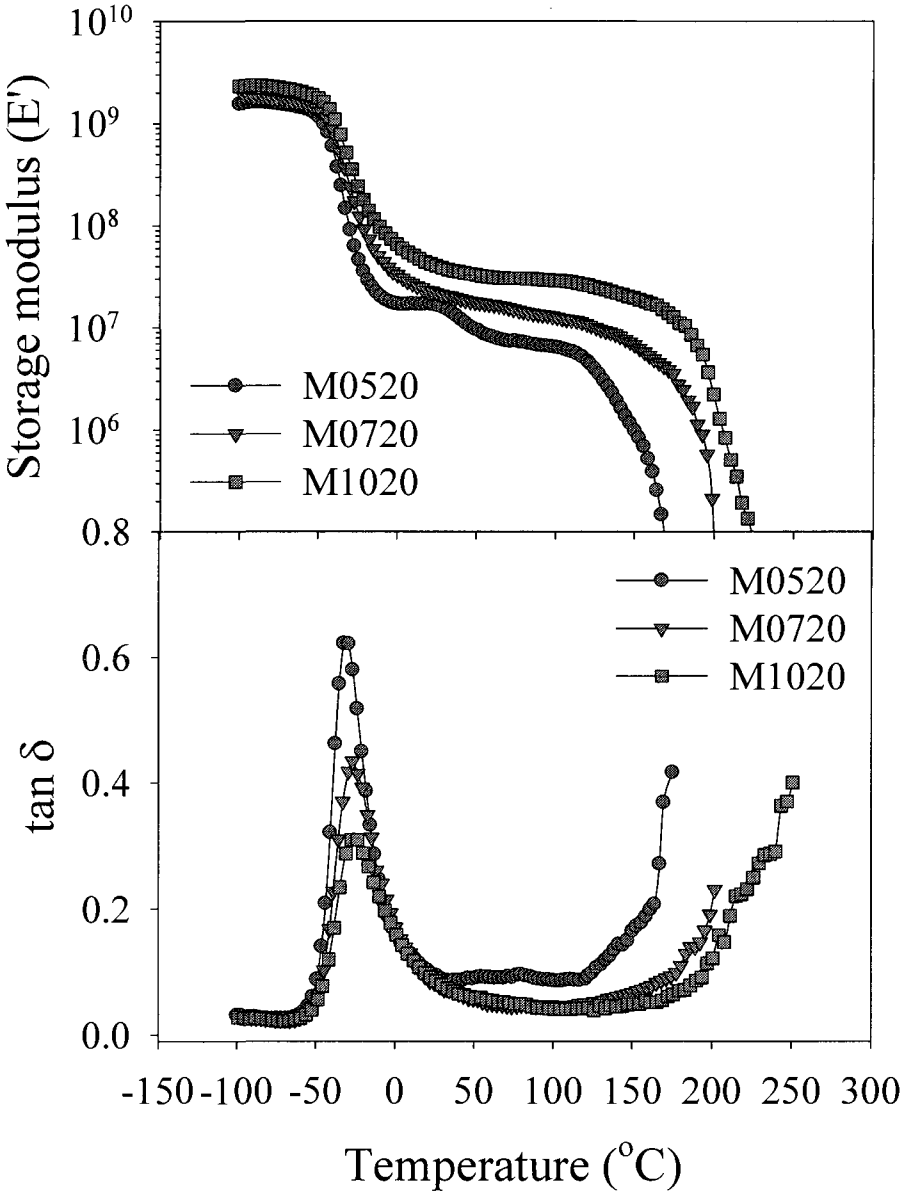

Figure 3.8. Dynamic mechanical properties of segmented polythiourethane elastomers with variation of hard segment length.

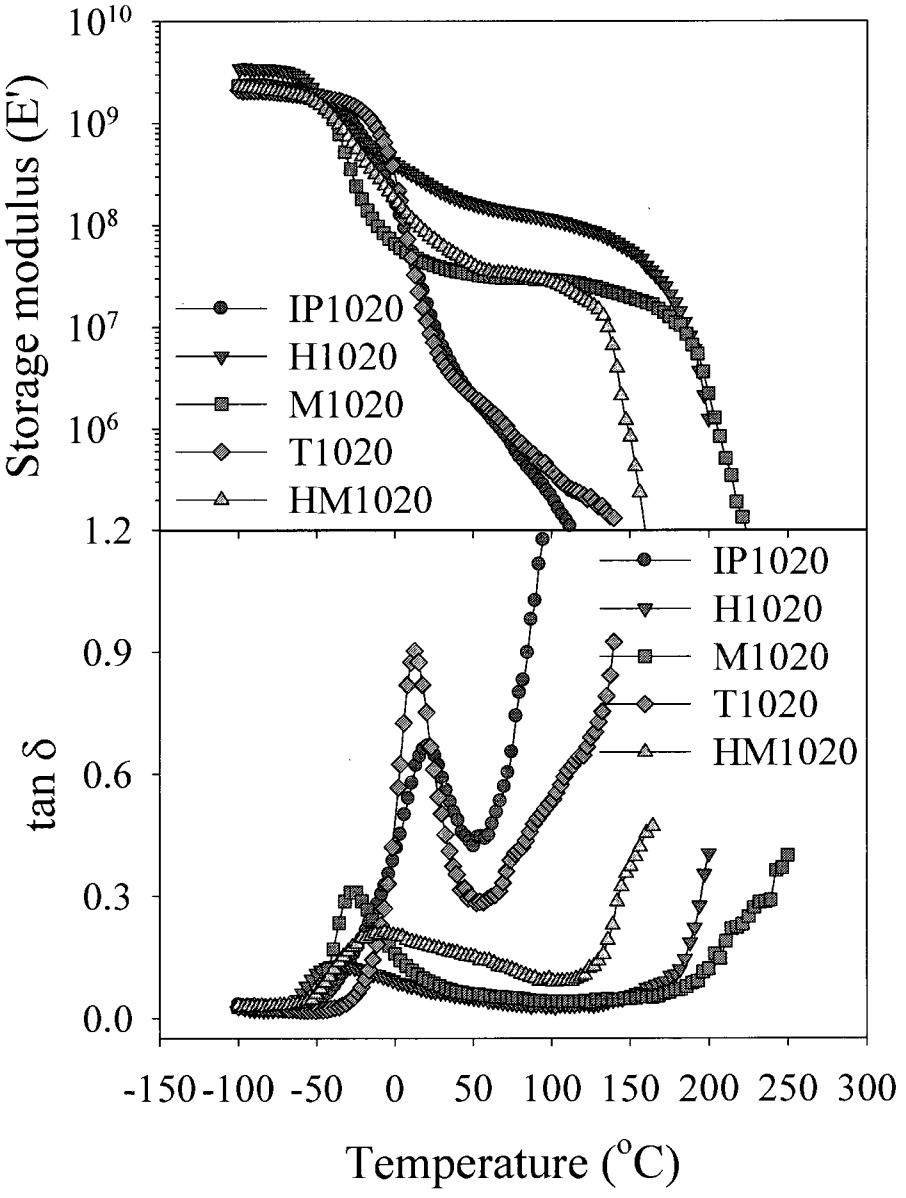

Figure 3.9. Dynamic mechanical properties of segmented polythiourethane elastomers with different diisocyanate structures.

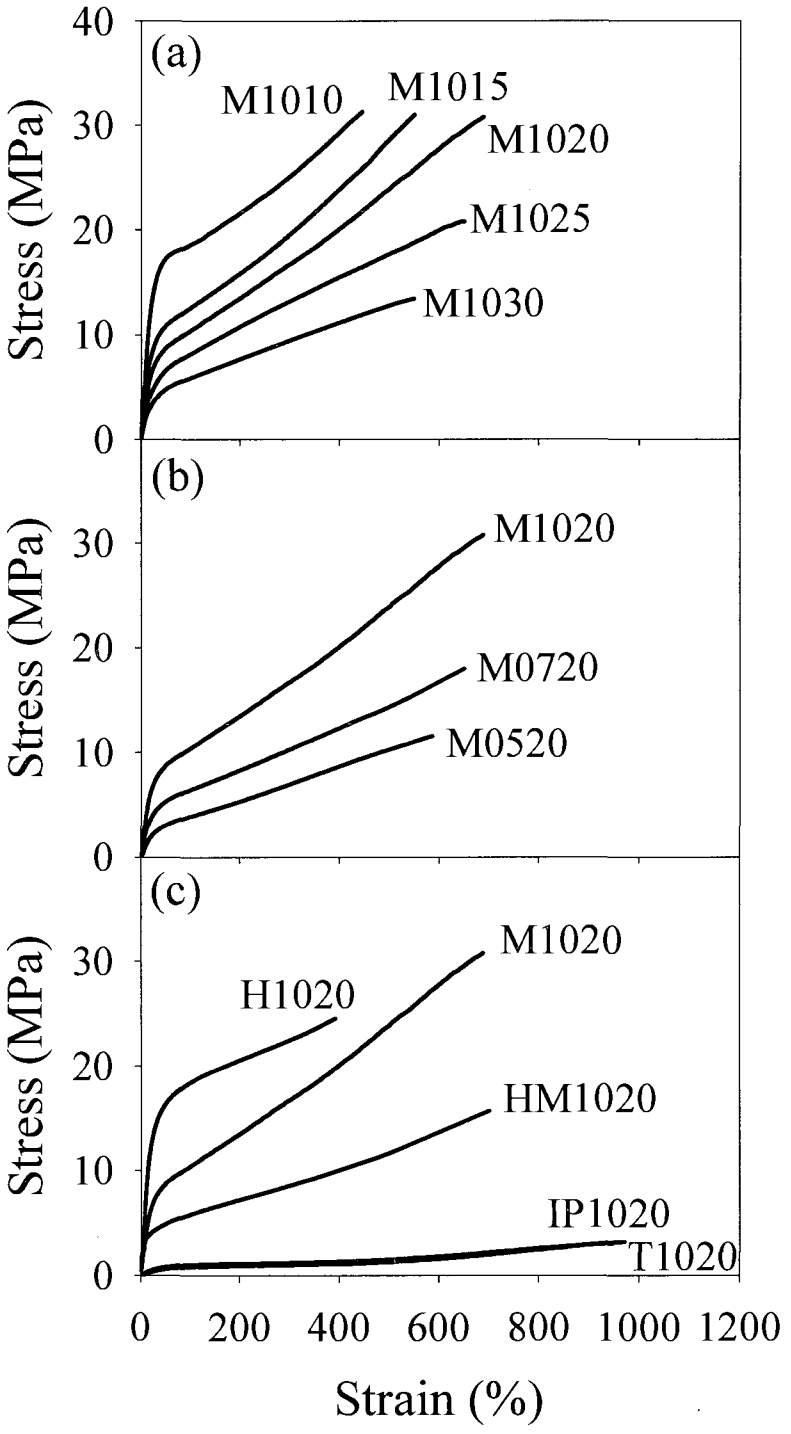

Figure 3.10. Tensile properties of segmented polythiourethane elastomers.

CHAPTER IV

THIOL-ISOCYANATE-ENE TERNARY NETWORKS BY SEQUENTIAL AND SIMULTANEOUS THIOL CLICK REACTIONS

Abstract

Thiol-isocyanate-ene ternary networks were prepared by sequential and simultaneous thiol click reactions. Both the base catalyzed thiol-isocyanate coupling and thiol-ene free-radical step reaction by UV light were quantitatively rapid and efficient. The thiol-isocyanate coupling reaction was triggered thermally and photolytically to control the sequence with the thiol-ene photo-polymerization. Triethyl amine (TEA) and 2,2-dimethoxy 2-phenyl acetophenone (DMPA) were used for the sequential thermally induced thiol-isocyanate coupling and thiol-ene free-radical step reaction by photolysis. A thermally stable photolatent base catalyst (tributylamine·tetraphenylborate salt, (TBA·$HBPh_4$)) capable of in-situ generating tributylamine by UV light was used with isopropylthioxanthone (ITX) for the simultaneous curing systems. The kinetics of the hybrid networks was investigated using real-time IR to follow the conversions of thiol, isocyanate, and ene during dual curing processes. The relationships between the chemical composition and physical/mechanical properties of Thiourethane-Thiolene hybrid networks were established. Highly uniform and dense network structures were obtained for both the sequential and simultaneous thiol click reactions resulting in identical thermal properties that are independent of the sequence of the curing processes.

Introduction

Thiol chemistry continues to attract attention due to its efficiency and versatility.[1] Thiol-ene free-radical photopolymerization proceeds by Click-type reaction and has been widely used in making polymeric materials.[2-8] The nucleophilic addition of thiols to electron poor isocyanate carbons in the presence of a strong base catalyst is also reported to give 100 % yield in a matter of seconds with no side products.[9] Each thiol based reaction has been suggested to proceed by free-radical or anionic chain process,[7-9] respectively. It has been reported that base catalysts have a pronounced effect on the thiol-isocyanate reaction since the base catalyst makes the carbonyl carbon of isocyanate more electron deficient while also producing a very strong nucleophilic thiolate ion,[9~13] that results in a rapid thiol-isocyanate coupling reactions. We recently reported the highly elastic novel segmented polythiourethanes elastomers synthesized by reacting a dithiol, an oligomeric dithiol, and a diisocyanate in the presence of triethylamine (TEA).[9] Results have shown that the conversion reached over 95 % within 10 min at room temperature and micro-phase separation of segmented structure was controllable by the efficient thiol-isocyanate Click-type reaction.

There have been several multi-component simultaneous or sequential systems based on thiol Click reactions. Wei et al. demonstrated that thiol-ene free-radical and vinyl ether cationic photopolymerization resulted in cross-linked networks that effectively coupled the thermal and mechanical properties inherent to each system.[14] Thiol-ene and thiol-epoxy hybrid networks reported by Carioscia et al. showed that highly crosslinked and high T_g polymer materials with significantly reduced shrinkage and stress were obtained by the tailorable polymerization kinetics.[15] Recently,

incorporation of urethane functional groups into thiol-ene networks to introduce strong hydrogen bonding for enhancing physical and mechanical properties has been reported.[1,16,17] However, these urethane-modified thiol-ene networks were essentially based on the simple photopolymerization of thiols and urethane-modified ene oligomers previously prepared by an isocyanate coupling reaction with hydroxyl enes. This presents a problem since the tetra-functional ene monomers have high viscosities due to extensive hydrogen bonding prior to the photo-polymerization process. To overcome this problem and generate cured networks with high levels of hydrogen bonding starting with the mixture of low viscosity monomers, thiol-isocyanate and thiol-ene reactions were carried out beginning from single component mixtures that proceed by dual curing processes.

Herein, we report thiol-isocyanate-ene based systems that react by both sequential and simultaneous thiol Click reactions, i.e. a base catalyzed thiol-isocyanate coupling reaction and a thiol-ene free-radical step reaction initiated by UV light. The sequence of the two reactions is controlled by the method of the triggering thiol-isocyanate coupling reaction. Using a thermally active base catalyst results in sequential reactions, while using a photolatent base catalyst which generates a tertiary amine upon exposure to light results in simultaneous curing system. In the first process, the thiol-isocyanate pre-curing in the presence of an externally added tertiary amine and subsequent thiol-ene photopolymerization result in a quantitatively controlled sequential dual curing process. Secondly, coproduction of the free-radical and tertiary amine by irradiating with light leads to simultaneous reactions of thiols with enes and isocyanates. Being able to control the sequence of thiol-isocyanate and thiol-ene reactions suggests an opportunity for

implementing suitable strategy to fabricate photocurable materials for both thin films and thick cross-linked materials. In addition, the inclusion of thiourethane groups in thiol-ene networks offers numerous advantages such as enhanced physical and mechanical properties resulting from extensive hydrogen bonding. The relationships between the chemical composition and physical/mechanical properties of thiol-isocyanate-ene based ternary networks are established in terms of thermal, dynamic thermal mechanical properties, refractive index, hardness, and tensile properties. The results reported are indicative of a wide range of properties achievable with thiol-isocyanate-ene based ternary networks.

Experimental

Materials

Hexanethiol, butyl 3-mercaptopropionate, butyl thioglycolate, benzenethiol, hexyl isocyanate, phenyl isocyanate, cyclohexyl isocyanate, 1,5-diazabicyclo[4.3.0]-5-nonene (DBN), 1,8-diazabicyclo[5.4.0]undec-7-ene (DBU), 1,4-diazabicyclo[2.2.2]octane (DABCO), 4-dimethylaminopyridine (DMAP), triethylamine (TEA), tributylamine (TBA), 1,8-bis (dimethylamino)naphthalene (proton sponge)), and 1,3,5-triallyl-1,3,5-triazine-2,4,6 (1H,3H,5H) -trione (TATAT) were purchased from Aldrich. Dithiol (glycol di-3-mercaptopropionate (GDMP)) and hexamethylene diisocyanate trimer (Desmodur N3600) were supplied by Bruno Bock Thio-Chemicals-S and Bayer Materials Science, respectively. Photoinitiators, 2,2-dimethoxy 2-phenyl acetophenone (DMPA) and isopropylthioxanthone (2 & 4-isomer mixture) (ITX), were obtained from Ciba Specialty Chemicals and Albemarle. The photogenerated amine (tributylamine·

tetraphenylborate salt, TBA·$HBPh_4$) was synthesized by reacting tributylamine and sodium tetraphenylborate in a hydrocholic acid (HCl) aqueous solution as reported in the literature.[18] The structures of all materials used are shown in Charts 4.1 and 4.2. All materials were used as received.

Kinetics

Real-time infrared (RTIR) spectra were recorded on a modified Bruker 88 spectrometer to obtain kinetic profiles of thiol-isocyanate model reactions in dilute benzene solution as well as thiol-isocyanate-ene network formation. For thiol-isocyanate model reactions, all samples were prepared by adding isocyanates to the thiol solutions with catalyst present (for detailed concentration and measurement conditions see Figure captions). Thin samples (25 μm) between two salt plates sealed with silicon were placed immediately in the RTIR after mixing the samples. The conversion of thiol and isocyanate as a function of time were measured by monitoring the peaks at 2570 and 2250 cm^{-1}, respectively. The results of both peaks are identical so only the plots for isocyanate conversion are given. It should be noted that there is some error in the measurements due to delay (~ 10 sec) in initiating the RTIR measurements. For the sequential thiol-isocyanate / thiol-ene curing process, samples were prepared by dissolving the photoinitiator (DMPA, 1 wt %) and base catalyst (TEA, 0.1 wt %) into GDMP followed by the add-on of TATAT and N3600. Mixtures were immediately placed in the RTIR and retained for 20 min before irradiating with UV light to selectively induce the TEA catalyzed thiol-isocyanate coupling reactions. The thiol-ene free-radical reaction was subsequently initiated by irradiating with light (20.5 mW/cm^2) from an Oriel lamp system equipped with a 200 W, high-pressure mercury-xenon bulb channeled

through an electric shutter and optical fiber cable into the sample chamber. Samples for the simultaneous thiol-isocyanate / thiol-ene reactions were prepared by dissolving TBA·$HBPh_4$ (0.61 wt %) and ITX (0.36 wt %) in GDMP followed by mixing of both monomer components, TATAT and N3600. Both thiol-isocyanate and thiol-ene reactions were triggered simultaneously by irradiating with UV light (1.41 mW/cm^2) passed through a 365-nm filter. The conversions of GDMP, N3600, and TATAT as a function of time were measured during the sequential and simultaneous thiol-isocyanate and thiol-ene reactions by monitoring peaks at 2570, 2250, and 3080 cm^{-1} for thiol, isocyanate, and ene, respectively.

Characterization

^1H NMR spectra was obtained to confirm the dissociation of TBA·$HBPh_4$ salt and generation of TBA before and after irradiation with light at 365 nm (1.5 mW/cm^2) and full arc (10.2 mW/cm^2) for 30 min in the presence and absence of ITX. All spectra were recorded on a Varian 300 MHz NMR for samples in $CDCl_3$ with tetramethysilane (TMS) as the internal reference.

Thiol-isocyanate-ene network films were prepared on glass plates using a 200 μm draw down bar. For sequential thiol-isocyanate / thiol-ene reaction processes, cast films were pre-cured at room temperature for 1 h to induce selectively GDMP-N3600 reactions followed by initiation of GDMP-TTT photopolymerization with a medium pressure mercury lamp (intensity = 10.2 mW/cm^2 for 5 min). Thiol-isocyanate coupling reactions and thiol-ene photopolymerizations were performed at the same time for simultaneous reaction systems by irradiating with a medium pressure mercury lamp passed through a 365 nm optical filter (1.5 mW/cm^2) for 30 min. All samples were post-cured at 80 °C for

24 h to obtain approximately quantitative 100 % conversion. The same concentration of TEA, DMPA, TBA·$HBPh_4$, and ITX as used for RTIR measurements were employed for the film preparation.

Thermal properties of the thiol-isocyanate-ene films prepared by both sequential and simultaneous reaction systems were characterized by differential scanning calorimetry (DSC, TA Instruments Q 1000) equipped with RCS 90 (Refrigerated Cooling System). Sample weights were 8.0 ± 1.0 mg and all experiments were carried out under nitrogen with a flow rate of 50 mL/min. DSC scans were conducted over a temperature range from -50 to 100 °C using 10 °C/min heating and cooling rates. On the first heating scan, samples were equilibrated at 100 °C (higher than the T_g of the Thiourethane neat film (GDMP : TTT : N3600 = 100 : 0 : 100)) for 10 min to erase thermal history and hysteresis of the samples possibly attained during curing process, followed by cooling to -50 °C and a subsequent second heating to 100 °C. The second heating scans were recorded for all thiol-isocyanate-ene network films.

Dynamic thermal mechanical properties of sequentially prepared thiol-isocyanate-ene samples were measured using a DMTA (MK VI, Rheometrics). Measurements were conducted using the vertical tension mode on samples with dimensions of 10 × 8.0 × 0.2 mm (L × W × T) from -50 to 150 °C at a 5 °C/min heating rate and 1 Hz frequency with 0.05 % strain.

Tensile property measurements were conducted with a mechanical testing machine (MTS, Alliance RT/10) according to ASTM D882 using a 100 N load cell with a specimen gauge length of 20 mm at a crosshead speed of 100 mm/min.

Refractive index was obtained using a Bausch&Lomb ABBE-3L refractometer at 24 °C. 1-Bromonaphthalene was applied between the sample film and the prism shield.

Pencil and Persoz pendulum hardness (ASTM D-4366 using a BYK-Gardner pendulum hardness tester with a square frame pendulum) were measured. The results reported are the average of ten tests.

Results and Discussion

Model kinetics for tertiary amine catalyzed thiol-isocyanate coupling reactions

To facilitate the discussion of the thermally and photolytically induced tertiary amine catalyzed thiol-isocyanate coupling reactions, the extensive model kinetics study was performed and the results evaluated in terms of the structures of the tertiary amine catalysts, thiols, and isocyanates. It is well known that the reactions between hydrogen containing compounds such as alcohols, thiols, and primary (or secondary) amines with isocyanates undergo via nucleophilic addition processes such that the reactivity is generally proportional to the nucleophilicity of -OH, -SH, and $-NH_2$ and the electron deficiency of the isocyanate carbon.[10,19]

The catalytic activity of tertiary amines is due to the coordination of the nitrogen electron lone pair with both active hydrogen containing compounds and isocyanates, with the result being an increase in the nucleophilicity of hydrogen donors and a more electron susceptible carbon, respectively. The catalytic efficiency of tertiary amines is dependent upon the availability of the electron pair for complex formation as determined by both the basicity of the nitrogen and steric hindrance.[10,19-21] The kinetic profiles of thiol-isocyanate reactions in dilute acetonitrile with a mono-functional thiol (hexanethiol) and

aliphatic isocyanate (hexyl isocyanate) in the presence of different types of tertiary amines were obtained by real-time IR (see Figure 4.S1 for kinetic plots) and the second order rate constants are summarized in Table 4.1. Note that the rate constants at the lower catalyst concentrations (Figure 4.S1(a)) could only be given for DBU and DBN since the rates for the other catalysts were too slow to measure by real time IR. The rate constants for the 1,5-diazabicyclo[4.3.0]-5-nonene (DBN) and 1,8-diazabicyclo[5.4.0]undec-7-ene (DBU) catalyzed model system are significantly greater than for (1,4-diazabicyclo[2.2.2]octane (DABCO), 4-dimethylaminopyridine (DMAP), triethylamine (TEA), tributylamine (TBA), and 1,8-bis(dimethylamino)naphthalene (proton sponge)). As stated above, this is due to the higher basicity (see Table 4.1) of DBN and DBU than DABCO, DMAP, TEA, TBA, and the proton sponge as determined by the pK_a values of the conjugate acids of each amine listed in Table 4.1.[22-24] The proton sponge as a strong base catalyst is almost a non-catalyst for the thiol-isocyanate coupling reaction due to the significantly crowded environment of nitrogen atoms so that it is very difficult for electron lone pairs to take part in thiol-isocyanate nucleophilic addition reactions.

It is well known that the addition of thiol reactions toward electron deficient carbons depends on the acid dissociation constant (pK_a) because the thiol nucleophilic addition reaction proceeds through the thiolate anion chain process as shown in Scheme 4.1.[10,25-28] In Table 4.1, the kinetic rate constants for the reaction with hexyl isocyanate and four different thiols in the presence of TEA (2.3 mM) is shown (see Figure 4.S2 for kinetic plots). The rate constants increase as the pK_a of the thiol decreases due to the

increase in the rate for the formation of the corresponding thiolate anion, which is a strong nucleophile.

As discussed above, the reactivity of isocyanates with active hydrogen containing compounds is affected by the electron deficiency of the carbon atom in isocyanates so that the substituents that stabilize positive character of the carbon atom enhance the isocyanate reactivity with the corresponding thiolate anion. Table 4.1 (see Figure 4.S3 for kinetic plots) shows the isocyanate structural effect on the thiol-isocyanate coupling reaction. The reaction of the aromatic isocyanate (phenyl isocyanate) with benzenethiol is significantly faster than the reaction between the aliphatic isocyanates (hexyl and cyclohexyl isocyanate) and benzenethiol due to the carbon cation formation of aromatic isocyanate by resonance structures (see Chart 4.3).[19]

Having established the relationship between structure and kinetic reactivity for the basic components (thiol, isocyanate, catalyst) in thiol-isocyanate nucleophilic coupling reactions, results for the polymerization of a ternary mixture of thiol, isocyanate, and ene will be evaluated. To demonstrate the efficiency of this ternary approach to making networks highlighted by the presence of extensive urethane groups capable of hydrogen bonding, we selected a di-thiol based on the di-ester of mercaptopropionic acid and ethylene glycol, a tri-isocyanate which is the trimer (isocyanurate) of 1,6-hexane diisocyanate, and a corresponding tri-allyl tri-ene with the same isocyanurate cyclic ring structure as the tri-isocyanate.

Kinetics of Thiol-Isocyanate-Ene Ternary Systems

The real-time IR (RTIR) kinetic profile of thiol-isocyanate-ene polymerization was investigated in terms of compositional ratios of the reactive components as well as

the sequence of the reactions using different catalysts and photoinitiator combinations. Figures 4.1 and 4.2 present the resultant conversion vs. irradiation time plots of the sequential and simultaneous thiol-isocyanate-ene ternary networks, respectively. In Figures 4.1 (a) and (b), it is seen that both the glycol di-3-mercaptopropionate (GDMP) - 1,3,5-triallyl-1,3,5-triazine-2,4,6 (1H,3H,5H)-trione (TATAT) photopolymerization (2,2-dimethoxy 2-phenyl acetophenone (DMPA), 1wt%) and GDMP - hexamethylene diisocyanate trimer (Desmodur N3600) coupling reaction with triethylamine (TEA, 0.1 wt%) catalyst are very fast and essentially quantitative. The thiol-ene photopolymerization involves the photo-induced free-radical step process, while the base catalyzed thiol-isocyanate coupling reactions proceed by nucleophilic addition of thiolate anion to the electron deficient carbon of the isocyanate. This indicates that each reaction is independent of each other and can be controlled separately. In Figures 4.2 (a) ~ (d), the kinetic profiles of thiol-isocyanate-ene ternary mixture by sequential dual curing process with the variation of the molar ratio from 20:80 to 80:20 as a function of time are shown. The concentration of TEA and DMPA was fixed at 0.1 and 1.0 wt% based on the amount of mixture. GDMP-N3600 coupling reactions forming thiourethane networks proceeded for 20 min in the dark followed by irradiating UV light to trigger photo-polymerization of GDMP and TATAT. N3600 conversions reached 90~91 % in 20 min during selective TEA catalyzed thiol-isocyanate coupling reactions and the corresponding GDMP conversions were 19, 36, 54, and 73 % (~90 % of theoretical conversion of thiols based on stoichiometry) as increasing N3600 molar ratio (20, 40, 60, and 80 %). TATAT and excess GDMP based on stoichiometry underwent photo-polymerization by irradiating UV right after TEA catalyzed GDMP-N3600 coupling reactions for 20 min

and quantitative conversions were obtained. It should be noted that, for all compositions, the final conversions of GDMP, N3600, and TATAT obtained by RTIR were not 100 % due to restriction of molecular mobility at higher conversions. As shown in model studies, the rate of thiol-isocyanate coupling reactions can be controlled by using different types or concentration of tertiary amine catalysts. In addition, the thiol-ene photo-polymerization can also be initiated anytime before, during, or after thermally induced tertiary amine catalyzed thiol-isocyanate coupling reactions. Consequently, the sequence of thiol-isocyanate and thiol-ene reactions involving different reaction mechanisms is programmable based on property requirements of the final network structures.

For simultaneous thiol-isocyanate-ene ternary networks formation, both the thiol-isocyanate coupling and thiol-ene free-radical reactions can be triggered by UV light at 365nm using the photo-generate amine, tributylamine·tetraphenylborate salt, (TBA·$HBPh_4$, 0.61 wt %) and sensitizer, isopropylthioxanthone, (ITX, 0.36 wt %) which generates both free-radical and tributylamine catalysts upon photolytic decomposition as will be explained. First, consider photolysis of only TBA·$HBPh_4$ in solution. TBA·$HBPh_4$ absorbs UV light below 300nm as shown in Figure 4.3: upon direct photolysis at wavelength less than 300nm to give TBA and other by products.[18] Accordingly, in Figure 4.3, NMR spectra of tributylamine as well as TBA·$HBPh_4$ before and after irradiation with UV light at 365 nm and unfiltered are shown. The generation of TBA from TBA·$HBPh_4$ is only occured when TBA·$HBPh_4$ was photolyzed with the full arc of the unfiltered UV light. It is also well known that ITX efficiently sensitizes upon UV irradiation through photo-excitation and energy transfer to other molecules.

The sensitizing efficiency of ITX is highly dependent on the wavelength of irradiating UV light, i.e. the higher extinction coefficient around 254 and 365 nm as shown in Figure 4.4. Thus, it is expected that ITX abstracts hydrogen from thiols (hydrogen donor) producing thiol free-radicals upon UV irradiation at 365 nm, thus initiating the thiol-ene photopolymerization. If ITX is added, and TBA·$HBPh_4$ is irradiated at wavelength greater than 300nm, the excited triplet state of ITX transfers energy to TBA·$HBPh_4$ which subsequently decomposes as shown in Scheme 4.1 to give TBA and other by products. In Figure 4.5, the appearance of TBA is indeed confirmed by NMR peaks at 2.6 ppm upon photolysis of a solution of TBA·$HBPh_4$ and ITX by irradiating UV light at 365 nm. As a result, the thiol-isocyanate coupling reaction and thiol-ene free-radical photopolymerization can be triggered simultaneously by using ITX. Consequently, both Thiourethane and Thiolene formation can be essentially controlled by ITX. In Figure 4.6, kinetic profiles of simultaneous thiol-isocyanate-ene ternary networks as a function of SH : C=C : NCO ratio during UV irradiation at 365 nm in the presence of TBA·$HBPh_4$ and ITX are shown. Both thiol-isocyanate coupling reaction and thiol-ene photopolymerization are successfully initiated simultaneously and the conversion of GDMP, TATAT, and N3600 is quantitative based on the stoichiometry, i.e. $Conversion_{SH} \sim Conversion_{C=C} + Conversion_{NCO}$. However, thiol-ene photopolymerization proceeds faster than the thiol-isocyanate coupling reaction for a given system. The different reaction rates can be synchronized by either changing the type of tertiary amine used to make the salt with tetraphenyl borate. Of course, the rate of both reactions can be controlled at the same time by simply varying the amount of ITX.

Thermal properties

DSC measurements were conducted to investigate the effect of the compositional ratio and reaction sequence of Thiourethane-Thiolene hybrid networks on thermal properties. DSC thermograms of Thiourethane-Thiolene hybrid networks prepared by both sequential and simultaneous curing systems were almost identical. Glass transition temperatures obtained by DSC are summarized in Table 4.2 and 2nd heating scans of Thiourethane-Thiolene hybrid networks prepared by sequential curing system are shown in Figure 4.7 as a representative. With an increase in the N3600 concentration, T_g progressively increases due to the higher extent of hydrogen bonding resulting from the increase in the number of thiourethane linkages in the thiol-isocyanate-ene ternary networks. In addition, as shown in Figure 4.7, the glass transition range ($T_{g,e}$-$T_{g,i}$) is very narrow (~5 °C) for all compositions. It is clear that thiol-isocyanate-ene ternary networks are highly uniform as found for typical thiol-ene based systems.[1,29] Also, the sequence of the thiol-isocyanate and thiol-ene reactions does not affect the uniformity or thermal transition of the network structure since both reactions are essentially independent of each other with no side products, resulting in homogeneous chemical structures as long as the conditions used ensure quantitative conversions for all components.

Thermal mechanical properties

In addition to thermal properties, dynamic mechanical properties of Thiourethane-Thiolene hybrid networks are expected to be largely dictated by the compositional ratio. In Figure 4.8, the storage modulus and tan δ of thiol-isocyanate-ene ternary networks are shown. The T_g determined by the inflection point of the storage modulus and tan δ peak (see Table 4.4) increases as a function of N3600 content due to increased hydrogen

bonding consistent with DSC results. The rubbery plateau modulus (Table 4.4) also increases monotonically with increasing thiourethane content indicating that hydrogen bonding acts to physically crosslink the thiol-isocyanate-ene ternary networks so that the apparent network density increases. The broadness of the glass transition determined by FWHM (Full Width at Half Maximum) of the tan δ plots is about 10 °C for all compositions (Table 4.3) implying that the distribution of relaxation times of thiol-isocyanate-ene ternary networks is narrow due to uniformity of the chemical structure. Consequently, the T_g of thiol-isocyanate-ene ternary networks can be tuned by varying the composition over wide temperature range without sacrificing the characteristic uniform network structure typically associated with thiol-ene based materials.

Mechanical properties and refractive index

Tensile properties, pencil hardness, and pendulum hardness of Thiourethane-Thiolene hybrid networks prepared by the sequential curing process are shown in Figure 4.9 and Table 4.4. It is well known that the mechanical properties of thiol-ene based materials may be enhanced by using (thio)urethane modified thiols or enes for the preparation of thiol-ene networks to improve hardness and increase T_g.[16,17] However, (thio)urethane linkages have strong hydrogen bonding and, if present in the thiol or ene monomers, increase the viscosity of the unpolymerized system. For thiol-isocyanate-ene ternary networks cured by both the sequential and simultaneous curing methods, thiourethane linkages are formed during the curing process eliminating the initial viscosity issues and ensuring high conversion. As seen in Figure 4.9, Young's modulus and the stress at break are significantly improved by increasing the thiourethane content due to the large extent of hydrogen bonding in the hybrid networks, consistent with the

DMA results (storage modulus at room temperature) in Figure 4.8 and Table 4.3. The elongation at break also increases from 50 % for the thiol-ene neat network (Figure 4.5(a)) to 230 % for the Thiourethane-Thiolene 60:40 hybrid network (Figure 4.5(d)). Surface hardness was also measured using pencil hardness. As shown in Table 4.4, the pencil hardness increases as a function of thiourethane content. The pendulum hardness, which simply measure energy damping, has a minimum for the Thiourethane : Thiolene = 40 : 60 composition, which has a glass transition temperature near room temperature. Finally, refractive index is one of the most important physical properties of thiol based materials. It has been reported that refractive index of thiol-ene, thiol-yne, and thiourethane systems is largely determined by the sulfur contents although other factors related to additional components in the networks are also important.[4,30] The refractive index of the thiol-isocyanate-ene ternary networks shown in Table 4.4 are all relatively high and increase slightly with increase in wt% of sulfur.

Conclusions

In this study, thiol-isocyanate coupling and thiol-ene free radical step reactions, which are independent each other, were sequentially and simultaneously employed to form Thiourethane-Thiolene hybrid networks with tunable network properties. A conventional base catalyst, TEA, and photoinitiator, DMPA, were used for Thiourethane-Thiolene hybrid networks to be cured sequentially. For simultaneous systems, a photo-generated amine catalyst (TBA·$HBPh_4$) was used in the presence of ITX to trigger both thiol-isocyanate coupling and thiol-ene free radical step reaction simultaneously by UV light. TBA was successfully generated by irradiating UV light at 365 nm due to the

sensitization by ITX and efficiently catalyzed thiol-isocyanate coupling reaction. Thiol-ene free radical reaction was also initiated by ITX at 365 nm without additional photoinitiator. Kinetic profiles clearly showed that both thiol-isocyanate and thiol-ene reactions are quantitative. Thermal properties of hybrid network films prepared by both methods were identical regardless of the sequence. Consequently, Thiourethane-Thiolene hybrid systems can form the uniform and dense network structure that is the characteristic of thiol click type reaction based materials. Very narrow glass transition temperature range for all compositions measured by DSC and DMA supported this conclusion. Compositional variation of the ratio between polythiourethanes and thiolene networks allowed us to control the mechanical properties such as tensile, pencil, and pendulum hardness. Refractive index was more dependent on the sulfur content than the amount of hydrogen bonding in the hybrid networks.

Thiourethane-Thiolene hybrid polymerization strategy offers many advantages in tailoring physical/mechanical properties and manufacturing process of materials based on the thiol click type reactions by manipulating polymerization kinetics and varying chemical composition. Since thiols undergo various chemical reactions with corresponding reactants and initiators (or catalysts) associated with different mechanisms such as free-radical and anionic step reactions, it is sure that many different combinations of thiol click type reactions to form hybrid networks can be designed as different requirements in chemistry as well as physical/mechanical properties.

References

1. Hoyle, C. E.; Lee, T. Y.; Roper, T. *J. Polym. Sci.: Part A: Polym.Chem.* **2004**, *42*, 5301.
2. Killops, K. L.; Campos, L. M.; Hawker, C. J. *J. Am. Chem. Soc.* **2008**, *130*, 5062.
3. Fairbanks, B. D.; Scott, T, F.; Kloxin, C. J.; Anseth, K. S.; Bowman, C. N. *Macromolecules* **2009**, *42*, 211.
4. Chan, J. W.; Zhou, H.; Hoyle, C. E.; Lowe, A. B. *Chem. Mat.* **2009**, *21*, 1579.
5. Campos, L. M.; Killops, K. L.; Sakai, R.; Paulusse, J. M. S.; Damiron, D.; Drockenmuller, E.; Messmore, B. W.; Hawker, C. J. *Macromolecules* **2008**, *41*, 7063.
6. Dondoni, A. *Angew. Chem. Int. Ed.* **2008**, *47*, 2.
7. Chan, J. W.; Hoyle, C. E.; Lowe, A. B. *J. Am. Chem. Soc.* **2009**, *131*, 5751.
8. Chan, J. W.; Yu, B.; Hoyle, C. E.; Lowe, A. B. *Chem. Comm.* **2008**, 4959.
9. Shin, J.; Matsushima, H.; Chan. J. W.; Hoyle, C. E. *Macromolecules* **2009**, *42*, 3294.
10. Dyer, E.; Glenn, J. F.; Lendrat, E. G. *J. Org. Chem.* **1961**, *26*, 2919.
11. Dyer, E.; Osborne, D. W. *J. Polym. Sci.* **1960**, *47*, 361.
12. Dyer, E.; Glenn, J. F. *J. Am. Chem. Soc.* **1957**, *79, 366.*
13. Klemm, E.; Stockl C. *Macromol. Chem.* **1991**, *192*, 153.
14. Wei, H.; Li, Q.; Ojelade, M.; Madbouly, S.; Otaigbe, J. U.; Hoyle, C. E. *Macromolecules*, **2007**, *40*, 8788.
15. Carioscia, J. A.; Stansbury, J. W.; Bowman, C. N. *Polymer* **2007**, *48*, 1526.
16. Li, Q.; Zhou, H.; Wicks, D. A.; Hoyle, C. E. *J. Polym. Sci.: Part A: Polym. Chem.* **2007**, *45*, 5103.

17. Senyurt, A. F.; Hoyle, C. E.; Wei, H.; Piland, S. G.; Gould, T. E *Macromolecules*, **2007**, *40*, 3174.

18. Sun, X.; Gao, J. P.; Wang, Z. Y. *J. Am. Chem. Soc.* **2008**, *130,* 8130.

19. Randall, D.; Lee, S. *The polyurethanes book*; John Wiley & Sons Ltd.: The United Kingdom, **2002**.

20. Hepburn, C. *Polyurethane Elastomers*; Elsevier: Essex, **1992**.

21. Szycher, M. *Szycher's Handbook of Polyurethanes*; CRC Press LLC: Boca Raton, FL, **1999**; Chapter 3.

22. Li, J-N.; Fu, Y.; Liu, L.; Guo, Q-X. *Tetrahedron* **2006**, *62*, 11801.

23. Kaljurand, I.; Kütt, A.; Sooväli, L.; Rodima, T.; Mäemets, V.; Leito, I.; Koppel, I. A. *J. Org. Chem.*, **2005**, *70*, 1019.

24. Serjeant, E. P.; Dempsey, B. Ionisation Constants of Organic Acids in Aqueous Solution; Pergamon Press: New York, **1979**.

25. Bernasconi, C. F.; Killion, R. B. *Am. Chem. Soc.* **1988**, *110*, 7506.

26. Bordwell, F. G; Hughes, D. L. *J. Org. Chem.*, **1982**, *47*, 3224.

27. Kreevoy, M. M.; Harper, E. T.; Duvall, R. E.; Wilgus III, H. S.; Ditsch, L. T. *J. Am. Chem. Soc.* **1960**, *82*, 4899.

28. Hupe, D. J.; Jencks, W. P. *J. Am. Chem. Soc.*, **1977**, *99*, 451.

29. Cramer, N. B.; Scott, J. P.; Bowman, C. N. *Macromolecules* **2002**, *35*, 5361.

30. Li, Q.; Zhou, H.; Wicks, D. A.; Hoyle, C. E.; Magers, D. H.; McAlexander, H. R. *Macromolecules*, **2009**, *42*, 1824.

Table 4.1. The second order rate constant (k_2) of amine catalyzed thiourethane reactions with mono-functional thiols and isocyanates in benzene

Isocyanate	Thiol (p*K*a)	Catalyst (p*K*a)	$k_2 \times 10^2$ ($L \cdot mol^{-1} \cdot s^{-1}$)
Hexyl isocyanate	Hexanethiol (10.53)	DBU (11.6)	10,700[a]
		DBN (13.5)	8,300[a]
		DABCO (8.2)	3.0[b]
		DMAP (9.2)	0.6[b]
		TEA (10.75)	0.7[b]
		TBA (10.7)	0.3[b]
		Proton sponge (12.1)	slow[b]
Hexyl isocyanate	Hexanethiol (10.53)	TEA (10.75)	3.0[c]
	Butyl 3-Mercaptopropionate (9.33)		21.7[c]
	Butyl thioglycolate (7.91)		67.8[c]
	Benzenethiol (6.43)		2,097[c]
Hexyl isocyanate	Benzenethiol (6.43)	DABCO (8.2)	4.7[c]
Cyclohexyl isocyanate			4.7[c]
Phenyl isocyanate			212[c]

[a][SH] = [NCO] = 570 mM, [Catalyst] = 0.24 mM
[b][SH] = [NCO] = 730 mM, [Catalyst] = 80 mM
[c][SH] = [NCO] = 730 mM, [TEA] = 2.3 mM
[d][SH] = [NCO] = 570 mM, [DABCO] = 0.12 mM

Table 4.2. Glass transition temperatures of thiol-isocyanate-ene ternary networks through the sequential and simultaneous dual cure systems obtained by DSC

SH : C=C : NCO (molar ratio)	TEA + I 651 (^{o}C)	TBA·$HBPh_4$ + ITX (^{o}C)
100 : 100 : 0	-6	-5
100 : 80 : 20	4	3
100 : 60 : 40	10	8
100 : 40 : 60	16	16
100 : 20 : 80	30	28
100 : 0 : 100	36	35

Table 4.3. Glass transition temperatures and rubbery modulus (E' at 80 °C) of thiol-isocyanate-ene ternary networks through the sequential and simultaneous dual cure systems obtained by DMTA

SH : C=C : NCO (molar ratio)	TEA + I 651		TBA·$HBPh_4$ + ITX	
	T_g (°C)[a]	E' (MPa)[b]	T_g (°C)[a]	E' (MPa)[b]
100 : 100 : 0	11	5.1	11	4.9
100 : 80 : 20	23	7.4	20	7.6
100 : 60 : 40	32	8.4	33	8.1
100 : 40 : 60	41	9.5	38	9.3
100 : 20 : 80	50	9.6	52	10.2
100 : 0 : 100	56	13.5	54	12.1

[a]the peak temperature of tan δ
[b]the storage modulus (E') at 80 °C

Table 4.4. Mechanical properties and refractive index of thiol-isocyanate-ene ternary networks by sequential dual cure system

SH : C=C : NCO (molar ratio)	Pendulum Hardness	Pencil Hardness	Refractive Index (Sulfur content, wt %)
100 : 100 : 0	30	3B	1.5535 (15.8)
100 : 80 : 20	23	HB	1.5510 (14.4)
100 : 60 : 40	16	H	1.5490 (13.2)
100 : 40 : 60	18	2H	1.5475 (12.2)
100 : 20 : 80	82	4H	1.5460 (11.3)
100 : 0 : 100	220	8H	1.5440 (10.6)

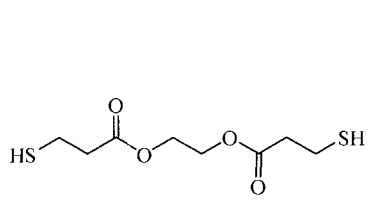

GDMP

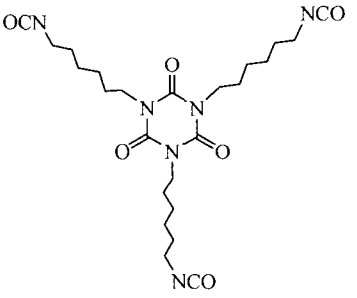

N3600

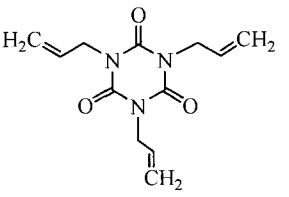

TATAT

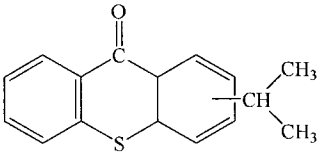

ITX

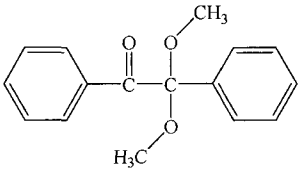

DMPA

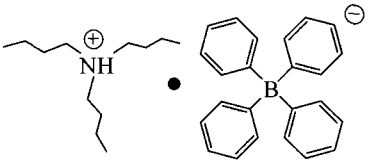

TBA·HBPh$_4$

Chart 4.1. Molecular structures of thiol, ene, isocyanate, photointitiator, and photo-generated amine catalyst.

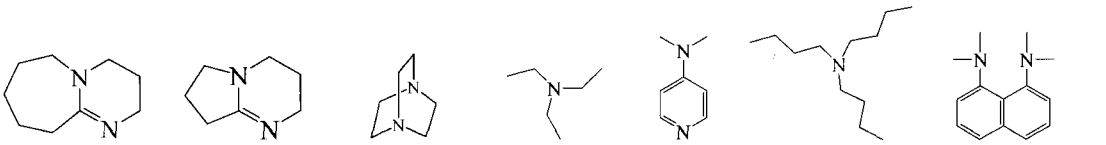

Chart 4.2. Molecular structures of tertiary amine catalysts.

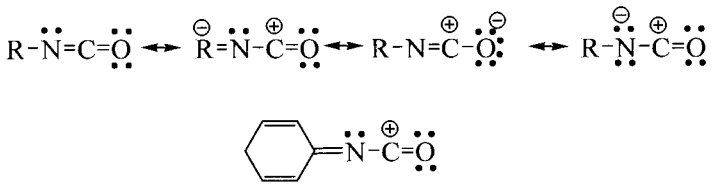

Chart 4.3. Resonance structure of isocyanate.

Initiation

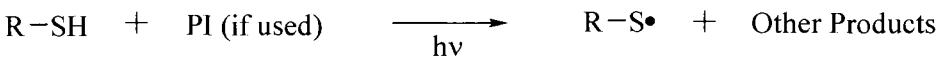

Propagation

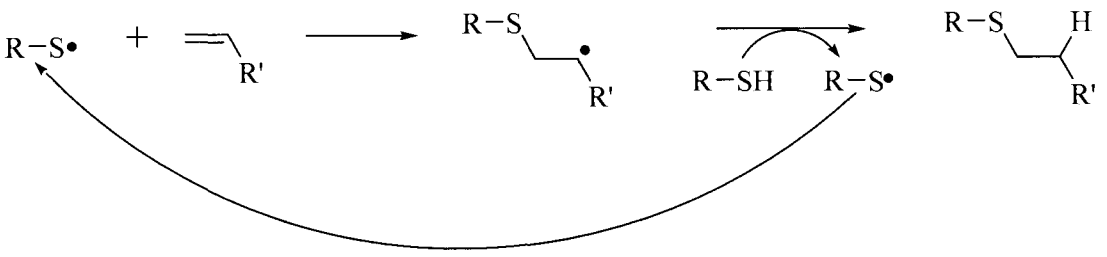

Termination Coupling of radicals

Scheme 4.1. Free-radical step growth mechanism of thiol-ene photopolymerization.

Initiation

Propagation

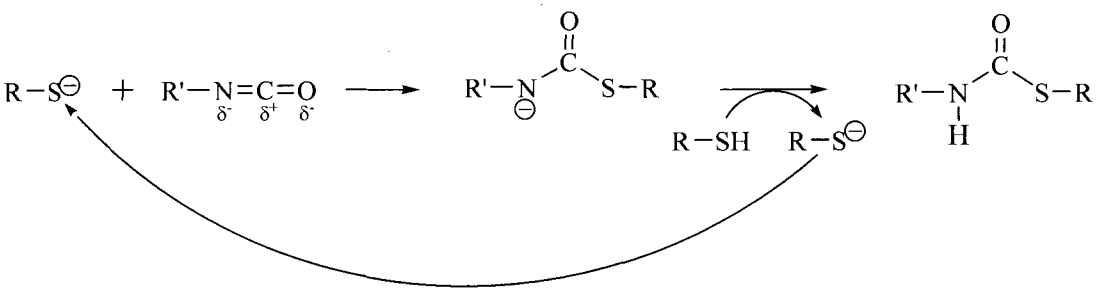

Scheme 4.2. Tertiary amine catalyzed thiol-isocyanate nucleophilic coupling reaction mechanism.

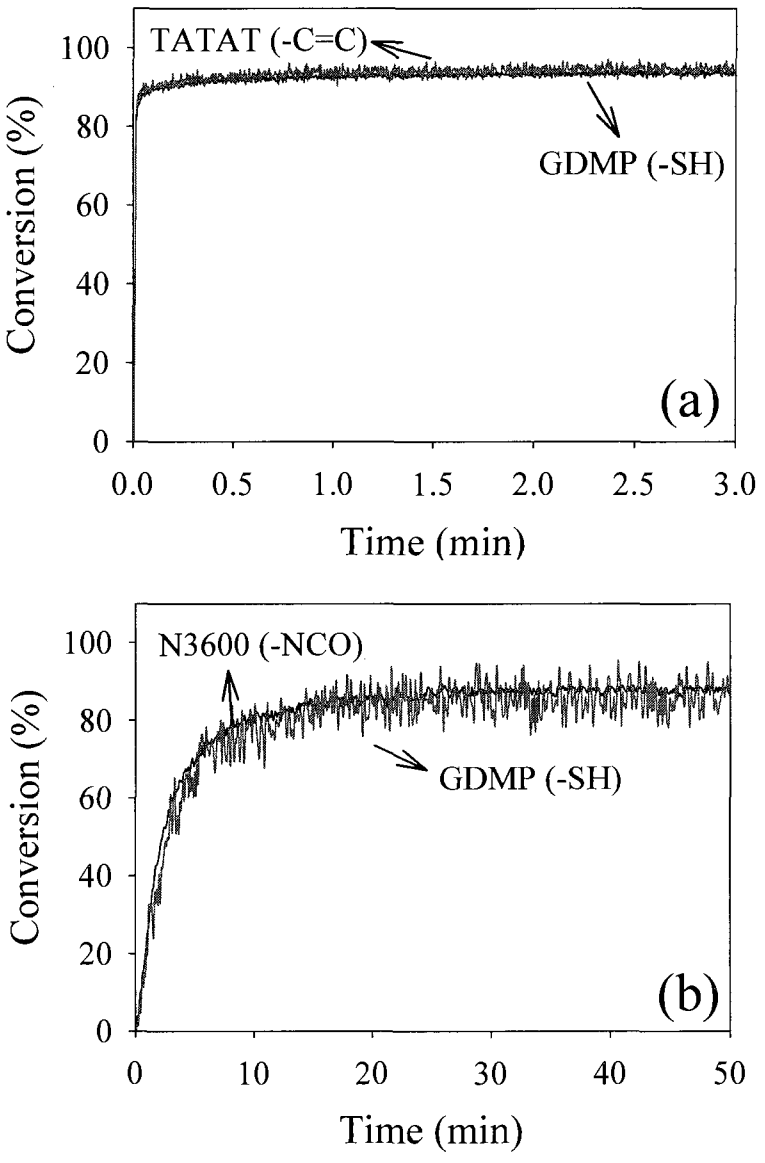

Figure 4.1. Kinetic profiles (a) thiol-ene (SH:C=C = 100:100; DMPA 1 wt%, intensity of high pressure mercury lamp: 20.5mW/cm^2) and (b) thiol-isocyanate networks (SH:NCO = 100:100; TEA 0.1 wt%).

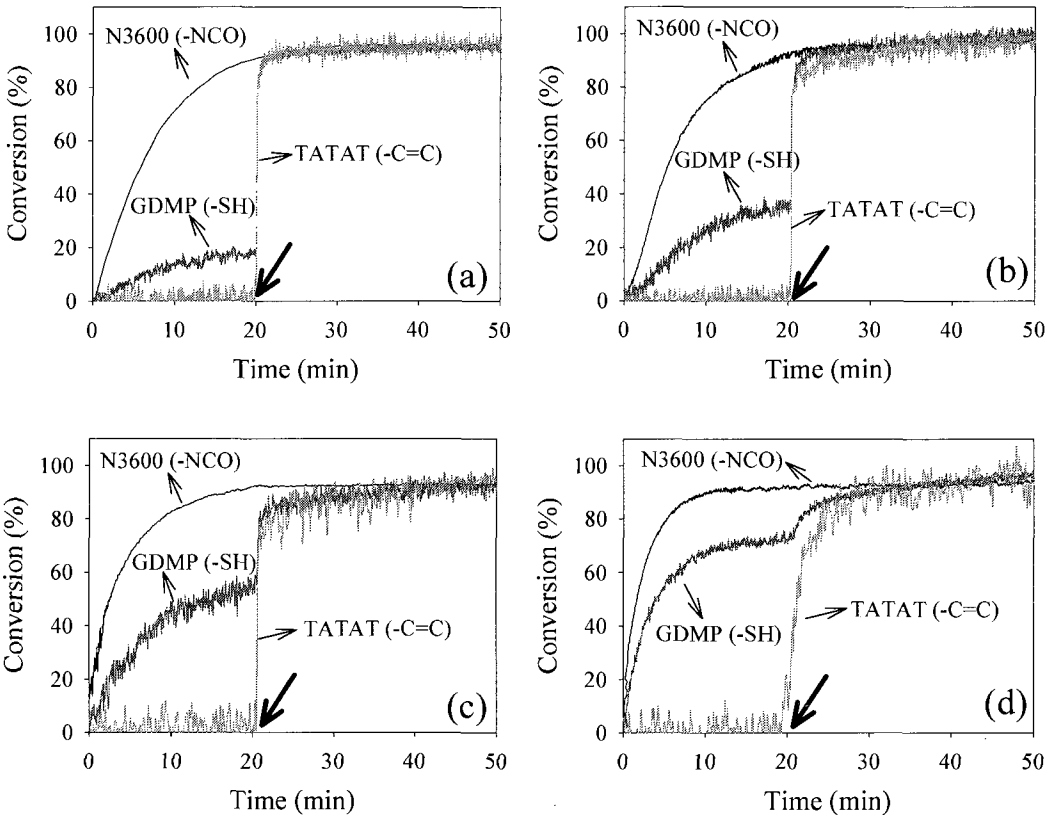

Figure 4.2. Kinetic profiles of thiol-isocyanate-ene ternary networks by sequential curing process; SH:C=C:NCO = (a) 100:80:20, (b) 100:60:40, (c) 100:40:60, (d) 100:20:80 (DMPA 1 wt%; TEA 0.1 wt%; intensity of high pressure mercury lamp: 20.5 mW/cm^2).

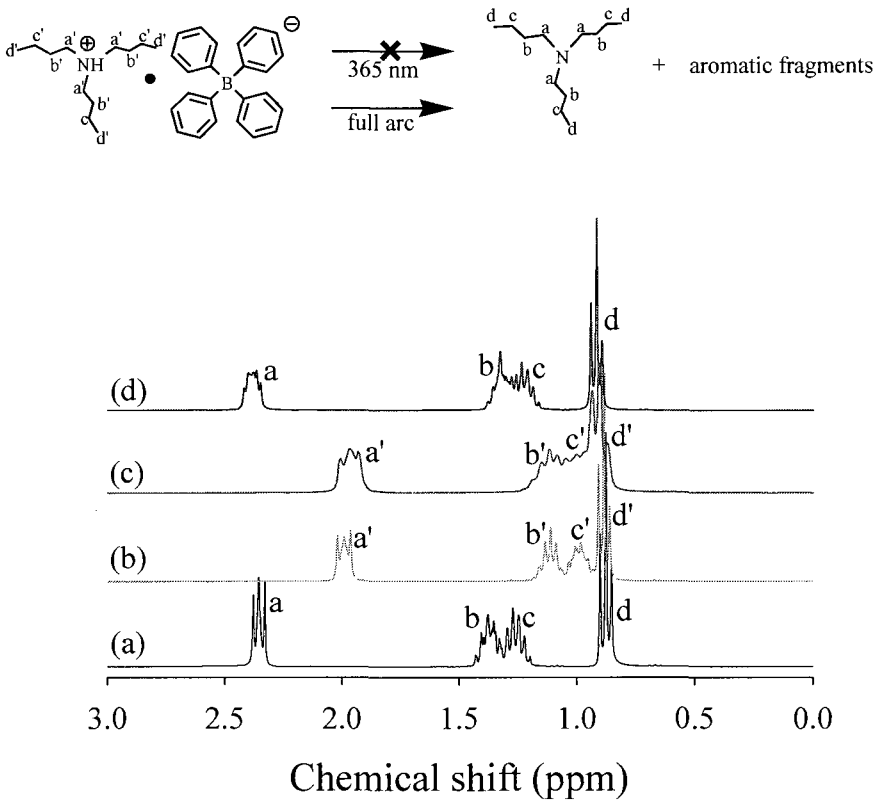

Figure 4.3. ^{1}H NMR spectra ($CHCl_3$-*d*) of (a) tributylamine (TBA), (b) TBA·HBPh4 before, (c) after irradiation at 365 nm (1.5 mW/cm^2), and (d) full arc (10.2 mW/cm^2) in $CHCl_3$-*d* solution (5 wt%).

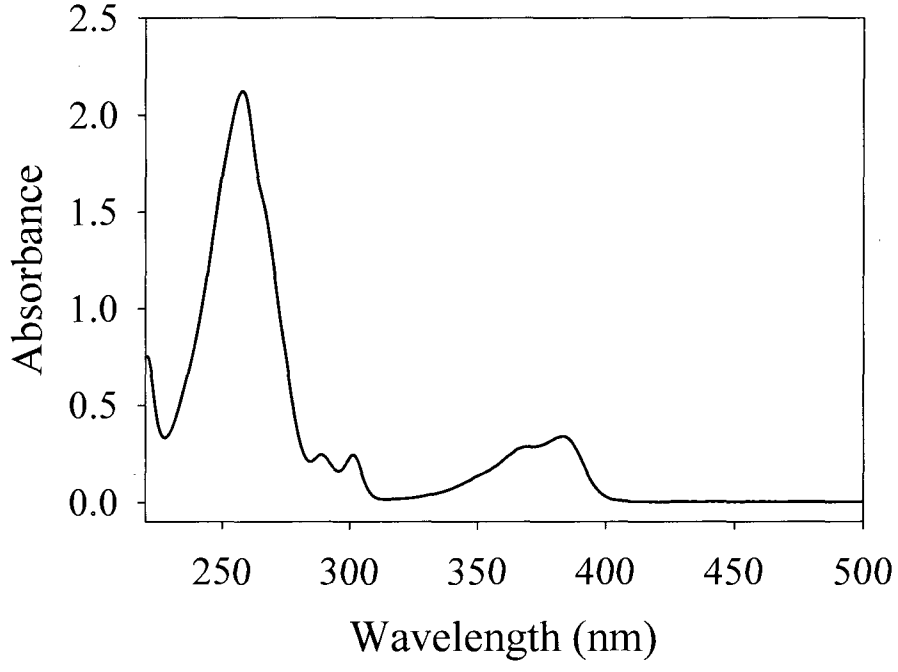

Figure 4.4. UV absorption spectra of ITX in acetonitrile (concentration: 5.8×10^{-5} M).

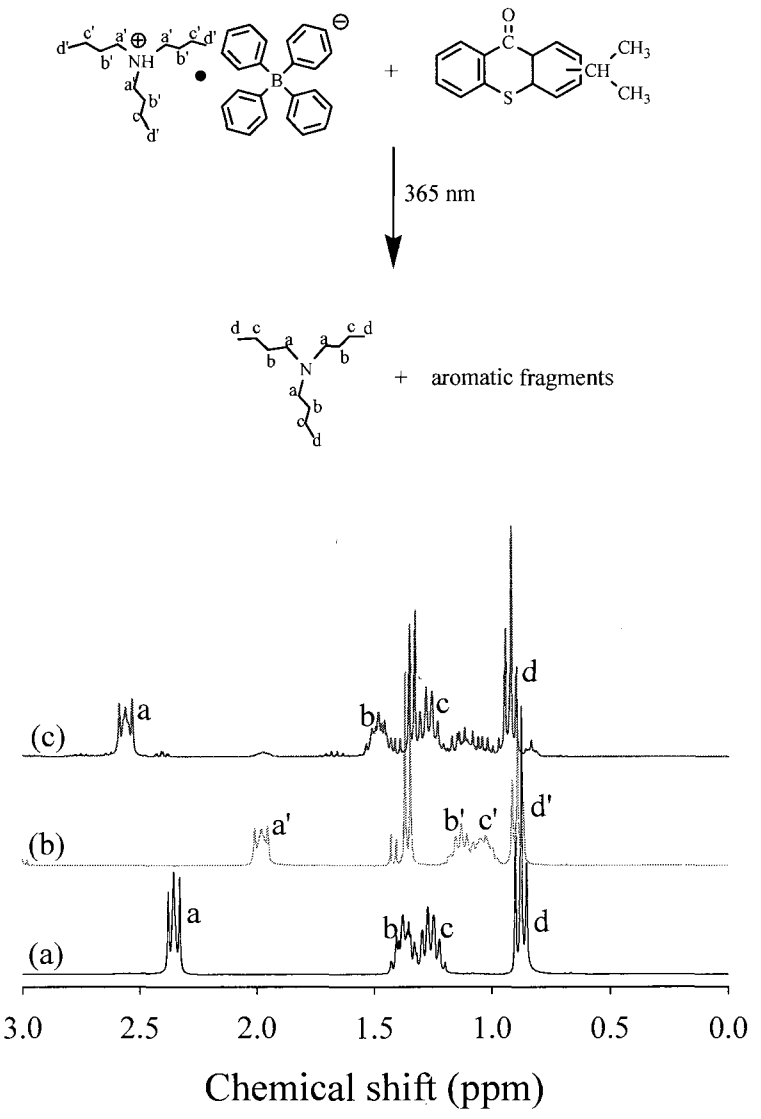

Figure 4.5. ^{1}H NMR spectra ($CHCl_3$-*d*) of (a) tributylamine (TBA) and TBA·$HBPh_4$ with ITX ((b) before and (c) after irradiation at 365 nm (1.5 mW/cm^2) in $CHCl_3$-*d* solution (5 wt%; ITX:TBA·$HBPh_4$ = 0.36:0.61).

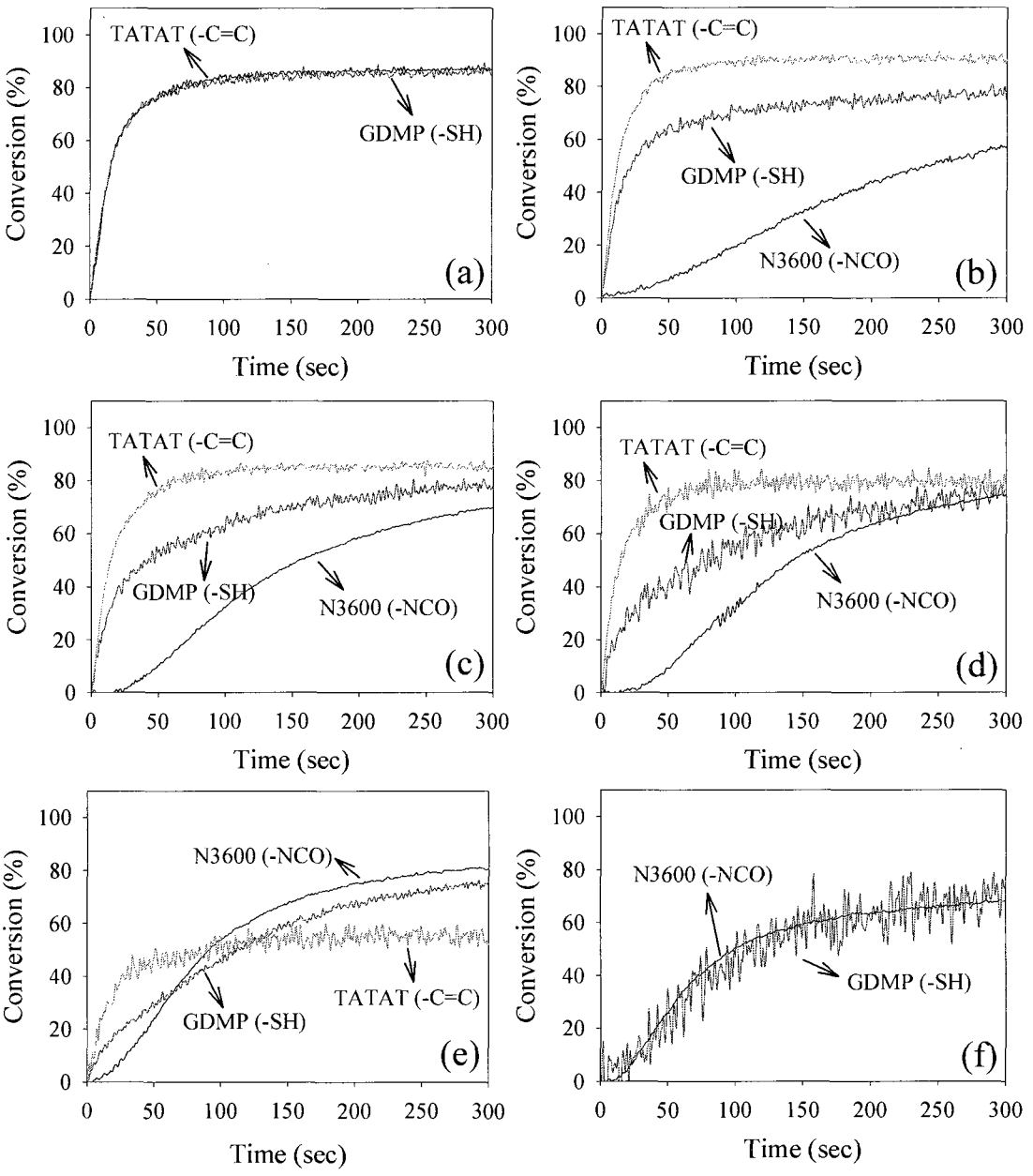

Figure 4.6. Kinetic profiles of thiol-isocyanate-ene ternary networks by simultaneous curing process; SH:C=C:NCO = (a) 100:100:0, (b) 100:80:20, (c) 100:60:40, (d) 100:40:60, (e) 100:20:80, (f) 100:0:100 (ITX 0.36 wt%; TBA·$HBPh_4$ 0.61 wt%; intensity of high pressure mercury lamp: 1.41 mW/cm^2 through 365-nm filter).

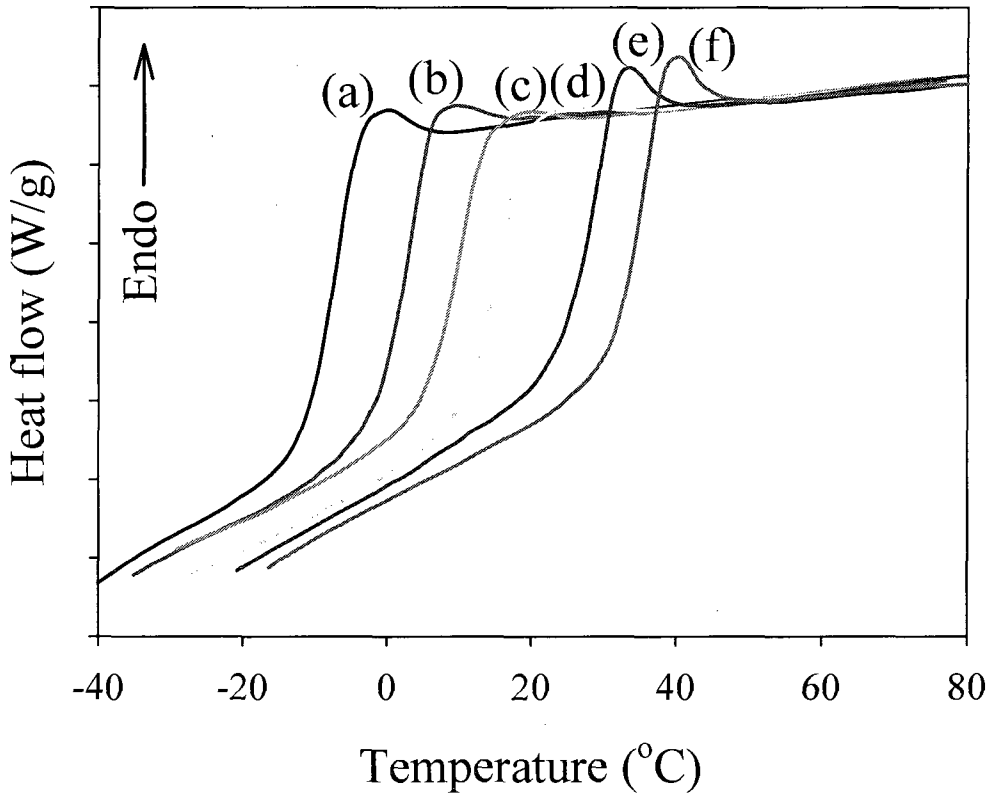

Figure 4.7. DSC thermograms of thiol-isocyanate-ene hybrid networks by sequential curing process; SH:C=C:NCO = (a) 100:100:0, (b) 100:80:20, (c) 100:60:40, (d) 100:40:60, (e) 100:80:20, (f) 100:0:100 (DMPA 1 wt%; TEA 0.1 wt%; pre-cure at room temperature for 1h; intensity of medium pressure mercury lamp 10.2 mW/cm^2; irradiation time: 5 min; post-cure at 80 °C for 24h).

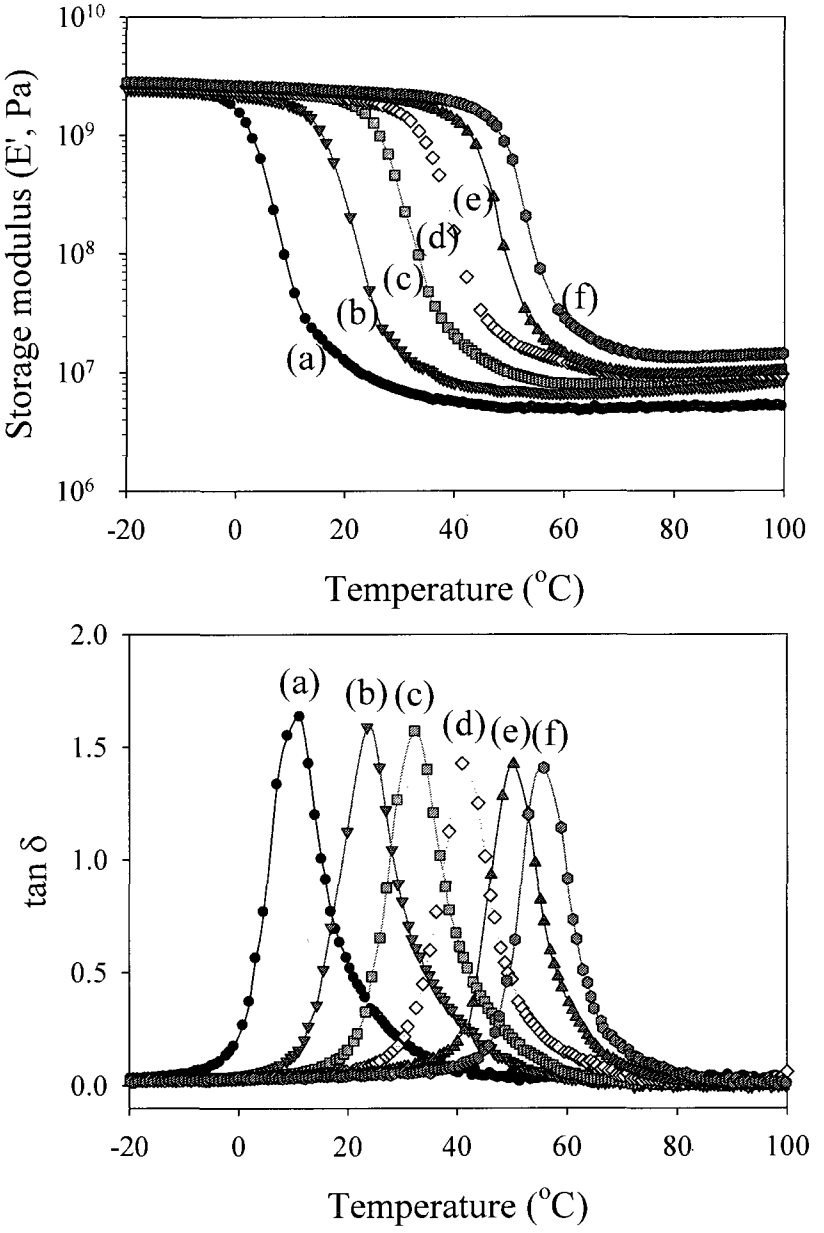

Figure 4.8. Dynamic mechanical thermal properties of thiol-isocyanate-ene ternary networks by sequential curing process; SH:C=C:NCO = (a) 100:100:0, (b) 100:80:20, (c) 100:60:40, (d) 100:40:60, (e) 100:80:20, (f) 100:0:100 (DMPA 1 wt%; TEA 0.1 wt%; pre-cure at room temperature for 1h; intensity of medium pressure mercury lamp 10.2 mW/cm^2; irradiation time: 5 min; post-cure at 80 °C for 24h).

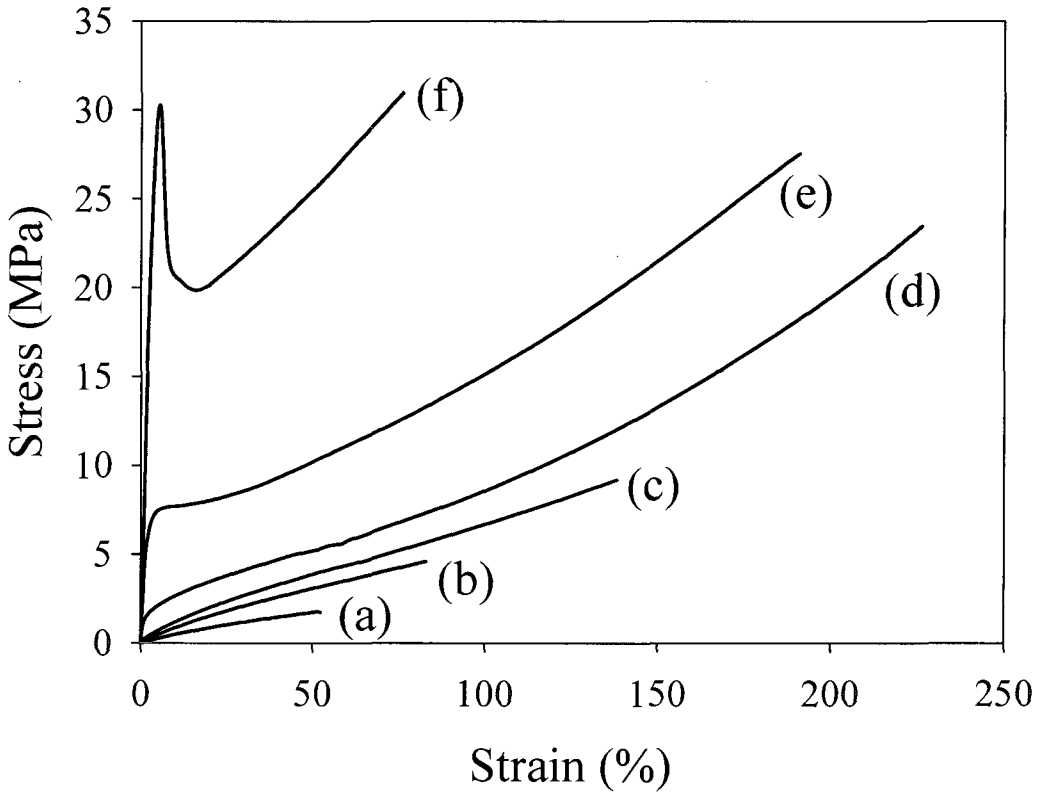

Figure 4.9. Tensile properties of Thiourethane-Thiolene hybrid networks by sequential dual cure system; SH:C=C:NCO = (a) 100:100:0, (b) 100:80:20, (c) 100:60:40, (d) 100:40:60, (e) 100:80:20, (f) 100:0:100 (DMPA 1 wt%; TEA 0.1 wt%; pre-cure at room temperature for 1h; intensity of medium pressure mercury lamp 10.2 mW/cm^2; irradiation time: 5 min; post-cure at 80 ^{o}C for 24h).

Supporting Information

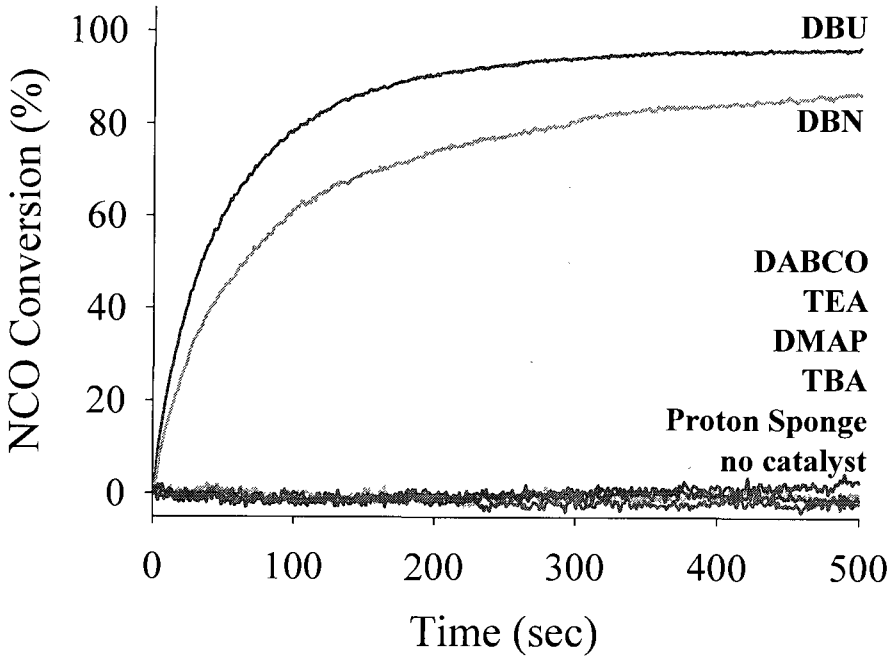

Figure 4.S1 (a). Kinetic profiles of thiourethane model reaction with different amine catalysts monitored by measuring the isocyanate conversion with real-time IR at 2250 cm^{-1} ([Hexanethiol] = [Hexyl isocyanate] = 570 mM; [Amine] = 0.24 mM in benzene).

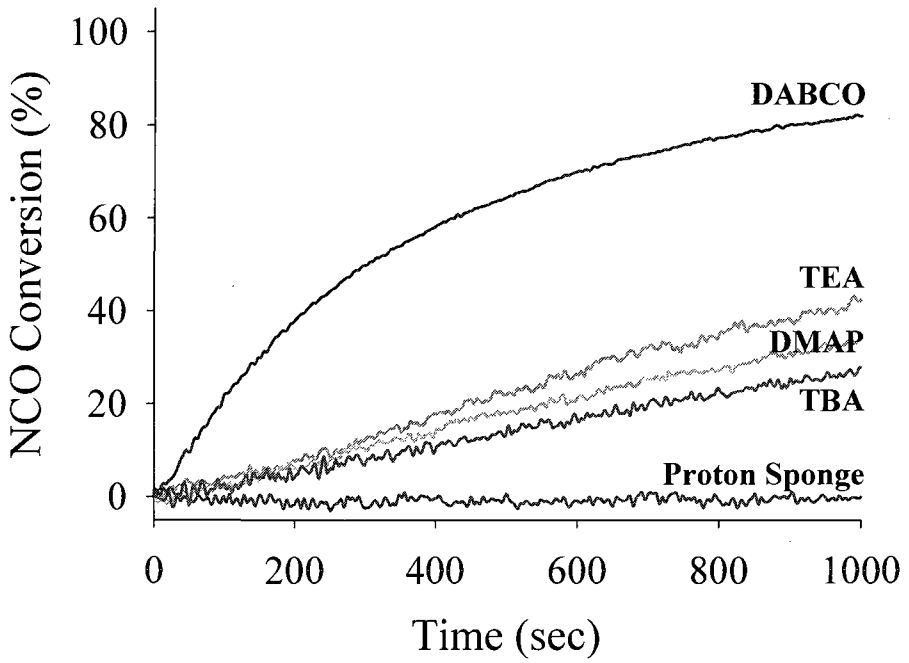

Figure 4.S1 (b). Kinetic profiles of thiourethane model reaction with different amine catalysts monitored by measuring the isocyanate conversion with real-time IR at 2250 cm^{-1} ([Hexanethiol] = [Hexyl isocyanate] = 730 mM; [Amine] = 80 mM in benzene).

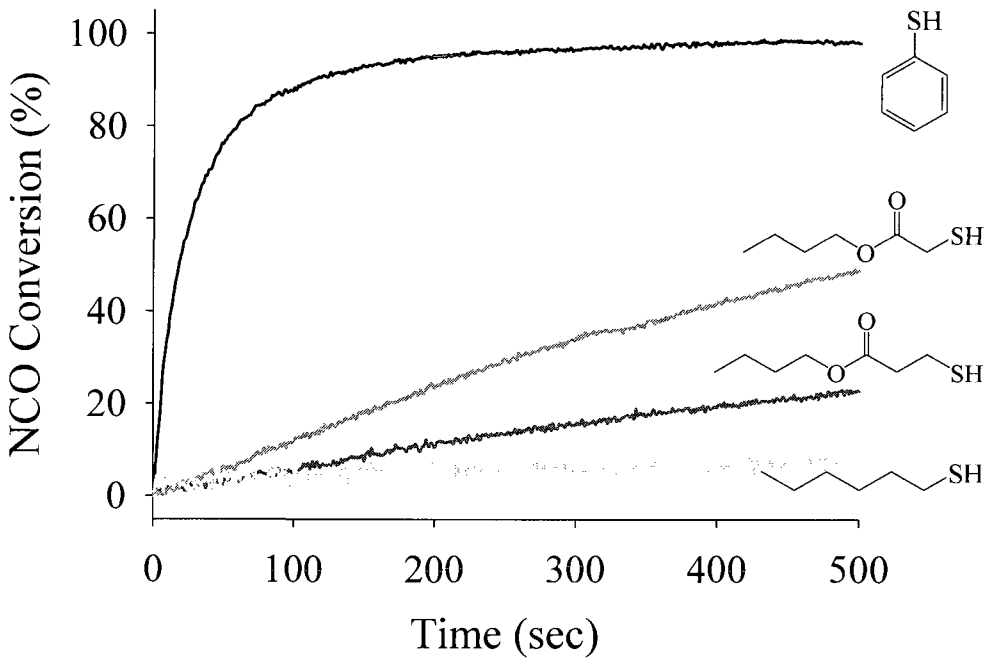

Figure 4.S2. Kinetic profiles of thiourethane model reaction with different thiol structure monitored by measuring the isocyanate conversion with real-time IR at 2250 cm^{-1} ([Thiol] = [Hexyl isocyanate] = 730 mM; [TEA] = 2.3 mM in benzene).

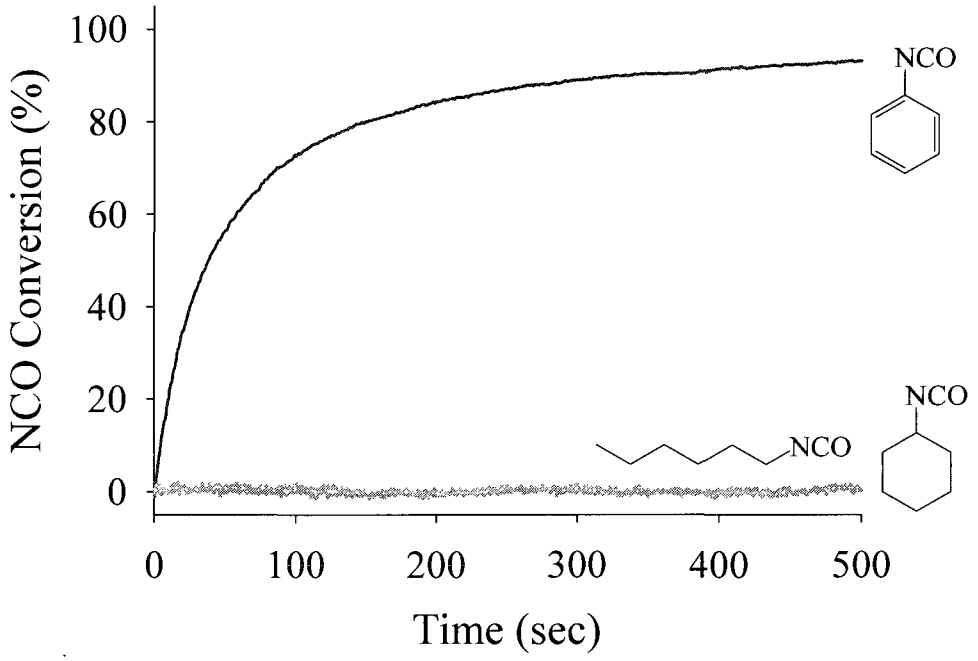

Figure 4.S3 (a). Kinetic profiles of thiourethane model reaction with different isocyanate structure monitored by measuring the isocyanate conversion with real-time IR at 2250 cm^{-1} ([Benzenthiol] = [Isocyanate] = 570 mM; [DABCO] = 0.12 mM in benzene).

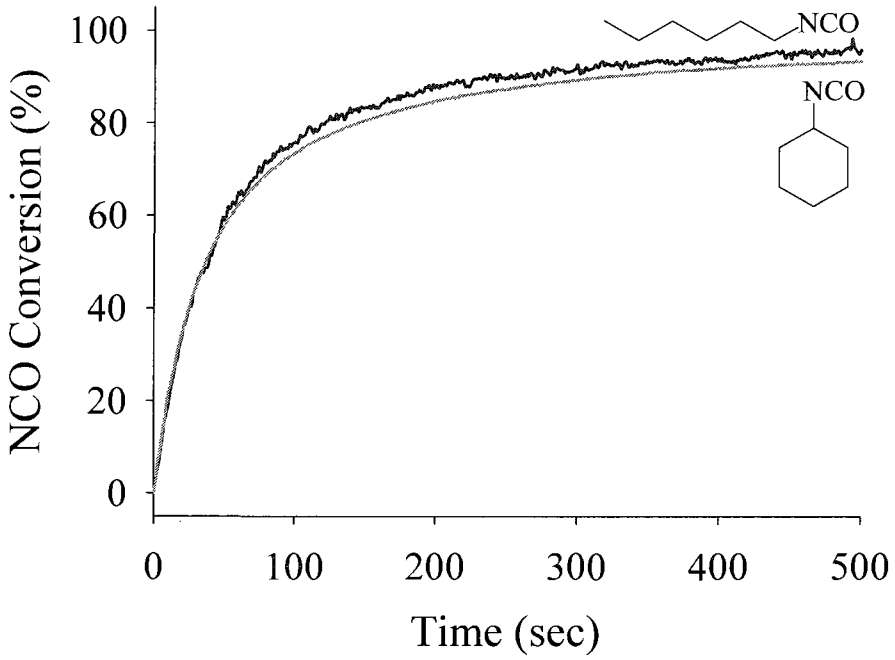

Figure 4.S3 (b). Kinetic profiles of thiourethane model reaction with different isocyanate structure monitored by measuring the isocyanate conversion with real-time IR at 2250 cm^{-1} ([Benzenthiol] = [Isocyanate] = 570 mM; [DABCO] = 5 mM in benzene.

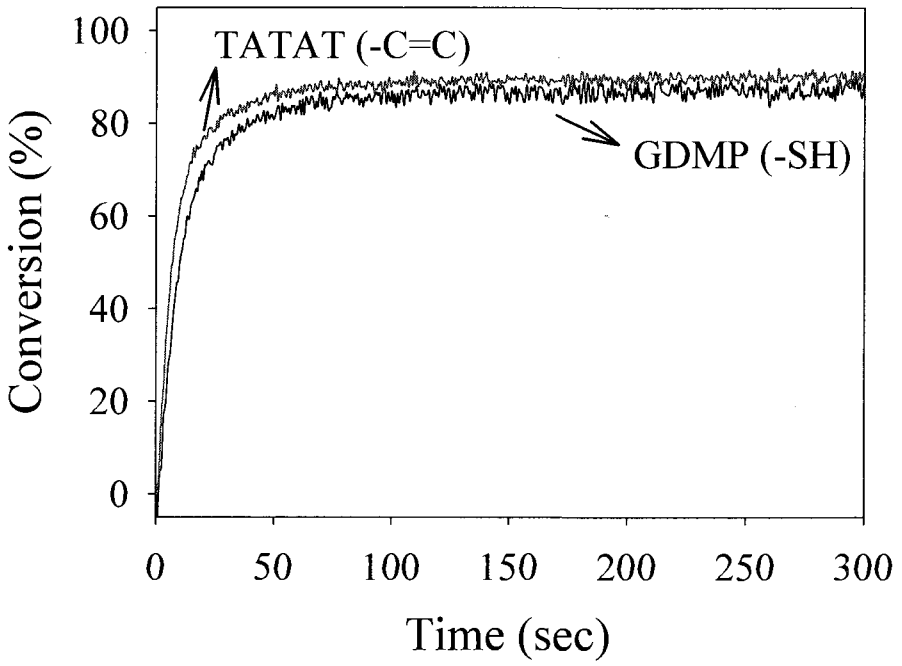

Figure 4.S4. Kinetic profiles of GDMP-TATAT binary networks by UV curing; SH:C=C = 100:100 (ITX 0.36 wt%; intensity of high pressure mercury lamp: 1.41 mW/cm^2 through 365-nm filter).

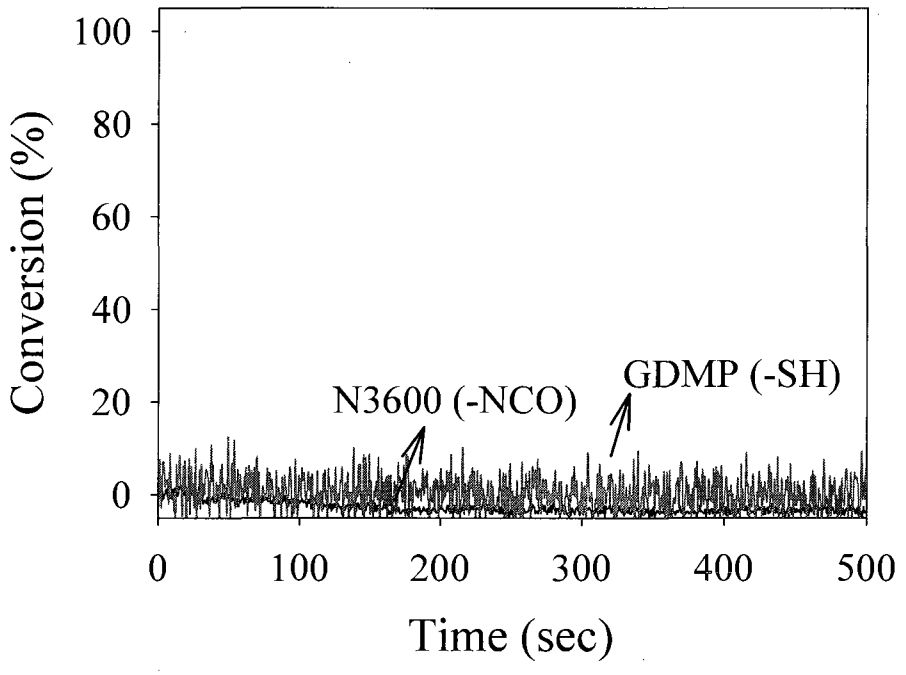

Figure 4.S5. Kinetic profiles of GDMP-N3600 binary networks by thiol-isocyanate coupling reaction; SH:NCO = 100:100 (ITX 0.36 wt%; intensity of high pressure mercury lamp: 1.41 mW/cm^2 through 365-nm filter).

CHAPTER V

ENTHALPY RELAXATION OF PHOTOPOLYMERIZED THIOL-ENE NETWORKS: STRUCTURAL EFFECTS

Abstract

Physical aging behavior of photo-polymerized Thiol-Ene networks was investigated by measuring the extent of enthalpy relaxation in terms of network density and molecular structure. The homogeneous network structure of the Thiol-Enes, having narrow glass transition temperature ranges, showed characteristic temperature and time dependency relationships for enthalpy relaxation. All Thiol-Ene films annealed at different temperatures (T_a) for 1 h according to the isochronal method, showed maximum enthalpy relaxation peaks at approximately T_g-10 °C by DSC. The extent of enthalpy relaxation as a function of annealing time (t_a) was obtained by the isothermal aging method. Correlations between the extent of enthalpy relaxation and the heat capacity difference at T_g were made and related to Thiol-Ene chemical group rigidity and network linking density. Pendulum hardness values for a selected Thiol-Ene film showed a clear change in hardness upon aging indicating sub-T_g mechanical relaxation, consistent with the related enthalpy relaxation process.

Introduction

Polymer sub-T_g aging behavior is related to the molecular structure and chemical environment which control chain mobility and conformational states. Hence, the chemical structure of linear, crosslinked, and network polymers can potentially have a

profound effect on the extent of enthalpy relaxation. As examples of linear polymers, poly(vinyl acetate),[1] polycarbonate,[2] poly(methyl methacrylate),[3-4] polystyrene[5-7] and phenolphthalein poly(ether sulfone)[8] have been investigated in terms of the effect of molecular weight, chain conformation and entanglement on enthalpy relaxation. The role of hydrogen bonding and bulky side chains of linear polymers have also been reported.[9] Since physical aging is directly related to segmental relaxation, the effect of chain mobility, cross-link density and the molecular weight between crosslinks is important.[10] Accordingly, the segmental relaxation behavior of crosslinked poly(ethylene oxide) copolymers showed an increase in broadening of the segmental relaxation distribution.[11] Attention has also been paid to epoxy systems which are well known to form polymer network structures that undergo physical aging.[12-16] Since epoxy networks are chemically complex due to significant effects from hydrogen bonding, the difficulty in controlling the extent of reaction, and chemical side reactions, correlation of structure-property relationships can be challenging.

Thiol-Enes are important in the fields of coatings, adhesives, and energy damping because of important attributes such as insensitivity to oxygen during photo-polymerization, high conversion, and low shrinkage.[17-21] Unlike other photo-initiated polymerization processes, Thiol-Enes follow a free-radical step-growth reaction mechanism that proceeds by a two-step propagation process.[17] Thiol-Ene mixtures still exist as low molecular weight prepolymers until the gel point, resulting in a combination of low stress-induced shrinkage and high conversion. Due to essentially quantitative conversions and a free-radical step-growth process, photopolymerized Thiol-Ene films

are highly uniform with dense network structures as depicted pictorially in Chart 5.1 for a generic tri-functional Thiol and tri-functional Ene.

Compared to conventional linear or crosslinked polymers, Thiol-Ene based networks have a highly uniform dense structure and inherently narrow glass transition.[17-21] This suggests that Thiol-Ene networks might be very sensitive to annealing temperature and time, resulting in a large amount of enthalpy or volume relaxation in a short period of time under specific physical aging conditions (temperature, pressure). Since Thiol-Ene networks have significance as coatings, energy absorbing materials, and optical components, any changes that may occur due to sub-T_g relaxation process are essential to identify and characterize. As already described, the near perfect network structure of photopolymerized Thiol-Ene systems which proceed to quantitative conversion with no side reactions, except for a small amount of radical coupling, presents a unique opportunity to evaluate enthalpy relaxation fundamentals in network systems. Accordingly, in the research described herein, the aging of photo-polymerized Thiol-Ene networks was evaluated by measuring the extent of enthalpy relaxation in terms of network density and chemical structural effects. The role of chemical structural features such as rigidity and network density are established.

Experimental

1,6-Hexanedithiol (Thiol 1), 2,4,6-triallyloxy-1,3,5-triazine (Ene 2) and 1,3,5-triallyl-1,3,5-triazine-2,4,6(1H,3H,5H)-trione (Ene 3) were purchased from Aldrich, and the other thiols (trimethrylolpropane tri(3-mercapto-propionate) (Thiol 2) and pentaerythritol tetrakis(3-mercaptopropionate) (Thiol 3)) and Ene monomer (Allyl

pentaerythritol (Ene 1)) were obtained from Bruno Bock Thio-Chemicals-S and Perstorp Specialty Chemicals, respectively. All Thiol and Ene monomers used in the investigation are shown in the Chart 5.2. The photoinitiator, 2,2-dimethoxy 2-phenyl acetophenone (DMPA), was supplied by Ciba Specialty Chemicals. All materials were used as received.

The photoinitiator (DMPA, 1 wt%) was dissolved in the Thiol and Ene mixtures by sonication for 10-20 min. All Thiol-Ene films were cast on glass plates (200 μm draw down bar) and cured by passing 10 times on a Fusion UV curing line system equipped with a D bulb (400 W/cm^2 with belt speed of 10 feet/min and 3.1 W/cm^2 irradiance). Surface temperature of films during curing reached 70~80 °C, and all samples were post-cured at 80 °C for 24 h to complete reaction and remove chemical any conversion effect on enthalpy relaxation.

Kinetic profiles of Thiol-Ene photopolymerization were obtained using real-time infrared (RTIR) spectroscopy. Infrared spectra were recorded on a modified Bruker 88 Fourier transform infrared spectrometer designed to allow light to impinge on a horizontal sample with a fiber-optic cable as a function of the irradiation time. An Oriel 200 W, high pressure mercury-xenon lamp equipped was directed to a 20 micron sample between two salt plates. The light impinging on the sample had an irradiance of 7.8 mW/cm^2 at 365nm. The temperature was isothermally controlled at 80 °C to provide a similar temperature environment to that experienced by samples cured using the Fusion lamp. The conversion rates of Enes were monitored at 3080 cm^{-1} for Enes and 2570 cm^{-1} for Thiols.

TA Q1000 DSC with RCS 90 (Refrigerated Cooling System) was used to measure thermal behavior of Thiol-Ene networks before and after sub-T_g annealing. An RCS 90 cooling head mounted on the DSC Q1000 furnace encases the DSC cell preventing frost building-up during operation. Three calibration steps for the TA Q1000 were performed periodically. First, the T_{zero} calibration, both without and with standard material (Sapphire), was conducted from -90 to 400 °C to compensate thermal lag between samples and temperature control sensors. Through the enthalpy constant calibration comparing the heat of fusion of a standard material (Indium, 28.58 J/g) with the measured value, the cell constant was determined by the ratio of these two values (1±0.05). Temperature calibration was performed by comparing the known melting point of Indium (156.6 °C) with the recorded value during a heating scan. All experiments were carried out under nitrogen with a flow rate of 50 mL/min. Sample weights were 8.0±1.0mg to ensure sufficient sensitivity for heat capacity measurements. DSC scans were conducted over the temperature range from T_g-50 to T_g+50 °C using 10 °C/min heating (q_h) and cooling (q_c) rates. It was assumed that initializing the Thiol-Ene network before each aging process at T_g+50 °C was sufficient to erase the internal stress from the photo-polymerization and/or any previous physical aging history. Enthalpy relaxation behavior of the networks was studied by two different methods. First, Thiol-Ene film samples were annealed directly in the DSC at various temperatures (T_a was varied by every 5 °C from T_g+10 to T_g-50 °C) for 60 min (t_a) in order to obtain information on the temperature dependency of the enthalpy relaxation rate (isochronal method, Figure 5.1a). Second, the enthalpy relaxation was studied as a function of annealing time (up to 24 h) at the temperature where the enthalpy relaxation rate was found to be the fastest by the

isochronal method (isothermal method, Figure 5.1b). The schematic diagrams of the DSC measurement procedures for both methods are shown in Figure 5.2. Each sample was measured twice. In the isochronal case, samples were measured first sequentially from $T_{a,1}$ to $T_{a,7}$ and then from $T_{a,7}$ to $T_{a,1}$ (Figure 5.2a). In isothermal process, samples were processed sequentially from $t_{a,1}$ to $t_{a,4}$, and then from $t_{a,4}$ to $t_{a,1}$ (Figure 5.2b). Identical results were obtained thus eliminating the possibility that chemical changes occurred during heating/cooling/annealing cycles. Agreement between the two sets of results illustrates the absence of significant contributions from instrument drift.

The enthalpy relaxation during the sub-T_g aging was calculated from the difference thermograms generated by subtracting the reference DSC curve generated without annealing from the DSC curve obtained after the sub-T_g annealing process based on equation (1),

$$\Delta H_r(T_a,t_a) = \int_{T_g-50^oC}^{T_g+50^oC} C_p(T_a,t_a)dT - \int_{T_g-50^oC}^{T_g+50^oC} C_p(T_a,0)dT \qquad (1)$$

where $C_p(T_a, t_a)$ and $C_p(T_a, 0)$ represent specific heat capacities for samples annealed at T_a for $t=t_a$ and unannealed samples, respectively.[23-25]

A BYK Gardner pendulum hardness tester was used to determine Persoz pendulum hardness of the annealed networks. The hardness was determined for Thiol 3 + Ene 3 system which exhibited a glass transition temperature above room temperature. The hardness was measured after annealing the network film at T_g-10 °C (43 °C) as a function of annealing time to investigate the effect of physical aging on hardness. Measurements were conducted at room temperature on network films coated onto glass

substrates. Three different samples, prepared and annealed using the same conditions, were used and the hardness was measured at least 10 times for each sample. The results of these measurements were averaged.

Results and Discussion

A series of Thiols and Enes (Chart 5.2) with significant variation in functionality (2 to 4) and structural rigidity were chosen to answer the basic questions of how network density and the rigidity of chemical groups influence enthalpy relaxation in networks. Although discussed in the Introduction, we reiterate that since photopolymerized Thiol-Ene networks are characterized by essentially quantitative conversions of the monomer components with little or no residual chemical groups that may further react upon thermal cycling or aging. Since they are mechanically and physically highly uniform polymer networks,[17-19] the photocured Thiol-Ene films made from the components in Chart 5.2 are ideal for determination of how basic features such as rigidity and network density can influence sub-T_g aging.

DSC heating scans of all nine photo-polymerized Thiol-Ene network samples, after they were heated above their corresponding glass transitions (T_g+50 °C) and cooled at 10 °C/min down to well below T_g (T_g-50 °C), are shown in Figure 5.3. This series of Thiol-Ene films exhibited a fairly large range of glass transition temperatures, the lowest at about -40 °C for Thiol 1 + Ene 1, and the highest at about +50 °C for Thiol 3 + Ene 3 system. All of the photopolymerized Thiol + Ene networks had fairly narrow glass transitions ranges of about 15-20 °C due to the uniform network structure of Thiol-Enes, as already discussed. To illustrate that essentially quantitative conversion was obtained

for each of the samples, in Figure 5.4, the polymerization kinetic profile for the Thiol-Ene (Thiol 3 + Ene 3) with the highest T_g was recorded (see Experimental for details) as a representative example. The percent conversion versus irradiation time plots, along with the IR spectra of the monomer mixture before and after exposure, clearly illustrates essentially complete conversion even for the relatively low light intensity used in this real-time infrared analysis. From this representative example, which is consistent with an extensive literature as reported in the review reference 17, it is clear that all of the samples in Figure 5.3 attained quantitative conversion. All samples used for the aging studies were prepared by exposing 10 times at 10 feet/min to the output of a Fusion D bulb with irradiance of 3.1 W/cm^2 followed by oven aging at 80 °C. This ensures quantitative conversion for all samples prior to beginning the enthalpy relaxation measurements.

Upon closer evaluation of the results in Figure 5.3, it is apparent that the glass transition temperature is a function of network density (i.e. the linking or connecting density) and the bulkiness (rigidity) of the network components. For a given Ene, the films made with Thiol 1 have the lowest glass transition temperature, consistent with the low functionality of Thiol 1. The glass transition temperature increased with increasing thiol functionality, i. e., the films made from the tetra-functional Thiol (Thiol 3) had the highest glass transition temperatures for a given Ene. Also, samples incorporating Ene 2 and Ene 3 with the rigid triazine rings have consistently higher glass transition temperatures than those prepared using Ene 1. This is consistent with previous results for other Thiol-Ene networks.[17]

The Thiol-Ene films were annealed at specific temperatures (T_a-annealing temperature) every 5 °C from T_g+10 to T_g-50 °C for a time, t_a, to investigate the temperature dependency of enthalpy relaxation. Figure 5.5 shows DSC heating scans of a selected Thiol-Ene system (Thiol 2+Ene 1) after annealing at different temperatures. A similar annealing process followed by DSC scans was performed for each of the Thiol-Ene samples. The resultant areas of the relaxed enthalpy peaks as a function of ΔT_a (T_g-T_a) for all of the Thiol-Ene systems are plotted in Figure 5.6. The plots in Figure 5.6 resemble asymmetric bell-shaped curves with the maxima located at about T_g-10 °C. At temperatures well below T_g, i. e., (T_g-T_a) > 30 °C, the structural relaxation rate is slow as exemplified by longer characteristic relaxation times. Hence, during the 1 hour annealing time, the relaxed enthalpy is small. As the annealing temperature increases, (T_g-T_a) becomes smaller and the relaxation process becomes progressively faster. Thus, the relaxed enthalpy achieved during the 1 hour annealing time increases. At annealing temperatures near the glass transition, the extent of relaxed enthalpy achieved in the 1 hour annealing period will be limited not by the characteristic relaxation time, but rather the actual enthalpic departure from equilibrium at that temperature. Hence, the maximum in the relaxed enthalpy occurs at about T_g-10 °C for each of the systems depicted in Figure 5.6. Based on the results presented in Figure 5.6, two molecular factors controlling the relaxed enthalpy maximum, the network density and the bulkiness (rigidity) of network constituents, are considered. It is obvious from the results in Figure 5.6 that the relaxed enthalpy maximum decreases with an increase of either of these two network parameters. Specifically, the films made from monomer combinations having higher Thiol functionalities (Thiol 3 > Thiol 2 > Thiol 1) and Enes with more rigid

structure (Ene 3 > Ene 2 > Ene 1) exhibit less enthalpy relaxation during the 1 hour annealing period.

Figure 5.7 shows DSC heating scans for a representative system (Thiol 2 + Ene 1) after annealing for different time periods at T_g-10 °C, the temperature where enthalpy relaxation exhibited a maximum during the isochronal analysis. The enthalpy relaxation peaks consistently increased with annealing time (t_a). The isothermal annealing results in Figure 5.7 for the Thiol 2 + Ene 1 system and equivalent results obtained for the other eight Thiol-Ene systems are plotted in Figure 5.8. A simple method for analyzing the general overall relaxation rate (β_H)[26-30] according to equation (2) can be applied to the plots in Figure 5.8.

$$\beta_H = \frac{d\delta_H}{d\log t_a} \tag{2}$$

It is clear that the β_H values obtained from the extent of enthalpy relaxation (δ_H) vs. logarithmic annealing time (t_a) at T_a in Figure 5.8 decrease with the Thiol functionality (network density) and Ene bulkiness (rigidity) which, as already discussed, are molecular factors which influence the relaxation process. The low 24 hour enthalpy relaxation values (ΔH_{24h}) for the systems with the more rigid triazine ring structures might well have been expected from a literature reference which indicates that bulky groups, albeit on the side groups in linear polymers, also result in low enthalpy relaxation values.[9]

Additional evidence for the difference in the relaxation processes for the films produced from the nine Thiol-Ene combinations can be suggested by calculating ΔC_p at T_g for the original DSC scans in Figure 5.4. According to the definition of fictive

temperature and assuming that equilibrium conditions (T_f=T_a at t_a=∞) are attained, the ultimate enthalpy relaxation values (ΔH_∞) at a given annealing temperature (T_a) can be approximated by the product of ΔC_p at T_g and ΔT_a (T_g–T_a).[1,2]

$$\Delta H_\infty (T_a) \approx \Delta C_p (T_g) \times \Delta T_a \qquad (3)$$

The resultant values for ΔC_p at T_g and $\Delta C_p \times \Delta T_a$ in Table 5.1, like the results for ΔH_{24h}, decrease as the Thiol functionality increases from 2 to 4 and the Ene rigidity increases. This results from the relationship between the amount of excess enthalpy and ΔC_p at T_g.

Finally, to demonstrate the effect of annealing on Thiol-Ene film hardness, Thiol 3 + Ene 3 films coated on glass plates were isothermally annealed at 43 °C (T_g-10 °C) and after each annealing time period, cooled to room temperature (20 °C) for measurement. A linear relationship between the Persoz hardness and the logarithm of the annealing time clearly illustrates the effect of sub-T_g aging on physical property changes (Figure 5.9).

Conclusions

Photopolymerized Thiol-Ene films were evaluated in terms of enthalpy relaxation. Maximum enthalpy relaxation was observed at T_g-10 °C for all Thiol-Ene films investigated. The extent of enthalpy relaxation after at 24 hours of annealing (ΔH_{24h}) and the overall relaxation rate (β_H) determined by the slope of the extent of enthalpy relaxation (δ_H) vs. the logarithm of the annealing time (t_a) decreased with Ene rigidity and the functionality of the Thiols used to fabricate the Thiol-Ene network. The assumed maximum enthalpy relaxation (ΔH_∞) at the annealing temperature as well as the heat

capacity difference (ΔC_p) at T_g also showed that the relaxation process is largely affected by the molecular structural features, i.e. rigidity and functionality. Physical property changes monitored by Persoz hardness increased as a function of annealing time coincident with the enthalpy relaxation. Considering that Thiol-Ene networks are used at temperatures, the effect of sub-T_g aging on other physical and mechanical properties would be critical and will be extensively studied in future work.

References

1. Hutchinson, J. M.; Kumar, P. *Thermochimica Acta* **2002**, 391, 197.
2. Huang, D.; Yang, Y.; Zhuang, G.; Li, B. *Macromolecules* **1999**, 32, 6675.
3. Andreozzi, L.; Faetti, M.; Giordano, M.; Zulli, F. *Macromolecules* **2005**, 38, 6056.
4. Andreozzi, L.; Faetti, M.; Giordano, M.; Palazzuoli, D. *Journal of Non-Crystalline Solids*, **2003**, 332, 229.
5. Privalko, V.; Demchenko, S. S.; Lipatov, Y. S. *Macromolecules*, **1986**, 19, 901.
6. Aras, L.; Richardson, M. J. *Polymer Comm.*, **1985**, 26, 77.
7. Tsitsilianis, C.; Mylonas, I. *Makromolekulare Chemie-Rapid Communications*, **1992**, 13, 207.
8. Huang, D.; Yang, Y.; Zhuang, G.; Li, B. *Macromolecules* **2000**, 33, 461.
9. McGonigle, E. A.; Cowie, J. M. G.; Arrighi, V.; Pethrick, R. A. *Journal of Materials Science* **2005**, 40, 1869.
10. Roe, R. J.; O'Reilly, J. M. *Structure, Relaxation, and Physical Aging of Glassy Polymers*, Materials Research Society: Pittsburgh **1991**.
11. Kalakkunnath, S.; Kalika, D. S.; Lin, H.; Freeman, B. D. *Macromolecules* **2005**, 38, 9679.
12. Lin, Y. G.; Sauterreau, H.; Pascault, J. P. *Journal of Applied of Polymer Science* **1986**, 32, 4595.
13. Lee, A.; McKenna, G. B. *Polymer* **1988**, 29, 1812.
14. Plazek. D. J.; Frund, Z. N. Jr. *Journal of Polymer Science: Part B: Polymer Physics* **1990**, 28, 431.
15. Calventus, Y.; Montserrat, S.; Hutchinson, J. M. *Polymer* **2001**, 42, 7081.

16. Cortes, P.; Montserrat, S.; Hutchinson, J. M. *Journal of Applied of Polymer Science* **1997**, 63, 17.

17. Hoyle, C. E.; Lee, T. Y.; Roper, T. *Journal of Polymer Science: Part A: Polymer Chemistry* **2004**, 42, 5301.

18. Roper, T. M.; Rhudy, K. L.; Chandler, C. M.; Hoyle, C. E.; Guymon, C. A. *RadTech NA Tech Conf Proc.* **2002**, 697.

19. Roper, T. M.; Guymon, C. A.; Hoyle, C. E. *Polymer* **2004**, 45, 2921.

20. Lub, J.; Broer, D. J.; Allan, J. F. *Mol Cryst Liq Cryst Sci Tech Sect A: Mol Cryst Liq Cryst* **1999**, 332, 2769.

21. Toh, H. K.; Chen, F.; Kok, C. M. U.S. Patent 6,172,140, **2001**.

22. Cerrada, M. L.; McKenna, G. B. *Macromolecules*, **2000**, 33, 3065.

23. Roe, R-J.; Millman, G. M. *Polymer Engineering and Science*, **1983**, 23, 318.

24. Montserrat, S.; Calventus, Y.; Hutchinson, J. M. *Progress in Organic Coatings*, **2006**, 35, 42.

25. Pellerin, C.; Pelletier, I.; Pezolet, M.; Prud'homme, R. R. *Macromolecules* **2003**, 36, 153.

26. Hutchinson, J. M. *Prog. Polym. Sci.* **1995**, 20, 703.

27. Pan, P.; Zhu, B.; Inoue, Y. *Macromolecules* **2007**, 40, 9664.

28. Ju, H.; Nutt, S. *Macromolecules* **2003**, 36, 4010.

29. Struik, L. C. E. *Polymer*, **1987**, 28, 1869.

30. Struik, L. C. E. *Physical Aging in Amorphous Polymers and Other Materials*, Elsevier Publishing Company: New York, **1978**.

Table 5.1. The extents of enthalpy relaxation at 24h (ΔH_{24h}), overall relaxation rates (β_H), heat capacities at T_g (ΔC_p), and assumed maximum enthalpy relaxation ($\Delta C_p \cdot \Delta T_a$) for photo-polymerized Thiol-Ene networks

Sample #	ΔH_{24h} (J/g)	β_H (J/g per decade)	ΔC_p (J/g·°C)	$\Delta C_p \cdot \Delta T_a^*$ (J/g)
Thiol 1+Ene 1	3.331	1.501	0.5624	5.624
Thiol 1+Ene 2	2.600	1.254	0.5251	5.251
Thiol 1+Ene 3	2.089	0.912	0.3739	3.739
Thiol 2+Ene 1	3.231	1.451	0.4985	4.985
Thiol 2+Ene 2	2.103	1.160	0.3633	3.633
Thiol 2+Ene 3	1.903	0.863	0.3360	3.360
Thiol 3+Ene 1	2.356	1.058	0.3847	3.847
Thiol 3+Ene 2	1.798	0.813	0.3079	3.079
Thiol 3+Ene 3	1.409	0.656	0.2514	2.514

*$\Delta T_a = T_g - T_a = 10$ °C

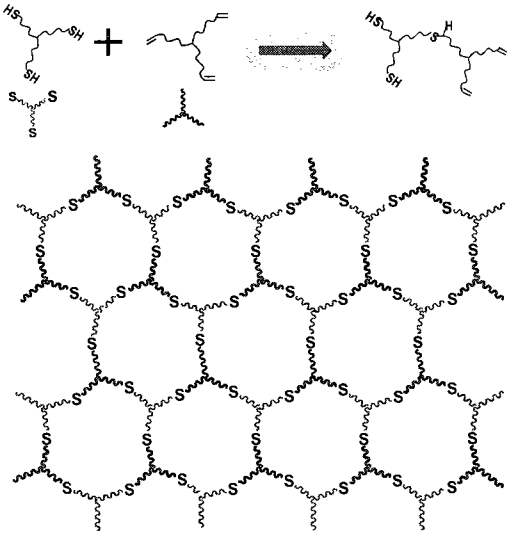

Chart 5.1. Uniform network structure of generic TriThiol-TriEne network.

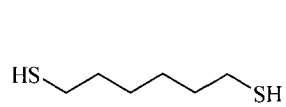

Thiol 1

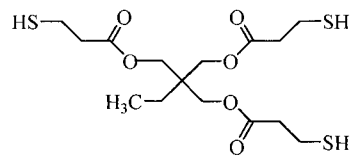

Thiol 2

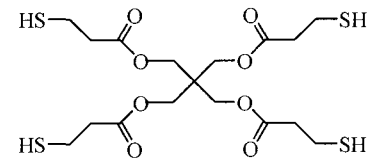

Thiol 3

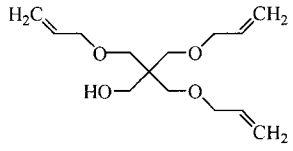

Ene 1

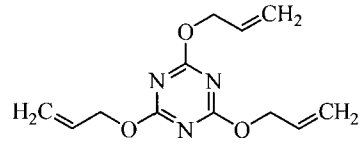

Ene 2

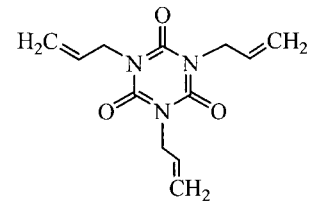

Ene 3

Chart 5.2. The structure of Thiol and Ene monomers.

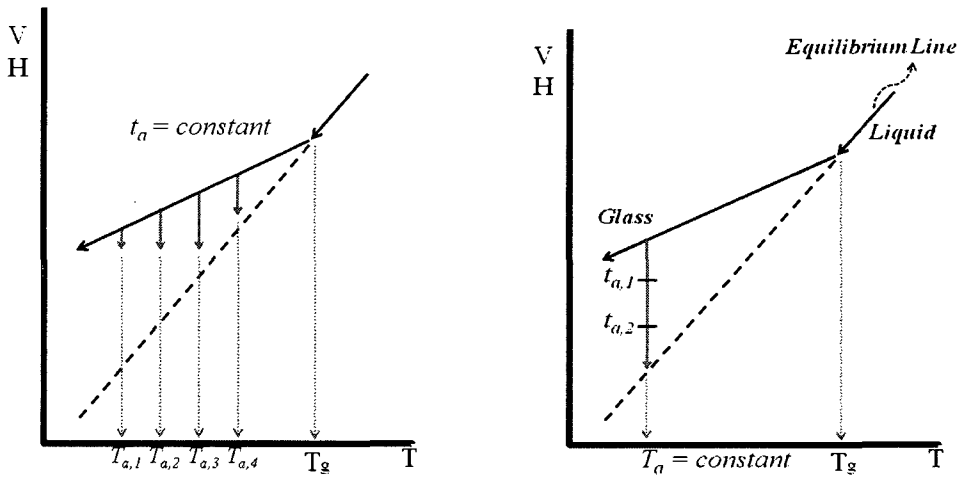

(a) Isochronal method (b) Isothermal method

Figure 5.1. Schematic representation of two annealing methods.[22]

(a) Isochronal process

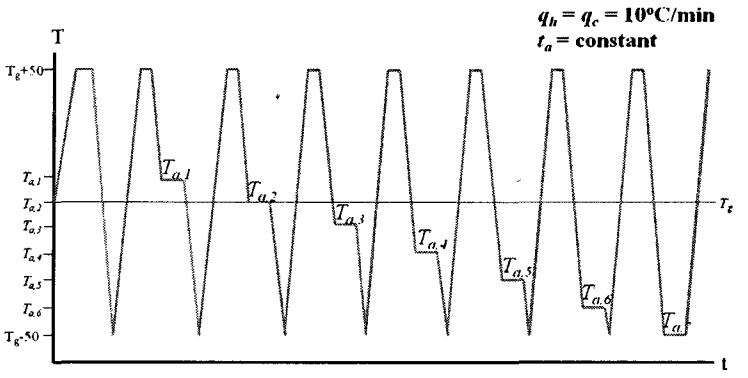

(b) Isothermal process

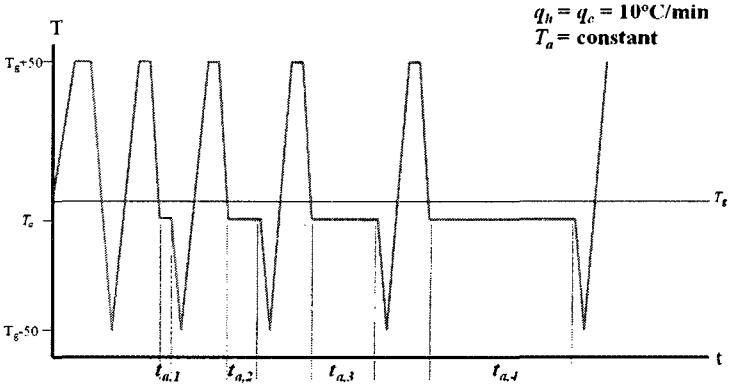

Figure 5.2. Schematic diagrams of isochronal and isothermal physical aging processes.

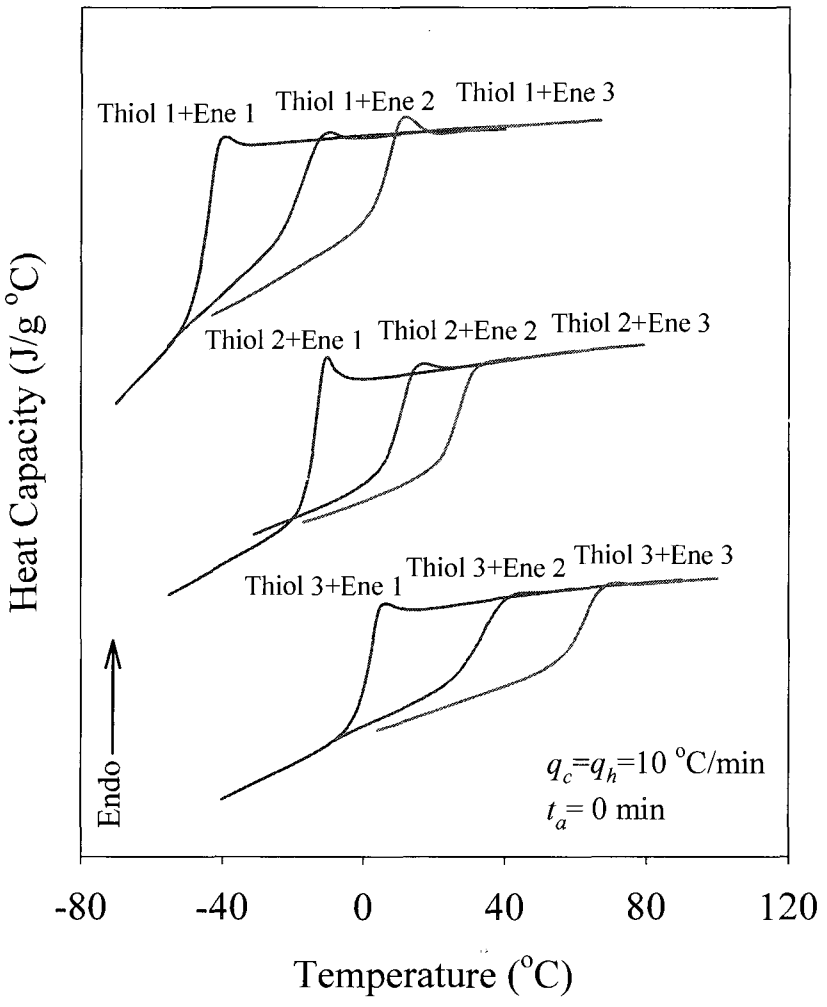

Figure 5.3. DSC thermograms of photo-polymerized Thiol-Ene films (q_c=q_h=10 °C/min, t_a=0 min).

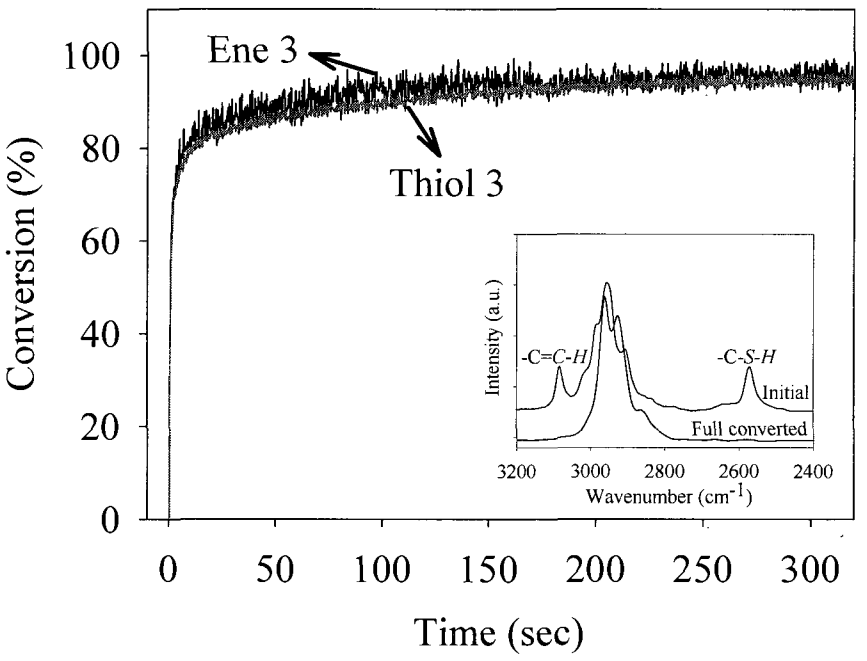

Figure 5.4. Conversion of –SH and -C=C- vs. irradiation time for Thiol 3+Ene 3 system.

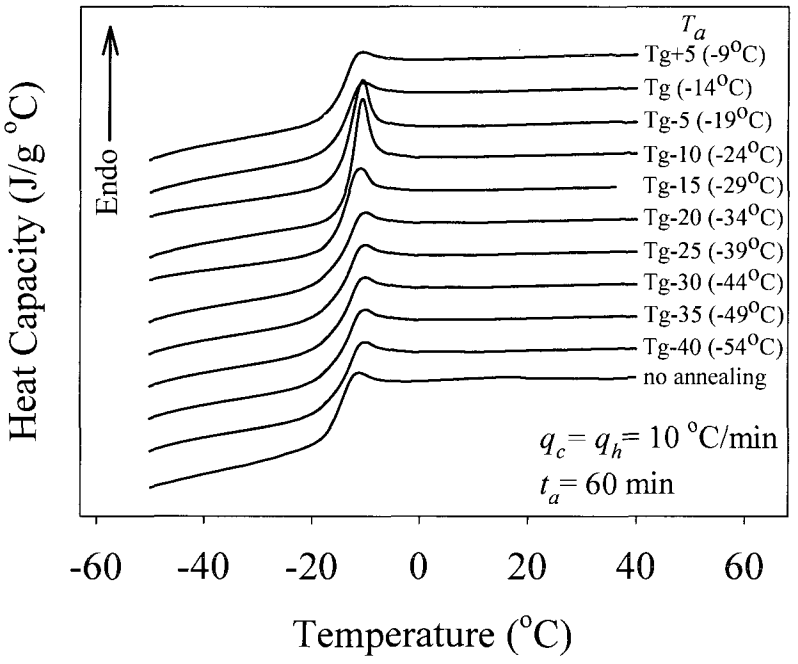

Figure 5.5. DSC heating scans a Thiol-Ene film (Thiol 2+Ene 1) after annealing at different temperatures (t_a=60 min, q_h=q_c=10 °C/min).

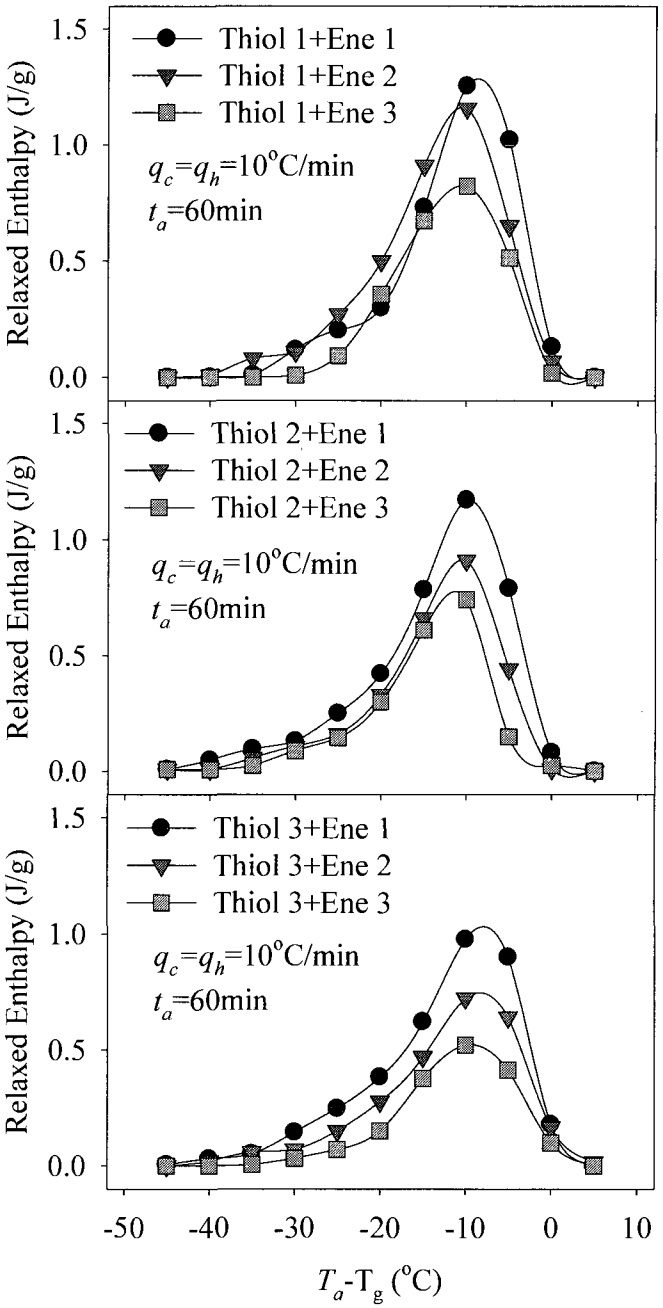

Figure 5.6. Temperature dependency and monomer structural effect on enthalpy relaxation of Thiol-Ene films (t_a=60 min, q_h=q_c=10 °C/min).

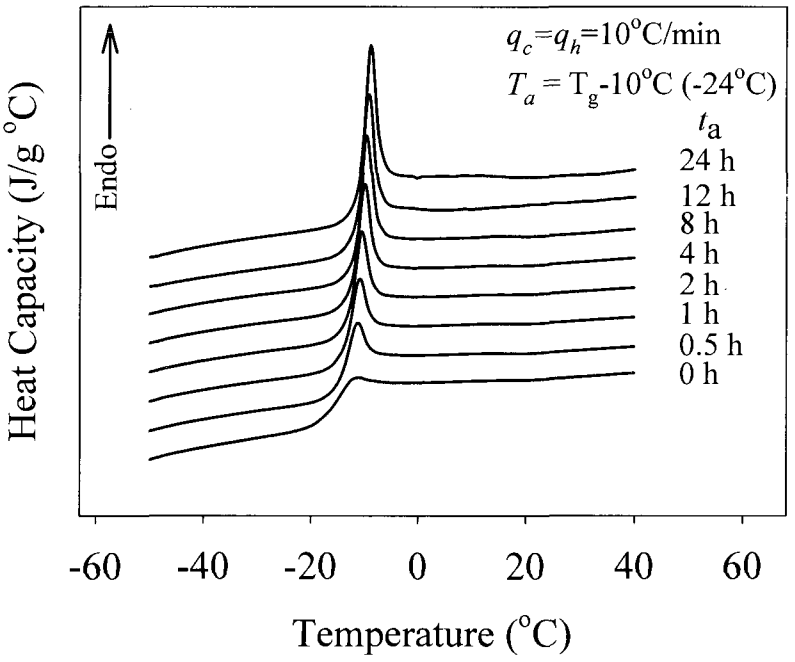

Figure 5.7. DSC heating scans of a Thiol-Ene film (Thiol 2 + Ene 1) after annealing for different annealing time (T_a=T_g-10 °C, q_h=q_c=10 °C/min).

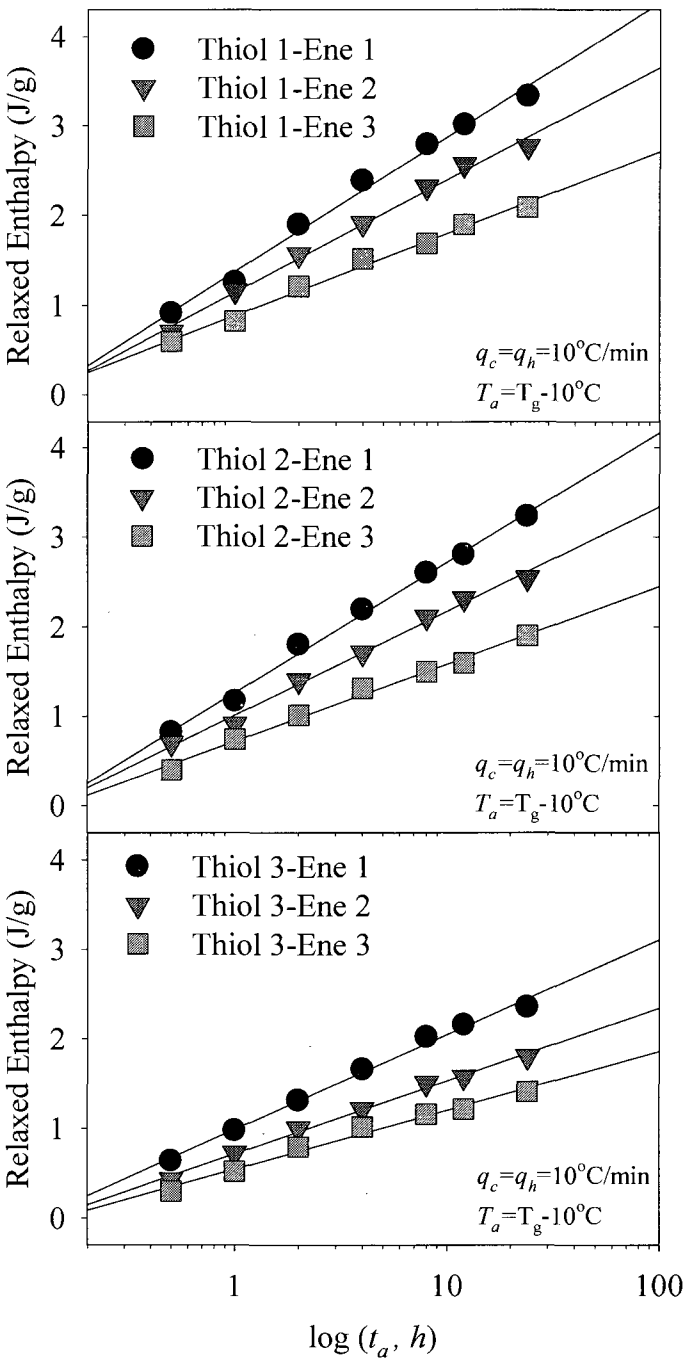

Figure 5.8. Relaxed enthalpy vs. logarithmic annealing time of Thiol-Ene networks (T_a=T_g-10 °C, q_h=q_c=10 °C/min).

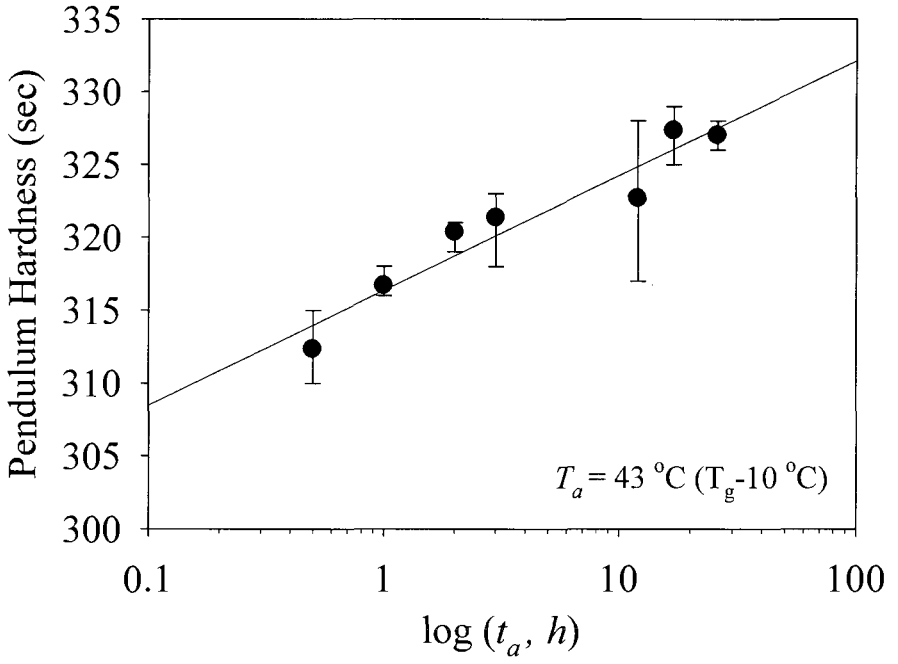

Figure 5.9. Persoz pendulum hardness for Thiol 3-Ene 3 as a function of annealing time (t_a).

CHAPTER VI

EFFECTS OF CHEMICAL MODIFICATION OF THIOL-ENE NETWORKS ON ENTHALPY RELAXATION

Abstract

The highly uniform and dense network structure of photopolymerized thiol-enes was chemically modified, and the enthalpy relaxation of the networks was measured. N-alkyl acrylate and hydroxyl acrylate groups were incorporated into thiol-ene networks using a phosphine catalyzed Michael addition reaction. The effect of flexible alkyl side chains and hydrogen bonding on sub-T_g relaxation was evaluated without sacrificing network uniformity. Overall both the rate and extent of enthalpy relaxation decreased as a function of the flexible n-alkyl chain length, while hydrogen bonding resulted in enhanced enthalpy relaxation. A trithiol-triene-triacrylate ternary system was investigated by correlating enthalpy relaxation and network uniformity. A multifunctional acrylate (TMPTA), being capable of homopolymerization as well as thiol-acrylate copolymerization, was incorporated into a thiol-ene network structure, thereby decreasing the network uniformity and significantly affecting the enthalpy relaxation behavior. In all cases, the extent and rate of enthalpy relaxation were directly related to the heat capacity change at the glass transition which defines the enthalpic departure from equilibrium at a given temperature below T_g.

Introduction

Thiol-ene based networks have many advantages as a result of the unique reaction mechanism (free-radical step growth) by which they are formed and their uniform, high density molecular structures (Figure 6.1(a)).[1-11] The kinetics of formation and physical characterization of thiol-ene networks has attracted much attention during the past decade. Due to their current and future use in a variety of applications as basic network films, there has been considerable interest in characterizing the basis of the thiol-ene networks with several hundred publications in the past 5-7 years, many dealing with applications including nano-lithography, microfluidics, gradient films, frontal polymerization, pillar arrays, and nano-structured networks provided herein for reference.[1-21] An important implication of the uniform highly dense thiol-ene network structure on sub-T_g aging properties was recently reported.[22] It was found that considerable enthalpy relaxation upon physical aging was observed within a narrow temperature range with a maximum relaxation rate at about T_g-10 ^oC for several thiol-Ene films. The extent of the enthalpy relaxation exhibited a linear relationship with the logarithmic annealing time (t_a). Both temperature and time dependency of the enthalpy relaxation process were directly affected by two molecular parameters, the network connectivity density, hereafter referred to as the crosslink density, and the flexibility of the chemical units comprising the network. It was reported that the maximum enthalpy relaxation decreased with the rigidity of the ene structure and an increase in crosslink density resulting from an increase in the thiol functionality. Physical aging of polymers below their glass transition temperature involves the densification of chains resulting in an increase in the apparent glass transition temperature and changes in physical properties. Since many thiol-ene

systems have glass transitions approximately 10 - 30 °C above room temperature, it might be expected that potential problems due to changes in physical and mechanical properties can develop when such materials are aged near room temperature for time periods up to several months.[22]

It is well known that chain mobility and conformational structure changes of polymer systems that affect enthalpy and volume relaxation during physical aging are dependent on molecular weight and molecular weight distribution for linear polymers, and the crosslink-density and distribution of molecular weight between crosslinks for crosslinked polymers.[23-29] It has been shown that molecular mobility in linear polymers can be controlled by structural parameters such as flexible n-alkyl side groups substitutents[30-32] and hydrogen bonding.[33,34] Flexible n-alkyl substituents do not limit backbone rotation of linear polymers, but rather reduce interaction between chains resulting in lowering T_g by an internal plasticization type of effect.[30] Accordingly, it has been suggested that the n-alkyl groups begin movement below T_g resulting in a concomitant increase in heat capacity in the glassy phase and an overall decrease in the heat capacity change (ΔC_p) at T_g. This, of course, affects the rate and extent of sub-T_g physical aging by reducing the thermodynamic force, i.e. ΔC_p, for relaxation. For polymers containing hydroxyl substituents which are capable of forming hydrogen bonding, inter- or intramolecular interactions increase and, as a result, the thermodynamics/kinetics of physical aging and enthalpy relaxation are largely affected. Enthalpy relaxation and free volume changes in linear polystyrene and modified polystyrene copolymer with hydroxyl substituents have been reported.[33,34] The larger extent of enthalpy relaxation for the copolymer was attributed to an enhanced

thermodynamic driving force for relaxation due to a higher heat capacity in the rubbery phase and hence higher ΔC_p value at T_g.

While there have been significant efforts to modify linear polymers and alter their sub-T_g relaxation processes, a systematic chemical structural approach with the intention of restricting or controlling physical aging has not been investigated in detail for thiol-ene networks. A general depiction of a strategy for binding n-alkyl and hydroxyl alkyl acrylate groups chemically into thiol-ene networks is shown in Figure 6.1(b). As thiol-ene networks are highly uniform, they are an excellent platform for assessing how chemical structural parameters can alter the physical phenomenon associated with cross-linked networks in general. In view of the reported effects for linear polymers of n-alkyl groups to induce motion below T_g and hydrogen bonding via hydroxyl groups to enhance heat capacity above T_g, we purport that such effects should also be effective in controlling sub-T_g enthalpy relaxation in thiol-ene networks. This presents an excellent opportunity to not only corroborate a range of effects reported in the literature for linear polymers, but it also provides a systematic approach to defining chemical structural control of sub-T_g relaxation phenomena for networks in general. Using the generalized format in Figure 6.1(b), n-alkyl (i.e. methyl, ethyl, butyl, and hexyl) acrylates and hydroxyl ethyl acrylate were used to functionalize thiol used in the formation of thiol-ene networks, and the extent and rate of enthalpy relaxation was correlated to the heat capacity difference in the glassy and rubbery states and the corresponding enthalpic departure from equilibrium in the glassy phase as determined by ΔC_p. In addition to the modification of thiol-ene networks by substituents, incorporating a third monomer[35-39] (multi-functional (meth)acrylate) that both copolymerizes (with thiol functional groups)

and homopolymerizes is an effective method for altering the physical and mechanical properties of thiol-enes over a very broad range, thus leading to a new class of network architecture that combines the uniformity of thiol-ene networks with the heterogeneity of multi-functional acrylates. Unlike binary thiol-ene based systems which gel at relatively high conversions as dictated by the Flory-Stockmayer gel equation,[40] multi-acrylates gel at much lower conversions (microgelation) and are characterized by very inhomogeneous networks and broad density distributions (Figure 6.1(c)).[41-46] The copolymerization of a multi-functional acrylate (i.e. TMPTA-trimethylolpropane triacrylate) with a thiol-ene system hinders the formation of the traditional thiol-ene uniform dense network structure, leading to a more inhomogeneous network with a broader crosslink density distribution. The appearance of defects in the network uniformity should affect the physical character of thiol-ene networks related to conformational degree of freedom, free volume, and ultimately relaxation processes. In this third approach, the rate and degree of enthalpy relaxation, as influenced by microgelation in the context of the thiol-ene network, was delineated with respect to changes in uniformity and ΔC_p at T_g.

Experimental

Materials

TMPMP (Trimethylolpropane tri-(3-mercapto-propionate), PETMP (Pentaerythritol tetra-(3-mercaptopropionate)), APE (allyl pentaerythritol), and TMPTA (trimethylolpropane triacrylate) were obtained from Bruno Bock Thio-Chemicals-S and Perstorp Specialty Chemicals, respectively. All n-alkyl and hydroxyl ethyl acrylates, TTT (1,3,5-triallyl-1,3,5-triazine-2,4,6(1H,3H,5H)-trione), and DMPPh (dimethyl phenyl

phosphine) were purchased from Aldrich. The structures of all components and corresponding acronyms are shown in Chart 6.1. The photoinitiator, 2,2-dimethoxy 2-phenyl acetophenone (DMPA), was supplied by Ciba Specialty Chemicals. All materials were used as received.

Preparation of n-alkyl/hydroxyl ethyl acrylate modified thiols

The basic structural units used to make the thiol-ene networks which are the subject of the investigation in this paper are shown in Charts 1 and 2. The three and four functional thiols, TMPMP and PETMP, and the two tri-functional enes, TTT and APE, in Chart 6.1 are standard multi-functional thiols and enes typically used to make thiol-ene networks. Several new difunctional and trifunctional thiols (modified di- and trithiols) shown in Chart 6.2 were made by the dimethylphenyl phosphine catalyzed reaction in Scheme 6.1 between the five acrylates in Chart 6.1 (MA, EA, BA, HA and HEA) and PETMP. The thiol structures shown in Chart 6.2 are representative of the predominant chemical structure, with the samples actually consisting of a mixture of un-substituted and multi-substituted components. N-Alkyl and hydroxyl ethyl acrylate modified trithiols were prepared through phosphine catalyzed nucleophilic thiol Michael addition reaction to acrylates.[47-50] PETMP was first mixed with 0.1 wt% of DMPPh while nitrogen purging. N-alkyl or hydroxyl ethyl acrylate was dripped into the mixture for 10 min and the temperature was controlled below 30 ^{o}C with an ice bath in order to prevent acrylates from undergoing thermally initiated free-radical polymerization. 1:1 and 1:2 molar ratios between PETMP and acrylates were used for the modified dithiol and trithiol systems, respectively. After adding acrylates, the mixture was further reacted for 3 h at room temperature until all acrylates were consumed.

Preparation of thiol-ene network films

EATT-TTT and HEATT-TTT mixtures with 1 wt% of DMPA were photo-cured to produce thiol-ene networks. For thiol-ene-acylate ternary systems, equimolar concentrations of TMPMP and APE were used and the molar ratio of TMPTA to TMPMP-APE was varied from 0 to 100% to form ternary networks. DMPA was first dissolve in the n-alkyl / hydroxyl ethyl acrylate modified di- and trithiols for the corresponding thiol-ene systems and TMPMP for thiol-ene-acrylate ternary systems by sonication for 30 minutes. Thiol (-SH) and ene (-C=C-) concentrations were held constant at 1:1 equiv for all thiol-ene networks. Films were cast on glass plates (200 μm) and cured on a Fusion UV curing line system with a D bulb (400 W/cm^2) having a belt speed of 10 feet/min and irradiance of 3.1 W/cm^2. All samples were post-cured at 80 °C for 24 h to insure complete reaction and eliminate any possibility of chemical conversion effect on enthalpy relaxation during sub-T_g annealing.

Characterization

The thiol Michael addition reaction with PETMP and acrylates using DMPPh catalyst was monitored by FT-infrared (FTIR) spectroscopy and NMR. The complete disappearance of acrylate carbon double bonds was confirmed by peaks at 812 cm^{-1} for FTIR, 5.71(q), 5.99(q), and 6.23(q) ppm for ^{1}H NMR, and at 128.3 and 130.5 ppm for ^{13}C NMR. A modified Bruker IFS 88 FTIR spectrometer was equipped with a horizontal sample accessory and thin samples (25 μm) were placed between two salt plates sealed with silicon in the FTIR. A small sample was taken every 30 min during reaction for FTIR measurements. After confirmation with FTIR, NMR measurements were conducted. ^{1}H and ^{13}C NMR spectra of the modified di- and trithiols in Chart 6.2 were

obtained on a Varian 300 MHz NMR in $CDCl_3$ with tetramethysilane (TMS) as the internal reference. FTIR and NMR spectra of the thiol Michael addition reaction with acrylate have been reported in the literature.[47-50]

Glass transition temperatures and enthalpy relaxation for all networks were characterized with a TA Q1000 differential scanning calorimeter (DSC) with RCS 90 (Refrigerated Cooling System). A RCS 90 cooling head mounted on the DSC Q1000 furnace encases the DSC cell preventing frost building-up during operation. Three calibration steps (T_{zero} calibration, enthalpy constant calibration, and Temperature calibration) for the TA Q1000 were performed periodically. Detailed calibration protocol has been well described in a previous report.[22] The glass transition region and heat capacity change (ΔC_p) at T_g were characterized as described in the literature.[51-52] The beginning ($T_{g,i}$) and end ($T_{g,e}$) of the glass transition were determined as the temperature where the heat capacity starts to increase from the glassy phase and where it finally attains a constant value in the liquid state, respectively. T_g was defined by the temperature of the inflection point in the heat capacity versus temperature plot in the glass transition region. ΔC_p was obtained by the heat capacity difference between the extrapolated lines of the glass and rubber heat capacities at T_g. Special attention was paid to running the DSC to ensure the accuracy of the enthalpy relaxation measurement. For two different annealing methods described in Figure 6.2, the measurement was conducted twice and the sequence of annealing was reversed in the second running. Equivalent results were obtained in each case, i.e., instrumental drift did not play a factor, and the results were reproducible despite the different order in obtaining the data sets. Furthermore, the heat flow and heat capacity of the TMPMP-APE sample without aging,

as a standard, were measured after every calibration and time-sequence scan to ensure consistency. Finally, in order to remove sampling errors, the same DSC pans (samples) were used for all measurements. All experiments were carried out under nitrogen with a flow rate of 50 mL/min. Sample weights were 8.0±1.0 mg to ensure sufficient sensitivity for heat capacity measurements. DSC scans were conducted over the temperature range of ±50 °C from the glass transition region ($T_{g,i}$~$T_{g,e}$). Annealing temperature (T_a) and annealing time (t_a) were controlled to establish different annealing methods. Detailed descriptions of measurement techniques are described in the text.

Results and Discussion

In this chapter, we focus on defining the role of chemical structure of the basic thiol-ene networks and the modified dithiol-ene and modified trithiol-ene networks (see Charts 1 and 2 for component structures) on enthalpy relaxation. Sub-T_g aging is both a temperature and time dependent physical phenomenon. Hence, the thiol-ene networks were equilibrated above T_g to remove prior thermal history and quenched to a temperature T_a (< T_g), at which the aging process occurs. The subsequent enthalpy was monitored upon reheating a sample through its glass transition. Equilibration achieved by maintaining the sample for 10 minutes at a temperature above T_g ($T_{g,e}$+50 °C) effectively erases the previous thermal history, and is necessary in order to initialize the sample for physical aging. Enthalpy relaxation was studied by two different approaches whose schematic representations are shown in Figure 6.2: (a) *isochronal* and (b) *isothermal*.[53] The isothermal method provides information on the time dependency of the

enthalpy relaxation processes, while the isochronal method assesses the temperature dependency of the relaxation processes.

n-Alkyl acrylate modified thiol-ene networks

To evaluate the effect of flexible alkyl side chains on the sub-T_g annealing of thiol-ene networks, equimolar functional group mixtures of all of the MA, EA, BA, and HA modified trithiols in Chart 6.2 with TTT were photopolymerized. Thermal transitions of the resultant thiol-ene networks were characterized by DSC, and the results are summarized in Table 6.1. First, it is noted that the DSC glass transition breadth ($T_{g,e}$-$T_{g,i}$) for four different n-alkyl acrylate modified thiol-TTT networks is almost identical indicating that the uniformity of the thiol-ene networks is very high and not affected by the flexible n-alkyl substituent. Second, the glass transition temperature decreases progressively as the length of the n-alkyl chain in the modified trithiol-TTT network increases from methyl to hexyl, consistent with the results observed for n-alkyl acrylate homopolymers where the longer more flexible n-alkyl chain acts as an internal plasticizer.[30,32,54] Concomitantly, the heat capacity change (ΔC_p) at T_g (see Table 6.1) also decreases as the number of methylene groups on the acrylate increases from methyl to hexyl. Hatakeyama et al.[31] has reported that side chain n-alkyl groups on linear polymer can sustain rotational motion below T_g, hence raising the specific heat capacity in the glassy state and thus lowering the change in heat capacity going from the glassy to rubbery state at T_g. We thus project that flexible n-alkyl side chains incorporated into thiol-ene networks also begin rotational motion at a temperature below T_g, thereby increasing the specific heat capacity below T_g, with the concomitant decrease in ΔC_p with increase in the n-alkyl chain length (Table 6.1).

The n-alkyl acrylate modified trithiol-TTT networks were next annealed at specific temperatures (T_a-annealing temperature) every 5 °C from T_g+10 to T_g-45 °C for a time, t_a (60 min), to investigate the temperature dependency of enthalpy relaxation. The schematic diagram of the isochronal process is shown in Figure 6.2(b). The extent of enthalpy relaxation was calculated from the difference thermograms using Equation (1),[22,55-57]

$$\Delta H_r(T_a,t_a) = \int_{T_g-50^oC}^{T_g+50^oC}[C_p(T_a,t_a)-C_p(T_a,0)]dT \qquad \text{Equation (1)}$$

where $C_p(T_a, t_a)$ and $C_p(T_a, 0)$ represent specific heat capacities for samples annealed at T_a for $t=t_a$ and unannealed samples, respectively. The relaxed enthalpies as a function of T_a-T_g for all n-alkyl acrylate modified trithiol-TTT networks are shown in Figure 6.3. The asymmetric bell-shaped enthalpy relaxation curves occur over a narrow temperature range (~20 °C) with the maxima at about T_g-10 °C for each system, consistent with the results found for basic un-modified thiol-ene networks.[22] The position of the maxima are dictated by the relaxation rates which are set by a combination of the enthalpic departure from equilibrium and the characteristic enthalpic relaxation time at an annealing temperature (T_a) for a given time (t_a, 60 min).[22,58] Based on the results in Figure 6.3, the extent of enthalpy relaxation at the peak maxima of each T_a-T_g versus relaxed enthalpy plot decreases as the n-alkyl chain length increases. If each sample is annealed at T_a-T_g = -10 °C, the $\Delta T_{maximum}$ for each network in Figure 6.3, the relaxed enthalpy after 24 hours (ΔH_{24}) can be obtained. As shown in Table 6.1, the ΔH_{24} values also decrease with increasing n-alkyl chain length. Furthermore, the product of ΔC_p and ΔT ($|T_a$-$T_g|$) in

Table 6.1, where ΔT = 10 °C, also decreases with the n-alkyl chain length. The $\Delta C_p \cdot \Delta T$ product is indicative of the ultimate departure of enthalpy from equilibrium conditions at the annealing temperature. Hence, based on the extent of enthalpy relaxation at the peak maximum in Figure 6.3, the value for ΔH_{24}, and the $\Delta C_p \cdot \Delta T$ product (Table 6.1), it can be concluded that the supposition of increased rotational motion afforded by increasing alkyl chain length in side chain substituent of linear polymers in the glassy phase[30-31] also applies to n-alkyl chain substituent in uniform thiol-ene networks.

Figure 6.4 shows the plot of enthalpy relaxation of n-alkyl acrylate modified trithiol-TTT networks as a function of annealing time (t_a) at T_g-10 °C, the temperature where enthalpy relaxation exhibited a maximum during the isochronal analysis in Figure 6.3. The extent of enthalpy relaxation consistently increased with annealing time at T_a-T_g = -10 °C and a linear relationship between the extents of enthalpy relaxation vs. logarithmic annealing time is obtained. A simple quantitative method is used to analyze the general overall relaxation rate (β_H)[22,59-62] according to Equation (2),

$$\beta_H = \frac{d\delta_H}{d\log t_a} \qquad \text{Equation (2)}$$

where δ_H is the extent of enthalpy relaxation and t_a is the annealing time at T_a-T_g. The general overall relaxation rate (β_H) obtained by the slopes of each plot in Figure 6.4 (see Table 6.1) shows that the enthalpy relaxation rate of n-alkyl acrylate modified trithiol-TTT networks decreases with the length of n-alkyl acrylate substituent, consistent with the decrease in departure of the enthalpy from equilibrium as defined by the $\Delta C_p \cdot \Delta T$

product in Table 6.1. It is clear that the smaller excess enthalpy obtained by incorporating flexible n-alkyl acrylates into the thiol-ene networks results in a slower overall enthalpy relaxation rate (β_H), corroborating the results found for ΔH_{24}.

Hydroxyl alkyl acrylate nodified thiol-ene networks

The hydrogen bonding effect on enthalpy relaxation was next investigated by comparing networks formed from HEATT -TTT, EATT-TTT, HEADT-TTT, and EADT-TTT systems (see Chart 6.2 for description of components). Results of the basic DSC heating scans, T_gs and ΔC_ps, are summarized in Table 6.2. According to the speculation in the Introduction based on linear polymers,[31,33,34] the HEADT-TTT and HEATT-TTT networks have higher T_gs and ΔC_p values than for the EADT-TTT and EATT-TTT networks. The increase in T_g and ΔC_p is more pronounced for the HEADT-TTT based networks since the effect of hydrogen bonding would be expected to be more effective in a system of lower chemical crosslink density. The higher ΔC_p values at T_g for the hydrogen bonding networks containing HEA mainly results from the onset of contributions from hydrogen bonding to the heat capacity at temperatures greater than T_g (rubbery state). In other words, hydrogen bonding opens up another mode (breaking or bending of hydrogen bonds) for dissipation of the thermal energy needed to increase temperature in the rubbery state in additional to translational, rotational, and vibrational contributions to the heat capacity.[31,33,34,63]

The effect of hydrogen bonding on temperature and time dependency of enthalpy relaxation were next investigated using isochronal and isothermal DSC measurements. In Figure 6.5, the relaxed enthalpies as a function of T_a-T_g for the HEADT-TTT and HEATT-TTT networks obtained using Equation (1) are seen to exhibit similar peak

maxima at T_g-10 °C to that observed for EADT-TTT and EATT-TTT networks, with the caveat that the extent of enthalpy relaxation of the networks from HEADT-TTT and HEATT-TTT are higher than the corresponding EADT-TTT and EATT-TTT networks. In order to more clearly characterize the effect of hydrogen bonding on enthalpy relaxation, isothermal annealing measurements were conducted. Based on the general overall relaxation rate (β_H) and ΔH_{24h} (Figure 6.6 and Table 6.2), it is obvious that the enthalpy relaxation rates for thiol-ene networks is enhanced by incorporating hydrogen bonding, consistent with the values for $\Delta C_p \cdot \Delta T$ (Table 6.2), an estimate for the enthalpic departure from equilibrium at the annealing temperature. The greater incremental increase in $\Delta C_p \cdot \Delta T$ and ΔH_{24h} for the HEADT-TTT network compared to the HEATT-TTT network results from the lower chemical network crosslink density for the dithiol based networks.

TMPMP-APE-TMPTA ternary system

Thiol-ene-acrylate ternary systems were next used to investigate the effect of network uniformity on sub-T_g aging. Figure 6.7 shows the DSC heating scans and glass transition for the photopolymerized binary TMPMP-APE network and TMPTA homopolymer. As discussed already, due to the network uniformity, TMPMP-APE has a very narrow glass transition temperature region and a distinct enthalpy relaxation peak around T_g obtained by DSC scanning of the pre-cooled sample at 10 °C/min cooling (q_c) followed by an immediate (no time for extended aging at a single annealing temperature) subsequent heating at a rate (q_h) of 10 °C/min (Figure 6.7 (a)). Concomitantly, photopolymerized TMPTA has an inhomogeneous crosslinked structure with a wide variation of crosslink densities and corresponding microgel structures,[41-46] as well as

dangling chain ends,[6,35] resulting in a very broad glass transition region and no clearly defined enthalpy relaxation peak (Figure 6.7 (b)).

To define the effect of sub-T_g annealing of ternary thiol-ene-acrylate networks, systems were prepared by mixing TMPMP-APE with increasing TMPTA concentrations (10, 20, 30, 40, 50, and 60 mole %). The basic DSC glass transition temperature and breadth ($T_{g,e}$-$T_{g,i}$) increases as a function of TMPTA content (Figure 6.8 and Table 6.3). It is clear that incorporating TMPTA into the thiol-ene network successfully decreases the network uniformity due to the microgel formation by TMPTA homopolymerization, acting like rigid amorphous region, restricts molecular mobility of thiol-ene networks, consistent with previous reports for other ternary thiol-ene-(meth)acrylate systems.[6,35]

The restriction of molecular mobility in the thiol-ene network by incorporation of the third component leads to a reduction of ΔC_p values. As shown in Figure 6.9, ΔC_p at T_g of TMPMP-APE-TMPTA also significantly decreases as a function of TMPTA content due to restriction of internal degrees of freedom resulted from the microgelation of TMPTA accompanied by broadened distribution of network/crosslink density and consequent broad glass transition temperature range and distribution of relaxation times. The restriction of molecular mobility above T_g which reduces the heat capacity in the rubbery phase, obviously results in a decrease in the relaxed enthalpy after 24 h (ΔH_{24h}) as well as ultimate enthalpy relaxation ($\Delta C_p \cdot \Delta T$) as a function of TMPTA content as shown in Table 6.3.

The broadening of the temperature range and restrictive effect on enthalpy relaxation by incorporating TMPTA into the TMPMP-APE network is even more obvious when characterized by temperature dependent (isochronal) analysis (Figure 6.10)

and time-dependency (isothermal) measurements (Figure 6.11 and 4.12). The relaxed enthalpy (δ_H) versus sub-T_g aging temperature for TMPMP-APE-TMPTA ternary films in Figure 6.10 obtained by Equation 1 using isochronal analysis clearly exhibits a dramatic broadening and decrease in δ_H at a given temperature below T_g as a function of TMPTA content, consistent with the decrease in $\Delta C_p \cdot \Delta T$, the enthalpic departure from equilibrium at the annealing temperature. Interestingly, the maximum values for δ_H for all TMPMP-APE-TMPTA samples are still observed at about T_g-10 °C, consistent with results for the n-alkyl/hydroxyl ethyl acrylate modified thiol-ene networks discussed in previous sections and reported for several binary thiol-ene systems.[22] In Figure 6.11, the overshoot effect for enthalpy relaxation decreases progressively with increasing TMPTA content. The overall enthalpy relaxation rate (β_H) obtained from the slopes of the plots in Figure 6.12 in Table 6.3 decreases as a function of TMPTA content indicating that β_H is affected by inclusion of the third monomer (TMPTA) in the TMPMP-APE network, i.e., the multifunctional acrylate both copolymerizes (with TMPMP) and homopolymerizes thereby decreasing the network uniformity and reducing the physical aging process. In other words, the enthalpy relaxation is not concentrated over a narrow temperature breadth.

Conclusions

Thiol-ene networks were chemically modified to provide unprecedented control of enthalpy relaxation via three methods: incorporation of (1) n-alkyl side chains, (2) hydrogen bonding hydroxyl substituents, and (3) a third (acrylate) component (ternary system). n-Alkyl and hydroxyl alkyl side chain groups were incorporated into the

network using chemically modified multi-functional thiols to investigate the effect of flexible alkyl side chains and hydrogen bonding on enthalpy relaxation of thiol-ene networks without sacrificing their characteristic network uniformity. In all of the modified networks, the breadth of the glass transition temperature was not affected by the side chain appendages since the base crosslink density and network chemical structure was not altered. T_g, ΔC_p, and ΔH_{24} decrease with an increase in the length of the alkyl chain due to the internal plasticizing effect of flexible alkyl side chains. Hydrogen bonding by hydroxyl substituents requires additional enthalpy involved in long-range segmental motions leading to higher heat capacity differences at T_g and, as a resultant, a larger extent of enthalpic deviation from equilibrium at temperature below T_g. For the networks with appended alkyl and hydroxyl side groups, the rate of enthalpy relaxation at a specific temperature below T_g was found to be directly related to the deviation from enthalpic equilibrium as determined by the product $\Delta C_p \cdot \Delta T$. A triacrylate (TMPTA) was also incorporated into the thiol-ene network structure to investigate the effect of the network uniformity on physical aging behavior. The extent of enthalpy relaxation decreased and the distribution was drastically broadened as a function of TMPTA content. It is concluded that network uniformity is a critical factor affecting sub-T_g relaxation of thiol-ene based networks. In addition, the restrictive effect of the rigid amorphous region by microgelation of TMPTA homopolymerization results in decreasing the enthalpic relaxation rate and corresponding extent of the relaxed enthalpy in 24 h (ΔH_{24h}) based on the decrease in the enthalpic deviation from equilibrium at the annealing temperature ($\Delta C_p \cdot \Delta T$).

References

1. Hoyle, C. E.; Lee, T. Y.; Roper, T. *J. Polym. Sci., Part A: Polym. Chem.* **2004**, 42, 5301.
2. Cramer, N. B.; Bowman, C. N. *J. Polym. Sci., Part A: Polym. Chem.* **2001**, 39, 3311.
3. Cramer, N. B.; Reddy, S. K; Cole, M.; Hoyle, C. E.; Bowman, C. N. *J. Polym. Sci., Part A: Polym. Chem.* **2004**, 42, 5817.
4. Khire, V. S.; Harant, A. W.; Watkins, A. W.; Anseth, K. S.; Bowman, C. N. *Macromolecules* **2006**, *39,* 5081.
5. Senyurt, A. F.; Hoyle, C. E.; Wei, H.; Piland, S. G.; Gould, T. E. *Macromolecules* **2007**, 40, 3174.
6. Wei, H.; Senyurt, A. F.; Jönsson, S.; Hoyle, C. E. *J. Polym. Sci., Part A: Polym. Chem.* **2007**, 45, 822.
7. Roper, T. M.; Guymon, C. A.; Jönsson, E. S.; Hoyle, C. E. *J. Polym. Sci., Part A: Polym. Chem.* **2004**, 42, 6283.
8. Lee, T. Y.; Roper, T. M.; Jönsson, E. S.; Guymon, C. A.; Hoyle, C. E. *Macromolecules* **2004**, 37, 3606.
9. Li, Q.; Zhou, H.; Wicks, D. A.; Hoyle, C. E. *J. Polym. Sci., Part A: Polym. Chem.* **2007**, 45, 5103.
10. Wei, H.; Li, Q.; Ojelade, M.; Madbouly, S.; Otaigbe, J. U.; Hoyle, C. E. *Macromolecules* **2007**, 40, 8788.
11. Senyurt, A. F.; Warren, G.; Whitehead, J. B.; Hoyle, C. E. *Polymer* **2006**, 47, 2741.
12. Moran, I. W.; Briseno, A. L.; Loser, S.; Carter, K. R.; *Chem. Mater.* **2008**, *20*, 4595.

13. Yi, Y. W.; Khire, V.; Bowman, C. N.; Maclennan, J. E.; Clark, N. A. *J. Appl. Phys.* **2008**, *103*, 6.

14. Good, B. T.; Reddy, S.; Davis, R. H.; Bowman, C. N. *Sensors and Actuators B-Chemical* **2007**, *120*, 473.

15. Pojman, J. A.; Varisli, B.; Perryman, A.; Edwards, C.; Hoyle, C. E. *Macromolecules* **2004**, *37*, 691.

16. Khire, V. S.; Benoit, D. S. W.; Anseth, K. S.; Bowman, C. N. *J. Polym. Sci., Part a-Polym. Chem.* **2006**, *44*, 7027.

17. Khire, V. S.; Harant, A. W.; Watkins, A. W.; Anseth, K. S.; Bowman, C. N. *Macromolecules*, **2006**, 39, 5081.

18. Dickey, M. D.; Collister, E.; Raines, A.; Tsiartas, P.; Holcombe, T.; Sreenivasan, S. V.; Bonnecaze, R. T.; Willson, C. G. *Chem. Mater.* **2006**, *18*, 2043.

19. Fox, A. E.; Fontecchio, A. K. *App. Phys. Lett.* **2007**, *91*, 3.

20. Campos, L. M.; Meinel, I.; Guino, R. G.; Scheirhorn, M.; Gupta, N.; Stucky, G. D.; Hawker, C. J. *Adv. Mater.* **2008**, 20, 3728.

21. Sangermano, M.; Gross, S.; Priola, A.; Rizza, G.; Sada, C. *Macro. Chem. and Phys.* **2007**, *208*, 2560.

22. Shin, J.; Nazarenko, S.; Hoyle, C. E. *Macromolecules* **2008**, 41, 6741.

23. Lin, Y. G.; Sauterreau, H.; Pascault, J. P. *J. App. Polym. Sci.* **1986**, 32, 4595.

24. Lee, A.; McKenna, G. B. *Polymer* **1988**, 29, 1812.

25. Huang, D.; Yang, Y.; Zhuang, G.; Li, B. *Macromolecules* **1999**, 32, 6675.

26. Huang, D.; Yang, Y.; Zhuang, G.; Li, B. *Macromolecules* **2000**, 33, 461.

27. Privalko, V. P.; Demchenko, S. S.; Lipatov, Y. S. *Macromolecules* **1986**, 19, 901.

28. Andreozzi, L.; Faetti, M.; Giordano, M.; Zulli, F. *Macromolecules* **2005**, 38, 6056.

29. Mark, J. E.; Erman, B. *Elastomeric Polymer Network*, Prentice Hall, Inc.: New Jersey, **1992**.

30. Mays, J. W.; Siakali-Kioulafa, E.; Hadjichristidis, N. *Macromolecules* **1990**, 23, 3530.

31. Hatakeyama, T.; Hatakeyama, H. *Thermochimica Acta* **1995**, 267, 249.

32. Cypcar, C. C.; Camelio, P.; Lazzeri, V.; Mathias, L. J.; Waegell, B. *Macromolecules* **1996**, 29, 8954.

33. Schroeder, M. J.; Roland, C. M.; Kwei, T. K. *Macromolecules* **1999**, 32, 6249.

34. McGonigle, E. A.; Cowie, J. M. G.; Arrighi, V.; Pethrick, R. A. *J. Mat. Sci.* **2005**, 40, 1869.

35. Senyurt, A. F.; Wei, H.; Phillips, B.; Cole, M.; Nazarenko, S.; Hoyle, C. E.; Piland, S. G.; Gould, T. E. *Macromolecules* **2006**, 39, 6315.

36. Lee, T. Y.; Smith, Z.; Reddy, S. K.; Reddy, S. K.; Cramer, N. B., Bowman, C. N. Macromolecules **2007** 40, 1466.

37. Lee, T. Y.; Carioscia, J.; Smith, Z.; Bowman, C. N. *Macromolecules* **2007**, 40, 1473.

38. Rydholm, E.; Held, N. L.; Bowman, C. N.; Anseth, K. S. *Macromolecules* **2006**, 39, 7882.

39. Carioscia, J. A.; Stansbury, J. W.; Bowman, C. E. *Polymer*, 2007, 48,

40. Jacobian, A. F. *In Radiation Curing in Polymer Science and Technology III*; Fouassier, J. D.; Rabek, J. F., Eds; Elsevier: London, **1993**; Chapter 7.

41. Boots, H. M. J.; Kloosterboer, J. G.; van de Hei, G. M. M. *Bri. Polym. J.* **1985**, 17, 219.

42. Elliott, J. E; Bowman, C. N. *Macromolecules* **1999**, 32, 8621.

43. Lovestead, T. M.; Bowman, C. N. *Macromolecules* **2005**, 38, 4913.

44. Kloosterboer, J. G.; Lijten, G. F. C. M.; Boots, H. M. J. *Makromol. Chem., Macromol. Symp.* **1989**, 24. 223.

45. Bowman, C. N.; Anseth, K. S. *Macromol. Symp.* **1995**, 93, 269.

46. Kannurpatti, A. R.; Anseth, J. W.; Bowman, C. N. *Polymer* **1998**, 39, 2507.

47. Lee, T. Y.; Kaung, W.; Jonsson, E. S.; Lowery, K.; Guymon, C. A.; Hoyle, C. E. *J. Polym. Chem.: Part A: Polym. Chem.* **2004**, 42, 4424.

48. Kilambi, H.; Stansbury, J. W.; Bowman, C. N. *J. Polym. Chem.: Part A: Polym. Chem.* **2008**, 46, 3452.

49. Chan, J. W.; Yu, B.; Hoyle, C. E.; Lowe, A. B. *Chem.Commun.* **2008**, 4959.

50. Shin, J.; Matsushima, H.; Chan. J. W.; Hoyle, C. E. *Macromolecules* **2009**, 42, 3294.

51. Cheng, S. Z. D.; Cao, M.-Y.; Wunderlich, B. *Macromolecules* **1986**, 19, 1868.

52. Mathot, B. F. *Calorimetry and Thermal Analysis of Polymers*, Munich: Hanser; **1993**.

53. Cerrada, M. L.; McKenna, G. B. *Macromolecules*, **2000**, 33, 3065.

54. Sperling, L. H. *Introduction to Physical Polymer Science*, John Wiley & Sons, Inc.: New York, **1992**.

55. Pellerin, C.; Pelletier, I.; Pezolet, M.; Prud'homme, R. R. *Macromolecules* **2003**, 36, 153.

56. Roe, R-J.; Millman, G. M. *Polym. Eng. Sci.* **1983**, 23, 318.

57. Montserrat, S.; Calventus, Y.; Hutchinson, J. M. *Prog. Org. Coat.* **2006**, 55, 35.

58. Gedde, U. W. *Polymer Physics*, Chapman & Hall: London, **1995**.

59. Hutchinson, J. M. *Prog. Polym. Sci.* **1995**, 20, 703.

60. Pan, P.; Zhu, B.; Inoue, Y. *Macromolecules* **2007**, 40, 9664.

61. Struik, L. C. E. *Polymer*, **1987**, 28, 1869.

62. Struik, L. C. E. *Physical Aging in Amorphous Polymers and Other Materials*, Elsevier Publishing Company: New York, **1978**.

63. Cooper, A. *Biophysical Chem.* **2000**, 85, 25.

Table 6.1. The extents of enthalpy relaxation at 24 h (ΔH_{24}), overall relaxation rate (β_H), T_g, $T_{g,e}$-$T_{g,i}$, and assumed maximum enthalpy relaxation ($\Delta C_p \cdot \Delta T$) for photopolymerized n-alkyl acrylate modified thiol-ene networks

Sample #	β_H (J/g per decade)	ΔH_{24} (J/g)	T_g (°C)	ΔC_p (J/g·°C)	$\Delta C_p \cdot \Delta T^*$ (J/g)	$T_{g,e}$-$T_{g,i}$ (°C)
MATT-TTT	1.18	2.32	9.8	0.47	4.75	10.9
EATT-TTT	1.15	2.26	6.2	0.46	4.59	12.0
BATT -TTT	1.06	2.09	-0.2	0.44	4.39	13.5
HATT -TTT	0.96	1.91	-3.2	0.40	3.99	14.5

$^*\Delta T = |T_a - T_g| = 10$ °C

Table 6.2. The extents of enthalpy relaxation at 24 h (ΔH_{24}), overall relaxation rate (β_H), T_g, $T_{g,e}$-$T_{g,i}$, and assumed maximum enthalpy relaxation ($\Delta C_p \cdot \Delta T$) for photopolymerized ethyl/hydroxyl ethyl acrylate modified thiol-ene networks

Sample #	β_H (J/g per decade)	ΔH_{24} (J/g)	T_g (°C)	ΔC_p (J/g·°C)	$\Delta C_p \cdot \Delta T^*$ (J/g)	$T_{g,e}$-$T_{g,i}$ (°C)
EADT-TTT	1.35	2.70	-26.8	0.54	5.45	11.8
HEADT-TTT	1.57	3.30	-14.0	0.62	6.24	15.7
EATT-TTT	1.15	2.26	6.2	0.46	4.59	11.3
HEATT -TTT	1.24	2.42	12.8	0.48	4.79	12.4

*$\Delta T = |T_a - T_g| = 10$ °C

Table 6.3. The extents of enthalpy relaxation at 24 h (ΔH_{24}), overall relaxation rate (β_H), T_g, $T_{g,e}$-$T_{g,i}$, and assumed maximum enthalpy relaxation ($\Delta C_p \cdot \Delta T$) for photopolymerized TMPMP-APE-TMPTA ternary system

Sample #	β_H (J/g per decade)	ΔH_{24} (J/g)	T_g (°C)	ΔC_p (J/g·°C)	$\Delta C_p \cdot \Delta T^*$ (J/g)	$T_{g,e}$-$T_{g,i}$ (°C)
TMPMP-APE	1.46	3.25	-15.1	0.50	4.99	4.0
TMPMP -APE-10mol% TMPTA	1.34	3.01	-8.1	0.48	4.82	6.2
TMPMP -APE-20mol% TMPTA	1.02	2.19	5.7	0.41	4.05	11.5
TMPMP -APE-30mol% TMPTA	0.79	1.74	5.2	0.37	3.65	17.3
TMPMP -APE-40mol% TMPTA	0.64	1.40	21.1	0.31	3.12	24.3
TMPMP -APE-50mol% TMPTA	0.48	1.02	42.9	0.24	2.44	37.2
TMPMP -APE-60mol% TMPTA	0.32	0.73	ND**	ND**	ND**	ND**

*$\Delta T = |T_a - T_g| = 10$ °C

**not defined by DSC

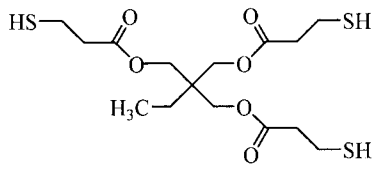

TMPMP

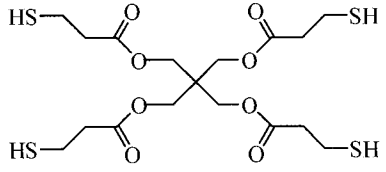

PETMP

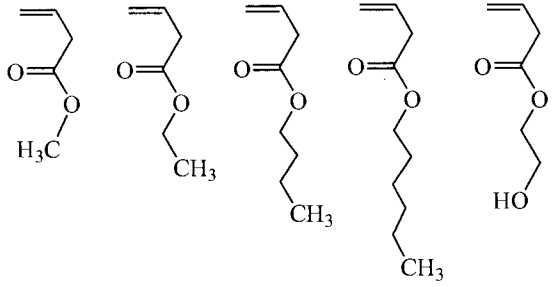

MA EA BA HA HEA

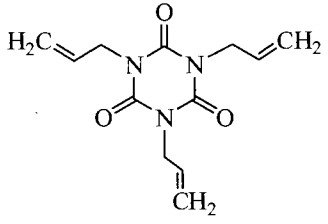

TTT

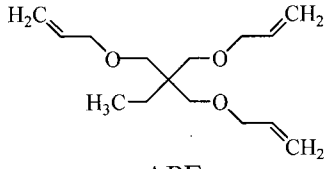

APE

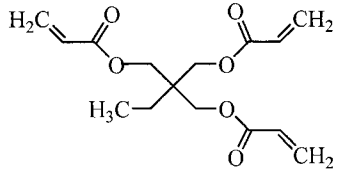

TMPTA

Chart 6.1. The molecular structures of thiols, enes, and acrylates.

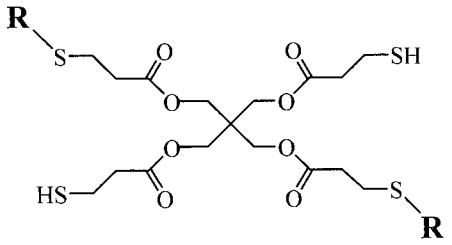

modified dithiol

EADT R = $-(CH_2)_2CO_2CH_2CH_3$

HEADT R = $-(CH_2)_2CO_2CH_2CH_2OH$

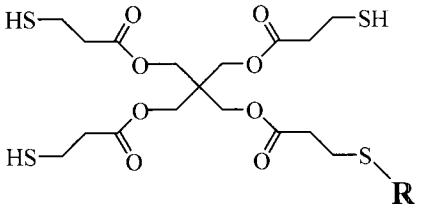

modified trithiol

MATT-TTT R = $-(CH_2)_2CO_2CH_3$

EATT-TTT R = $-(CH_2)_2CO_2CH_2CH_3$

BATT-TTT R = $-(CH_2)_2CO_2(CH_2)_3CH_3$

HATT-TTT R = $-(CH_2)_2CO_2(CH_2)_5CH_3$

HEATT-TTT R = $-(CH_2)_2CO_2CH_2CH_2OH$

Chart 6.2. The molecular structures of n-alkyl and hydroxyl ethyl acrylate modified di- and trithiols.

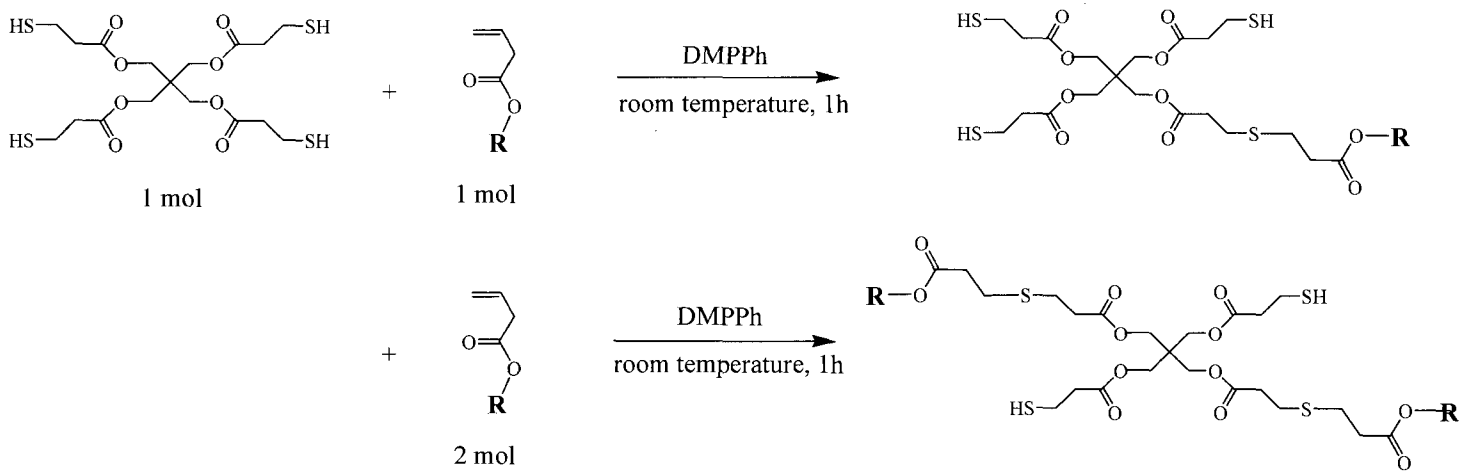

Scheme 6.1. The overall reaction procedure for the synthesis of modified di- and trithiols from PETMP and acrylate monomers.

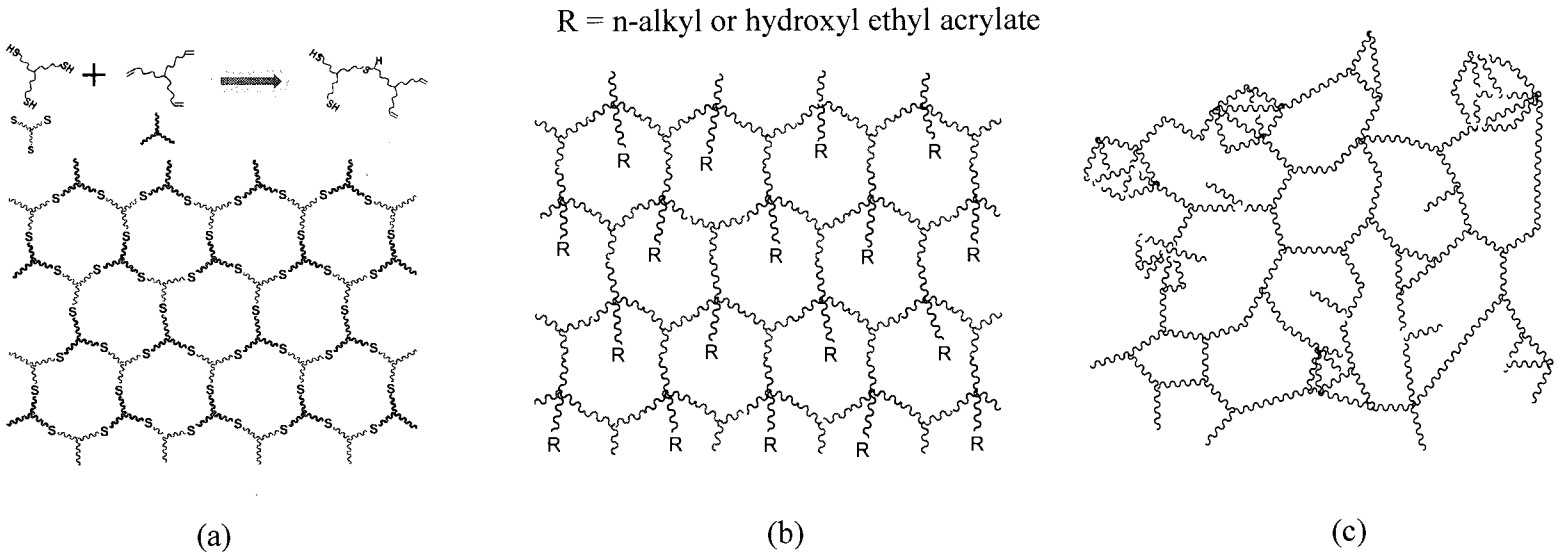

Figure 6.1. (a) uniform and dense network structure of photopolymerized thiol-ene made with trithiol and triene, (b) modified thiol-ene networks with n-alkyl or hydroxyl ethyl acrylate and tritne, (c) inhomogeneous crosslinked structure of multifunctional acrylate homopolymer by forming microgel.

(a) Isochronal

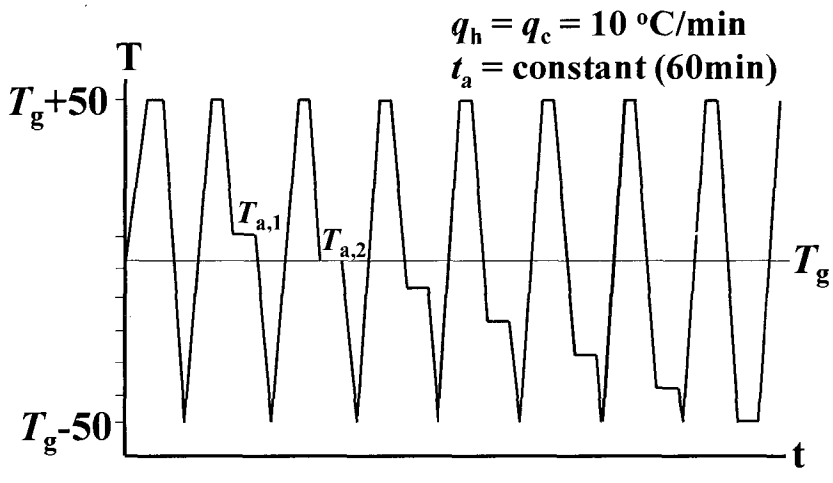

(b) Isothermal

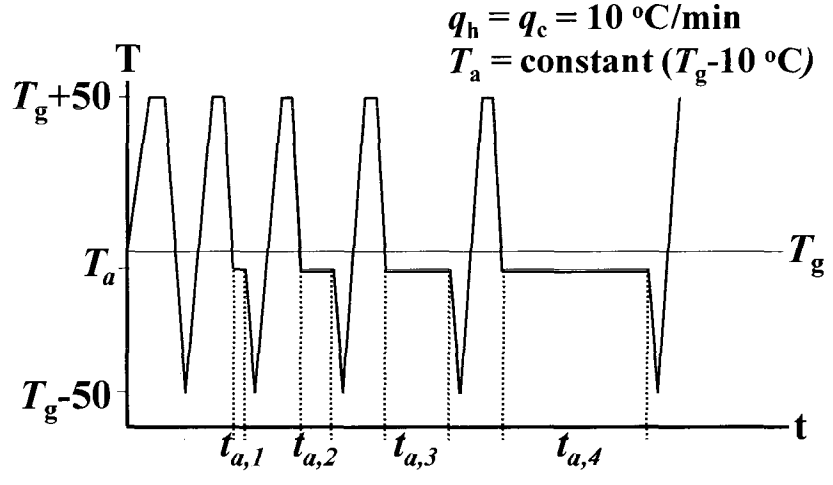

Figure 6.2. The schematic representation of two different annealing methods. The symbols q_h and q_c represent heating/cooling rates.

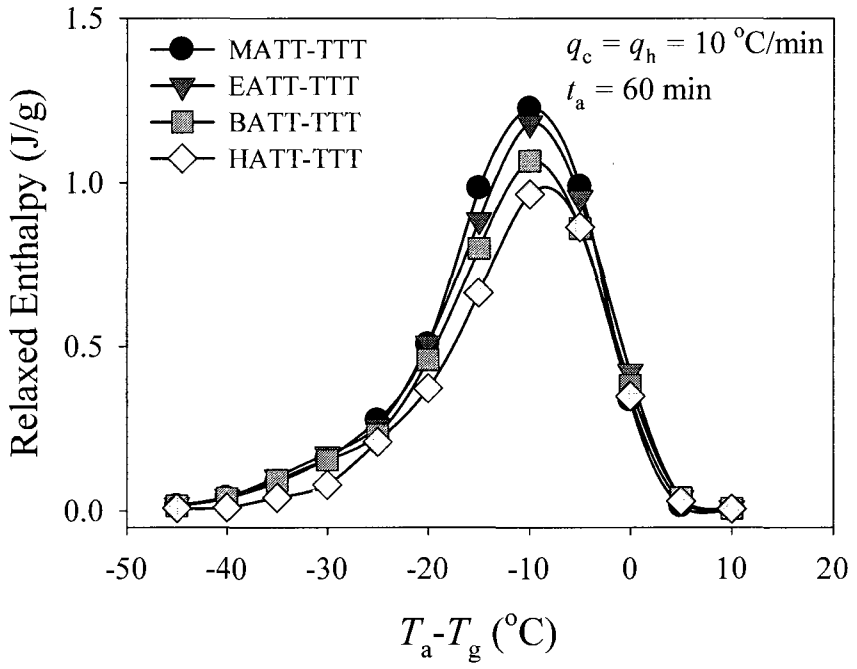

Figure 6.3. Enthalpy relaxation of photopolymerized n-alkyl acrylate modified trithiol-TTT networks as a function of the annealing temperature and alkyl chain length (q_h=q_c=10 °C/min, t_a=60 min).

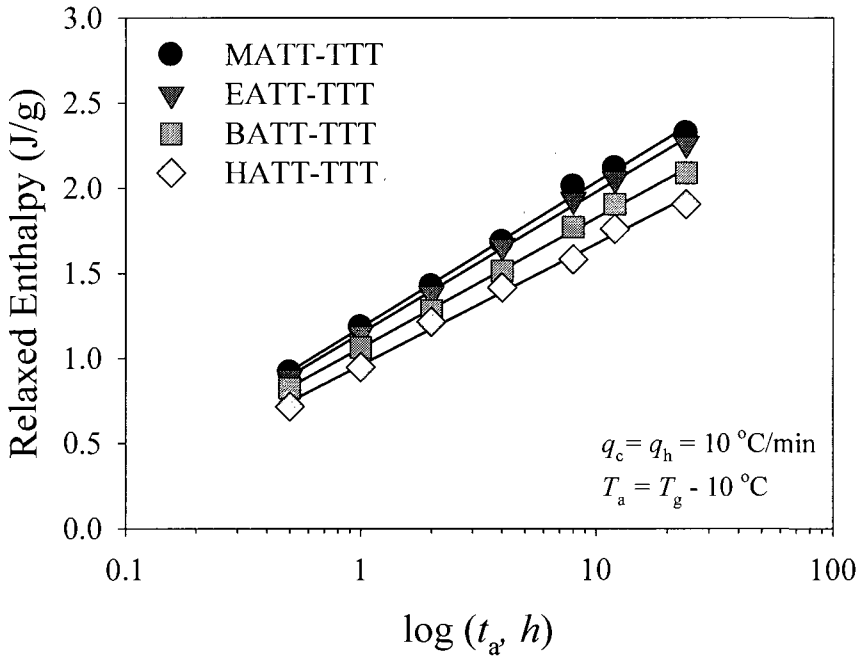

Figure 6.4. Relaxed enthalpy (δ_H) vs. logarithmic annealing time (t_a) of photopolymerized n-alkyl acrylate modified trithiol-TTT networks (q_h=q_c=10 °C/min, T_a=T_g-10 °C).

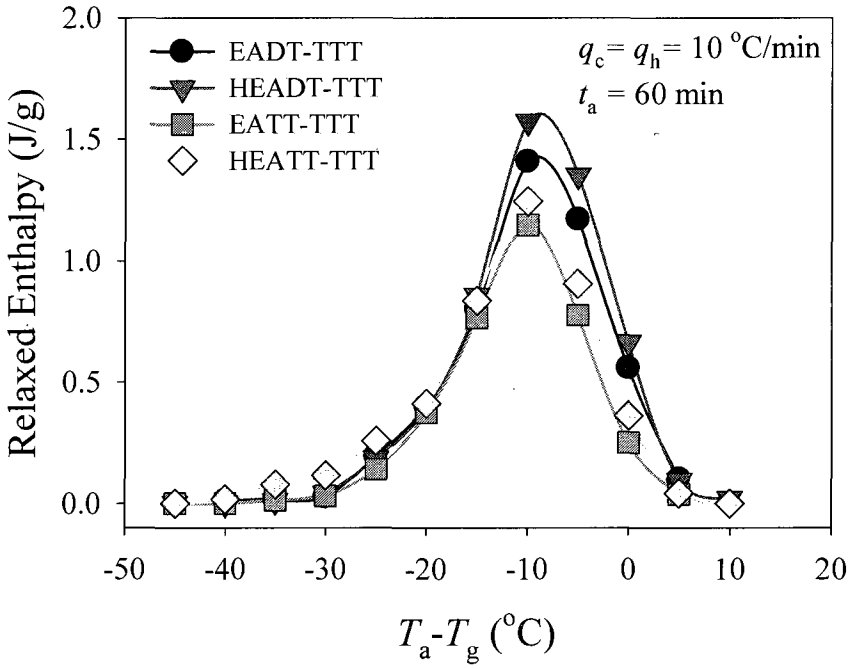

Figure 6.5. Enthalpy relaxation of photopolymerized ethyl/hydroxyl ethyl acrylate modified di-/trithiol-TTT networks as a function of the annealing temperature (q_h=q_c=10 °C/min, t_a=60 min).

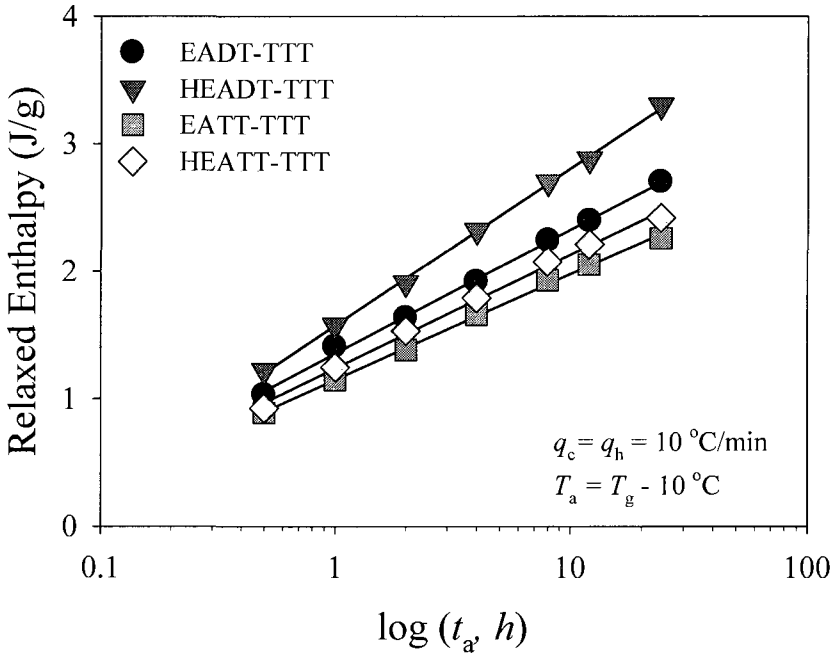

Figure 6.6. Relaxed enthalpy (δ_H) vs. logarithmic annealing time (t_a) of photopolymerized ethyl/hydroxyl ethyl acrylate modified di-/trithiol-TTT networks (q_h=q_c=10 °C/min, T_a=T_g-10 °C).

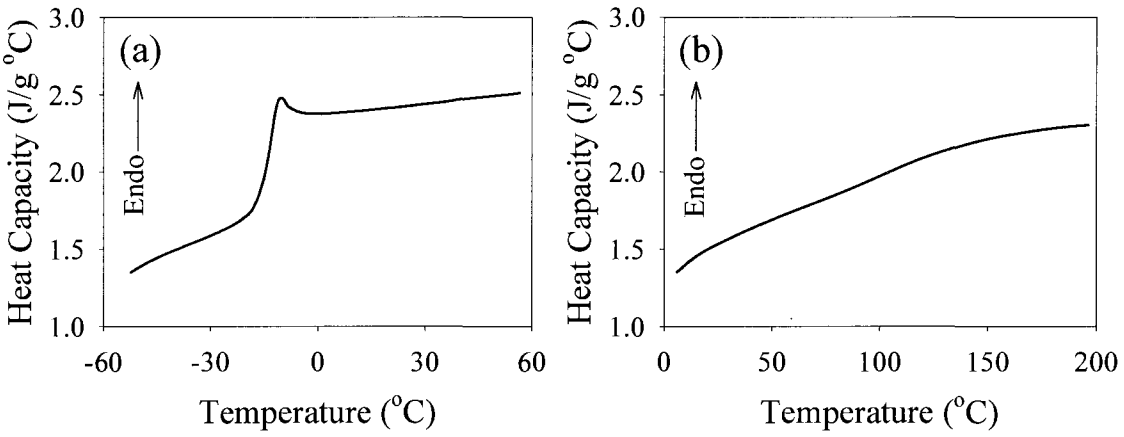

Figure 6.7. DSC heating scans of films of photopolymerized TMPMP-APE network (a) and TMPTA homopolymer (b) without annealing (cooling (q_c) and heating rate (q_h) : 10 °C/min).

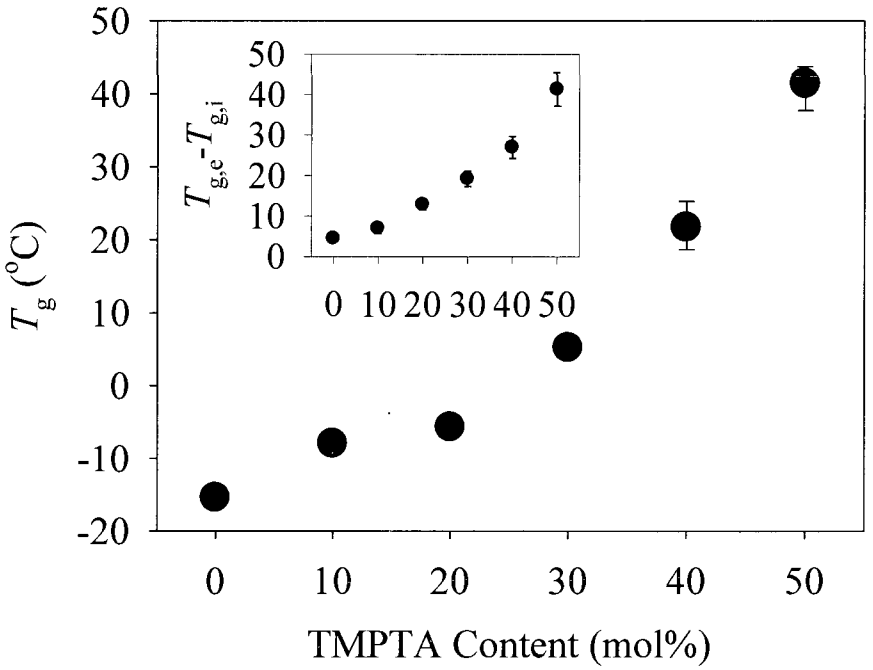

Figure 6.8. The effect of TMPTA on T_g of photopolymerized TMPMP-APE-TMPTA ternary system.

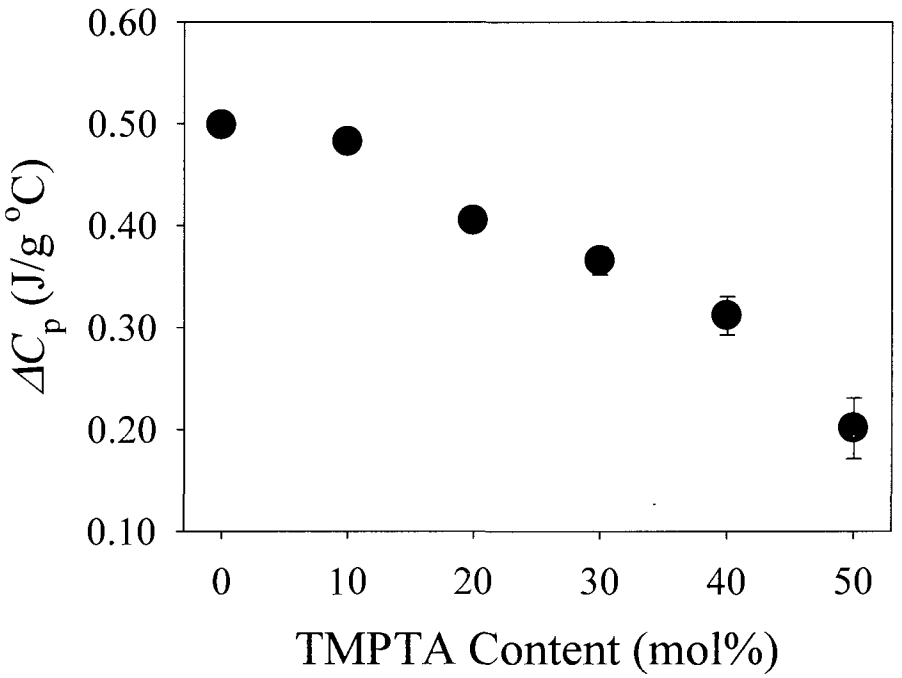

Figure 6.9. The effect of TMPTA on heat capacity of photopolymerized TMPMP-APE-TMPTA ternary system.

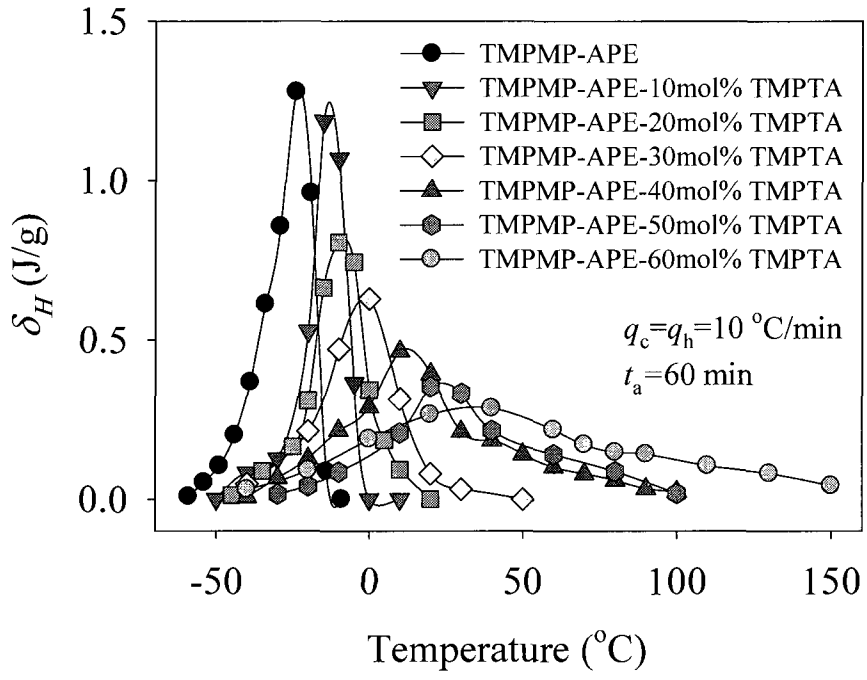

Figure 6.10. Temperature dependency of enthalpy relaxation of photopolymerized TMPMP-APE-TMPTA ternary system ($q_c = q_h = 10$ °C/min, $t_a = 60$ min).

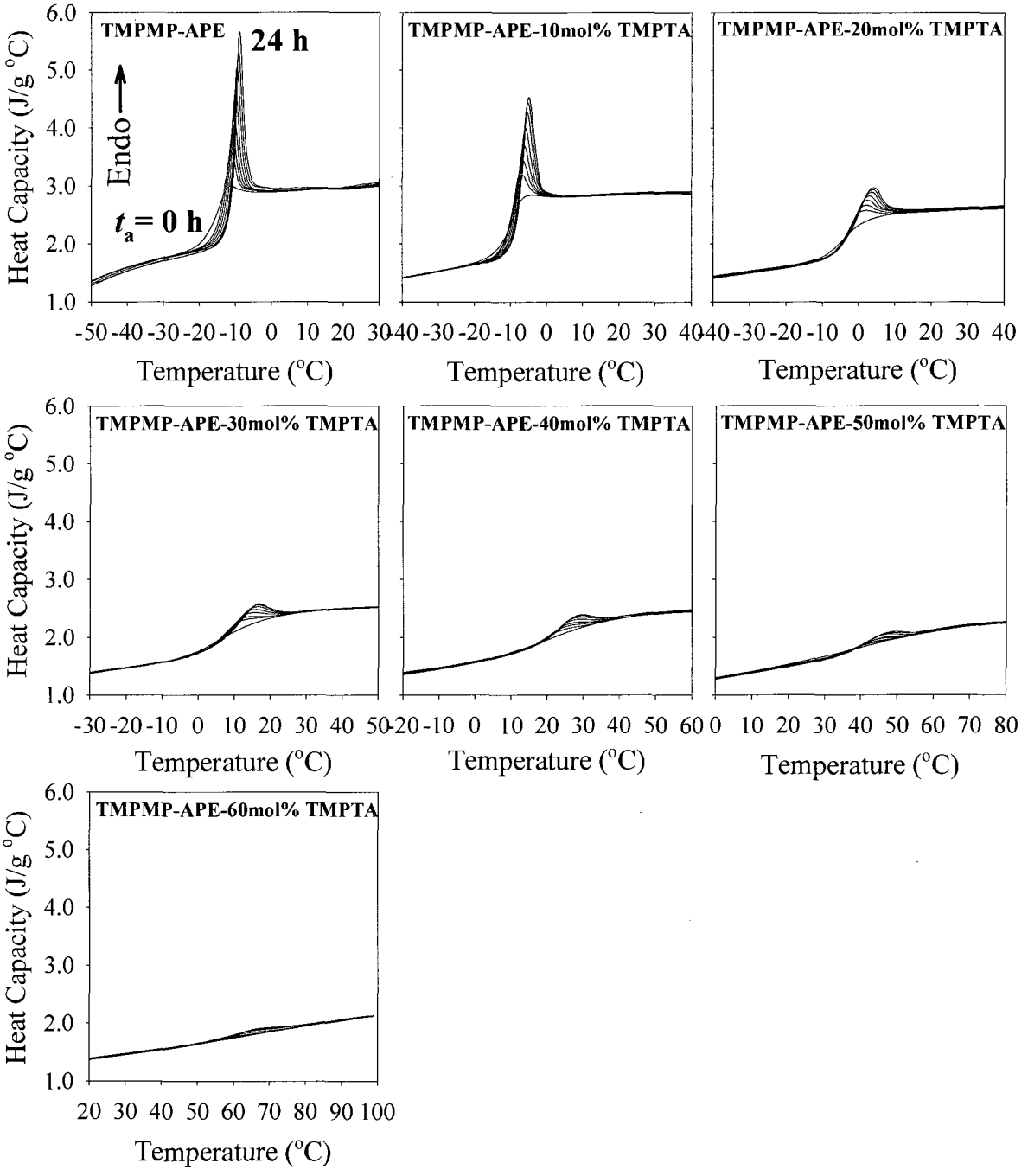

Figure 6.11. DSC heating scans of photopolymerized TMPMP-APE-TMPTA ternary system as a function of annealing time (t_a) ($q_c = q_h = 10$ °C/min, $T_a = T_g$-10 °C).

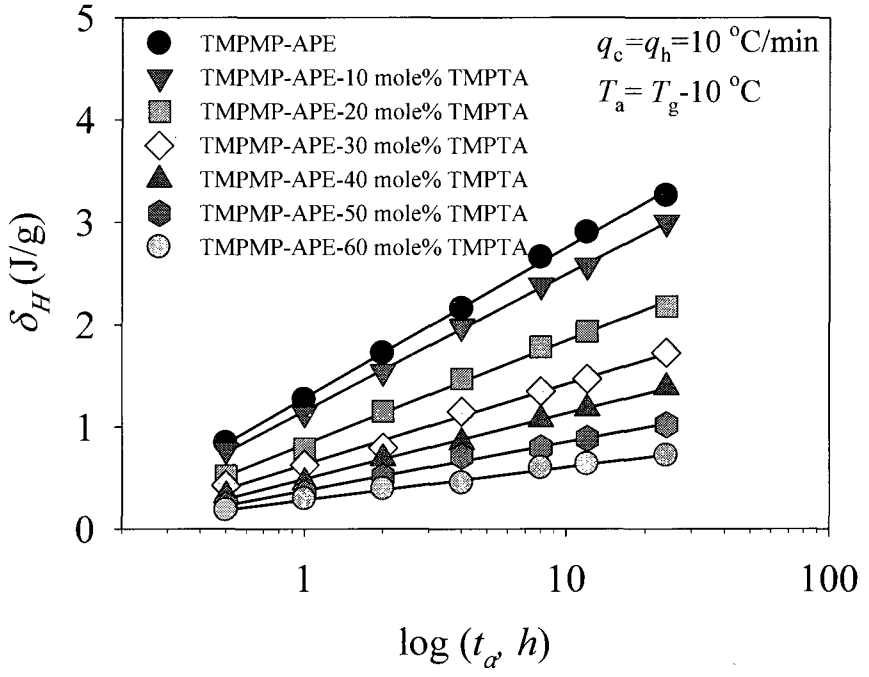

Figure 6.12. Relaxed enthalpy (δ_H) vs. logarithmic annealing time (t_a) of photopolymerized TMPMP-APE-TMPTA ternary system ($q_c = q_h = 10$ °C/min, $T_a = T_g$-10 °C).

CHAPTER VII

PHYSICAL AND CHEMICAL MODIFICATIONS OF THIOL-ENE NETWORKS TO CONTROL ACTIVATION ENERGY OF ENTHALPY RELAXATION

Abstract

Gold nanoparticles and multi-functional acrylate (TMPTA) were incorporated into a photopolymerized thiol-ene (TMPMP-APE) network as a physical and chemical approach to intentionally control sub-T_g aging. The degree of the restriction effect was evaluated by differential cooling rate measurements allowing the quantification of the apparent activation energy for enthalpy relaxation (Δh^*) upon sub-T_g aging. Incorporation of gold nanoparticles (0.01 to 1 wt%) into the TMPMP-APE network increased T_g and decreased ΔC_p at T_g due to molecular mobility restrictions. The extent of enthalpy relaxation and apparent activation energy for enthalpy relaxation (Δh^*) clearly indicated the significant restrictive effect of the gold nanoparticles on the molecular mobility in the thiol-ene network. A TMPMP-APE-TMPTA ternary system was investigated in order to correlate Δh^* and network uniformity as a chemical approach. TMPTA, being capable of homopolymerization as well as TMPMP-TMPTA copolymerization, was incorporated into a TMPMP-APE network structure, thereby decreasing the network uniformity and significantly affecting the sub-T_g aging. The extent of enthalpy relaxation decreased and the distribution was drastically broadened as a function of TMPTA content due to molecular mobility restrictions, which were also quantified by measuring values for the apparent enthalpy relaxation activation energy (Δh^*).

Introduction

Thiol-ene photo-polymerization has attracted much attention as an emerging area in industry as well as academia as detailed in a review in 2004.[1] The advantages of thiol-ene radical polymerization include initiatorless photopolymerization, low oxygen inhibition, and versatility in hybridization with other thiol click type reactions that provide the potential for opening up many new applications.[1-20] In addition, the unique chemical reaction mechanism, i.e. free-radical step-growth, yields matrices with highly uniform network structure (Figure 7.7.1(a)). The effect of thiol-ene network uniformity on physical / mechanical properties has been extensively studied and comparisons made with inhomogeneous multi-functional acrylate homopolymer networks (Figure 7.1(b)).[5,6,21] The uniform photopolymerized thiol-ene network structure is characterized by a very narrow glass transition region (FWHM ~ 10 °C). It is believed that this uniform network structures has very narrow chain relaxation times and physical / mechanical properties are sensitive to environmental conditions, i.e. temperature.

Sub-T_g aging is a thermodynamic phenomenon involving volume and enthalpy relaxation upon annealing below the glass transition temperature of a polymer resulting in physical / mechanical property changes. Sub-T_g aging of thiol-ene photo-polymerized networks with uniform chemical structure and a narrow distribution of relaxation times has been extensively investigated in terms of enthalpy relaxation by Shin et al.[22,23] Thiol-ene networks showed temperature and time dependency relationships for enthalpy relaxation as generally observed in conventional polymers. However, the extent of enthalpy relaxation and overall relaxation rate significantly decreased with the rigidity of the ene chemical structures and functionality of the thiols forming thiol-ene networks.

The effect of chemical and physical modification of thiol-ene network structure on enthalpy relaxation also has been reported. Overall both the rate and extent of enthalpy relaxation decreased by inclusion of flexible n-alkyl side chains as a function of alkyl chain length, while hydroxyl side chain incorporated into thiol-ene networks resulted in enhanced enthalpy relaxation. A multi-functional acrylate forming an inhomogeneous cross-linked structure by homopolymerization was copolymerized into thiol-ene networks to correlate enthalpy relaxation and network uniformity. The extent and distribution of enthalpy relaxation of thiol-ene networks were significantly affected by disruption of the uniformity.

Because the rate of enthalpy / volume relaxation and corresponding rearrangement of polymer chains depend on the local environment surrounding mobile segments, sub-T_g aging can be restricted by various chemical and physical environmental effects such as thin films on substrates, the rigid amorphous regions of semi-crystalline polymers, highly cross-linked polymer networks, and nanocomposites.[24-32] In addition, the restriction of molecular mobility and enthalpy relaxation is directly related to configurational energy barriers in the relaxation process. Thus, the activation energy for the enthalpy relaxation (Δh^*) has been used to quantify the extent of the restrictive effect upon sub-T_g aging.[32-39] It has been reported that rigid chains and high cross-link density increase Δh^*.[33-36] Similarly, an increase in Δh^* of an epoxy matrix by incorporation of nano-clay due to the anchoring of epoxy chains to the nano-clay surface was also reported.[32]

In the research described herein, gold nanoparticles and highly cross-linked TMPTA based rigid nano-domains as a physical and chemical approaches, respectively,

were employed to control molecular relaxation dynamics upon sub-T_g aging. The restrictive effect on enthalpy relaxation was quantified by measuring values for the apparent enthalpy relaxation activation energy (Δh^*).

Experimental

Materials

TMPMP (Trimethylolpropane tri(3-mercapto-propionate), APE (allyl pentaerythritol), and TMPTA (trimethylolpropane triacrylate) were obtained from Bruno Bock Thio-Chemicals-S and Perstorp Specialty Chemicals, respectively. Gold nanopowder (99.9+ %) was purchased from Aldrich. The structures of all components and corresponding acronyms are shown in the Chart 7.1. The photoinitiator, 2,2-dimethoxy 2-phenyl acetophenone (DMPA), was supplied by Ciba Specialty Chemicals. All materials were used as received.

Preparation of TMPMP-APE-gold and TMPMP-APE-TMPTA network films

TMPMP-APE-gold networks were prepared with gold dispersed in TMPMP and APE. Gold nanoparticles were added and dispersed in TMPMP with weight percents from 0.01 to 1.0. A detailed procedure for the dispersion of gold nanoparticles into TMPMP was described in the literature.[43] For TMPMP-APE-TMPTA ternary systems, the molar ratio of TMPTA to TMPMP-APE was varied from 0 to 100% to form TMPMP-APE-TMPTA ternary networks. 1 Wt% of DMPA was first dissolve in gold nanoparticles dispersed TMPMP for TMPMP-APE-gold networks and TMPMP for TMPMP-APE-TMPTA ternary systems by sonication for 10 minutes. Thiol (-SH) and ene (-C=C-) concentrations were held constant at 1:1 functional group molar equivalent

for all networks. Films were cast on glass plates (200 μm) and cured on a Fusion UV curing line system with a D bulb (400 W/cm^2) having a belt speed of 10 feet/min and irradiance of 3.1 W/cm^2. All samples were post-cured at 80 °C for 24 h to insure complete reaction and eliminate any possibility of chemical conversion effect on enthalpy relaxation during sub-T_g annealing.

Characterization

Glass transition temperatures and enthalpy relaxation for all modified thiol-ene networks were characterized with a TA Q1000 differential scanning calorimeter (DSC) with RCS 90 (Refrigerated Cooling System). A RCS 90 cooling head mounted on the DSC Q1000 furnace encases the DSC cell preventing frost build-up during operation. Three calibration steps (T_{zero} calibration, enthalpy constant calibration, and Temperature calibration) for the TA Q1000 were performed periodically. Detailed calibration protocol has been well described in previous reports.[22] For sub-T_g aging experiment, the differential cooling rate method was used as described in Figure 7.2. The measurement was conducted twice and the sequence of cooling rate variation was reversed in the second running. Equivalent results were obtained in each case, i.e., instrumental drift did not play a factor, and the results were reproducible despite the different order for obtaining the data sets. Furthermore, the heat capacity of TMPMP-APE sample without aging, as a standard, was measured after every calibration and set of experiments to ensure consistency. All experiments were carried out under nitrogen with a flow rate of 50 mL/min. Sample weights were 8.0±1.0 mg to ensure sufficient sensitivity for heat capacity measurements. DSC scans were conducted over the temperature range of ±50 °C from the glass transition region ($T_{g,i}$~$T_{g,e}$). Cooling rate (q_c) was differentiated at a

fixed heating rate (q_h, 10 °C/min) to provide samples the different degree of non-equilibrium state in the glass and enthalpy recovery upon reheating. The detailed description of the experimental measurement technique is described in the text.

Results and Discussion

The basic structural units used to make the thiol-ene and thiol-ene-acrylate ternary networks which are the subject of the investigation in this paper are shown in Charts 1 (gold structure is not shown). The three functional thiol (TMPMP) and ene (APE) are standard thiol and ene monomers typically used to make thiol-ene networks. Herein, we focus on defining the role of physically incorporated gold nanoparticles and chemical structure uniformity of the basic thiol-ene networks on sub-T_g aging behavior in terms of the apparent activation energy for enthalpy relaxation. The degree of non-equilibrium state in the glassy is determined by thermal treatment, i.e. by controlling the cooling rate in DSC measurements. Hence, the thiol-ene networks were equilibrated above T_g to remove prior thermal history and cooled down at different cooling rate (q_c). The subsequent heat capacity was monitored upon reheating the sample through its glass transition. Equilibration achieved by maintaining the sample for 10 minutes at a temperature above T_g ($T_{g,e}$+50 °C) effectively erases the previous thermal history, and is necessary in order to initialize the sample for sub-T_g aging. The differential cooling rate method measures the apparent activation energy for enthalpy relaxation and can potentially highlight changes in enthalpy relaxation distribution.

TMPMP-APE-gold networks

The effect of gold nanoparticles on sub-T_g aging of thiol-Ene photopolymerized films was investigated as a physical approach to intentionally control enthalpy relaxation and molecular mobility by binding the network structure to a non-reactive nanoparticle additive. The TMPMP-APE-gold photopolymerized networks made from mixtures of TMPMP, APE, and dispersed gold nanoparticles (0.01 ~ 1 wt%) were analyzed by DSC with varying cooling rate (q_c) from 0.2 to 10 °C/min and a fixed heating rate (q_h=10 °C/min). As shown in Figure 7.3, with decreasing cooling rate, the intensity of the endothermic peak upon subsequent heating progressively increases for all TMPMP-APE-gold films. However, for results obtained at each cooling rate, the overall peak intensity of the subsequent heating scan decreases and T_g shifts to higher temperature as a function of gold nanoparticle content (Figure 7.4). For reference, we note that the T_g values of the un-aged samples (q_h=q_c=10 °C/min) increase from -15 to -7 °C, leveling off at 0.5 wt% due to dispersion problems encountered in the pre-polymerized TMPMP and APE mixtures resulting in some aggregation of the gold nanoparticles as identified by light scattering.[43] Figure 7.5 shows a plot of ΔC_p as a function of the gold nanoparticle wt % in the TMPMP-APE network. It is clear that restriction of molecular mobility and hence lower ΔC_p in the rubbery phase upon incorporation of gold up to 0.5 wt % in the TriThiol-APE network is consistent with the T_g results in Figure 7.4. This certainly results from a binding interaction between sulfide linkages (or un-reacted thiol groups) in the network structure and the gold surface which restricts molecular motion, raises the T_g, and correspondingly reduces ΔC_p at T_g. The gold nanoparticles effectively restrict

conformational degrees of freedom otherwise operative in the TMPMP-APE network above T_g.

The logarithmic cooling rate (q_c) vs. reciprocal fictive temperature (T_f) for each of the TMPMP-APE-gold photopolymerized films are readily fit to straight lines with different slopes as shown in Figure 7.6. The restriction of molecular relaxation can be mathematically quantified by the apparent activation energy for enthalpy relaxation (Δh^*) as defined in Equation (1),

$$\frac{d(\ln q_c)}{d(1/T_f)} = -\frac{\Delta h^*}{R} \qquad \text{Equation (1)}$$

where R is the universal gas constant and q_c is cooling rate in DSC measurement.[36-42] The fictive temperature (T_f), which is defined as the temperature at which the extrapolation of thermodynamic parameters such as enthalpy, volume or entropy at a given temperature and annealing time in the glassy region intersects the extension of the liquid equilibrium line, can be used to characterize the structure of certain glassy states under a given set of conditions.[44-46] The apparent activation energy (Δh^*) obtained from the slopes in Figure 7.6 increases from 353 kJ/mol for the neat Thiol-Ene network to 836 kJ/mol for the sample with 1 wt % gold nanoparticles in the network (Figure 7.7). As with the T_g and ΔC_p results in Figures 4 and 5, Δh^* increases substantially with an increase in gold nanoparticles up to approximately 0.5 wt%, whereupon aggregation of the gold nanoparticles occurs,[43] thus limiting the gold surface area for interaction with the TMPMP-APE network. The increase in activation energy for enthalpy relaxation (Δh^*)

is thus consistent with the reduction in the enthalpic departure from equilibrium with increasing gold concentration already noted.

TMPMP-APE-TMPTA ternary networks

TMPMP-APE-TMPTA ternary networks were next used to investigate the effect of network structural uniformity on sub-T_g aging. As reported in references,[22,23] due to the network uniformity, TMPTA-APE has a very narrow glass transition temperature region and a distinct enthalpy relaxation peak around T_g obtained by DSC scanning of the pre-cooled sample at 10 °C/min cooling (q_c) followed by an immediate (no time for extended aging at a single annealing temperature) subsequent heating at a rate (q_h) of 10 °C/min. Concomitantly, photopolymerized TMPTA has an inhomogeneous crosslinked structure with a wide variation of crosslink densities and corresponding microgel structures, as well as dangling chain ends,[47-52] resulting in a very broad glass transition region and no clearly defined enthalpy relaxation peak.

To define the effect of sub-T_g aging of ternary TMPTA-APE-TMPTA networks, systems were prepared by mixing TMPMP+APE with increasing TMPTA molar concentrations (10, 20, 30, 40, 50, and 60 mole %). The basic DSC glass transition temperature (see plots for q_c=10 °C/min in Figure 7.8) increases as a function of TMPTA content (Figure 7.9), and the enthalpy relaxation peak is absent for TMPTA concentrations greater than 20 %. It is clear that incorporating TMPTA into the TMPMP-APE network successfully decreases the network uniformity and microgel formation by TMPTA homopolymerization, acting like rigid amorphous region, restricts molecular mobility of thiol-ene networks, as previously reported.[6,21,23]

The restriction of molecular mobility in the Thiol-Ene network by incorporation of the third component leads to a reduction of ΔC_p values. As shown in Figure 7.10, ΔC_p at T_g of TMPMP-APE-TMPTA also significantly decreases as a function of TMPTA content due to restriction of internal degrees of freedom resulted from the microgelation of TMPTA accompanied by a broadened distribution of network/crosslink density and broad glass transition temperature range and distribution of relaxation times. The broadening of the temperature range and restrictive effect on enthalpy relaxation by incorporating TMPTA into the TMPMP-APE network is even more obvious when characterized by a differential cooling rate sub-T_g aging method (Figure 7.8) from 0.2 to 10 °C/min at a fixed heating rate (q_h=10 °C/min). This allows investigation of enthalpy relaxation behavior independent of temperature and time dependency, i.e., enthalpy relaxation distribution over a temperature range can be observed. In Figure 7.8, the intensity of the endothermic peak progressively increases as the cooling rate decreases for all of the TMPMP-APE-TMPTA ternary systems, and the enthalpy relaxation peak maximum is lower as well as the distribution broadened with increasing TMPTA content. The apparent activation energy Δh^* from Equation 1 obtained from slopes of linear regression lines in Figure 7.11 (semi-log plots of cooling rate (q_c) vs. T_f^{-1}) increases from 349 kJ/mol for the neat TMPMP-APE network to 1,962 kJ/mol for the network with 60 mol % of TMPTA in the TMPMP-APE-TMPTA ternary system (Figure 7.12). This correlates with the decrease in the heat capacity changes at T_g (ΔC_p) and clearly indicates that the enthalpy relaxation decreases with increasing TMPTA content.

Conclusions

Thiol-Ene networks were physically and chemically modified to provide control of apparent activation energy for enthalpy relaxation caused upon sub-T_g aging via two methods; addition of gold nanoparticles and chemical addition of a third (acrylate) component (ternary system). The effect of gold nanoparticles as a physical blending approach to reduce the extent of enthalpy relaxation on TMPMP-APE network was first demonstrated. The decrease in the amount of relaxed enthalpy upon sub-T_g aging, increase in T_g, decrease in ΔC_p, and increase in Δh^* all occur with an increase in the gold nanoparticle content and attain limiting values at a gold nanoparticles concentration of 0.5 wt%. Effective incorporation of higher gold content at levels of 1 wt% or greater will require new mixing protocols due to the tendency for aggregation. Multifunctional acrylate (TMPTA) was incorporated into a TMPMP-APE network structure as a chemical approached to investigate the effect of the network uniformity on the apparent activation energy for enthalpy relaxation. The extent of enthalpy relaxation decreased and the distribution was drastically broadened as a function of TMPTA content. It can be concluded that network uniformity manipulated by chemical structural change is responsible for manipulation of the activation energy for enthalpy relaxation, i.e. sub-T_g relaxation of TMPMP-APE based networks. The restrictive effect of inorganic gold nanoparticles and rigid amorphous regions due to microgelation of TMPTA homopolymerization successfully decreases segmental chain mobility of TMPMP-APE networks resulting in significant reduction of activation energy for enthalpy relaxation. The physical and chemical approaches demonstrated for the model thiol-ene network provides a guide for control and restriction of sub-T_g aging of polymer networks.

References

1. Hoyle, C. E.; Lee, T. Y.; Roper, T. *J. Polym. Sci., Part A: Polym. Chem.* **2004**, 42, 5301.
2. Cramer, N. B.; Bowman, C. N. *J. Polym. Sci., Part A: Polym. Chem.* **2001**, 39, 3311.
3. Cramer, N. B.; Reddy, S. K; Cole, M.; Hoyle, C. E.; Bowman, C. N. *J. Polym. Sci., Part A: Polym. Chem.* **2004**, 42, 5817.
4. Khire, V. S.; Harant, A. W.; Watkins, A. W.; Anseth, K. S.; Bowman, C. N. *Macromolecules* **2006**, *39,* 5081.
5. Senyurt, A. F.; Hoyle, C. E.; Wei, H.; Piland, S. G.; Gould, T. E. *Macromolecules* **2007**, 40, 3174.
6. Wei, H.; Senyurt, A. F.; Jönsson, S.; Hoyle, C. E. *J. Polym. Sci., Part A: Polym. Chem.* **2007**, 45, 822.
7. Roper, T. M.; Guymon, C. A.; Jönsson, E. S.; Hoyle, C. E. *J. Polym. Sci., Part A: Polym. Chem.* **2004**, 42, 6283.
8. Lee, T. Y.; Roper, T. M.; Jönsson, E. S.; Guymon, C. A.; Hoyle, C. E. *Macromolecules* **2004**, 37, 3606.
9. Li, Q.; Zhou, H.; Wicks, D. A.; Hoyle, C. E. *J. Polym. Sci., Part A: Polym. Chem.* **2007**, 45, 5103.
10. Wei, H.; Li, Q.; Ojelade, M.; Madbouly, S.; Otaigbe, J. U.; Hoyle, C. E. *Macromolecules* **2007**, 40, 8788.
11. Senyurt, A. F.; Warren, G.; Whitehead, J. B.; Hoyle, C. E. *Polymer* **2006**, 47, 2741.
12. Moran, I. W.; Briseno, A. L.; Loser, S.; Carter, K. R.; *Chem. Mater.* **2008**, *20*, 4595.

13. Yi, Y. W.; Khire, V.; Bowman, C. N.; Maclennan, J. E.; Clark, N. A. *J. Appl. Phys.* **2008**, *103*, 6.

14. Good, B. T.; Reddy, S.; Davis, R. H.; Bowman, C. N. *Sensors and Actuators B-Chemical* **2007**, *120*, 473.

15. Pojman, J. A.; Varisli, B.; Perryman, A.; Edwards, C.; Hoyle, C. E. *Macromolecules* **2004**, *37*, 691.

16. Khire, V. S.; Benoit, D. S. W.; Anseth, K. S.; Bowman, C. N. *J. Polym. Sci., Part a-Polym. Chem.* **2006**, *44*, 7027.

17. Khire, V. S.; Harant, A. W.; Watkins, A. W.; Anseth, K. S.; Bowman, C. N. M*acromolecules*, **2006**, 39, 5081.

18. Dickey, M. D.; Collister, E.; Raines, A.; Tsiartas, P.; Holcombe, T.; Sreenivasan, S. V.; Bonnecaze, R. T.; Willson, C. G. *Chem. Mater.* **2006**, *18*, 2043.

19. Fox, A. E.; Fontecchio, A. K. *App. Phys. Lett.* **2007**, *91*, 3.

20. Campos, L. M.; Meinel, I.; Guino, R. G.; Scheirhorn, M.; Gupta, N.; Stucky, G. D.; Hawker, C. J. *Adv. Mater.* **2008**, 20, 3728.

21. Senyurt, A. F.; Wei, H.; Phillips, B.; Cole, M.; Nazarenko, S.; Hoyle, C. E.; Piland, S. G.; Gould, T. E. *Macromolecules* **2006**, 39, 6315.

22. Shin, J.; Nazarenko, S.; Hoyle, C. E. *Macromolecules* **2008**, 41, 6741.

23. Shin, J.; Nazarenko, S.; Hoyle, C. E. *Macromolecules* **2009**, 42, 6549.

24. Forrest, J. A.; Dalnoki-Veress, K. *Adv. Colloid Interface Sci.* **2001**, *94*, 167.

25. Zhu, L.; Cheng, S. Z. D.; Calhoun, B. H.; Ge, Q.; Quirk, R. P.; Thomas, E. L.; Hsiao, B. S.; Yeh, F. J.; Lotz, B. *J. Am. Chem. Soc.* **2000**, *122*, 5957.

26. Nogales, K.; Ezquerra, T. A.; Batallan, F.; Frick, B.; Lopez-Cabarcos, E.; Balta-Calleja, F. J. *Macromolecules* **1999**, *32*, 2301.

27. Dobbertin, J.; Hannemann, J.; Schick, C.; Potter, M.; Dehne, H. *J. Chem. Phys.* **1998**, *108*, 9062.

28. Zhao, J.; Wang, J.; Li, C.; Fan, Q. *Macromolecules* **2002**, *35*, 3097.

29. Zhukov, S.; Geppert, S.; Stuhn, B.; Staneva, R.; Ivanova, R.; Gronski, W. *Macromolecules* **2002**, *35*, 8521.

30. Jackson, C. L.; McKenna, G. B. *Rubber Chem. Technol.* **1991**, *64*, 760.

31. Barut, G.; Pissis, P.; Pelster, R.; Nimtz, G. *Phys. Rev. Lett.* **1998**, *80*, 3543.

32. Lu, H.; Nutt, S. *Macromolecules* **2003**, 36, 4010.

33. Karasz, F. E.; MacKnight, W. J. *Macromolecules* **1968**, *1*, 537.

34. Shen, M. C.; Eisenberg, A. *Rubber Chem. Technol.* **1970**, *43*, 95.

35. Cheng, S. Z. D.; Heberer, D. P.; Janimak, J. J.; Lien, S. H. -S.; Harris, F. W. *Polymer* **1991**, *32*, 2053.

36. Hutchinson, J. M. *Prog. Polym. Sci.* **1995**, 20, 703.

37. Hutchinson, J. M.; Kumar, P. *Thermochimica Acta* **2002**, 391, 197.

38. Pan, P.; Zhu, B.; Inoue, Y. *Macromolecules* **2007**, 40, 9664.

39. Qin, Q.; McKenna, G. B. *J. Non-crystal. Sol.* **2006**, 352, 2977.

40. Montserrat, S.; Calventus, Y.; Hutchinson, J. M. *Prog. Org. Coat.* **2006**, 55, 35.

41. Calventus, Y.; Montserrat, S.; Hutchinson, J. M. *Polymer*, **2001**, 42, 7081.

42. Cortes, P.; Montserrat, S.; Hutchinson, J. M. *J. App. Polym. Sci.* **1997**, 63, 17.

43. Phillips, J. P.; Mackey, N. M.; Confait, B. S.; Heaps, D. T.; Deng, X.; Todd, M. L.; Stevenson, S.; Zhou, H.; Hoyle, C. E. *Chem. Mater.* **2008**, 20, 5240.

44. Ritland, H. N. *J. Am. Ceram. Soc.* **1954**, *37*, 370.

45. Moynihan, C. T.; Easteal, A. J.; DeBolt, M. A. *J. Am. Ceram.Soc.* **1976**, *59*, 12.

46. Mathot, V. B. F. *Calorimetry and Thermal Analysis of Polymers*, Hanser: New York, **1994**.

47. Boots, H. M. J.; Kloosterboer, J. G.; van de Hei, G. M. M. *Bri. Polym. J.* **1985**, 17, 219.

48. Elliott, J. E; Bowman, C. N. *Macromolecules* **1999**, 32, 8621.

49. Lovestead, T. M.; Bowman, C. N. *Macromolecules* **2005**, 38, 4913.

50. Kloosterboer, J. G.; Lijten, G. F. C. M.; Boots, H. M. J. *Makromol. Chem., Macromol. Symp.* **1989**, 24. 223.

51. Bowman, C. N.; Anseth, K. S. *Macromol. Symp.* **1995**, 93, 269.

52. Kannurpatti, A. R.; Anseth, J. W.; Bowman, C. N. *Polymer* **1998**, 39, 2507.

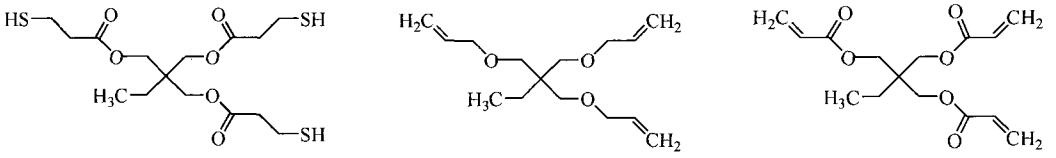

TMPMP APE TMPTA

Chart 7.1. The molecular structures of thiol, ene, and acrylate.

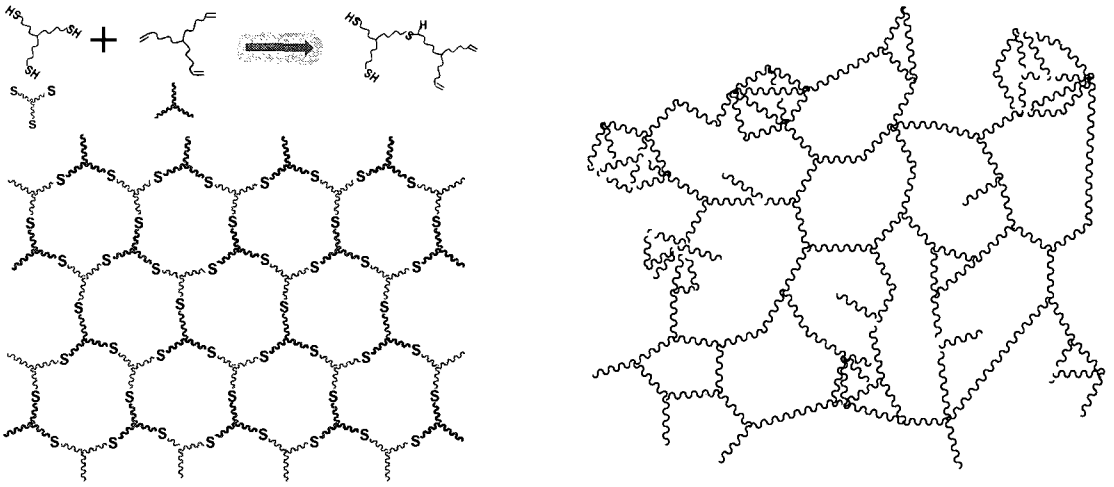

(a) (b)

Figure 7.1. (a) Uniform and dense network pictorial of photopolymerized thiol-ene made with trithiol and triene, and (b) inhomogeneous crosslinked pictorial of multi-acrylate homopolymer showing microgel formation.

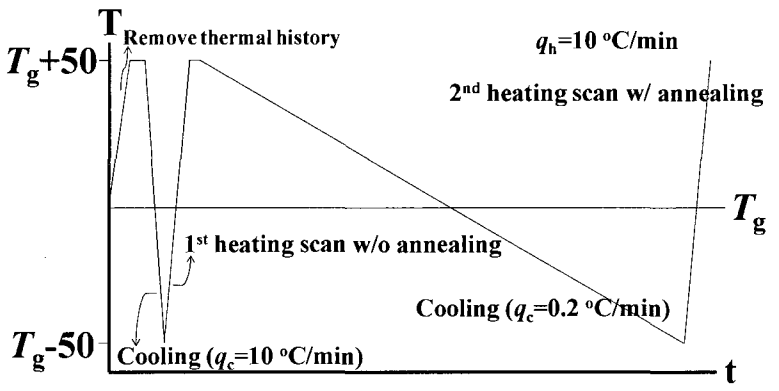

Figure 7.2. Schematic representation of the differential cooling rate method. The symbols q_h and q_c represent heating/cooling rates.

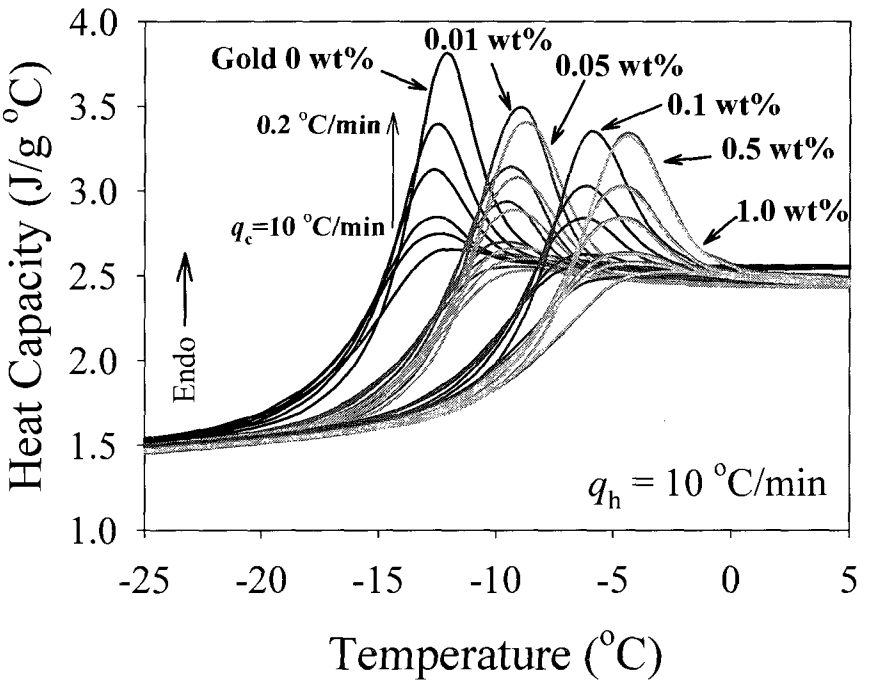

Figure 7.3. DSC heating scans of TMPMP-APE-gold photopolymerized films after cooling with differential cooling rate (q_c).

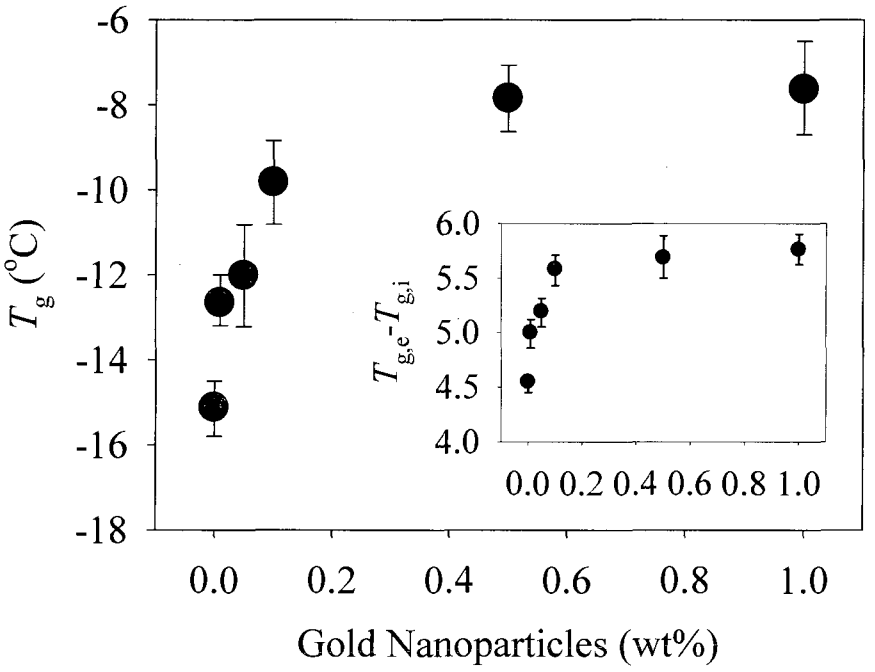

Figure 7.4. Effect of gold nanoparticles on T_g of TMPMP-APE-gold photopolymerized films.

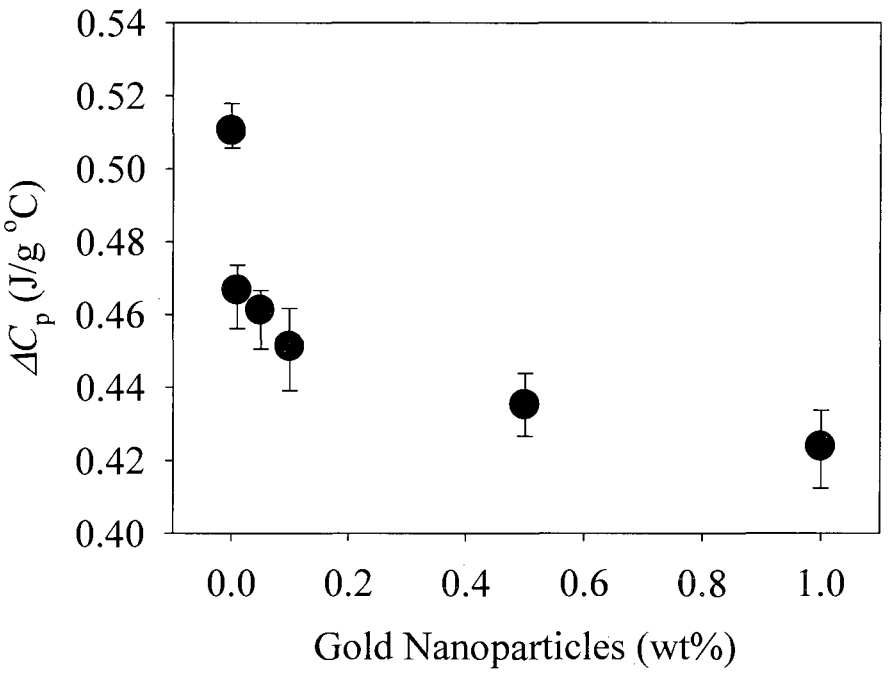

Figure 7.5. Effect of gold nanoparticles on heat capacity of TMPMP-APE-gold photopolymerized films.

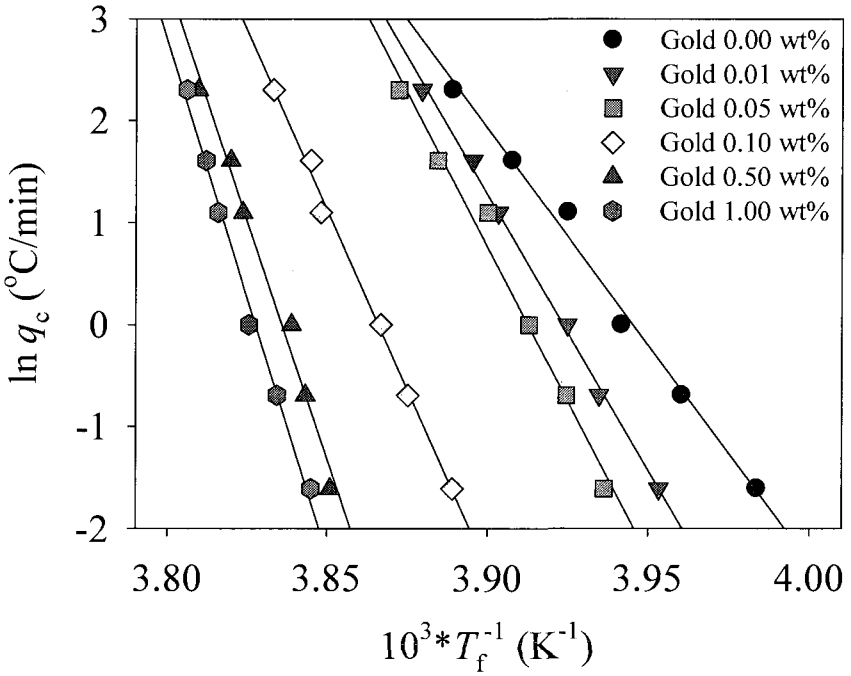

Figure 7.6. Plots of logarithmic cooling rate (q_c) vs. reciprocal fictive temperature (T_f) of TMPMP-APE-gold photopolymerized films.

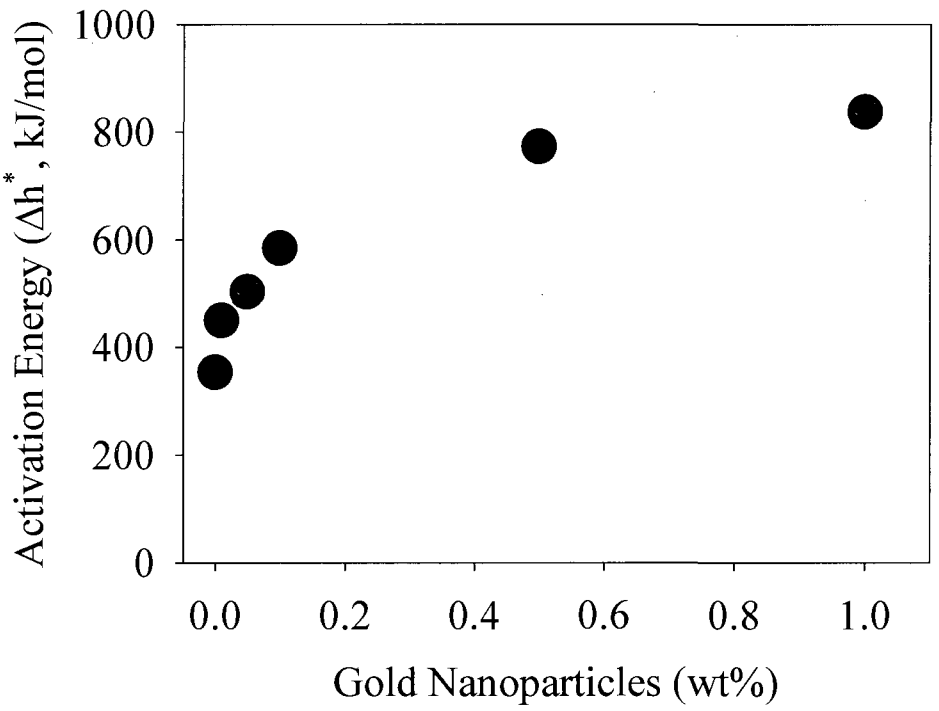

Figure 7.7. Apparent activation energy (Δh^*) for enthalpy relaxation of TMPMP-APE-gold photopolymerized films as a function of gold nanoparticle content.

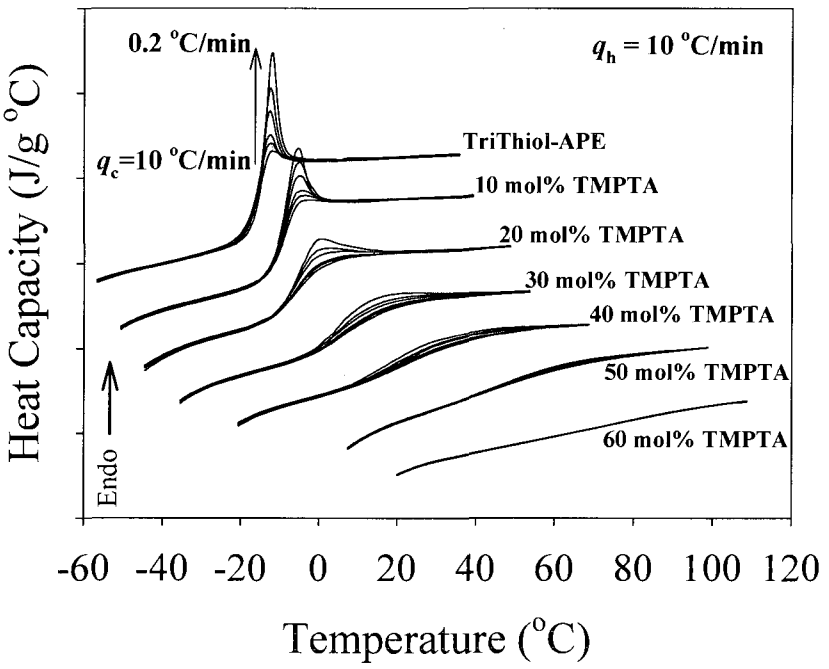

Figure 7.8. DSC heating scans of photopolymerized TMPMP-APE-TMPTA ternary networks upon differential cooling rates (10, 5, 3, 1, 0.5, and 0.2 °C/min).

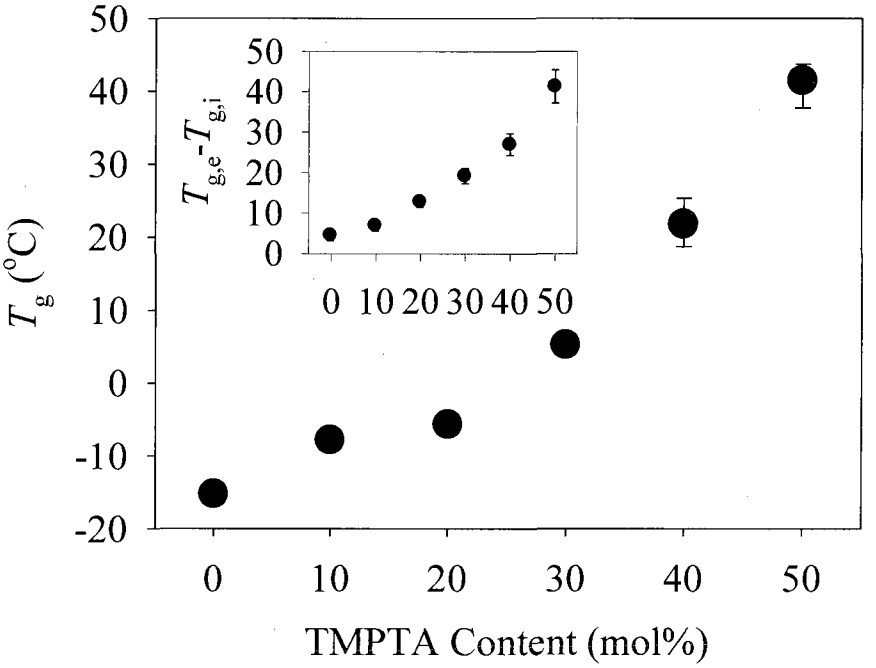

Figure 7.9. Effect of TMPTA on T_g of photopolymerized TMPMP-APE-TMPTA ternary networks.

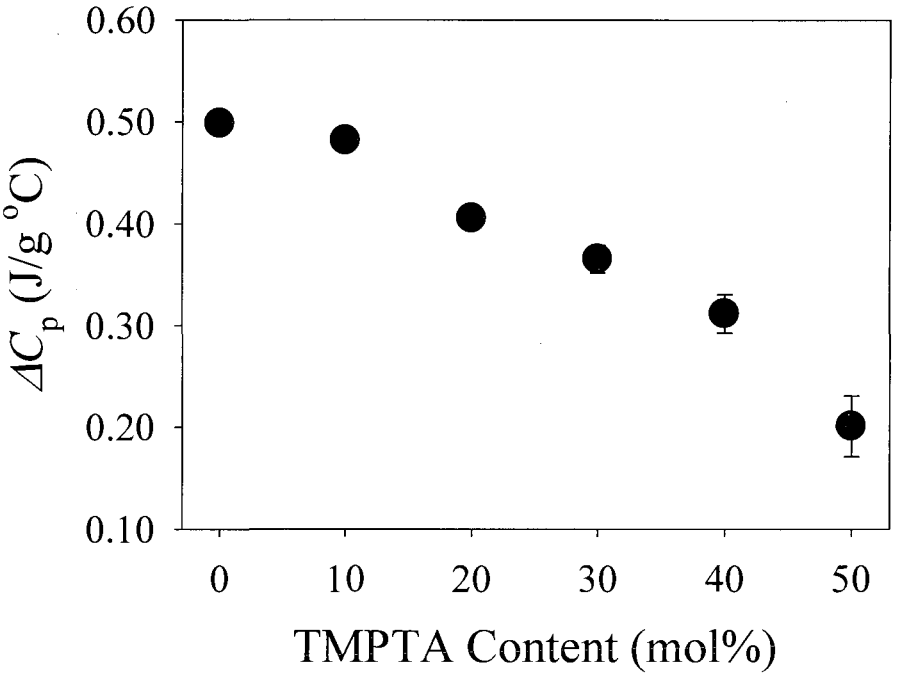

Figure 7.10. Effect of TMPTA on heat capacity of photopolymerized TMPMP-APE-TMPTA ternary networks.

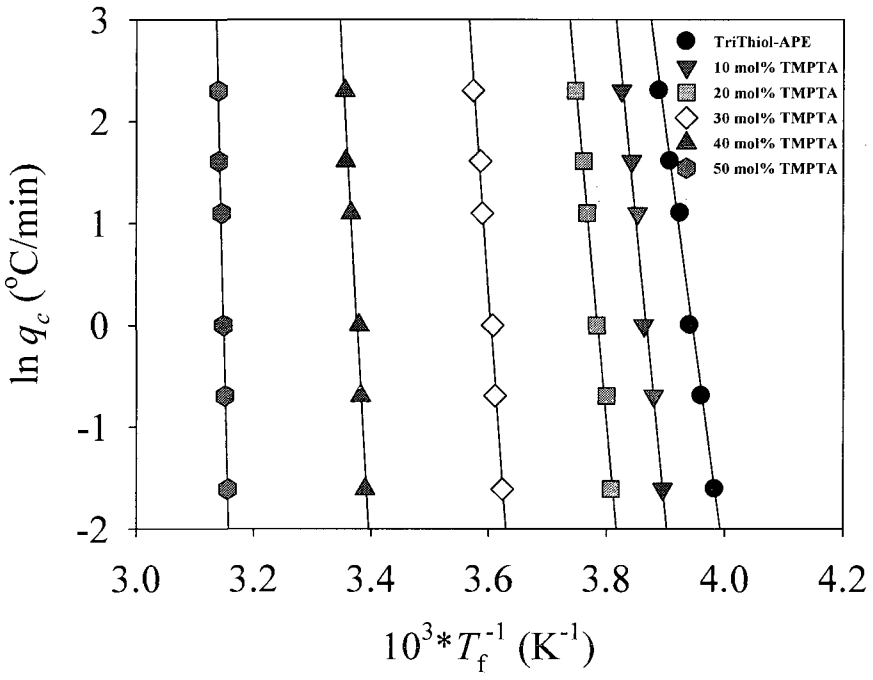

Figure 7.11. Plots of logarithmic cooling rate (q_c) vs. reciprocal fictive temperature (T_f) of photopolymerized TMPMP-APE-TMPTA ternary networks.

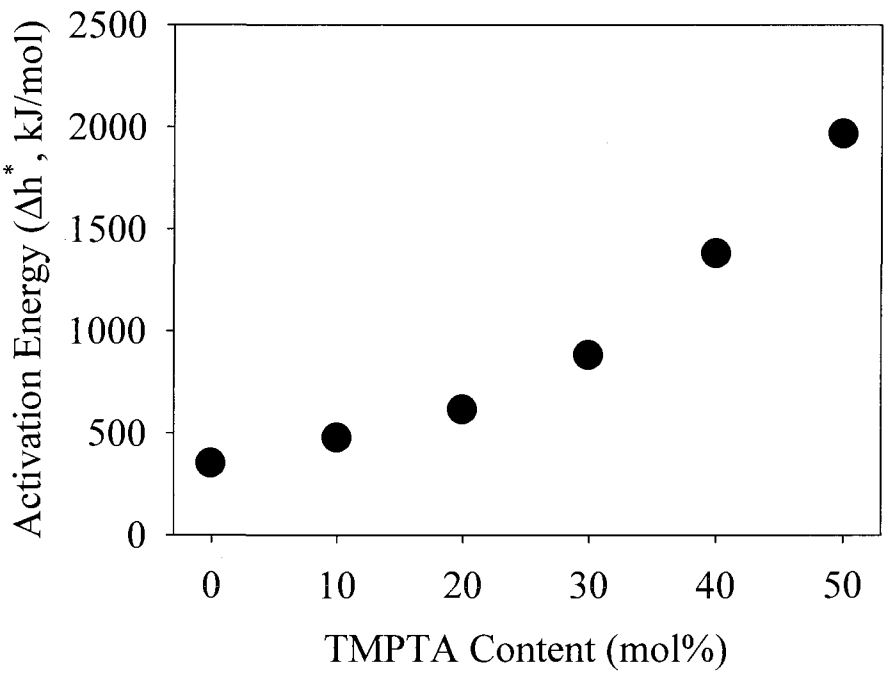

Figure 7.12. Apparent activation energy (Δh^*) for enthalpy relaxation of photopolymerized TMPMP-APE-TMPTA ternary networks as a function of TMPTA content.

CHAPTER VIII

ENTHALPY RELAXATION OF PHOTOPOLYMERIZED MULTI-LAYERED THIOL-ENE FILMS

Abstract

Multi-layered thiol-ene based films with two and three different components were fabricated by spin coating and photopolymerization. The distinctive glass transition temperatures of each component were observed at corresponding glass transition regions of each bulk sample. Sub-T_g aging of 10- and 32-layered thiol-ene films was investigated in terms of enthalpy relaxation. Enthalpy relaxation of each layer component occurred independently and presented the general time and temperature dependency. Overlapped unsymmetrical bell shaped enthalpy relaxation distribution having peak maximum at T_g-10 °C of each layer component was observed, resulting in wide distribution of enthalpy relaxation over wide temperature range. In addition, enthalpy relaxation of each layer component in the multi-layered thiol-ene films was significantly accelerated comparing to that of bulk thiol-ene samples. Dynamic mechanical thermal properties of multi-layered thiol-ene films also showed two and three separated glass transition temperature. However, for 32-layered thiol-ene film consisting of three different components, glass transition and damping region are overlapped and the width is extended over 100 °C.

Introduction

Thiol-ene photopolymerization has attracted much interest in academia as well as industries due to the unique reaction mechanism and chemical structure.[1-13] The kinetics of thiol-ene reactions following free-radical step reactions and resultant uniform networks structure have been extensively studied by Bowman and Hoyle since 2000.[6-13] Uniform and highly dense network structure results in narrow glass transition temperature (FWHM < 20 °C) and very high damping factor (tan δ < 1.6) due to probably narrow distribution of relaxation times.[1,14] Recently, the physical importance of the uniformity of thiol-ene networks has been reported by correlating chemical structure of thiol-ene networks and sub-T_g aging in terms of enthalpy relxation.[15,16] The overall relaxation is significantly affected by chemical parameters such as network uniformity, cross-link density, rigidity, bulky side groups, and hydrogen bonding. It is well known that apparent glass transition temperature and physical / mechanical properties of polymer materials can be potentially changed during the sub-T_g aging. In most cases, maximum enthalpy relaxation rate is observed at T_g-10 °C that resulted by the competition between thermodynamic driving force and molecular mobility.[15] Since thiol-ene photo-polymerized materials mostly have T_g near room temperature, the considerable property changes by sub-T_g aging are expected. Thus, it was also suggested that the overall rate (β_H) and extent of enthalpy relaxation (δ_H) can be intentionally restricted by chemical and physical modification of the thiol-ene network structure.[16]

Polymer thin films are widely being used as a membrane for gas separation and recently their application are expanding over many applications with the increasing demand of miniaturizing electronic devices.[17-20] It is known that as thickness decreases,

the physical properties of very thin polymer films appear to be different with what is observed in the bulk.[21-24] Special attention has been paid to study glass transition (T_g) behavior in confined thin films where the T_g is correlated to the chain mobility and interfacial interaction with substrate.[24,25] In the case of polymer films having weak interaction with the substrate, T_g usually decreases with decreasing film thickness.[21,22] If such a thin film is removed from the substrate, the resultant free-standing film has much different T_g than the film attached to the substrate.[23] On the contrary, an increase of T_g with decreasing film thickness has been shown for a PMMA (poly(methyl-methacrylate)) thin film on a hydrophilic modified substrate where there is strong interaction between the polymer thin film and the substrate.[24,25] Therefore, it can be concluded that, at least for linear, non-crosslinked or network polymers, the nature of the substrate-film interface is a critical factor affecting the T_g of polymer thin films. It can be speculated that the substrate-film interface will also affect relaxation processes upon physical aging. Interestingly, several recent reports have shown that the accelerated physical aging of thin films formed from linear polymers result in drastic changes of physical properties on very short time scales.[18-20,26-28] Huang et al. observed a more rapid increase in refractive index for thin films for linear polymer than for thick films of the same polymer.[26] Physical aging, as a function of film thickness as already noted, has also been reported to have a large effect on gas permeability.[19,20,26-28] Because gas permeation of polymeric materials is directly related to free volume, these results strongly suggest that accelerated physical aging is a direct contribution to volume changes of linear polymer films.

Multi-layered films of different polymers are commonly used in many applications such as gas barriers for food packaging and anti-reflective optical coatings.[29-

[31] These multi-layered films consist of a few to thousands layers with two or more different polymers. Each polymer has different physical properties so that the response of each layer to environment changes such as temperature and humidity. Thus, it is important to characterize and understand the physical and mechanical properties of each layer within the multi-layered films. For instance, if each polymer or layer is actually phase separated without any chemical bonding, they will undergo sub-T_g aging at different rate for a specific set of annealing conditions due to their different molecular structure.

In this article, 10 and 32-layered thiol-ene photo-polymerized films were fabricated with two and three different chemical compositions, respectively, by spin coating and evaluated in terms of sub-T_g aging monitored by enthalpy relaxation. The extent and rate of enthalpy relaxation of multi-layered thiol-ene networks were investigated and compared with them as in thick films of each composition. In addition, layering thiol-ene films, which have high uniform dense network resulting in glass transition occurring at narrow temperature region, provided a good venue as a damping material through the wide temperature range of loss modulus and tan δ.

Experimental

Materials

Thiols (Trimethylolpropane tris(3-mercaptopropionate) (Thiol 1) and pentaerythritol tetra(3-mercaptopropionate) (Thiol 2)) and ene monomers (allyl pentaerythritol (Ene 1), 2,4,6-triallyloxy-1,3,5-triazine (Ene 2), and 1,3,5-triallyl-1,3,5-triazine-2,4,6(1H,3H,5H)-trione (Ene 3)) were obtained from Bruno Bock Thio-

Chemicals-S and Perstorp Specialty Chemicals, respectively (Chart 8.1). The photoinitiator, 2,2-dimethoxy 2-phenyl acetophenone (DMPA), was obtained from Ciba Specialty Chemicals and directly used without purification.

Preparation of multi-layered thiol-ene films

Each layer has different glass transition temperature by the combination of different thiol and ene monomers that have different functionality and rigidity (Thiol 1-Ene 1 : T_g = -14 °C, Thiol 2-Ene 2 : T_g = 10 °C, and Thiol 2-Ene 3 : T_g = 45 °C). Thiols and enes for each layer were mixed with 1 wt% of photo-initiator (DMPA) and sonicated for 30 min in order to dissolve it. Multi-layered thiol-ene films were prepared by repeating spin coating and UV irradiation on the glass plate (2.5×2.5 cm). UV lamp was shuttered using electrically a automated optical shutter while each layer was spin-coated. Thickness of each layer was controlled by the spin rate and UV light was irradiated for 30 sec with low pressure mercury lamp (254 nm, 0.1 mW/cm^2). Photo-polymerized multi-layered thiol-ene films were post-cured at 80 °C for 12 hours in order to ensure full conversion of thiol-ene free-radical reaction and remove the feasibility of chemical structural change during physical aging. Figure 8.1 illustrates a diagram for multi-layered thiol-ene films consisting of three types of a thiol-ene network with three separate T_gs as well as physical aging behavior at specific temperature and time. Thickness of each layer and film was controlled by the amount of mixture and rpm of spin coater. Thickness of each layer was calculated with the weight, density of monomers, and area of glass plate. Two different types of multi-layered thiol-ene films were prepared with different thickness of each layer, the number of layers, and components of each layer. First sample has 10-layers with Thiol 1-Ene 1 and Thiol 2-Ene 2 by alternating two layers

whose average thicknesses were 47 and 43 μm, respectively. Total thickness was 450 μm and the weight ratio of two systems was 55:45. Second sample was prepared by layering three different system (Thiol 1-Ene 1, Thiol 2-Ene 1, and Thiol 2-Ene 2) and average thicknesses were 16, 20, and 17 μm, respectively. The number of each layer (9:10:13) and weight ratio (25:35:40) were determined based on the extent and rate of enthalpy relaxation of each thick film composition under the same condition (annealing time and temperature). Total thickness was 564 μm with 32-layers.

Characterization

Glass transition temperatures and thermal properties were measured with a TA Q800 dynamic mechanical analyzer (DMA) from -80 to 200 °C at a heating rate of 3 °C/min and frequency of 1 Hz using tensile mode, and a TA Q1000 differential scanning calorimeter (DSC) from -60 to 120 °C at a 10 °C/min heating and cooling rate. TA Q1000 was set up with RCS 90 (Refrigerated Cooling System). A RCS 90 cooling head mounted on the DSC Q1000 furnace encases the DSC cell preventing frost building-up during operation. Three calibration steps (T_{zero} calibration, enthalpy constant calibration, and Temperature calibration) for the TA Q1000 were performed periodically. Detailed calibration protocol has been well described in a previous literature.[15,16]

Three different aging methods were used to characterize enthalpy relaxation of multi-layered thiol-ene films as described in Figure 8.2 which showed time (isothermal) and temperature (isochronal) dependency of physical aging as well as different cooling rates potentially show the distribution of enthalpy relaxation (Figure 8.3). Special attention was paid to running the DSC to ensure the accuracy of the enthalpy relaxation measurement. For three different annealing methods described in Figure 8.2, the

measurement was conducted twice and the sequence of annealing was reversed in the second running. Equivalent results were obtained in each case, i.e., instrumental drift did not play a factor, and the results were reproducible despite the different order in obtaining the data sets. Furthermore, the heat flow and heat capacity of Thiol 1-Ene 1 sample without aging, as a standard, were measured after every calibration and time-sequence scan to ensure consistency. Finally, in order to remove sampling errors, the same DSC pans (samples) were used for all measurements. All experiments were carried out under nitrogen with a flow rate of 50 mL/min. Sample weights were 8.0±1.0 mg to ensure sufficient sensitivity for heat capacity measurements. DSC scans were conducted over the temperature range of ± 50 °C from the highest and lowest glass transition temperature of multi-layered thiol-ene films. Annealing temperature (T_a), annealing time (t_a), and cooling rate (q_c) were controlled to establish different annealing methods. Detailed descriptions of measurement techniques are described in mthe text.

The morphology of multi-layered thiol-ene films was obtained using scanning electron microscopy (SEM) (Quanta 200 SEM) in the high-voltage mode. Multi-layered thiol-ene films were quenched in liquid nitrogen and fractured followed by mounting on the SEM sample holders with epoxy. Samples were sputter-coated with a 5 nm gold layer using a Emitech K550X sputter coater to enhance the image quality.

Results and Discussion

Morphology

In Figure 8.4, the SEM images of fractured surface of 10 ad 32-layered thiol-ene films show that multi-layered structure is well defined for both samples and the de-

lamination between layers are not observed. Thickness of each layer for each sample is approximately consistent with the calculated average thickness, i.e. 40~50 μm for 10-layered film and 15~20 μm for 32-layered film.

Thermal properties

DSC thermograms and glass transition temperatures of 10- and 32-layered thiol-ene films and bulk samples of each layer composition were shown in Figure 8.5. Two and three distinctive separated T_gs were observed for 10-layered (a) and 32-layered films (b) respectively corresponding to glass transition temperature of each layer in bulk. It seems that adjacent layers and substrate (glass) do not affect much on chain mobility and thermal property each other because each layer has pretty great thickness (20~40 μm) to exhibit its own T_g and no chemical and physical interaction between layers.

Enthalpy relaxation

Figure 8.6 shows DSC heating scans of 10- and 32-layered thiol-ene films after cooling at different rates (q_c=10 °C/min and 0.2 °C/min) as described in Figures 2(a) and Figure 8.3(a). Differential cooling rate methodology was used to define the distribution and extent of enthalpy relaxation for 10- and 32-layered thiol-ene films independent to the annealing time and temperature dependency on the enthalpy relaxation. For both 10- and 32-layered thiol-ene films, the endothermic peaks by enthalpy relaxation of each layer were observed at its T_g region. The area of enthalpy relaxation produced by differential cooling rate for 10-layered films shows that the layers of Thiol 1-Ene 1 present greater endothermic peak by enthalpy relaxation than Thiol 2-Ene 3 layers (Figure 8.6(a)) even though the weight ratio between two components are almost the same (55:45). It is probably due to the different enthalpy relaxation rate of each layer

component. In our previous study, we systematically investigated the effect of chemical parameters of thiol-ene networks such as network density and rigidity on enthalpy relaxation.[15] The higher network density and more rigid chemical structure of thiol-ene networks result in the slower and less extent of enthalpy relaxation. For 32-layered thiol-ene film, the number and weight ratio of three network components were determined based on the characteristic enthalpy relaxation behavior of each component as in bulk (Table 8.1). It is concluded that multi-layered thiol-ene films exhibit enthalpy relaxation over wide temperature range due to the different T_gs of each layer as well as the inconsistent enthalpy relaxation will be occurred in a film at a specific annealing condition, i.e. annealing time (t_a) and temperature (T_a). As a result, there are potential problems due to the inconsistency of enthalpy relaxation between layers since each layer has different chemical structure and resultant relaxation times, which could be a potential problem in physical and mechanical properties of multi-layered thiol-ene films.

In Figure 8.7 to Figure 8.10, the temperature dependency of the enthalpy relaxation for both 10- and 32-layered thiol-ene films is shown. DSC heating scans of 10-layered thiol-ene film after annealing at different temperature from -39 to 49 °C for 1h in Figure 8.7 show that the enthalpy relaxation is temperature dependent. The endothermic peaks due to the enthalpy relaxation are maximum at T_g-10 °C of two different components (-24 °C for Thiol 1-Ene 1 and 35 °C for Thiol 2-Ene 3) and decrease as T_a is getting farther from T_g. This temperature dependency of enthalpy relaxation is affected by two factors such as chain mobility and thermodynamic driving force, and maximum at T_g-10 °C is the resultant temperature of the competition of them.[15,16] In general, chain mobility is extremely restricted below T_g-30 °C and there is

no relaxation over T_g+5 °C because liquid or rubbery state is already thermodynamic equilibrium. Therefore, no enthalpy relaxation was observed from -1~14 °C where temperature is too low for Thiol 2-Ene 3 to be relaxed and it is equilibrium for Thiol 1-Ene 1. Figure 8.8 shows the distribution of enthalpy relaxation as a function of temperature, which was calculated by the integration of enthalpy relaxation peak as following equation,

$$\Delta H_r(T_a,t_a) = \int_{T_g-50^oC}^{T_g+50^oC} C_p(T_a,t_a)dT - \int_{T_g-50^oC}^{T_g+50^oC} C_p(T_a,0)dT \qquad (1)$$

where $C_p(T_a, t_a)$ and $C_p(T_a, 0)$ represent specific heat capacities for samples annealed at T_a for $t=t_a$ and unannealed samples, respectively.

For 32-layered thiol-ene films, three different thiol-ene layer components showing different glass transition temperature (Thiol 1-Ene 1: T_g=-14 °C, Thiol 2-Ene 2: T_g=10 °C, and Thiol 2-Ene 3 : T_g=45 °C) were stacked, which results in three separated T_gs and endothermic peaks due to the enthalpy relaxation. In Figure 8.9, three different enthalpy relaxation peaks were observed and all of them have maximum at T_g-10 °C of each component indicating each layer is independent to adjacent layers. The distribution of enthalpy relaxation as a function of T_a in Figure 8.10 shows overlapped three peaks corresponding temperature dependency of each component (Thiol 1-Ene 1, Thiol 2-Ene 2, and Thiol 2-Ene from left to right).

The time dependency of enthalpy relaxation for 32-layered thiol-ene film characterized by isothermal aging method as described in Figure 8.2c and 3c is shown in Figure 8.11. The 32-layered thiol-ene film was annealed at three different temperatures

(-24, -1, and 34 °C), where the enthalpy relaxation showed maxima in isochronal aging method, as a function of annealing time (t_a). At each T_a, the extent of enthalpy relaxation increases as increasing t_a at the corresponding T_g region but no relaxation was observed at the region of the other two layer components, indicating that the enthalpy relaxation of layers are independent each other. In Figure 8.12, the extent of enthalpy relaxation (δ_H) of 32-layered thiol-ene film calculated by equation 1, normalized values by weight ratio of each layer component (Thiol 1-Ene 1 : Thiol 2-Ene 2 : Thiol 2-Ene 3 = 25 : 35 : 40), and that of bulk samples are plotted as a function of logarithmic annealing time. The calculated values are summarized in Table 8.1. In order to quantitatively analyze the general overall relaxation rate (β_H), a simple equation (2)[32-36] was applied to the plots in Figure 8.12.

$$\beta_H = \frac{d\delta_H}{d\log t_a} \tag{2}$$

It is clear that the β_H values obtained from the extent of enthalpy relaxation (δ_H) vs. logarithmic annealing time (t_a) at each T_a in Figure 8.11 smaller than β_H of bulk samples due to the weight ratio of each layer component in 32-layered film. However, the normalized δ_H per unit weight of each layer component is considerably greater than δ_H of bulk samples resulting in faster overall relaxation rate (β_H). It is concluded that the thin layers within 32-layered film that are not chemically bonded exhibit accelerated enthalpy relaxation compared to that of bulk samples because segmental chain mobility of each layer increases and each layer does not affect each other.

Dynamic mechanical thermal properties

In Figure 8.13, tan δ and loss modulus of 10- and 32-layered thiol-ene films are shown. Two and three distinctive transition peaks are observed at T_g of each layer component that is consistent with DSC results. Thus, for 32-layered thiol-ene film, glass transition regions of three different layer components are overlapped and ranges from -20 ~ 80 °C. Based on the viscoelasticity, the damping property of a polymer can be estimated by the intensity and area of tan δ or loss modulus (E").[37] Therefore, it has been reported that thiol-ene networks are a good candidate for high energy absorbing materials due to the high tan δ peak resulted by the highly dense and uniform chemical structure.[1,38-40] However, the narrow glass transition range of thiol-ene resulted by the highly dense and uniform network structure limits energy damping temperature, i.e. working temperature. Consequently, layering thiol-ene films exhibiting high and broad loss modulus (E") and tan δ as shown in Figure 8.13 could provide the solution to the existing problems of thiol-ene based materials as energy damping applications.

Conclusions

10- and 32-layered thiol-ene films were successfully prepared by sequentially repeating spin coating and photo-polymerization of two and three different thiol-ene compositions, respectively, to investigate thermal property and enthalpy relaxation behavior of multi-layered thiol-ene films. Two and three separated T_gs were observed for 10-layered (Thiol 1-Ene 1 and Thiol 2-Ene3) and 32-layered films (Thiol 1-Ene1, Thiol 2-Ene 2, and Thiol 2-Ene 3) indicating that each layer of multi-layered thiol-ene films is independent each other. As a resultant, distinctive enthalpy relaxation peaks were

observed for both 10- and 32-layerd thiol-ene films at the same temperature region, i.e. T_g of bulk thiol-ene samples. Isochronal annealing experiments showed temperature dependency of enthalpy relaxation for both 10- and 32-layered thiol-ene films that are distributed over wide temperature range. Time dependency of enthalpy relaxation for 32-layered thiol-ene film was obtained by isothermal annealing experiment at three annealing temperature (T_a). The extent (δ_H) as well as overall enthalpy relaxation rate (β_H) was significantly accelerated by layering of thin films compared to bulk samples. Consequently, the enthalpy relaxation of each layer component occur independently at a different temperature, so as a result the inconsistency in physical and mechanical property changes between layers by enthalpy relaxation could be a potential problem to affect the original performance of multi-layered thiol-ene films. In addition, the acceleration of enthalpy relaxation by the formation of multi-layered thin films is another parameter that has to be considered when designing thiol-ene films.

Loss modulus (E") and tan δ of 10- and 32-layered thiol-ene film showed two and three distinctive peaks corresponding to T_gs of different thiol-ene layer components. However, for 32-layered thiol-ene film consisting of three different components, glass transition and damping region are overlapped and the width is extended over 100 °C. It is proposed that multi-layered structure using thiol-ene exhibiting high damping factor (tan δ) could be a good candidate for an energy damping material in many applications.

Finally, this article mainly discussed about general enthalpy relaxation behavior of thiol-ene films as in multi-layered structure in terms of glass transition temperature and enthalpy relaxation of each layer component. However, the thickness effects of each layer on physical properties, especially enthalpy relaxation, are also very interesting

topic. In addition, actual energy damping properties such as impact, acoustic, and vibrational damping of multi-layered thiol-ene films will be reported in near future.

References

1. Hoyle, C. E.; Lee, T. Y.; Roper, T. *Journal of Polymer Science: Part A: Polymer Chemistry* **2004**, 42, 5301.
2. Roper, T. M.; Rhudy, K. L.; Chandler, C. M.; Hoyle, C. E.; Guymon, C. A. *RadTech NA Tech Conf Proc.* **2002**, 697.
3. Roper, T. M.; Guymon, C. A.; Hoyle, C. E. *Polymer* **2004**, 45, 2921.
4. Lub, J.; Broer, D. J.; Allan, J. F. *Mol Cryst Liq Cryst Sci Tech Sect A: Mol Cryst Liq Cryst* **1999**, 332, 2769.
5. Toh, H. K.; Chen, F.; Kok, C. M. U.S. Patent 6,172,140, **2001**.
6. Cramer, N. B.; Scott, J. P.; Bowman, C. N. *Macromolecules*, **2002**, 35, 5361.
7. Cramer, N. B.; Davies, T.; O'Brien, A. K.; Bowman, C. N. *Macromolecules*, **2003**, 36, 4631.
8. Cramer, N. B.; Reddy, S. K.; O'Brien, A. K.; Bowman, C. N. *Macromolecules*, **2003**, 36, 7964.
9. Okay, O.; Reddy, S. K.; Bowman, C. N. *Macromolecules*, **2005**, 38, 4501.
10. Reddy, S. K.; Cramer, N. B.; Bowman, C. N. *Macromolecules*, **2006**, 39, 3673.
11. Senyurt, A. F.; Wei, H.; Hoyle, C. E.; Piland, S. C.; Gould, T. E. *Macromolecules*, **2007**, 40, 4901.
12. Wei, H.; Li, Q.; Ojelade, M.; Madbouly, S.; Otaigbe, J. U.; Hoyle, C. E. *Macromolecules*, **2007**, 40, 8788.
13. Scott, T. F.; Kloxin, C. J.; Draughon, R. B.; Bowman, C. N. *Macromolecules*, **2008**, 41, 2987.

14. Shin, J.; Matsushima, H.; Comer, C. M.; Hoyle, C. E. *Thiol-Isocyanate-Ene Ternary Networks by Sequential and Simultaneous Thiol Click Reactions*, in preparation.

15. Shin, J.; Nazarenko, S.; Hoyle, C. E. *Macromolecules* **2008**, 41, 6741.

16. Shin, J.; Nazarenko, S.; Hoyle, C. E. *Macromolecules* **2009**, 42, 6549.

17. Frank, C. W.; Rao, V.; Despotopoulou, M. M.; Pease, R. F. W.; Hinsburg, W. D.; Miller, R. D.; Rabolt, J. F. *Science* **1996**, 273, 912.

18. Pfromm, P. H.; Koros, W. J. *Polymer* **1995**, 36, 2379.

19. McCaig, M. S.; Paul, D. R. *Polymer* **2000**, 41, 629.

20. McCaig, M. S.; Paul, D. R.; Barlow, J. W. *Polymer* **2000**, 41, 639.

21. Kim, J. H.; Jang, J.; Zin, W. C. *Langmuir* **2000**, 16, 4064.

22. Pham, J. Q.; Green, P. F. *Macromolecules* **2003**, 36, 1665.

23. Forrest, J. A.; Dalnoki-Veress, K.; Stevens, J. R.; Dutcher, J. R. *Physics Review Letter* **1996**, 77, 2002.

24. Keddie, J. L.; Jones, R. A. L.; Cory, R. A. *Faraday Discuss* **1994**, 98, 219.

25. Wallace, W. E.; van Zanten, J. H.; Wu, W. L. *Physical Review E* **1995**, 32, R3329.

26. Huang, Y.; Paul, D. R. *Macromolecules* **2006**, 39, 1554.

27. Dorkenoo, K. D.; Pfromm, P. H. *Journal of Polymer Science, Part B: Polymer Physics* **1999**, 37, 2239.

28. Pinnau, I.; Koros, W. J. *Journal of Applied Polymer Science* **1991**, 43, 1491.

29. Roth, C. B.; Torkelson, J. M.; *Macromolecules*, **2007**, 40, 3328.

30. Weber, M. F.; Stover, C. A.; Gilbert, L. R.; Nevitt, T. J.; Ouderkirk, A. J. *Science* **2000**, *287*, 2451.

31. Leibler, L. *Prog. Polym. Sci.* **2005**, *30*, 898.

32. Hutchinson, J. M. *Prog. Polym. Sci.* **1995**, 20, 703.

33. Pan, P.; Zhu, B.; Inoue, Y. *Macromolecules* **2007**, 40, 9664.

34. Ju, H.; Nutt, S. *Macromolecules* **2003**, 36, 4010.

35. Struik, L. C. E. *Polymer*, **1987**, 28, 1869.

36. Struik, L. C. E. *Physical Aging in Amorphous Polymers and Other Materials*, Elsevier Publishing Company: New York, **1978**.

37. Klempner, D.; Sperling, L. H.; Utracki, L. A.; Advances in Chemistry Series 239: Interpenetrating Polymer Networks; ACS, New York, **1991**.

38. Senyurt, A. F.; Wei, H.; Phillips, B.; Cole, M.; Nazarenko, S.; Hoyle, C. E.; Piland, S. G.; Gould, T. E.; *Macromolecules*, **2006**, 39, 6315.

39. Senyurt, A. F.; Wei, H.; Hoyle, C. E.; Piland, S. G.; Gould, T. E.; *Macromolecules*, **2007**, 40, 4901.

40. Senyurt, A. F.; Wei, H.; Hoyle, C. E.; Piland, S. G.; Gould, T. E.; *Macromolecules*, **2007**, 40, 3174.

Table 8.1. The extents of enthalpy relaxation at 24h (ΔH_{24h}) and overall relaxation rates (β_H) for three thiol-ene network components for 10- and 32-layered films

Sample #	ΔH_{24h}* (J/g)			β_H** (J/g per decade)		
	bulk	in layers	normalized	bulk	in layers	normalized
Thiol 1+Ene 1	3.7	2.2	8.7	1.5	0.9	3.7
Thiol 1+Ene 2	2.1	1.2	3.5	0.8	0.4	1.3
Thiol 2+Ene 3	1.7	0.9	2.3	0.6	0.3	0.8

*the extent of enthalpy relaxation after 24 h at T_g-10 °C

**the overall enthalpy relaxation rate at T_g-10 °C

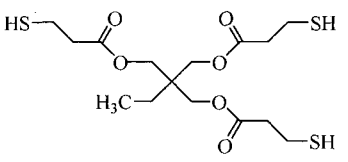

Thiol 1

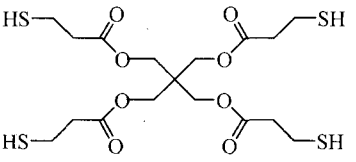

Thiol 2

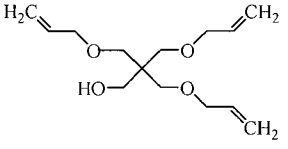

Ene 1

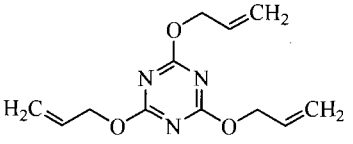

Ene 2

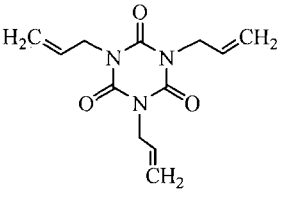

Ene 3

Chart 8.1. The structure of Thiol and Ene monomers.

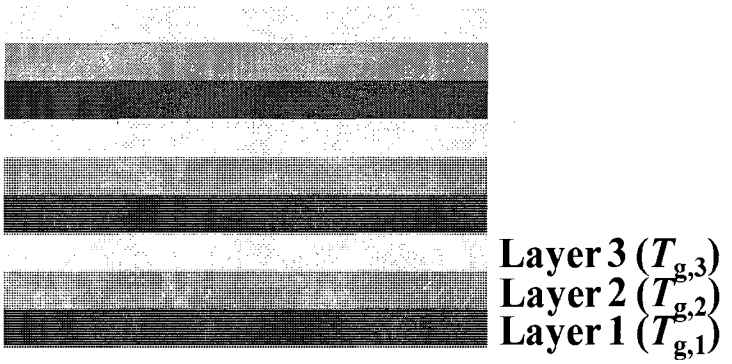

(a)

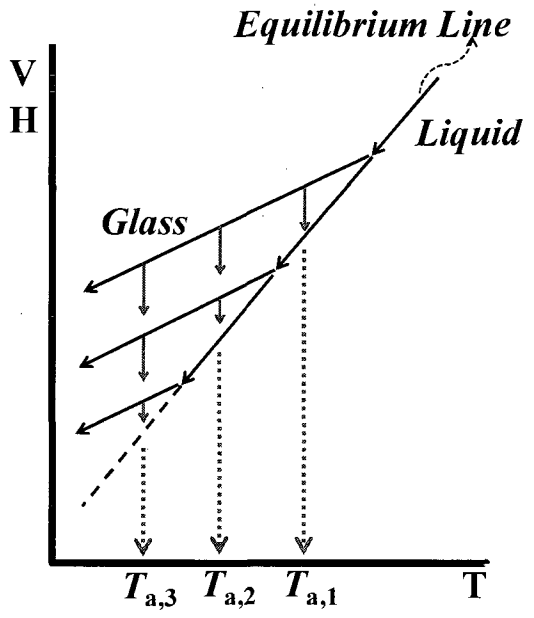

(b)

Figure 8.1. Diagram of physical aging of multi-layered films based on three different layers.

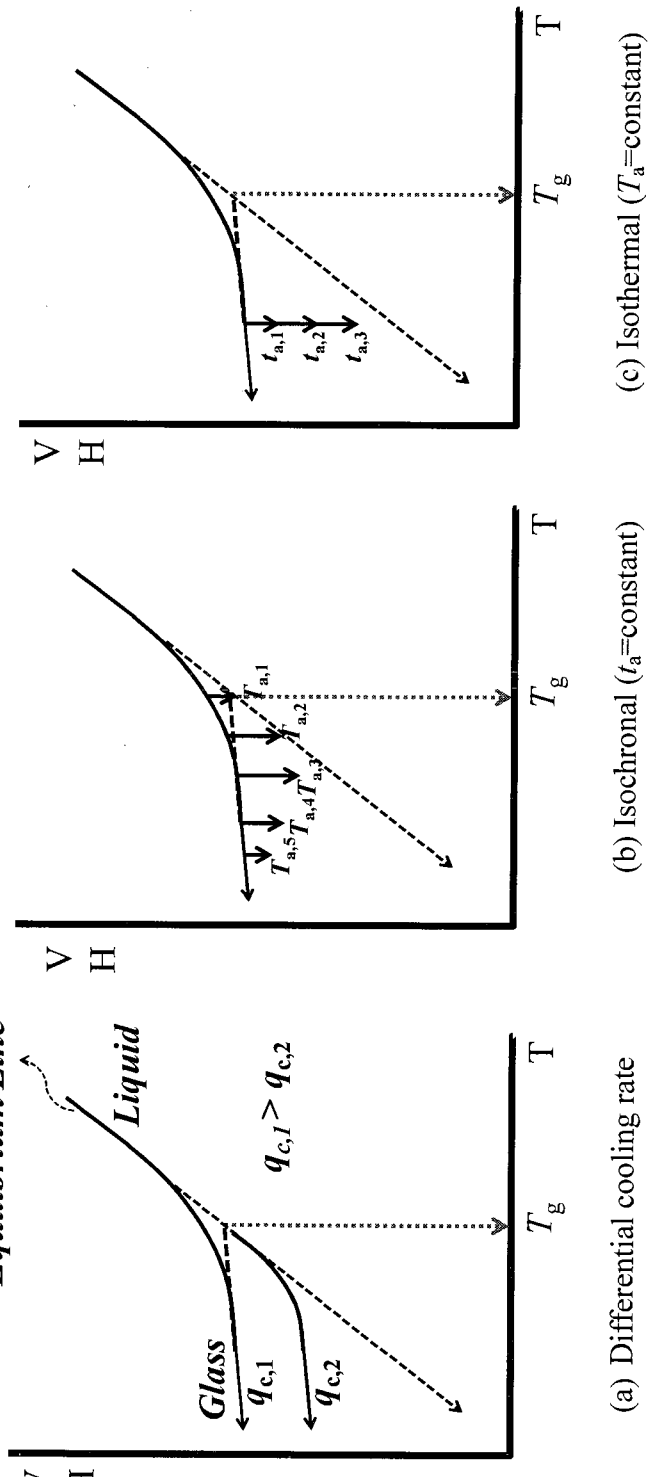

(a) Differential cooling rate (b) Isochronal (t_a=constant) (c) Isothermal (T_a=constant)

Figure 8.2. Physical aging behavior as different annealing methods.

(a) Differential cooling rate

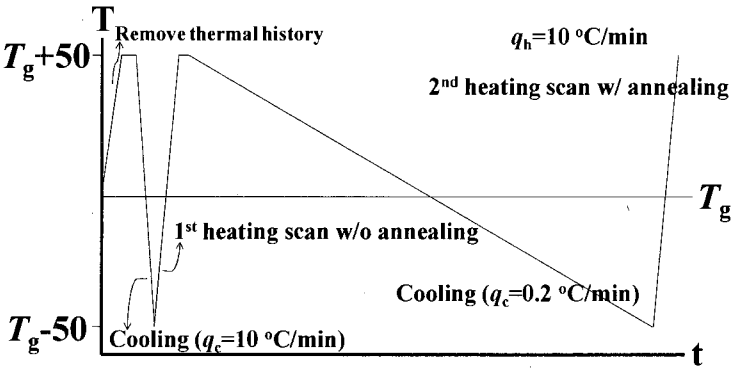

(b) Isochronal

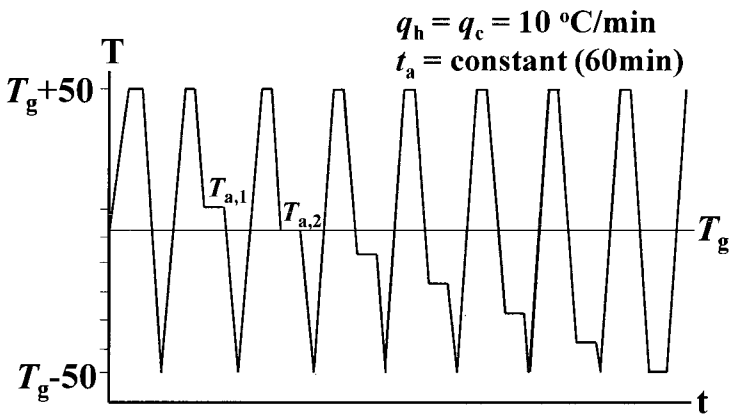

(c) Isothermal

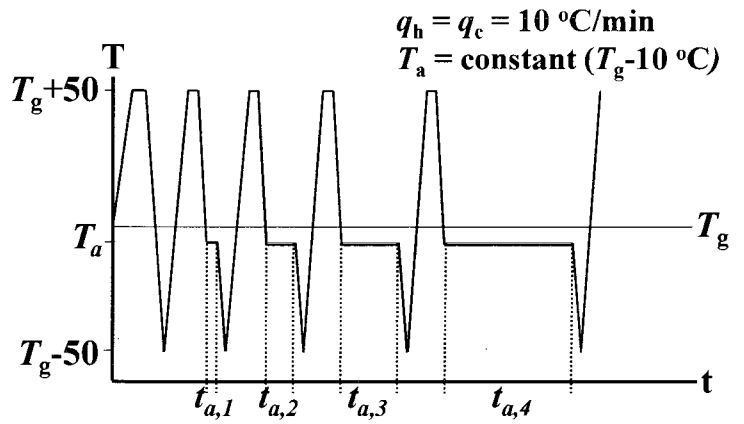

Figure 8.3. Three different types of physical aging methods.

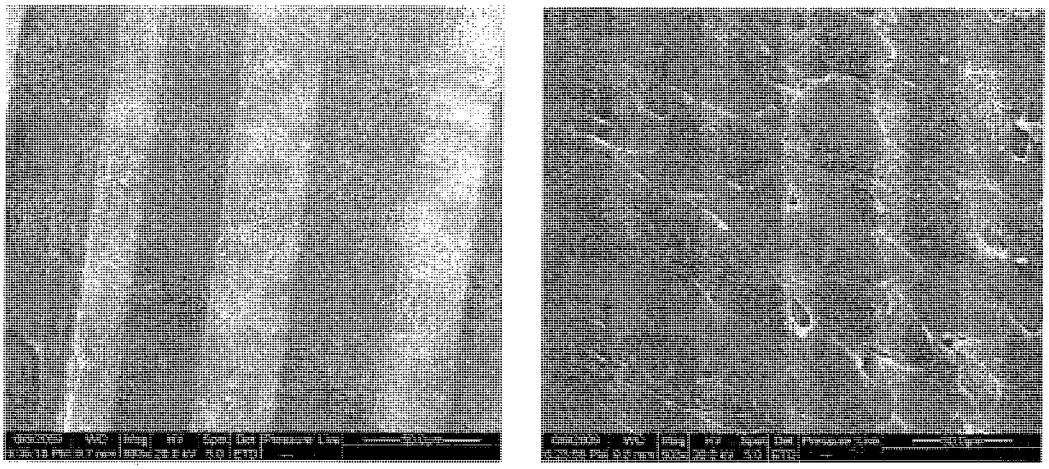

(a) 10-layered film (b) 32-layered film

Figure 8.4. SEM images of fractured surface of 10- and 32-layered thiol-ene films.

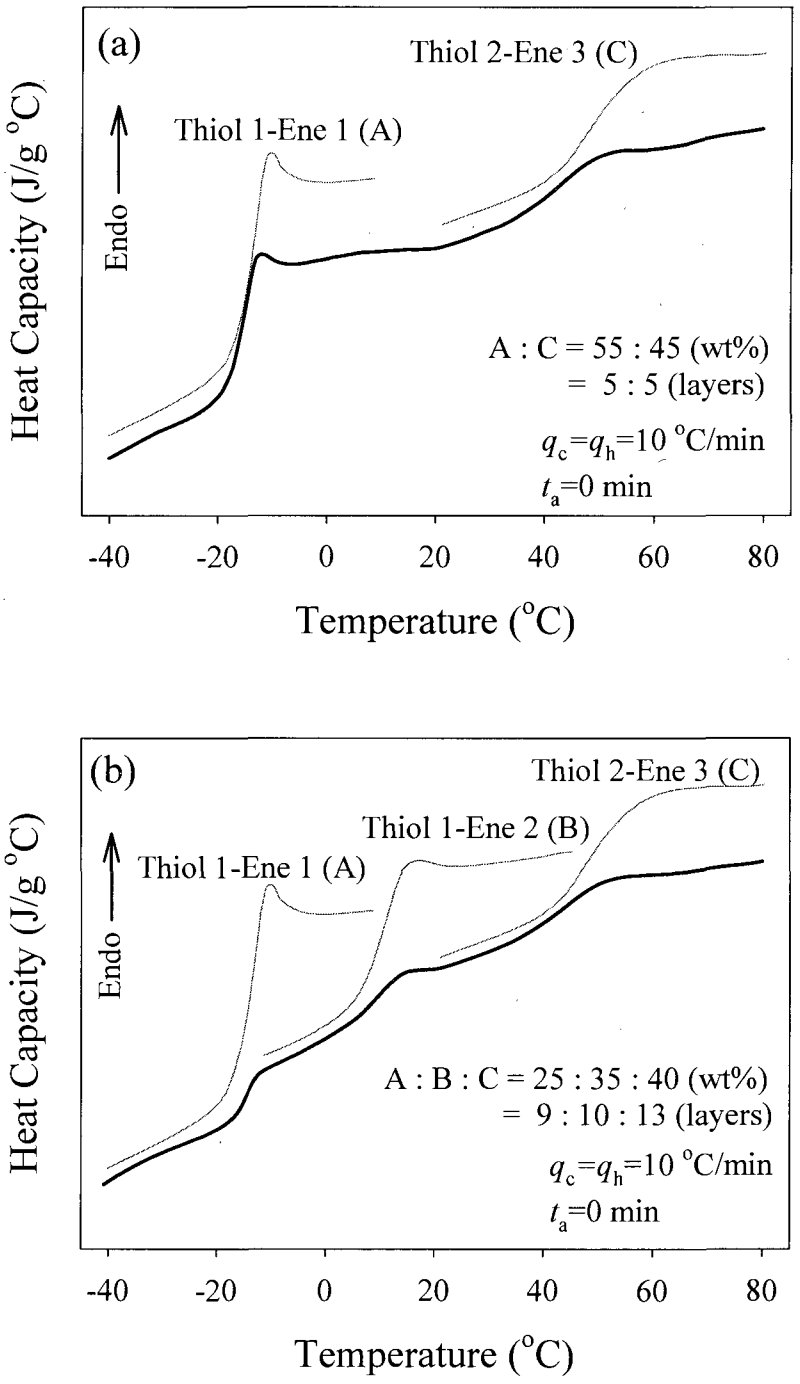

Figure 8.5. Thermal properties of (a) 10- and (b) 32-layered thiol-ene films with two and three different thiol-ene compositions, respectively.

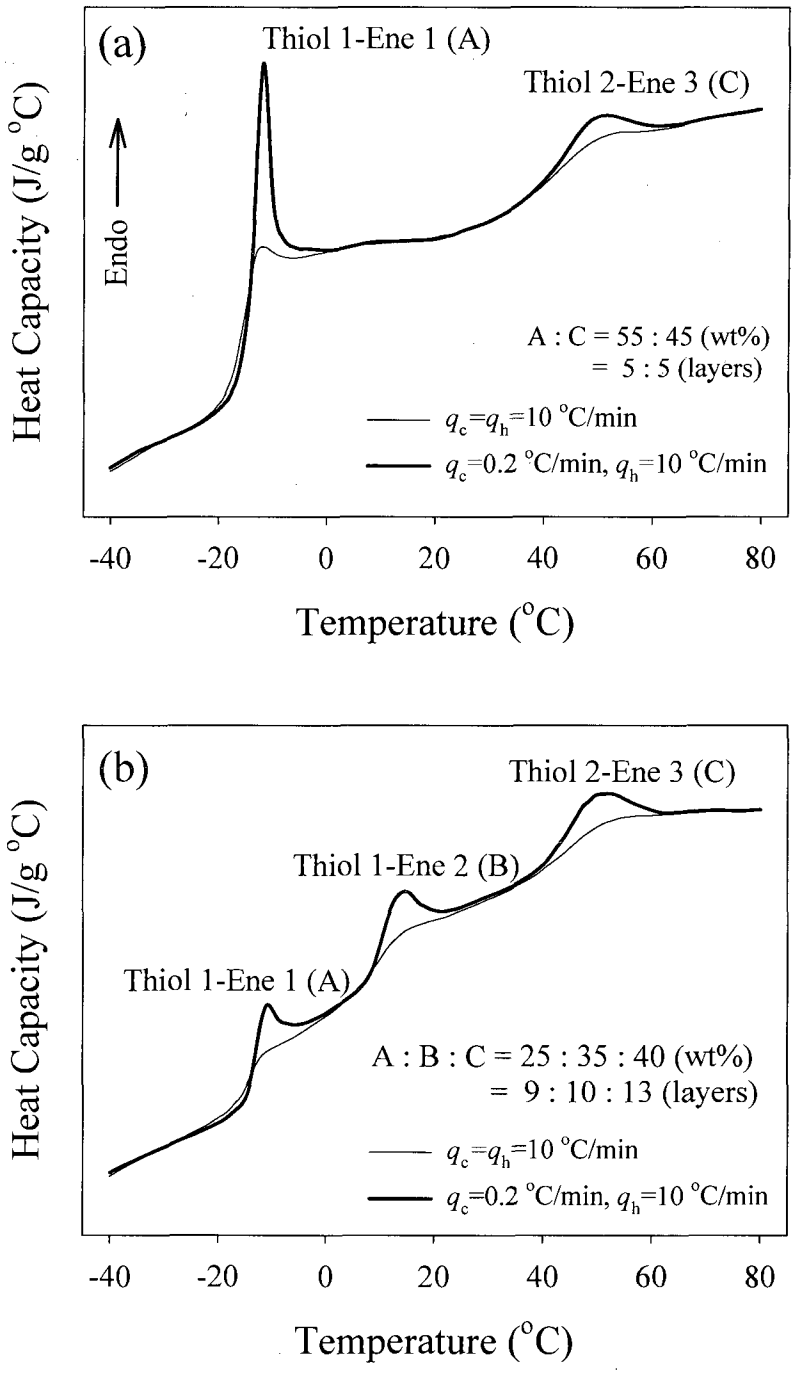

Figure 8.6. DSC heating scans of (a) 10- and (b) 32-layered thiol-ene films with two and three different thiol-ene compositions, respectively, after different cooling rate (q_c).

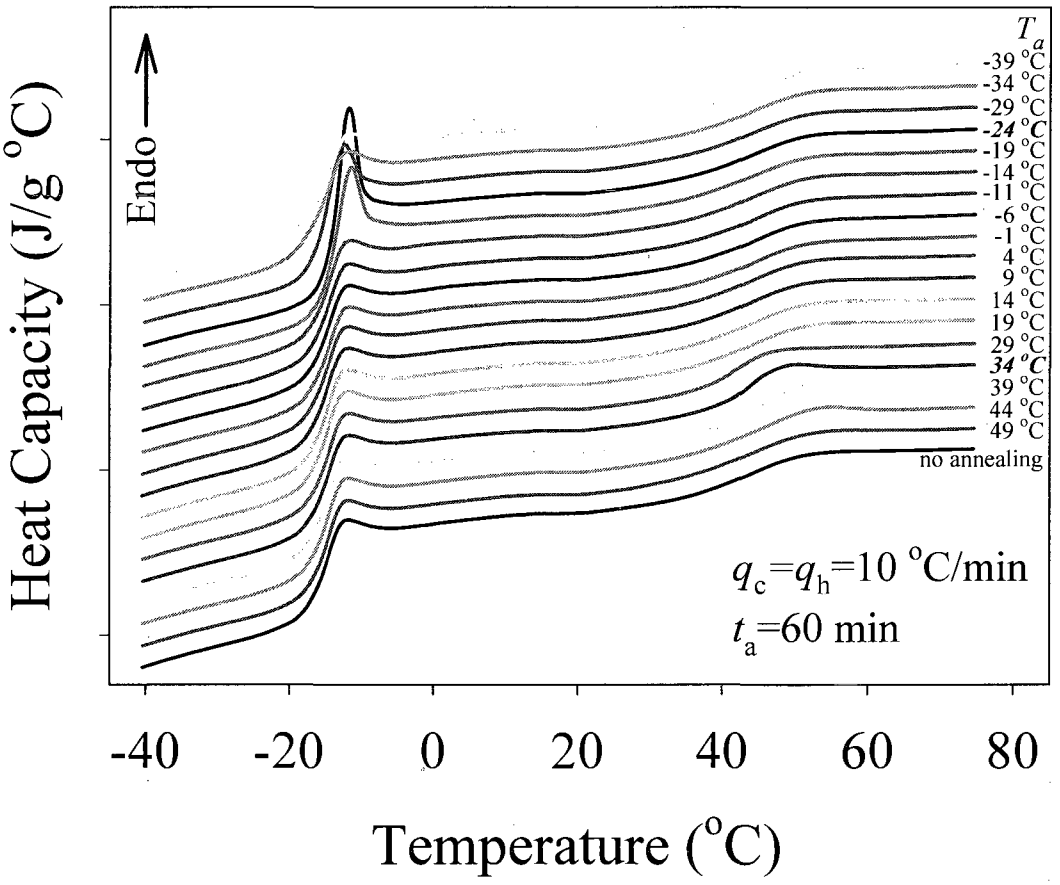

Figure 8.7. DSC heating scans of the 10-layered thiol-ene film after annealing for 1h at different temperature (T_a).

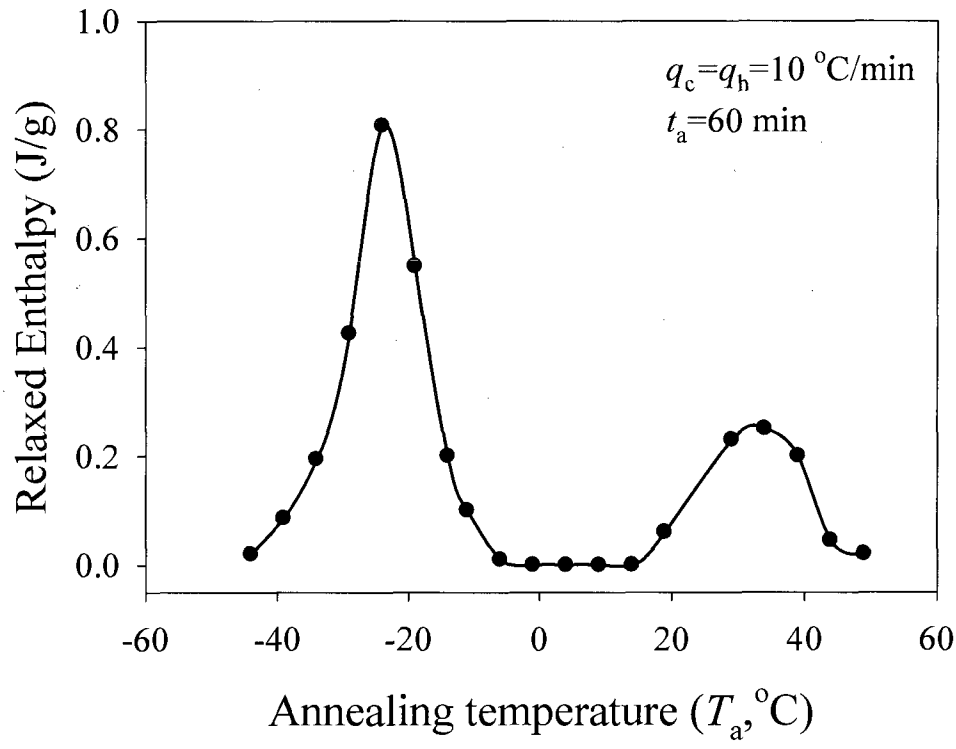

Figure 8.8. The distribution of enthalpy relaxation of the 10-layered thiol-ene film obtained by isochronal aging method.

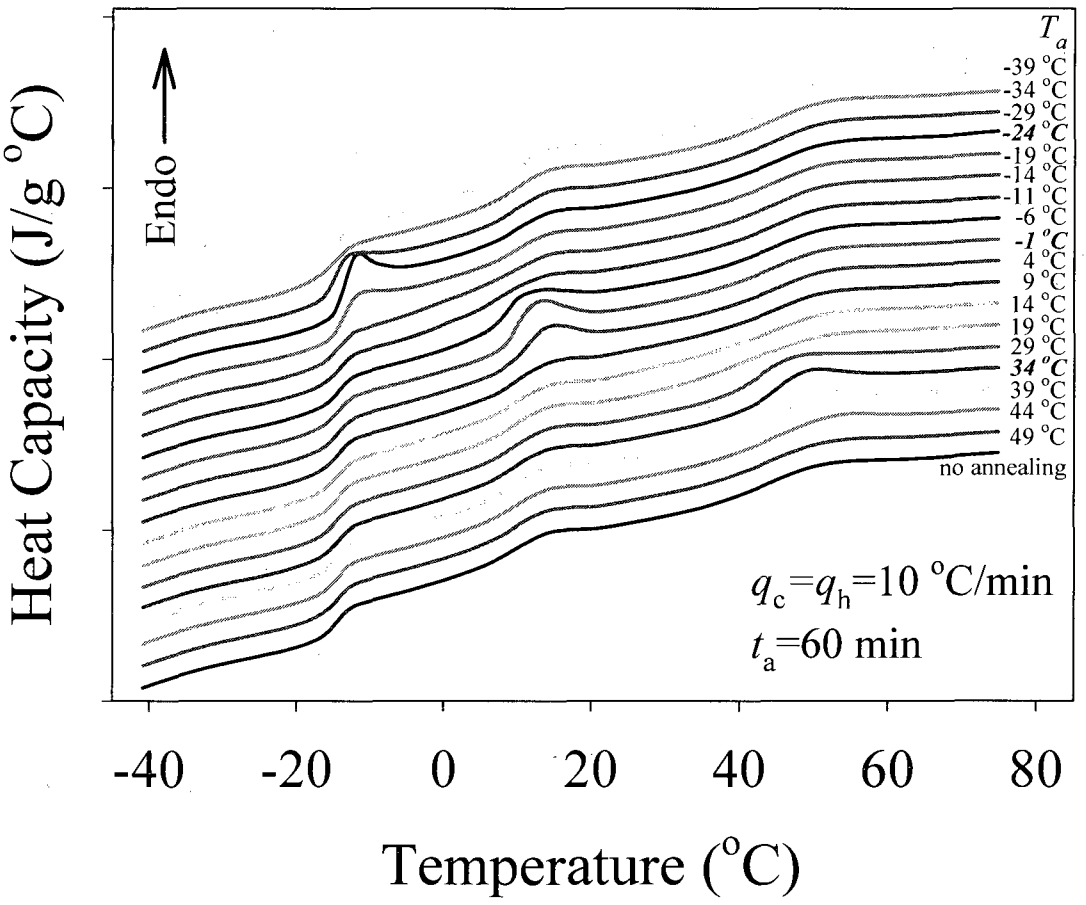

Figure 8.9. DSC heating scans of the 32-layered thiol-ene films after annealing for 1h at different temperature (T_a).

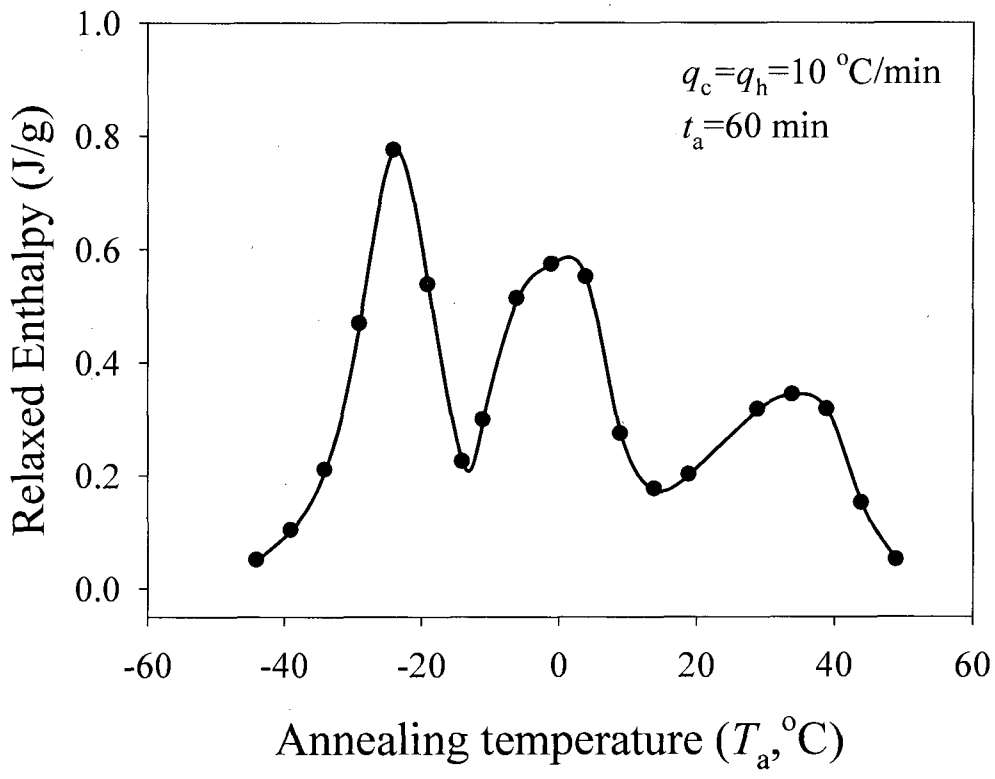

Figure 8.10. The distribution of enthalpy relaxation of the 32-layered thiol-ene film obtained by isochronal aging method.

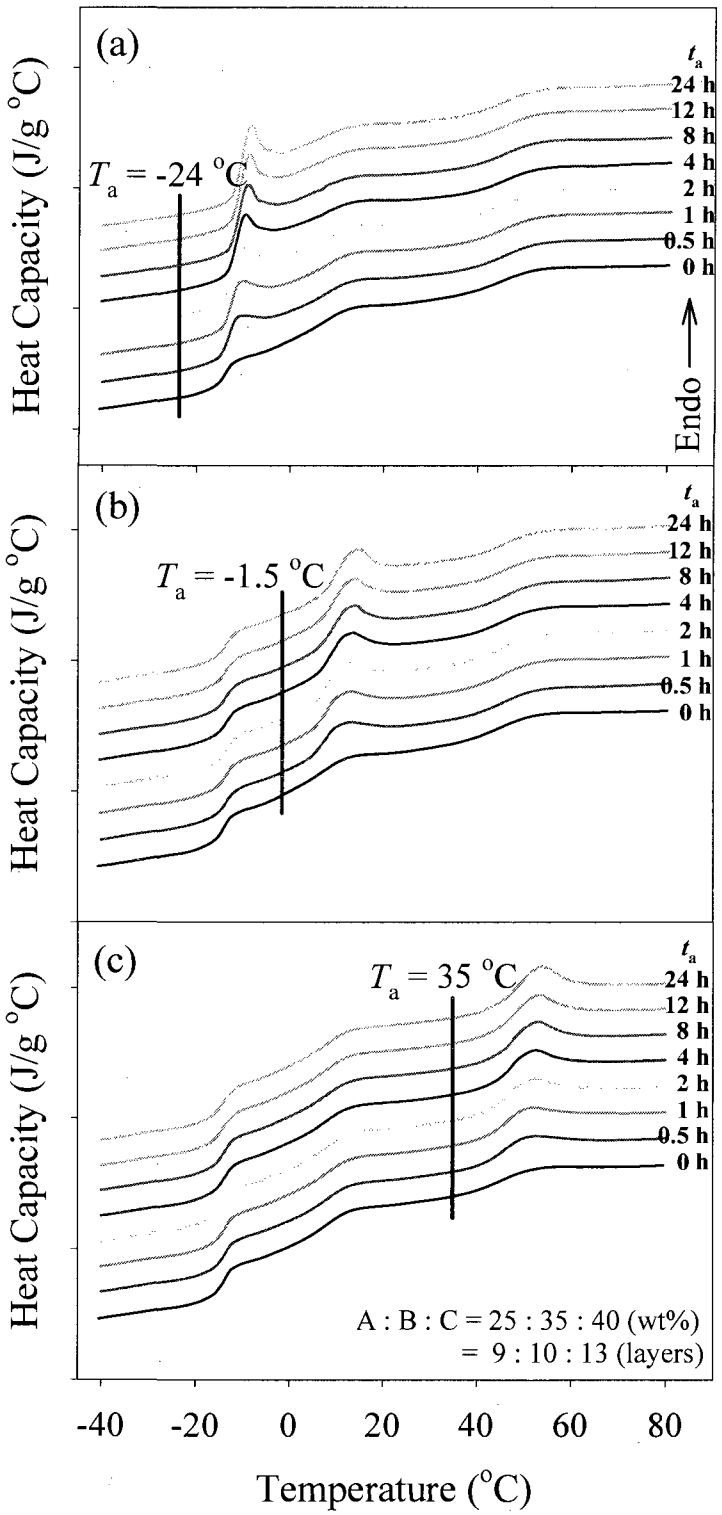

Figure 8.11. DSC heating scans of the 32-layered thiol-ene film after annealing at three different annealing temperatures as a function of annealing time.

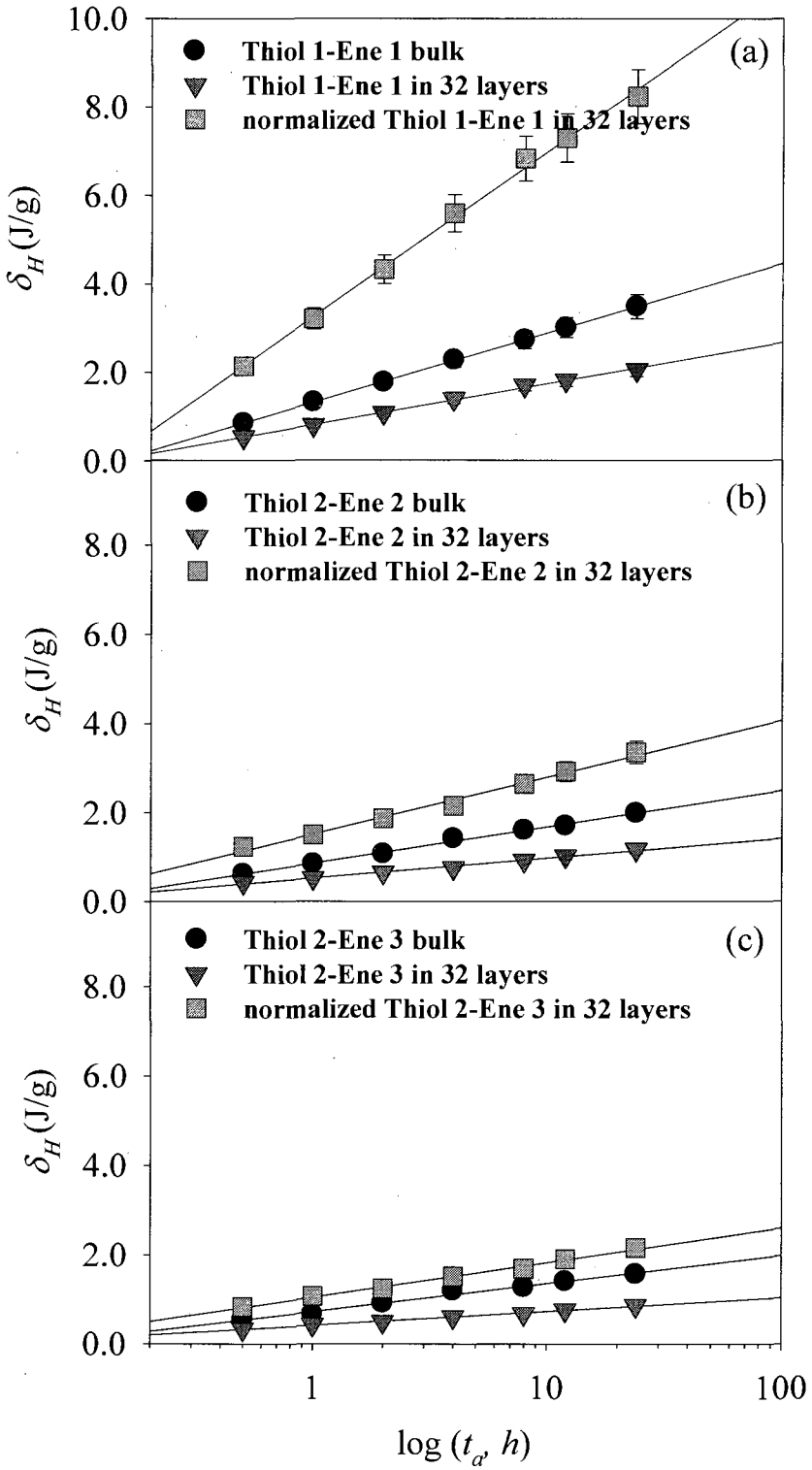

Figure 8.12. Enthalpy relaxation of 32 layered thiol-ene film as a function of annealing time at T_g-10 °C of each system.

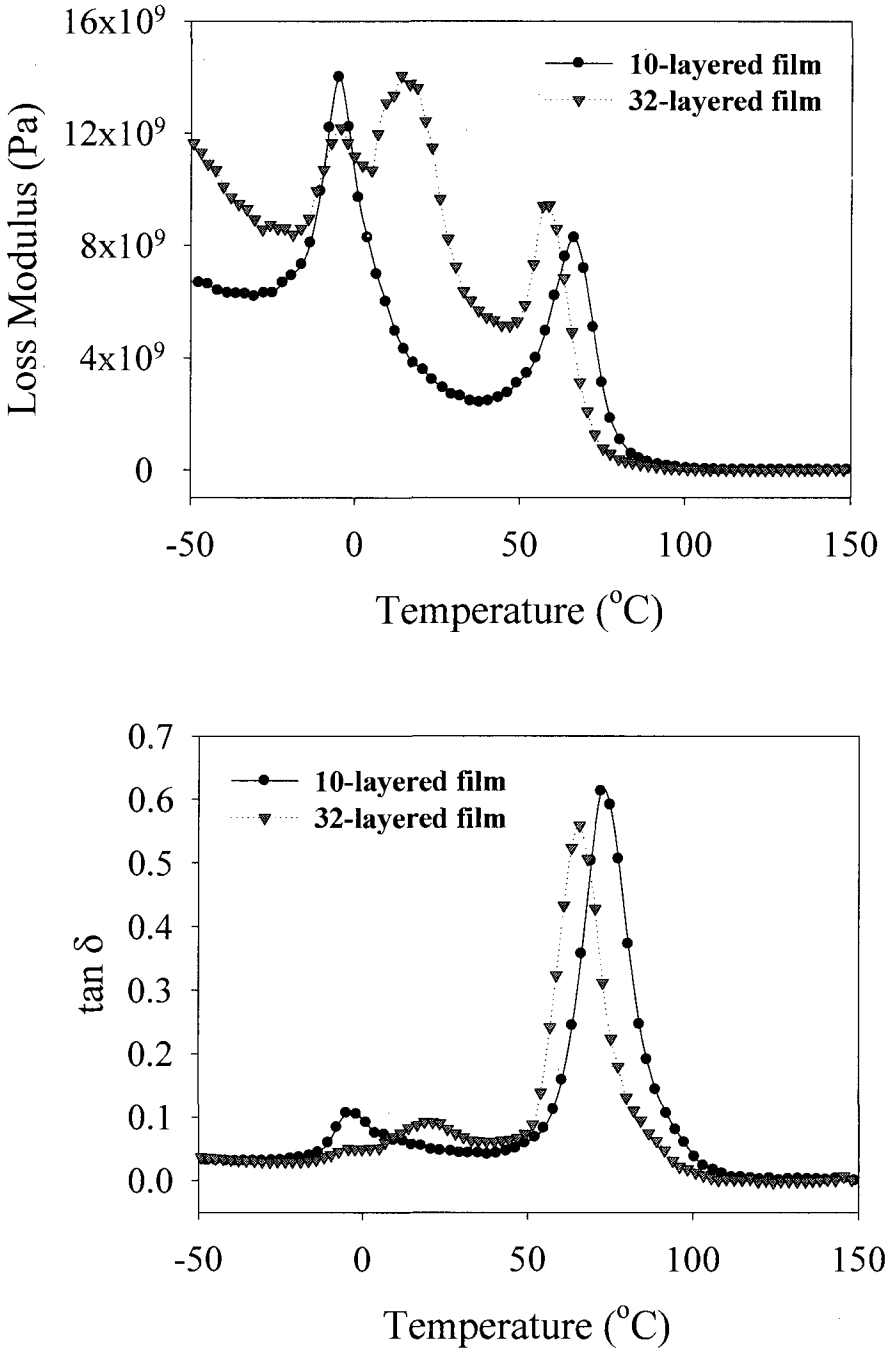

Figure 8.13. Loss modulus (E″) and tanδ of 10- and 32-layered thiol-ene films.

CHAPTER IX

CONCLUSIONS AND RECOMMENDATIONS

This dissertation has discussed three major thiol click-type reactions: thiol-electron rich carbon double bonds by free-radical, thiol-electron poor carbon double bonds by nucleophile catalyzed hetero-Michael addition, and thiol-isocyanate nucleophilic coupling reactions. Physical / mechanical properties of the resultant highly dense and uniform networks were also investigated. Chapter III and IV have focused on the advantages and usefulness of thiol click-type reactions in the chemical reaction point of view for the fabrication of high performance thiol based materials. In Chapters V to VIII, sub-T_g aging behavior of exceptionally uniform thiol-ene networks resulting from unique thiol click-type reactions has been investigated. The conclusions of each study are summarized as follows:

Chapter III represents a new and efficient procedure for the rapid synthetic methodology for highly elastic segmented polythiourethanes, and provides a clear rationale for designing and controlling micro-phase separation between hard and soft segments resulting in tunable thermal / mechanical properties. Both the thiol-acrylate phosphine catalyzed and tertiary amine catalyzed thiol-isocyanate reactions used to synthesize the segmented polythiourethanes under the conditions described herein exhibit the salient attributes of click type reactions as identified by kinetics and product analysis. Thermal, dynamic thermal mechanical, and tensile properties showed that the degree of phase separation can be controlled by varying the length of each segment, the ratio of two phases, and the chemical structure of the hard segment leading a very wide spectrum of

Young's modulus, tensile strength, and elongation at break. The efficient synthesis of segmented polythiourethanes reported in this chapter opens up a totally new materials platform since the thiol oligomers can be readily synthesized in high yields with no side products in a matter of seconds.

In Chapter IV, thiol-isocyanate nucleophilic coupling and thiol-ene free-radical step reactions, which are independent of each other, were sequentially and simultaneously employed to form thiourethane-thiolene co-networks. A conventional base catalyst, TEA, and photoinitiator, DMPA, were used for sequential thiourethane-thiolene co-networks formation. For simultaneous systems, a photo-generated amine catalyst (TBA·$HBPh_4$) was used in the presence of ITX to trigger both thiol-isocyanate coupling and thiol-ene free-radical step reactions simultaneously by UV light. Kinetic profiles clearly showed that both thiol-isocyanate and thiol-ene reactions are essentially fast and quantitative. Thermal properties of hybrid network films prepared by both methods were identical indicating that the uniform and dense network structure that is the characteristic of thiol click-type reaction based materials is not affected by the reaction sequence. Very narrow glass transition temperature ranges for all compositions measured by DSC and DMA supported this conclusion. Thiourethane-thiolene co-network systems offer many advantages in tailoring physical/mechanical properties and the manufacturing process of materials based on the thiol click-type reactions by manipulating polymerization kinetics and varying chemical composition. Since thiols involved in various click-type reactions depend on functional groups and initiating (or catalyst) systems associated with different mechanisms such as free-radical and anionic chain processes, it is suggested that many different combinations of thiol click-type reactions to

form co-networks can be designed as different requirements in chemistry as well as physical/mechanical properties.

In Chapter V, the fundamental sub-T_g aging study on photopolymerized thiol-ene network films was accomplished in terms of enthalpy relaxation. Thiol-ene networks present the characteristic temperature and time dependency of enthalpy relaxation, i.e. maximum enthalpy relaxation was observed at T_g-10 °C for all thiol-ene networks and the extent of enthalpy relaxation (δ_H) and the logarithm of the annealing time (t_a) show linear relationship. The overall relaxation rate (β_H) determined by the slope of δ_H vs. log t_a decreased with ene rigidity and the functionality of the thiols used to fabricate the thiol-ene network. The assumed ultimate enthalpy relaxation (ΔH_∞) at the annealing temperature as well as the heat capacity difference (ΔC_p) at T_g also showed that the relaxation process is largely dependent on the molecular parameters, i.e. rigidity and functionality. Mechanical properties measured by Persoz hardness increased as a function of annealing time consistent with the enthalpy relaxation.

In Chapter VI, sub-T_g aging of thiol-ene networks was intentionally controlled by chemical modification via three methods: incorporation of (1) n-alkyl side chains, (2) hydrogen bonding hydroxyl substituents, and (3) a third (acrylate) component (ternary system). n-Alkyl and hydroxyl alkyl side chain groups were incorporated into the network using modified multi-functional thiols to investigate the effect of flexible alkyl side chains and hydrogen bonding on enthalpy relaxation of thiol-ene networks without sacrificing their characteristic network uniformity. T_g, heat capacity difference at T_g (ΔC_p), and the extent of enthalpy relaxation (δ_H) decrease with an increase in the length of the alkyl chain due to the internal plasticizing effect of flexible alkyl side chains.

Hydrogen bonding by hydroxyl functional groups in thiol-ene networks requires additional energy involved in long-range segmental motions leading to higher heat capacity differences at T_g and, as a resultant, a larger extent of enthalpic deviation from equilibrium at temperatures below T_g. A triacrylate (TMPTA) was incorporated into the thiol-ene network structure to investigate the effect of the network uniformity on sub-T_g aging behavior. ΔC_p and δ_H decreased and the distribution of enthalpy relaxation was drastically broadened as a function of TMPTA content. It is concluded that the restrictive effect of the rigid amorphous region by microgelation of TMPTA homopolymerization results in decreasing the enthalpic relaxation rate based on the decrease in the enthalpic deviation from equilibrium at the annealing temperature ($\Delta C_p \cdot \Delta T$).

In Chapter VII, the restrictive effect of the rigid amorphous region by TMPTA homopolymers and gold nanoparticles in the thiol-ene networks was quantitatively investigated. A multifunctional acrylate (TMPTA) incorporated into thiol-ene networks as a chemical approach significantly decreased the extent of enthalpy relaxation (δ_H) and increased the activation energy for enthalpy relaxation (Δh^*) as a function of TMPTA content. The effect of gold nanoparticles as a physical blending approach to reduce δ_H on thiol-ene network was also demonstrated. The decrease in the amount of relaxed enthalpy upon sub-T_g aging, increase in T_g, decrease in ΔC_p, and increase in Δh^*, all consistently changed with the gold nanoparticles content. Consequently, the restriction effect of rigid amorphous region by microgelation of TMPTA homopolymerization and inorganic gold nanoparticles successfully decreased segmental chain mobility of the thiol-ene network resulted in significant reduction of activation energy for enthalpy relaxation. However, it should be noted that network uniformity manipulated by

chemical structural approach is a more critical factor than the incorporation of gold nanoparticles by simple physical mixing affecting the molecular mobility and Δh^*. Finally, chemical and physical approaches demonstrated in this chapter would be guidance for unprecedented control and restriction of sub-T_g aging.

In Chapter VIII, 10- and 32-layered thiol-ene films with two and three different chemical compositions for each layer, respectively, were prepared by spin coating and photo-polymerization to investigate thermal property and enthalpy relaxation behavior. Distinctive two and three separate T_gs were observed for 10-layered and 32-layered films indicating that each layer of multi-layered thiol-ene films exhibited independent thermal transitions. Consistently, two and three enthalpy relaxation peaks were obtained by the differential cooling rate DSC measurements for 10- and 32-layered thiol-ene films at the T_g region of bulk thiol-ene samples. The temperature dependency of enthalpy relaxation by isochronal annealing experiments showed that both 10- and 32-layered thiol-ene films have distributed enthalpy relaxation over a wide temperature range depending on the original T_g of each layer. The extent (δ_H) as well as overall enthalpy relaxation rate (β_H) obtained by isothermal annealing experiments were significantly accelerated by layering of thin films compared to bulk samples. It is concluded that the enthalpy relaxation of each layer occurs independently at the original T_g of components, so, as a result, the inconsistency in physical and mechanical property changes between layers by sub-T_g aging could affect the performance of multi-layered thiol-ene films. In addition, the accelerated enthalpy relaxation of thin films in the multi-layered systems is another parameter that has to be considered when designing thiol-ene films.

In summary, this dissertation has studied thiol click-type reactions as new strategies for the fabrication of high performance polymeric materials. Many aspects of thiol based reactions satisfying the classical click nature provided new methodologies that are more environmentally friendly and energy economical processes to synthesize polymers. Also, the versatility of functional groups involving many different thiol-click type reactions allowed thiol based materials to exhibit the tunability of physical and mechanical properties over a wide range. In addition to the investigation of thiol-click type reactions in the chemical reaction point of view, the relationships between the molecular parameters, i.e. chemical network density, structural rigidity of monomers, polar / non-polar side chains, network uniformity, and incorporation of gold nanoparticles, and physical / mechanical properties, specifically, sub-T_g aging have been established. The unique chemical structure of thiol based materials, i.e. highly dense and uniform network, resulted by the quantitative conversion with no side products that is an important click nature of thiol reactions provided excellent opportunity for the fundamental study.

APPENDIX A

CHARACTERIZATION OF MOUTHGUARD MATERIALS

Abstract

Five commercially representative thermoplastic mouthguard materials (Essix™ Resin, Erkoflex™, Proform™-regular, Proform™-laminate, and Polyshok™) were evaluated in terms of tear strength, thermal, dynamic thermal mechanical properties, and energy damping performance. Tear strength of EVA was strong enough satisfying the requirements for mouthguard materials. However, thermal properties measured by DSC and DMA showed that EVA materials are temperature sensitive and their performance can possibly change as a thermal treatment. Finally, energy damping efficiency of EVA materials evaluated using modified impact strength measurement method exhibits 50 ~ 60 % of absorption at 23 and 37 °C. The relationship between DMA results and energy damping performance was established and discussed.

Introduction

Interest in the performance of mouthguard materials began in the late 1960s and early 1970s when researchers made initial attempts to characterize the physical,[1] mechanical,[2] and stress transmission[3,4] properties of athletic mouth protectors. Over the past decade, a modest review of the literature demonstrates a renewed interest by the dental research community for salient issues such as mouthguard materials properties,[5-8] energy dissipation,[9-12] and their epidemiological efficacy[13-16] toward reducing the incidence of dental trauma. Cogent reviews of the literature surrounding the history,

material characterization, and prevention effectiveness of the mouthguard are available.[16,17]

It is general knowledge within the dental community that ethylene vinyl acetate (EVA) is the most common material used for commercial and custom mouthguard fabrication. EVA's widespread usage is most likely a function of the materials': abundant commercial availability, ability to be easily processed and adequate mechanical properties. The use of EVA is certainly not limited to mouthguards and is often seen in other sport materials applications such as shoe insoles and helmet cushioning liners. EVA is a random copolymer with a wide range of vinyl acetate content (10–60%) which is produced by the high pressure free radical ethylene polymerization process. As the vinyl acetate content increases, structural regularity decreases and hence crystallization decreases.[17] At 10–15% vinyl acetate content, EVA copolymers resemble plasticized polyvinyl chloride in flexibility but without the necessity of having a plasticizer present. EVA copolymers with about 30% vinyl acetate become soluble in organic solvent due to the increased polarity, which is useful in adhesives. EVA copolymers containing higher content vinyl acetate (30–40%) are used as rubber materials and may be vulcanized with peroxides as needed. As the vinyl acetate content varies, thermal properties such as melting temperature (T_m), crystallization temperature (T_c), and degree of crystallization change due to the different chain regularity and polarity. An example of how the thermal properties of a commercialized EVA (DuPont™ Elvax®) product change as a function of vinyl acetate content is illustrated in Figure A.1.

The ANSI and SAI standards are the only ones that specifically set physical and mechanical properties requirements that must be met by mouthguard materials

manufacturers. In each case, performance parameters were based upon a single manuscript investigating a basic set of physical and mechanical properties of commercialized EVA sheets and fabricated mouthguard specimens.[6] The properties investigated included hardness, water absorption, tear strength, and shock absorption. All of these measures minus shock absorption were conducted at an approximate intra-oral temperature of 37 ◦C.

Fundamentally, mouthguards should be tested and function well at theoretical end-use intra-oral temperature. However, because of the convectional influences of breathing and ambient temperature, it seems unlikely that mouth-guards would stay at this constant 37 ◦C temperature. On cooler days, one would expect the materials to be subjected to lower service temperatures and vice versa for warmer days. Therefore, a mouthguard material needs to perform consistently over a wide range of possible service temperatures (from -20 to 40 ◦C). Additionally, it is well known that a material's best viscoelastic (energy dissipation) response will be at its respective glass transition temperature (T_g).[18] Therefore, if impact attenuation is an important factor to consider for tooth, oral soft tissue, or head protection as some authors have posited,[19-21] then one would expect the T_g of commercialized mouthguard materials to be close to 37 ◦C. Under normal mouthguard service conditions, EVA is well into its rubbery state and is functioning as an elastomer and not a high energy absorbing material. Thus, it becomes important to replicate the physical and mechanical properties from previous research and extend them to other temperatures. Room temperature was chosen because it did not require sophisticated environmental chamber methods.

Two different analytical tools will be used to characterize the thermal properties: differential scanning calorimetry and dynamic thermal mechanical analysis. Differential scanning calorimetry (DSC) is a thermal analysis technique measuring temperatures and heat flow associated with thermal transitions in a material. Applications of DSC to polymers include detection and measurement of chemical reactions or phase transitions associated with temperature changes, which allow one evaluate end-use performance of materials and quality control. Especially, it is essential to investigate thermal properties of polymer materials having two important thermal transitions (T_g and T_m) with respect to determining application temperature and predicting thermal stability. Dynamic mechanical analysis (DMA) yields information about mechanical properties of materials as a function of time, temperature, and frequency. Unlike DSC for static thermal properties, DMA measures the response to dynamic stimuli such as stress or strain as temperature or frequency sweeping. For polymers which usually exhibit viscoelasticity, the response is always behind the mechanical stimuli with the phase lag between 0° ~ 90° due to the viscous character. In other words, perfect elastic materials show no phase lag (0°), but maximum phase lag (90°) can be observed for viscous liquid (Figure A.2). This behavior can be represented by a complex modulus consisting of the in-phase component and the 90° out-of-phase component, characterized by storage and loss modulus, respectively. At an applied stimulus, the energy loss due to the viscous character of polymer materials is given by the ratio of these moduli, which is loss tangent (tan δ). As the dynamic moduli and tan δ are both frequency and temperature dependent, DMA results may be expressed as a spectrum of the storage (E′) and loss modulus (E″) or of tan δ against temperature or frequency. Maximum loss, i.e. maximum energy damping,

occurs in the thermal transition region (usually glass transition, T_g) where the ratio of storage and loss modulus is maximum (see Figure A.3 for examples).

Herein, five different commercialized EVA copolymers are investigated to improve on previous studies[1,6] by adding the following three pieces of information to the extant literature: a complete set of room and intraoral temperature physical and mechanical measurements for comparison, a detailed test method and interpretation for shock absorption values not afforded by the main reference[6] used by standards organizations, and a more current and representative set of mouthguard materials. Therefore, tear strength measurements were conducted at room temperature and 37 °C to characterize mechanical properties of commercialized mouthguard materials. Impact damping performance was directly measured with modified impact strength measurement method using Tinius Olsen impact tester. DSC and DMA were used to measure thermal and dynamic thermal mechanical properties and correlate with impact absorption performance in terms of temperature.

Experimental

Tear strength of all mouthguard materials were measured according to ASTM guideline D624-00 which measures the force required to completely rupture across the width of a material.[22] The tear strength of thermoplastic elastomers is expressed by the ratio of the force to the thickness of samples (F/d) where F = the average maximum force in Newtons and d = the average thickness of the test specimen in meters. Prior to conducting tear strength measurements; the universal material testing machine (Model 3300, Instron, Norwood, MA, USA) was calibrated according to the manufacturer's

recommendations. Four test specimens were then prepared to conform to tear die shape C and placed at a consistent depth into the machine's constant pressure pneumatic grips to prevent slippage. Each test consisted of placing a force on the material with the test tabs pulling perpendicular to the flow direction of the material at 500±50 mm/min. The tests were conducted on four separate specimens for both approximate room 23±2 °C (73.4±3.6 °F) and intra-oral 37±2 °C (98.6±3.6 °F) temperatures.[22] Intraoral temperature was achieved via immersion in a water bath. Mean values were reported.

The energy absorption measurements were conducted using a Tinius Olsen instrument using modified impact strength test protocol to evaluate nondestructive impact energy absorption properties of thick polymer plates. Detailed procedures are described in Figure A.4 and below:

1. Ensure that the impact machine is in the 'normal' (clockwise) mode and is properly configured and calibrated as per manufacturer's recommendations.
2. When prompted for the 'free hang point' in the calibration process, place the radius edge of the tup against 8mm of mouthguard material stacked on the substrate (0.25 inch steel) material.
3. It was determined that 8mm of EVA material was needed to ascertain the material's true ability to dissipate energy. Thicknesses less than 8mm exhibited an elastic artifact from the steel substrate material.
4. Using the integrated, adjustable arm fixture, latch the pendulum and move arm with pendulum to an angle and height where 1.13 J (113Ncm) of energy will be delivered.
5. Record the angle. It will be negative because it is on the pre-impact side.

6. With no specimen on the anvils, rotate the pendulum clockwise and find the point where the pendulum reaches the same latch angle on the post-impact side.
7. Determine the distance from the top surface of the machine base to a good reference point on the pendulum. A reasonable reference point is the back edge of the tup. Using this distance, cut a length of rod to use as a spacer for a reliable latch point. A 12.8mm rod was used in this study.
8. Enter into the password protected configuration mode of the model 892 display and change the swing direction from counter-clockwise (CCW) to clockwise (CW).
9. Repeat the calibration process as amended in step 2, but latch the pendulum on the post-impact side using the spacer created in step 6.
10. Enter the 892's friction loss mode and enter the number of 'half-swings' at 3.
11. With no specimen on the anvils, rotate the pendulum to the artificial latch point using the spacer. Press enter. Lower the pendulum by hand counter-clockwise through the free-hanging point. The cycle count should advance to 1.
12. Continue to rotate counter-clockwise until it reaches the arm fixture and latch it. Please note that the arm fixture should still be positioning at an angle where 1.13 J of energy would be delivered.
13. Put the steel substrate on the anvils. Place an 8mm thick test specimen over the steel substrate.
14. Pull the latch release on the arm fixture to release the pendulum. The pendulum will drop and cross through the free-hanging point at which time the cycle count should advance to 2.

15. The impact tup should strike the 8mm thick specimen and rebound in the counter-clockwise direction back through the free-hanging point until it reaches some maximum height.
16. Quickly remove the specimen prior to the tup impacting the specimen again thereby letting the pendulum freely swing through the anvils. As the pendulum moves through the free-hanging point for the final time, the unit display will show the friction loss which is equivalent to the impact energy absorbed by the test specimen.
17. The friction loss test actually only looks at the last odd-numbered half-swing to height achieved by the pendulum. The display unit then performs the ASTM calculations for friction loss.

Thermal properties of EVA copolymers were characterized with differential scanning calorimetry (DSC, TA Instruments Q 1000) equipped with RCS 90 (Refrigerated Cooling System). Instrument calibration was performed before measurements as the instruction of the manufacturer (T_{zero}, enthalpy constant, and temperature calibration). In order to remove the effect of oxidation on DSC measurements, all experiments were carried out under nitrogen with a flow rate of 50 mL/min. Sample weights were 8.0±1.0 mg to ensure sufficient sensitivity for heat flow measurements. DSC scans were conducted over the temperature range from -70 to 150 ^{o}C using 10 ^{o}C/min heating and cooling rates to determine all thermal transitions of EVA copolymers. All samples equilibrated at -70 (lower than T_g of EVA) for 10 min before

first heating to 150 °C. After first heating scan, cooling and reheating were repeated three times and all scans were recorded.

Dynamic thermal mechanical properties of EVA copolymers were measured by using a DMTA (MK V, Rheometrics). Measurements were conducted in the vertical tension mode with dimensions of 10 × 3.5 × 0.8 mm (L × W × T) from -80 to 100 °C at 5 °C/min of heating rate and at 1Hz of frequency with 0.05 % of strain.

Results and Discussion

As shown in Table A.1, the tear strengths of the commercialized sheet materials ranged from 30.4 ~ 50.5 kN/m at room temperature (23 ◦C). These values are consistent with other research findings.[6] In all cases, the mouthguard sheet materials' tear strength decreased under the 37 ◦C condition (21.5 ~ 42.6 kN/m). However, all materials were within ANSI and SAI guidelines (above 20 kN/m). The maximum strain values for the commercialized sheet materials at 23 ◦C varied from about 90% (Proform™-laminate) to nearly 200% (Erkoflex™). The range changed slightly under the 37 ◦C from about 107% (Proform™-laminate) to about 204% (Proform™-regular). In addition, these commercially available EVA sheet mouthguard materials, once past the yield point, undergo substantial geometrical change (i.e., drawing) that is beyond the proportional limit (i.e., permanent). Yet, the guideline calls for the maximum force to be recorded at failure which is after all of the permanent deformation has occurred.

Thermal properties measured by DSC are shown from Figure A.5 ~ A.8 and Table A.2. Glass transition temperature defined as an inflection of heat flow is observed for all five different EVA copolymers at almost same temperature (-30 °C) on first

heating scan in Figure A.5. The endothermic peak by melting of crystalline domain of EVA copolymer is also observed at almost same temperature range (35 ~ 85 °C) except for Essix™ showing another small endothermic melting peak at 120 °C. It seems that broad melting ranges with two peaks are due to the different crystalline structures or size which usually created by different thermal history unless the sample is not a blend of different polymers. In other words, first heating scan shows that thermal properties of EVA copolymers can be changed by thermal treatment such as annealing. For this reason, T_g and T_m observed on the first heating scan are basically not considered as original thermal transition. In Figure A.6, DSC cooling scans of EVA copolymers are shown. In general, crystallization temperature (T_c) is defined on DSC cooling scan. For all EVA copolymers, T_c is observed from 51 ~ 56 °C with a single endothermic peak which means that commercialized EVA copolymers investigated in this study are evidently EVA neat system without any addition of polymer. However, as T_m defined by first heating scan in Figure A.5, Essix™ shows another T_c at 70 °C. It is assumed that Essix™ is a blend of EVA copolymer and small amount of an unknown polymer as additives. Second heating scans in Figure A.7 shows that T_g is at the same temperature as observed on first heating scan but endothermic melting peaks are broader and single implying that the crystalline structure and amount of crystalline domain are changed after first heating and cooling cycle. It is sure that first heating above T_m of EVA copolymer erases previous thermal history resulting in the initialization of chain conformation and configuration. Thus, T_g and T_m measured by second DSC heating scan can be basically considered as primitive thermal transition of EVA copolymers. The third and fourth DSC heating scans, not shown here, are identical to second heating scans for all EVA

copolymers. It is concluded that EVA copolymer has distinctive thermal transitions (T_g and T_m) and T_m and the amount of crystalline domains can be affected by thermal treatment, i.e. annealing or aging at a specific temperature. The effect of annealing on thermal transition of Polyshock^{TM} as a representative example is investigated as a function of annealing time at 37 °C. Sample was first heated up to 150 °C to erase all previous thermal history and followed by cooling to 37 °C and equilibrated for 1 ~ 8 h to give different thermal history to sample. After annealing for different time at 37 °C, sample was further cooled down to -70 °C and reheated to 150 °C which was recorded and are shown in Figure A.8. T_g of Polyshock^{TM} is almost identical regardless of annealing time. However, the endothermic melting peak changes from singlet to doublet with the appearance of a new peak at 45 ~ 50 °C which increases and shifts to higher temperature as a function of time. It is due to that, as discussed above, molecular conformation and configuration of Polyshock^{TM} changes by annealing at 37 °C resulting in altering thermal properties. Consequently, thermal properties of commercialized EVA copolymer as a mouthguard materials measured by DSC show that T_g and T_m are essentially the same for all samples with small difference, i.e. an additional endothermic melting peak at 120 °C for Essix^{TM}, indicating that five different samples are neat EVA copolymer containing about 18 % of vinyl acetate content. As a material for mouthguard, EVA copolymers investigated in this study have significant potential problems in changes of thermal properties depending on the temperature and time.

Dynamic thermal mechanical properties are shown in Figure A.9 ~ A.11 and Table A.3. All EVA copolymer exhibit single T_g at -10 °C defined by inflection of E′ and tan δ and melt flow starts at 90 °C which is corresponding to DSC results. It is also

expected that vinyl acetate content is almost the same for all samples. Considering EVA copolymers as a mouthguard material, damping factor (tan δ) is needed to be evaluated at a specific temperature, i.e. room temperature and 37 °C. In Figure A.11, tan δ of EVA copolymers are shown against temperature. As discussed in Introduction, maximum energy damping occurs in the glass transition, T_g for polymeric materials. However, the temperature of maximum tan δ is about -10 °C and transition range is -50 ~ 40 °C for all samples. Thus, EVA copolymers are basically elastomeric rubber at application temperature range of mouthguards. This is consistent with the impact energy damping properties of EVA copolymers shown in Figure A.12.

Impact results under the 23 and 37 ◦C condition showed that the commercialized mouthguard sheet materials absorbed approximately 50 ~ 60% of the impact energy (Table A.4). The impact resistance values for the commercialized sheet materials at 23 ◦C are more modest than previous research suggests[6] with materials dissipating from 0.556 J (49%) to 0.693 J (61%) of initial 1.13 J impact. Only slight changes in impact resistance were noted between the 23 ◦C and 37 ◦C conditions. Because these materials were tested off-the-shelf, these variations are possibly due to small variations in thermal history, hydrogen bonding, or changes in the crystallinity. Based on our results, none of the commercially available mouthguard sheet materials absorb impact energy over 70%. It should be noted that, under normal service conditions, EVA copolymers are in their rubbery state well above their T_g of ≈ -10 ◦C. As such, one would not expect these materials to function well as shock absorbing materials as has been previously suggested.[6] In order to verify EVA's change in energy absorption as a function of temperature, ProformTM-regular and ProformTM-laminate were tested over a 100 ◦C

thermal range (Figure A.12). As expected, energy absorption spectrum is perfectly consistent with tanδ peaks in Figure A.11. Note that the second rise in impact absorption that is occurring between the 40 and 50 ◦C range is due to the material undergoing its melt flow process. Consequently, commercialized EVA mouthguard materials should be reconsidered as energy damping materials for room temperature or inside-body applications.

Conclusions

Commercialized EVA mouthguard materials were characterized in terms of tear strength, thermal, and dynamic thermal mechanical properties. DMA results were correlated with energy damping performance. The tear strength of commercially available EVA sheet materials is adequate. High stress, low strain characteristics are desirable of mouthguard materials as it allows for adequate service length while at the same time limiting the deformation that occurs under load which is thereby related to the deformation translated to the substrate material (tooth) with which the material is protecting. DSC and DMA results of commercialized mouthguard materials showed that EVA as a thermoplastic is not acceptably good materials due to the temperature sensitivity of properties. Crystallinity and melting temperature of commercialized EVA mouthguard materials obtained by DSC changed as a function of annealing time. In addition, glass transition of commercialized mouthguard materials falls well below the targeted, end use intra-oral temperature. As such, these materials are functioning as elastomers and not optimal mechanical damping materials. Impact damping properties were well consistent with DMA results. It is concluded that even though EVA has many

advantages (e.g., easily fabricated), it need to be reconsidered by at least two significant hindrances (thermal stability and mechanical damping) that may affect overall performance.

References

1. Craig, R. G.; Godwin, W. C. *Journal of the Michigan State Dental Association* **1967**, 49, 34.
2. Going, R.; Loehman, R.; Chan, M. S. *Journal of the American Dental Association* **1974**, 89, 132.
3. Alexander, M. *Neurology* **1995**, 45, 1253.
4. Godwin, W. C.; Craig, R. G. *Journal of the American Dental Association* **1968**, 77, 1316.
5. Tran, D.; Cooke, M. S. *Dental Traumatology* **2001**, 17, 260.
6. Craig, R. G.; Godwin, W. C. *Journal of Oral Rehabilitation* **2002**, 29, 146.
7. Meng, F. H.; Schricker, S. R.; Brantley, W. A. et al. *Dental Materials* **2007**, 23, 1492.
8. Low, D.; Sumii, T.; Swain, M.V.; Ishigami, K.; Takeda, T. *Dental Materials* **2002**, 18, 211.
9. Greasley, A.; Imlach, G.; Karet, B. *British Journal of Sports Medicine* **1998**, 32, 17.
10. Warnet, L.; Greasley, A. *British Journal of Sports Medicine* **2001**, 35, 257.
11. Westerman, B.; Stringfellow, P. M.; Eccleston, J. A. *Dental Traumatology* **2002**, 18, 24.
12. Duhaime, C. F.; Whitmyer, C. C.; Butler, R. S.; Kuban, B. *Dental Traumatology* **2006**, 22, 186.
13. Wisniewski, J. F.; Guskiewicz, K.; Trope, M.; Sigurdsson, A. *Dental Traumatology* **2004**, 20, 143.
14. Mihalik, J. P.; MCaffrey, M. A.; Rivera, E. M.; et al. *Dental Traumatology* **2007**, 23, 14.

15. Beachy, G. *Journal of Athletic Training* **2004**, 39, 310.

16. Knapik, J. J.; Marshall, S. W.; Lee, R. B.; et al. *Sport Medicine* **2007**, 37, 117.

17. Gould, T. E.; Piland, S. G.; Hoyle, C. E.; Nazarenko, S. *Mouth protection in sports. In: Aleksandar Subic, editor. Materials in sports equipment*, vol. 2. Cambridge, England: Woodhead Publishing Limited; **2007**.

18. Seymour, R. B.; Carraher, C. E. *Polymer chemistry: an introduction.* New York: Marcel Dekker; **1981**.

19. Stenger, J.; Lawson, E.; Wright, J. et al. *Journal of the American Dental Association* **1964**, 69, 273.

20. Winters, J. E. *Journal of Athletic Training* **2001**, 36, 339.

21. Hickey, J.; Morris, A.; Carlson, L.; et al. *Journal of the American Dental Association* **1967**, 74, 735.

22. ASTM D 624. Standard test method for tear strength of conventional vulcanized rubber and thermoplastic elastomers. ASTM International; **2000** (Reapproved 2007).

Table A.1. Tear properties of commercialized EVA mouth guards

	Tear Force (kN/m)		Strain (%)	
	23 ± 2 °C	37 ± 2 °C	23 ± 2 °C	37 ± 2 °C
Essix™	50.5 (1.03)	42.6 (0.61)	161.1 (18.85)	172.83 (13.67)
Erkoflex™	46.6 (1.08)	34.8 (0.78)	199.8 (17.77)	167.73 (3.13)
Proform™ Laminate	41.4 (1.36)	38.7 (3.57)	90.2 (27.83)	204.63 (52.21)
Proform™ Regular	47.3 (2.52)	33.6 (0.42)	141.1 (10.59)	107.11 (2.29)
Polyshock™	30.4 (1.06)	21.5 (0.89)	95.0 (2.65)	161.43 (67.25)

- ASTM D624-00e1 standard test method for tear strength of conventional vulcanized rubber and thermoplastic elastomers

Table A.2. Thermal properties of commercialized EVA mouth guards by DSC

		Essix™	Erkoflex™	Proform™ Regular	Proform™ Laminated	Polyshock™
[a]$T_{g,DSC}$ (°C)		-32.6	-31.0	-30.8	-33.7	-31.4
[b]ΔC_p (T_g) (J/g·°C)		0.50	0.52	0.51	0.48	0.51
[c]$T_{m,onset}$ (°C)		40.4	40.3	40.3	40.0	42.6
[d]T_m (°C)	1st	46.7, 74.2	47.1, 71.0	46.8, 72.7	44.7, 72.2	48.4, 71.0
	2nd	74.2	71.7	73.3	73.3	71.7
[e]T_c (°C)		56.6	51.6	54.0	55.0	54.0
[f]ΔH_f (J/g)		45.7	37.4	45.4	38.5	37.5

[a] inflection of heat flow

[b] heat capacity change at T_g

[c] onset temperature of melting

[d] peak temperature at melting

[e] crystallization temperature on cooling

[f] heat of fusion (area of melting peak)

Table A.3. Thermal properties of commercialized EVA mouth guards by DMTA

	Essix™	Erkoflex™	Proform™ Regular	Proform™ Laminated	Polyshock™
[a]$T_{g,DMTA}$ (°C)	-6.5	-9.2	-6.3	-12.3	-9.1
[b]E′ at 37 °C (MPa)	29.7	21.9	24.5	23.2	20.0
[c]E″ at 37 °C (MPa)	1.76	1.96	1.31	2.71	1.15
[d]tan δ at 37 °C	0.06	0.09	0.05	0.12	0.06
[e]tan δ_{max}	0.28	0.30	0.30	0.27	0.31
[f]FWHM	44.2	50.7	39.8	61.4	38.6

[a] temperature at tan δ maximum

[b] storage modulus at 37 °C

[c] loss modulus at 37 °C

[d] tan δ value at 37 °C

[e] maximum value of tan δ

[f] full width at half maximum of tan δ

Table A.4. Impact energy damping of commercialized EVA mouth guards

	Essix™	Erkoflex™	Proform™ Regular	Proform™ Laminated	Polyshock™
25 °C	50.1	54.4	46.4	57.8	56.8
37 °C	49.2	50.1	46.0	56.2	62.5

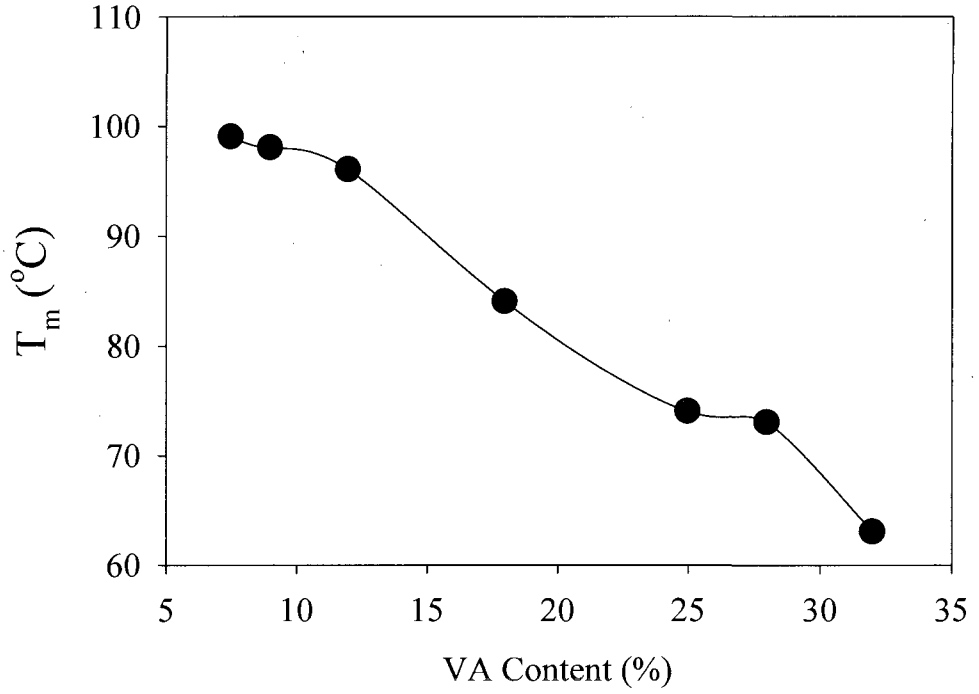

Figure A.1. Melting temperature of EVA copolymer as a function of vinyl acetate content (DuPont™ Elvax®).

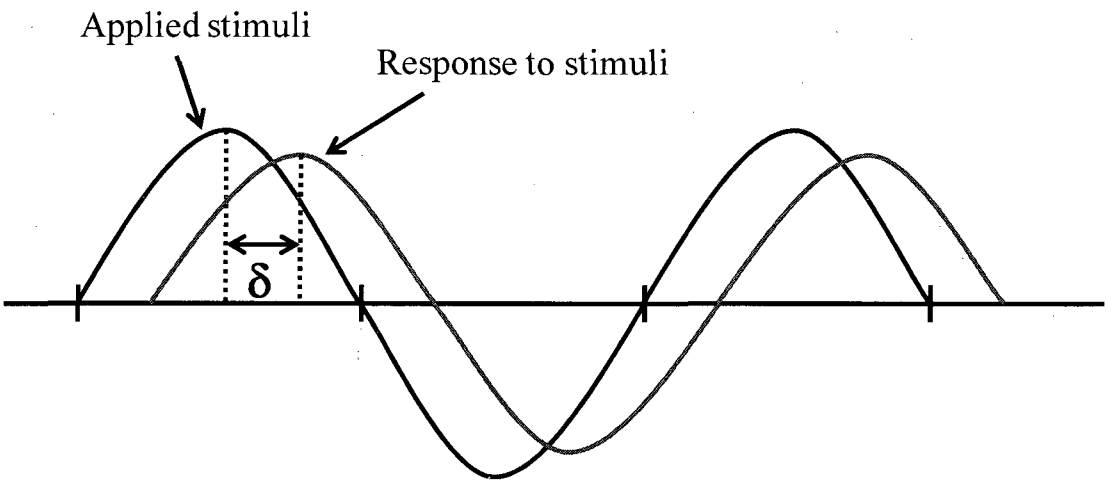

δ = damping factor

In phase (δ : 0^o) : ideal elastic materials
Out of phase (δ : 90^o) : viscous liquids
$0^o < \delta < 90^o$: viscoelasticity (most polymers)

Figure A.2. The schematic representation of viscoelasticity of polymeric materials.

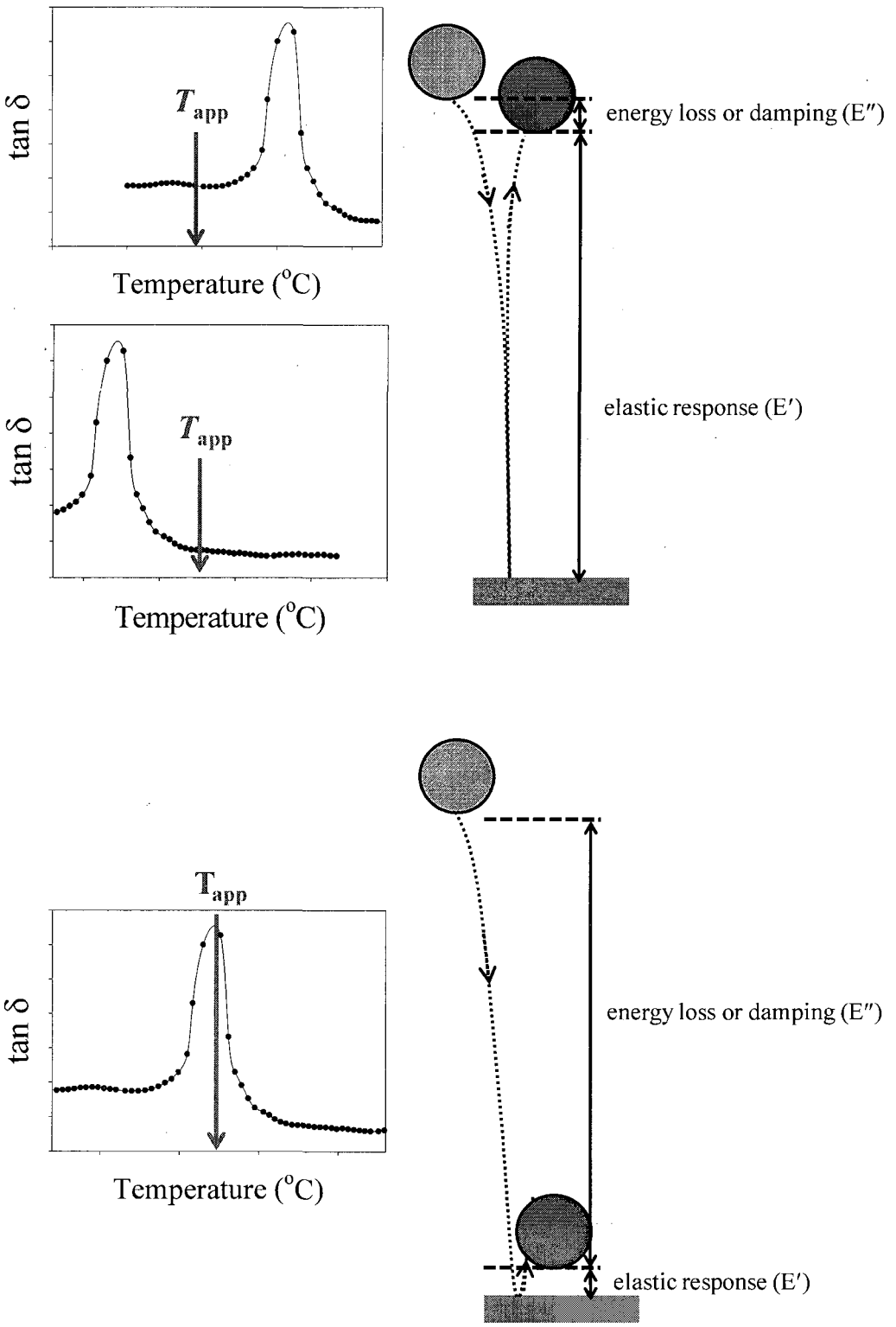

Figure A.3. The illustration of the relationship between glass transition temperature and energy damping performance of polymeric materials.

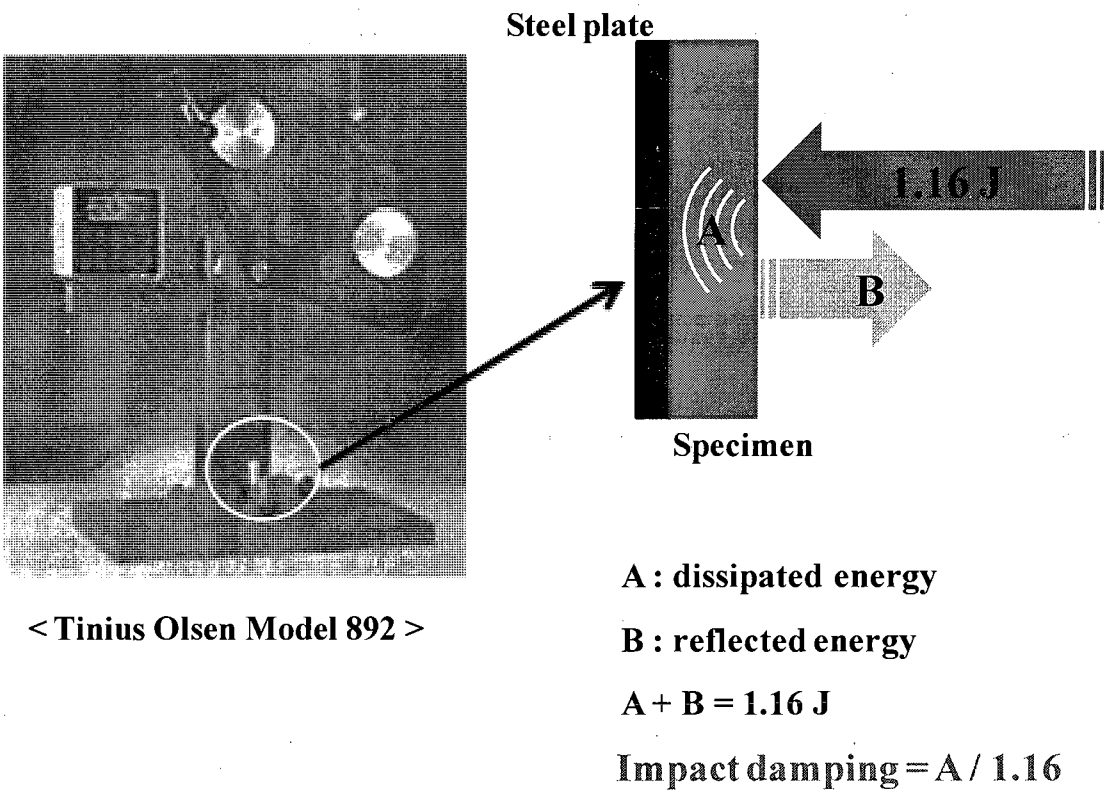

Figure A.4. The instrumentation of impact energy damping measurement.

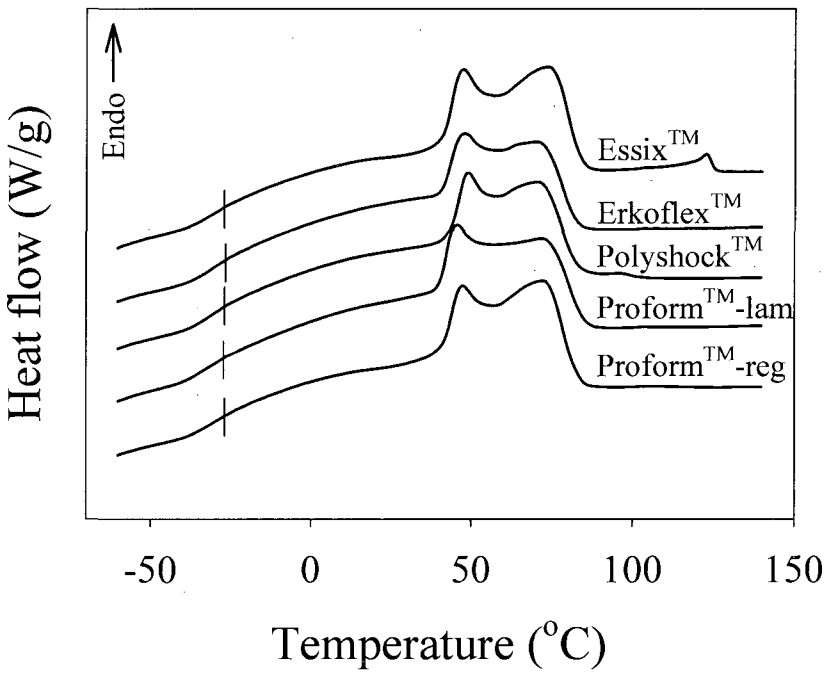

Figure A.5. DSC first heating scans of commercialized EVA copolymers.

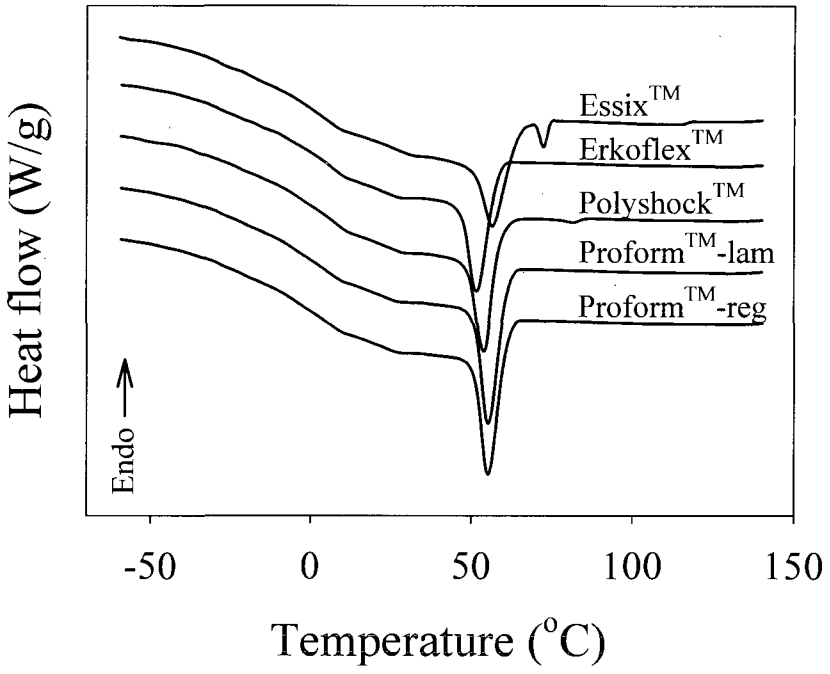

Figure A.6. DSC cooling scans of commercialized EVA copolymers.

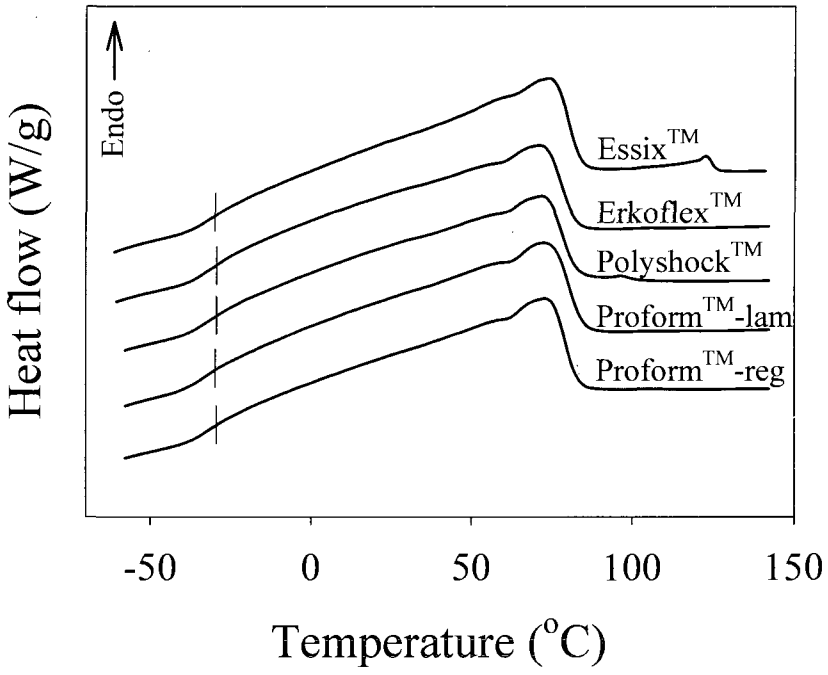

Figure A.7. Second DSC heating scans of commercialized EVA copolymers.

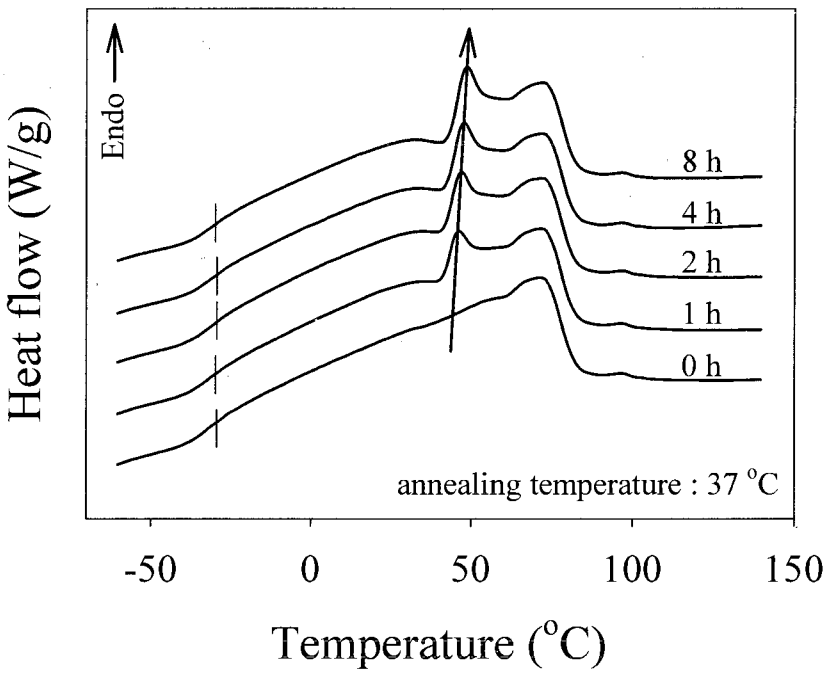

Figure A.8. DSC heating scans of Polyshock™ after annealing for different time at 37 °C.

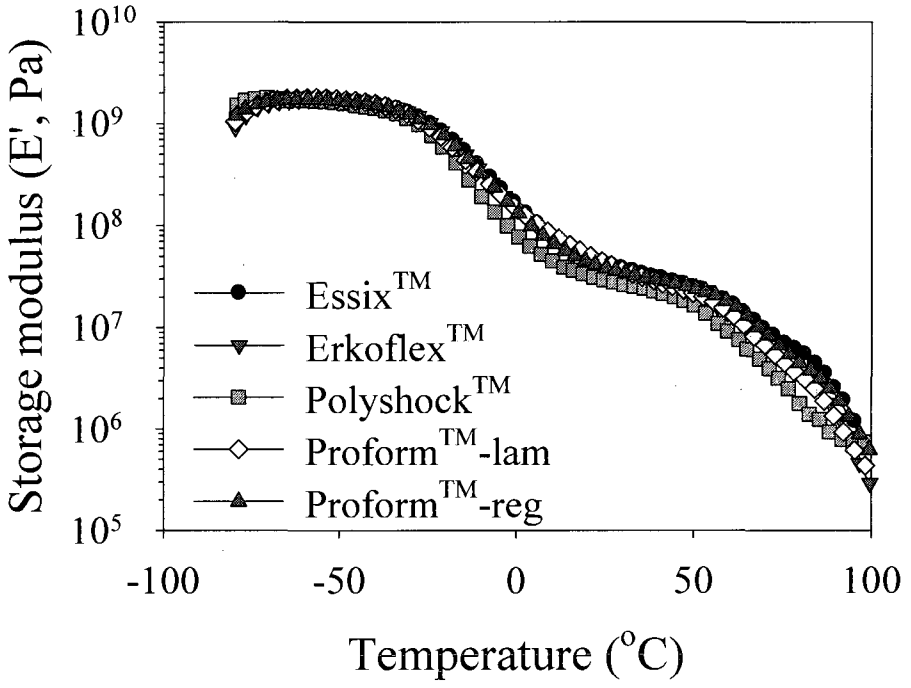

Figure A.9. Storage modulus (E′) of commercialized EVA copolymers.

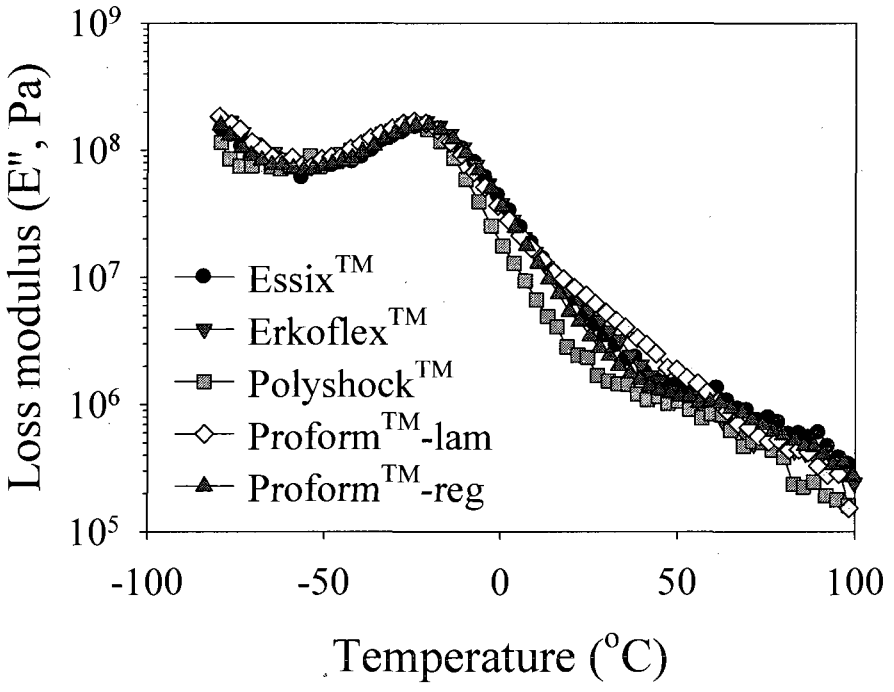

Figure A.10. Loss modulus (E″) of commercialized EVA copolymers.

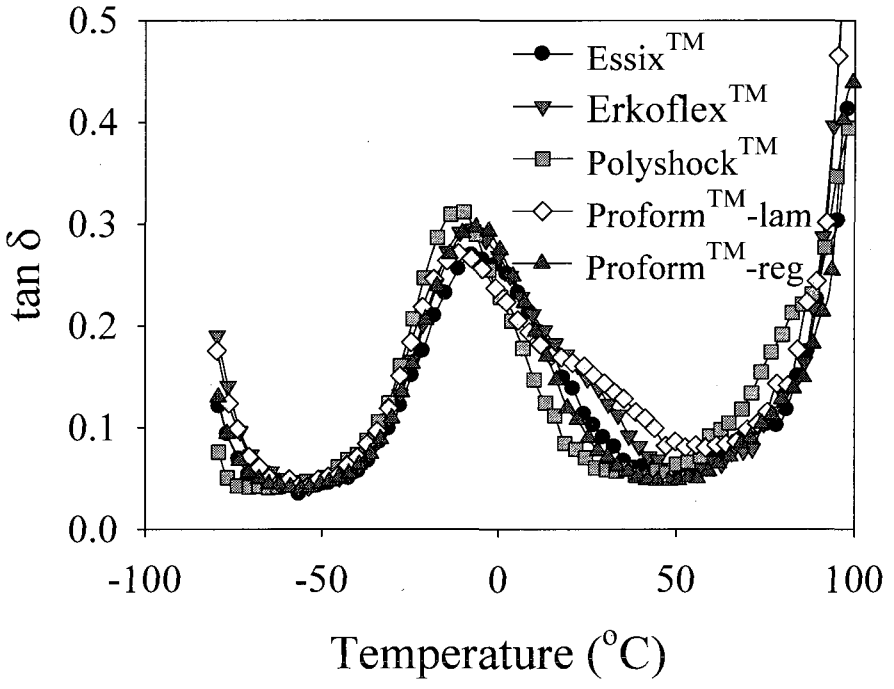

Figure A.11. tan δ of commercialized EVA copolymers.

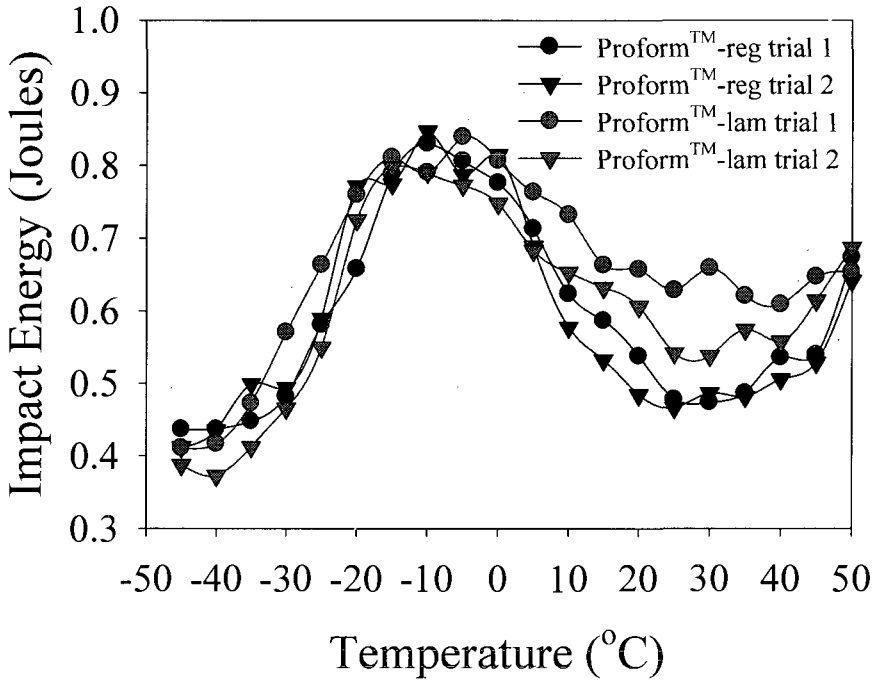

Figure A.12. The impact damping property of commercialized EVA mouth guards as a function of temperature.

APPENDIX B

ENERGY DAMPING PROPERTIES OF PHOTOPOLYMERIZED THIOURETHANE THIOL – URETHANE ENE NETWORKS

Introduction

The photopolymerization of thiol and ene mixtures follows free-radical step growth reaction mechanism involving the addition of the thiyl radical to the ene double bond to yield a carbon-centered radical and subsequent the hydrogen abstraction of a thiol from the carbon-centered radical to regenerate a thiyl radical.[1] Multifunctional thiol monomers readily react with carbon double bonds to form highly dense uniform networks structure resulting in narrow glass transition temperature region and corresponding concentrated high damping performance at a specific temperature (T_g). However, due to this highly dense chemical structure, photopolymerized thiol-ene networks exhibit serious problems in mechanical properties such as low elongations at break, insufficient fracture toughness, and poor tear strengths.[1,2]

In order to resolve the fundamental issues of thiol-ene networks, urethane groups forming strong intra- and intermolecular hydrogen bonds were introduced into thiol-ene networks in the literatures.[2] Several different types of diisocyanate were end capped with hydroxyl di-ene (trimethylolpropane diallyl ether) producing urethane modified tetra-enes, which were photopolymerized with thiols to form urethane incorporated thiol-ene. Also, aromatic diol (bisphenol A propoxylate) was used to extend urethane modified tetra-ene increasing urethane content in thiol-ene networks. Significant improvement in mechanical properties was achieved with this simple approach. However, increase in

hydrogen bonding results in high viscosity of modified ene monomers which can be another problem in the preparation of homogeneous reactant mixtures with thiols and affecting photopolymerization kinetics. Furthermore, there are still needs in improving mechanical properties in order for thiol-ene photopolymerized networks to be used in energy damping materials.

It has been reported that thiols can be efficiently coupled with isocyanate in the presence of a base catalyst at even room temperature.[3-6] Since the hydrogen bonding strength of thiourethane is about the same with urethane,[3,7] thiourethane modified thiols can be another approach in designing and modifying thiol-ene networks. Thus, in this chapter, in addition to the modification of enes, thiols were also modified by the formation of thiourethane linkages with diisocyanates to extensively improve mechanical properties. Also, urethane and thiourethane groups involving strong hydrogen bonds are formed in separated monomer compounds, i.e. enes and thiols, which can minimize the high viscosity issue of modified monomers.

As an energy damping material, there are two important requirements; tunability of transition temperature and high damping factor. The tunability should allow materials to have glass transition temperature at any specific temperature region as well as over wide temperature range where the specific frequency of energy can be dissipated by the resonance. Also, damping factor which can be interpreted by tan δ plots should be high enough to dissipate energy efficiently. In this chapter, thiol-ene networks are chemically modified using isocyanate chemistry in both enes and thiols to satisfy the requirements for energy damping materials.

Experimental

Materials

All thiols, glycol di-(3-mercapto-propionate) (GDMP), trimethylol-propane tri(3-mercapto-propionate) (TMPMP), pentaerythri-tol tetra (3-mercapto-propionate) (PETMP), propylene- glycol 3-mercapto-propionate 800 (PPGMP 800), and ethoxylated trimethylol-propane tri (3-mercapto-propionate) (ETTMP 1300) were obtained from Bruno Bock. Enes (butanediol vinyl ether (BDVE), trimethylolpropane diallyl ether (TMPDAE), 1,3,5-triallyl-1,3,5-triazine-2,4,6(1H,3H,5H)-trione (TTT)), 1,4-butane diol diacrylate (BDDA), trimethylol propane, and polytetramethylene glycol (PTMEG, Mw=650, 1000, and 2000 g/mole) were purchased from Aldrich. Diisocyanates (isophorone diisocyanate (IPDI), 4,4'-methylenebis(phenyl isocyanate) (MDI)) were obtained from Bayer as samples. Chemical structure of all monomers are shown in Chart B.1 and B.2.

Synthesis of modified thiols (m-PPGMP 3800, IP-m-DT, and IP-m-TT))

A 250 mL, round-bottom, three-necked flask with a magnetic stirrer equipped with an ice bath was used as a reactor. For longer polydithiol (m-PPGMP 3800), PPGMP 800 and BDDA were used. First, PPGMP 800 was mixed with 0.1 wt% of DMPPh in the flask while nitrogen purging. BDDA was dripped into the mixture while the temperature was controlled below 30 ^{o}C with an ice bath in order to prevent BDDA from undergoing thermally initiated free-radical polymerization. After completion of adding BDDA, the mixture was further reacted for 10 ~ 20 min at room temperature until all the BDDA was consumed. The complete disappearance of carbon double bonds in BDDA was confirmed by peaks at 812 cm^{-1} for FTIR, 5.71(q), 5.99(q), and 6.23(q) ppm for ^{1}H NMR,

and 128.3 and 130.5 ppm for ^{13}C NMR. The average molecular weights of PPGMP 3800 was controlled by stoichiometry with excess thiol and dictated by theoretical calculation using the Carothers equation.[8] Thiourethane modified di- and tetrathiol (IP-mDT and IP-m-TT) were synthesized by reacting IPDI with the thiols (GDMP and TMPMP), respectively, to produce di- and tetra-functional thiourethane modified thiols with 1:1 stoichiometry between NCO and OH. The reactions were carried out under nitrogen purging at room temperature in the presence of 0.1 wt% of triethylamine (TEA) for 1 h. The synthesized monomers were mixed with GDMP and TMPMP (see the formulations for the ratio of mixtures). Urethane modified enes (IP-m-DE, M-m-TE, and IP-m-TE) were synthesized by reacting diisocyanates (IPDI, MDI) with the hydroxyl functionality of BDVE and TMPDAE with 1:1 stoichiometry between NCO and OH. 0.1 Wt% of dibutyltin dilaurate (DBTDL) was used as catalyst and reaction was carried out at 60 °C for 12 h. For both, thiourethane modified thiols and urethane modified enes, the reactions were monitored with FTIR by following the decrease in the NCO band at 2250 cm^{-1}. The chemical structure of modified monomers is shown in Chart B.3.

Film preparation

The sample formulations were prepared on the basis of equal molar functional groups of thiol and ene monomer (see Table B.1 to B.9 for formulations). The photoinitiator, DMPA, with concentration of 1 wt % of total thiol and ene monomer was used for thiol-ene photopolymerization (200 μm). DMPA was dissolved in the thiols and mixed with ene monomers. Film samples were prepared on the glass plates and irradiated with UV Fusion line EPIQ 6000 with D bulb and intensity of 3.146 W/cm2 at a line speed of 10 feet/min (10 passes) and all samples were post-cured at 80 °C for 24 h to

complete reaction. For polyurethane and polyurethane/thiol-ene co-network films, DBTDL was used for the reaction of IPDI and PTMEG/TMP. 0.1 wt% of DBTDL and 1wt% of DMPA based on total weight of mixture were dissolved in thiols and all the other monomers (PTMEG, TMP, and enes) were mixed. Thiol-ene networks was first formed by irradiating the mixture with UV Fusion line as the same way used for the preparation of thiol-ene networks, followed by the polyurethane networks formation by thermal curing at 80 °C for 24 h.

Characterization

Dynamic thermal mechanical properties of thin cast films were measured using a DMTA (MK VI, Rheometrics). Measurements were conducted in the vertical tension mode with dimensions of 10 × 5.0 × 0.5 mm (L × W × T) from -110 to 250 °C at a 5 °C/min heating rate and 1 Hz frequency with 0.05 % strain.

Results and Discussion

In this chapter, both thiols and ene are modified by the reaction with isocyanates as shown in Chart B.3. In order to optimize energy damping performance (tan δ), nine different sets of modified thiol-ene combinations were prepared.

Set 1 and 2 were designed to investigate the effect of functionality and amount of thiourethane linkage in modified thiols on modified thiol-ene networks at a fixed urethane modified ene (M-m-TE).

1. Urethane ene (MDI + TMPDAE) + Urethane thiol (GDMP + IPDI)

In Chart B.4 and Table B.1, the chemical structure of reactants for this set of modified thiol-ene networks and their formulations are shown. The amount of

thiourethane linkages are varies from 0 to 30 mole % by reacting IPDI with GDMP and photopolymerized with a MDI modified tetra-functional ene (M-m-TE). As shown in Figure B.1, T_gs of modified thiol-ene networks increase as a function of thiourethane content due to the increased hydrogen bonding.

2. Urethane ene (MDI + TMPDAE) + Urethane thiol (TMPMP + IPDI)

In this set, tri-functional thiol (TMPMP) was modified with IPDI from 0 to 30 mole % producing thiourethane modified tetra-functional thiol (IP-m-TT). In Chart B.5 and Table B.2, the chemical structure of reactants for this set of modified thiol-ene networks and their formulations are shown. As shown in Figure B.2, T_gs of modified thiol-ene networks increase as a function of thiourethane content due to the increased hydrogen bonding.

The increase in T_g for both set 1 and 2 was observed as increasing the amount thiourethane linkage in the modified thiol. The higher average thiol functionality (IP-m-TT) resulted in higher glass transition temperature and lower tan δ peak height. However, the width of glass transition is almost identical for all samples implying that network uniformity was not affected.

3. Urethane ene (MDI + BDVE / TMPDAE) + Urethane thiol (GDMP + IPDI)

In this set, di-functional thiol (GDMP) was modified with IPDI from 0 to 50 mole % producing thiourethane modified di-functional thiol (IP-m-DT) as well as di- and tetra-ene was also synthesized using BDVE-IPDI and TMPDAE-IPDI combinations to investigate the effect of average functionality of enes and amount of hydrogen bond in the modified thiol on dynamic mechanical thermal properties. In Chart B.6 and Table B.3, the chemical structure of reactants for this set of modified thiol-ene networks and

their formulations are shown. In Figure B.3, rubbery modulus and T_g increase as a function of average functionality of modified ene from 2.5 to 3.0 at a constant thiourethane content (40 mole%). The effect of hydrogen bonding content on thiol-ene networks are shown in Figure B.4 to 6 at a constant average functionality of modified enes, i. e. 2.5, 3.0, and 4.0, respectively. As expected, T_g increases as increasing thiourethane content.

4. Polyurethane networks (IPDI + PTMEG + TMP)

In this set, simple cross-linked polyurethane networks were prepared to compare with thiol-ene networks. IPDI, PTMEG (MW = 650, 1000, and 2000 g/mole), and TMP were mixed in the presence of 0.1 wt% of DBTDL. Molar ratio was 1:1:1 based on functional groups (NCO and OH, see Table B.4 for formulation). In Figure B.7, storage modulus and T_g increase as decreasing molecular weight of PTMEG due to the decrease in molecular weight between crosslinks as observed in conventional cross-linked polymer systems. However, tan δ peak height is lower than 0.6 and T_g range is also much broader compared to thiol-ene networks, which is probably due to the inhomogeneous polyurethane network structure resulted by secondary reaction, i. e. allophanate formation between isocyanate and urethane groups, during film preparation.

5. Polyurethane networks (IPDI + PTMEG + TMP) / Thiol-ene (TMPMP + TTT) co-networks

In this set, polyurethane and thiol-ene networks were formed sequentially resulting in co-network structure to broaden glass transition temperature region. Chemical structure and formulation are shown in Chart B.8 and Table B.4. In Figure B.8, totally separated two T_gs were defined, implying that polyurethane and thiol-ene

networks are chemically as well as physically phase separated exhibiting independent thermal transition behaviors.

6. Polyurethane networks (IPDI + PTMEG + TMP) / Thiol-Urethane ene (TMPMP + M-m-TE) co-networks

In this set, polyurethane and thiol-urethane modified ene networks were formed sequentially resulting in co-network structure to broaden glass transition temperature region. Also, the effect of incorporated hydrogen bonding in thiol-ene networks on phase behavior of co-networks was investigated. Chemical structure and formulation are shown in Chart B.9 and Table B.6. In Figure B.9, single T_gs was defined between T_g of polyurethane and thiol-ene networks, implying that polyurethane and thiol-ene networks are fully phase mixed certainly due to the incorporation of urethane linkages in thiol-ene networks resulting in inter-network interaction and phase mixing.

7. Polythiourethane networks (IPDI + ETTMP 1300 + PETMP)

In this set, polythiourethane networks were prepared by the base (TEA, 0.01 wt%) catalyzed reaction of IPDI with tetra-functional (PETMP) and ethoxylated tri-functional (ETTMP 1300) thiols. The effect of network density controlled by the ratio between PETMP and ETTMP 1300 on damping factor (tan δ) and T_g was investigated. Chemical structure and formulation are shown in Chart B.10 and Table B.7. In Figure B.10, rubbery modulus and T_g increased as increasing PETMP content due to the increase in network density as observed polyurethane networks (see set 4). However, for all compositions, very narrow T_g was observed implying that polythiourethanes networks are essentially uniform and homogeneous structure as observed in thiol-ene networks. It has been reported that thiol-isocyanate reaction in the presence of a base catalyst does not

produce side product, i. e. allophanate. Thus, polythiourethanes networks from IPDI, PETMP, and ETTMP 1300 certainly exhibit more uniform chemical structure compared to polyurethane networks.

8. Polythiourethane networks (IPDI + ETTMP 1300 + PETMP + m-PPGMP)

In this set, polythiourethane networks were prepared by the base (TEA, 0.01 wt%) catalyzed reaction of IPDI with tetra-functional (PETMP), ethoxylated tri-functional (ETTMP 1300), and modified (extended) di-functional (PPGMP 3800) thiols. The effect of a long spacer (polydithiol, PPGMP 3800), prepared by Michael addition reaction between PPGMP 800 and BDDA, on damping factor (tan δ) and T_g of polythiourethanes networks was investigated. Chemical structure and formulation are shown in Chart B.11 and Table B.8. In Figure B.11, rubbery modulus and T_g decreased as increasing m-PPGMP 3800 content due to the increase in molecular weight between crosslinks. Interestingly, for the sample of higher long chain spacer content, overlapped double T_gs are observed. This is probably due to the phase separation between soft and hard segment by IPDI / m-PPGMP and IPDI / PETMP, respectively.

9. Polythiourethane networks (IPDI + ETTMP 1300 + PETMP + m-PPGMP + PPGMP 800)

In this set, polythiourethane networks were prepared by the base (TEA, 0.01 wt%) catalyzed reaction of IPDI with tetra-functional (PETMP), ethoxylated tri-functional (ETTMP 1300), and short / long poly di-functional (PPGMP 800 and 3800) thiols. Formulation was designed for polythiourethanes networks to exhibit broader T_g range around room temperature with maintaining damping factor (tan δ) higher than 0.3. Chemical structure and formulation are shown in Chart B.12 and Table B.9. As shown in

Figure B.12(c), T_g of all samples are single and narrow around room temperature. Due to the homogeneous chemical reaction and corresponding chemical structure of polythiourethanes networks, broadening T_g is challenging. However, T_g range can be broader by formulating the combination of thiols (width ~ 90 °C at 0.3 of tan δ). There is very limited number of commercially available thiols. Thus, the synthesis of various thiols such as high molecular weight dithiol for enough space and high molecular weight monofunctional thiol for dangling chains is necessary.

Conclusions

Nine different sets of modified thiol-ene and polythiourethanes networks were prepared to investigate the relationship between chemical structure and dynamic thermal mechanical properties, especially damping factor (tan δ). In set 1 to 3, both thiol and ene monomers were modified by incorporating thiourethane and urethane linkages. Results showed that T_g can be controlled by functionality of both modified ene and thiol monomers as well as the amount of thiourethane and urethane contents in thiol-ene networks. In set 4 to 6, polyurethane network and polyurethane /thiol-ene conetworks were investigated in terms of broadness of glass transition temperature range. While polyurethane / thiol-ene co-networks showed distinctive two T_gs due to the phase separation, polyurethane / thiol-urethane ene exhibited single T_g resulted by the inter-network strong hydrogen bonding. In set 7 to 9, polythiourethane networks were prepared by the base catalyzed coupling reaction between isocyanates and thiols and investigated in terms of damping factor (tan δ) and broadness of T_g range. Since thiol-isocyanate reaction essentially does not produce side products such as allophanate, T_g

was narrow for all cases. However, incorporation of long polydithiols as a spacer inducing controlled phase separation between soft and hard segments in the same polythiourethanes networks was suggested as an approach to broaden T_g. This study has been accomplished with limited number and types of monomers, i.e. thiols and enes. Thus, there are still a lot of works should be done to optimize the formulation for thiol based energy damping materials.

References

1. Hoyle, C. E.; Lee, T. Y.; Roper, T. *Journal of Polymer Science: Part A: Polymer Chemistry* **2004**, 42, 5301.
2. Senyurt, A. F.; Hoyle, C. E.; Wei, H.; Piland, S. G.; Gould, T. E *Macromolecules*, **2007**, *40*, 3174.
3. Shin, J.; Matsushima, H.; Chan. J. W.; Hoyle, C. E. *Macromolecules* **2009**, *42*, 3294.
4. Dyer, E.; Glenn, J. F.; Lendrat, E. G. *J. Org. Chem.* **1961**, *26*, 2919.
5. Dyer, E.; Osborne, D. W. *J. Polym. Sci.* **1960**, *47*, 361.
6. Dyer, E.; Glenn, J. F. *J. Am. Chem. Soc.* **1957**, *79, 366.*
7. Li, Q.; Zhou, H.; Wicks, D. A.; Hoyle, C. E.; Magers, D. H.; McAlexander, H. R. *Macromolecules*, **2009**, *42*, 1824.
8. Odian, G. Principle of Polymerization 4th Ed. John Wiley & Sons, Inc.: Hoboken, **2004**.

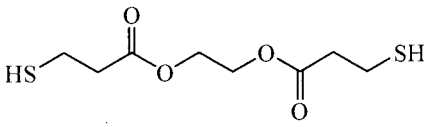

GDMP

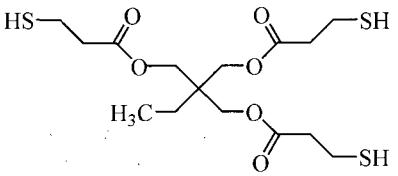

TMPMP

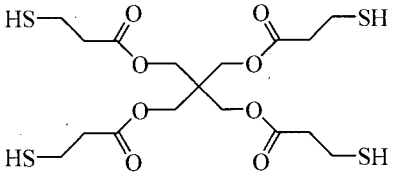

PETMP

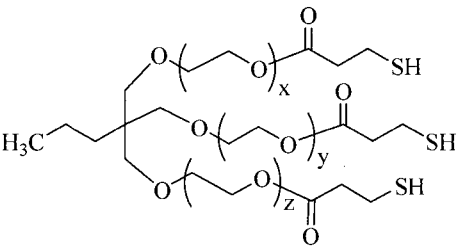

x + y + z = 20

ETTMP 1300

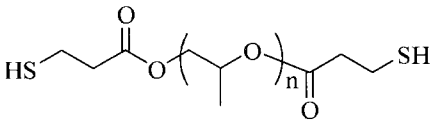

n = 10.3

PPGMP 800

Chart B.1. Chemical structure of thiols.

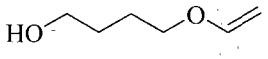

BDVE

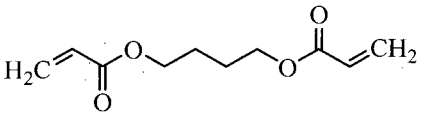

BDDA

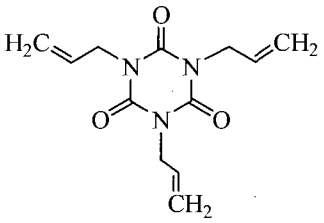

TTT

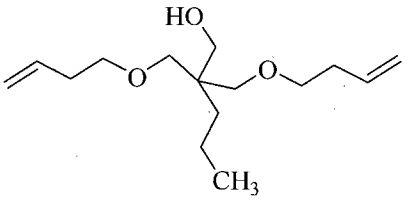

TMPDAE

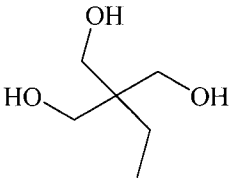

TMP

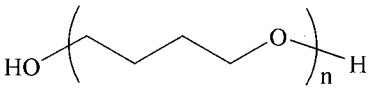

PTMEG

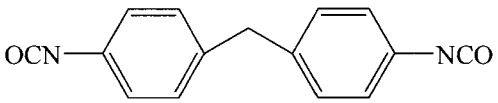

MDI

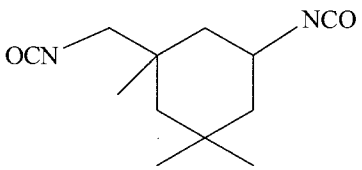

IPDI

Chart B.2. Chemical structures of enes, acrylate, alcohols, and isocyanates.

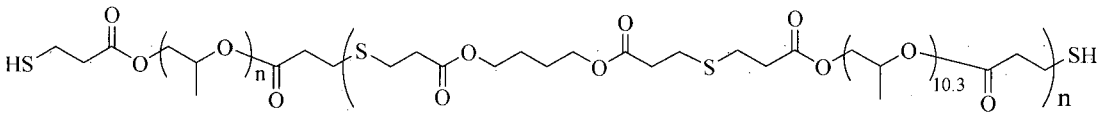

m-PPGMP3800

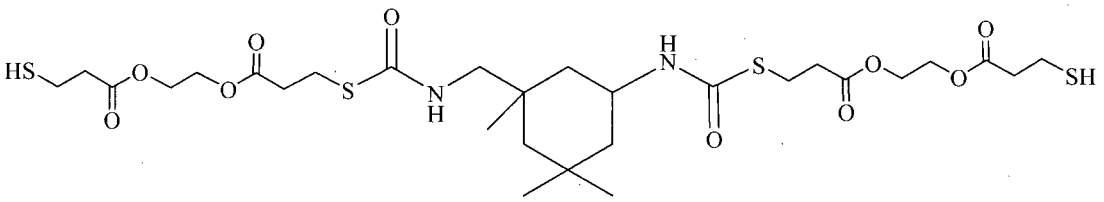

IP-m-DT

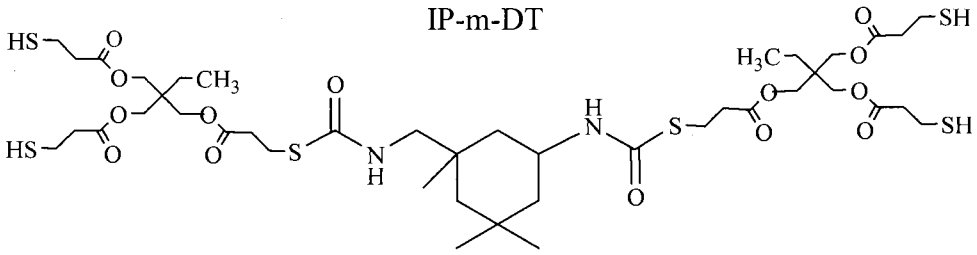

IP-m-TT

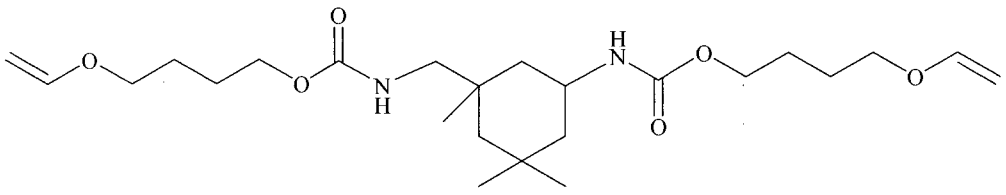

IP-m-DE

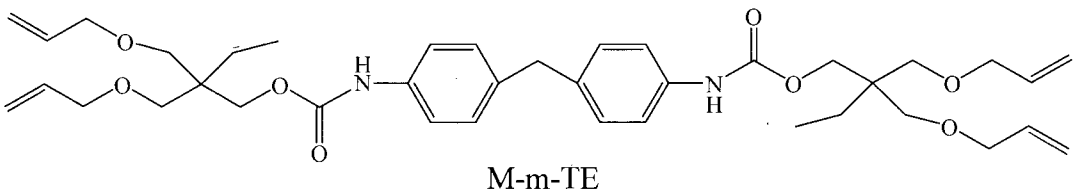

M-m-TE

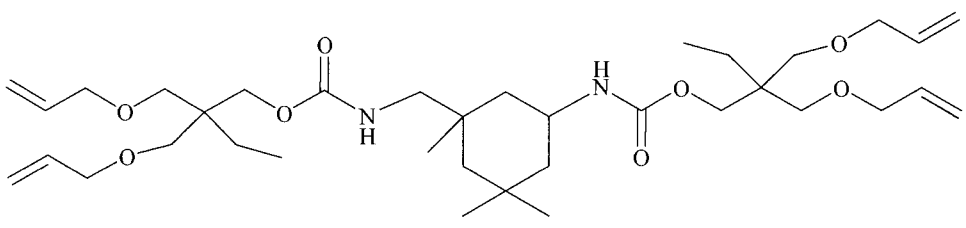

IP-m-TE

Chart B.3. Chemical structures of modified thiols and enes.

1. Urethane Ene (MDI + TMPDAE) + Urethane Thiol (GDMP + IPDI)

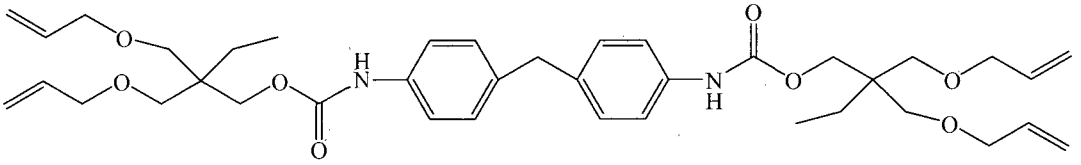

M-m-TE

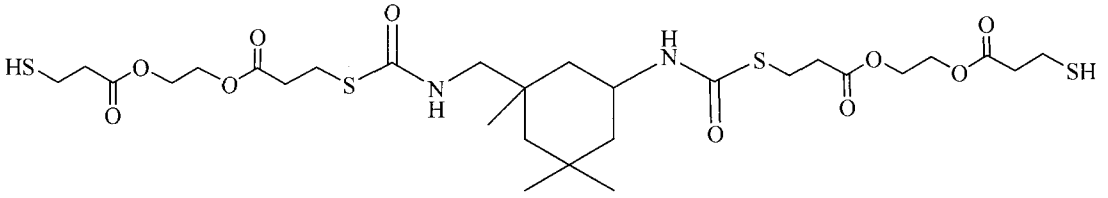

IP-m-DT

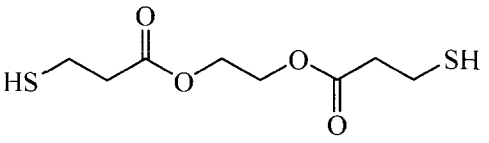

GDMP

Chart B.4. Chemical structures of modified thiol, ene, and GDMP.

Table B.1. Formulation of thiourethane modified thiol – urethane modified ene networks (molar ratio of functional groups)

	Thiol		Ene
	GDMP	IPDI	M-m-TE[a]
GDIP0-M4.0E	100	0	100
GDIP10-M4.0E	100	10	90
GDIP20-M4.0E	100	20	80
GDIP30-M4.0E	100	30	70

[a] urethane modified tetra-ene (MDI + TMPDAE)

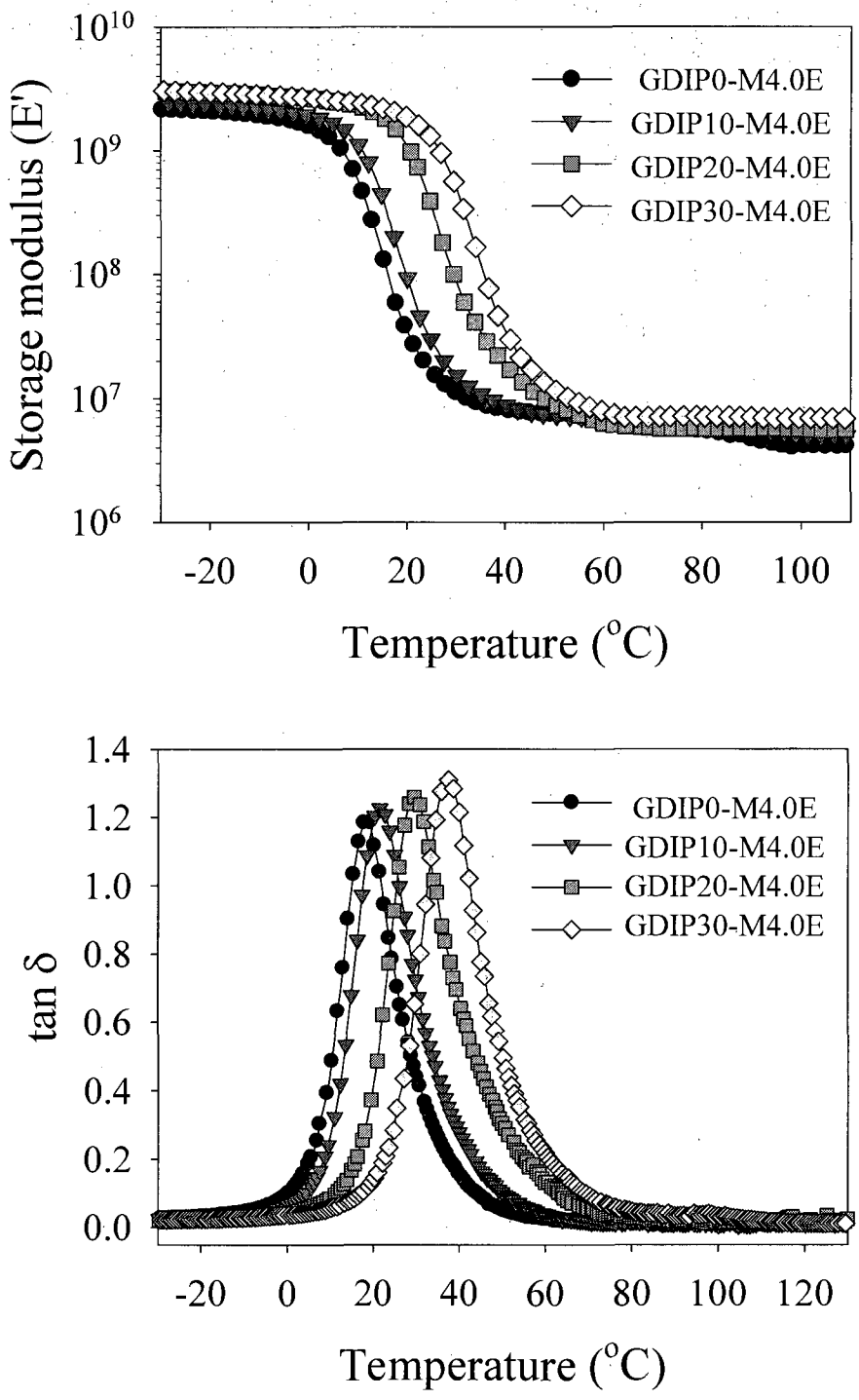

Figure B.1. Dynamic mechanical thermal properties of Urethane Ene (MDI + TMPDAE) + Urethane Thiol (GDMP + IPDI).

2. Urethane Ene (MDI + TMPDAE) + Urethane Thiol (TMPMP + IPDI)

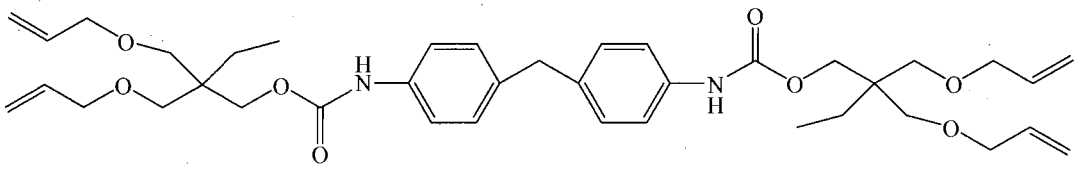

M-m-TE

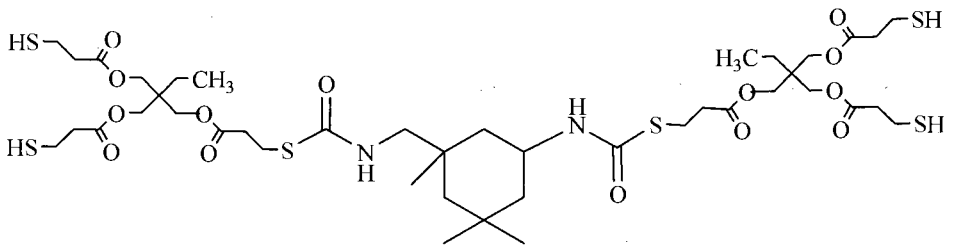

IP-m-TT

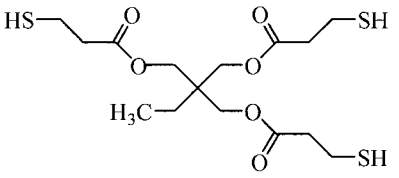

TMPMP

Chart B.5. Chemical structures of modified thiol, ene, and TMPMP.

Table B.2. Formulation of thiourethane modified thiol – urethane modified ene networks (molar ratio of functional groups)

	Thiol		Ene
	TMPMP	IPDI	M-m-TE[a]
TMIP0-M4.0E	100	0	100
TMIP10-M4.0E	100	10	90
TMIP20-M4.0E	100	20	80
TMIP30-M4.0E	100	30	70

[a] urethane modified tetra-ene (MDI + TMPDAE)

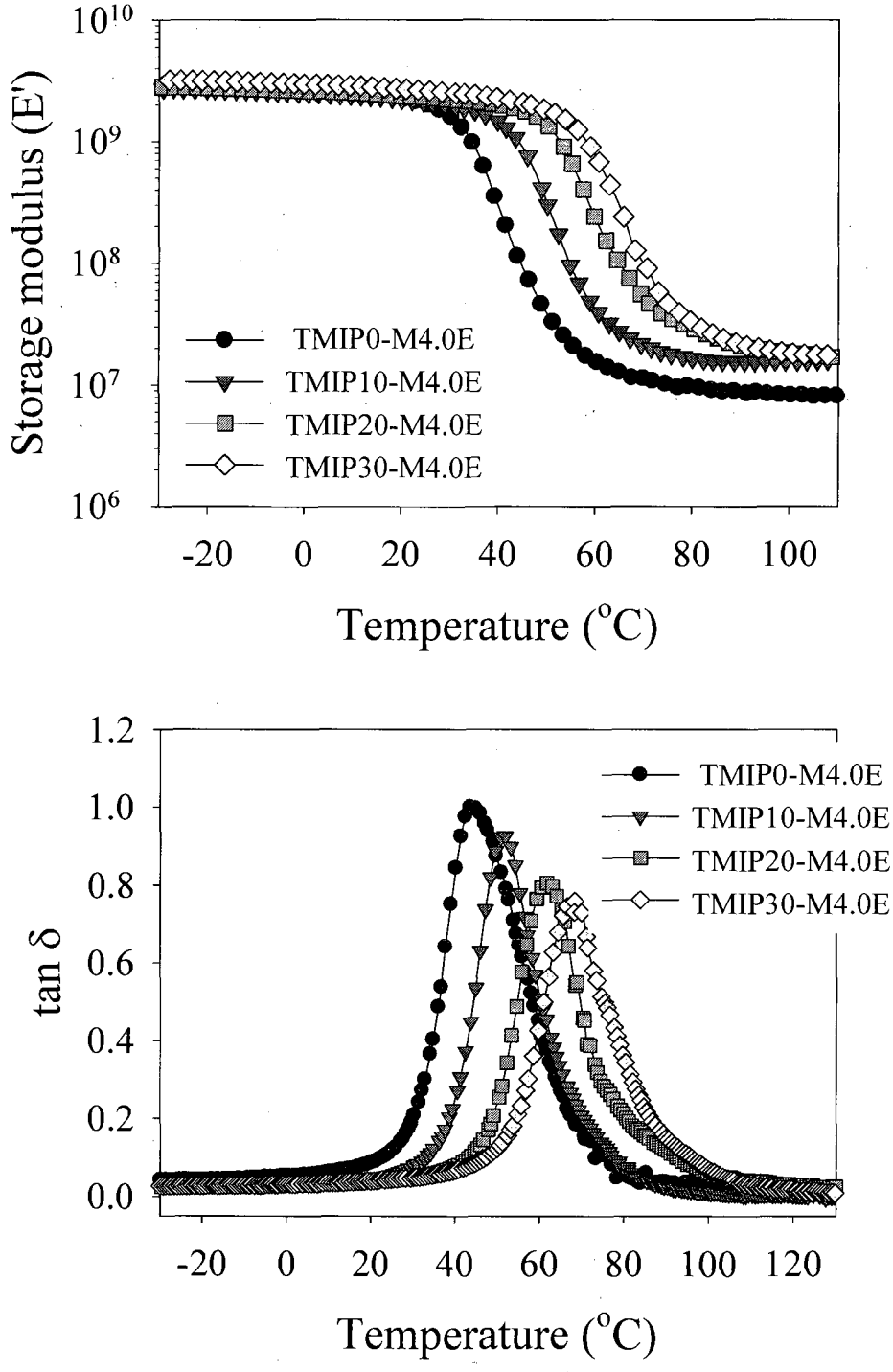

Figure B.2. Dynamic mechanical thermal properties of Urethane Ene (MDI + TMPDAE) + Urethane Thiol (TMPMP + IPDI).

3. Urethane Ene (IPDI + BDVE / TMPDAE) + Urethane Thiol (GDMP + IPDI)

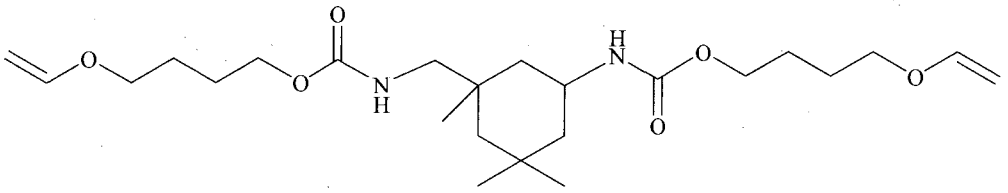

IP-m-DE

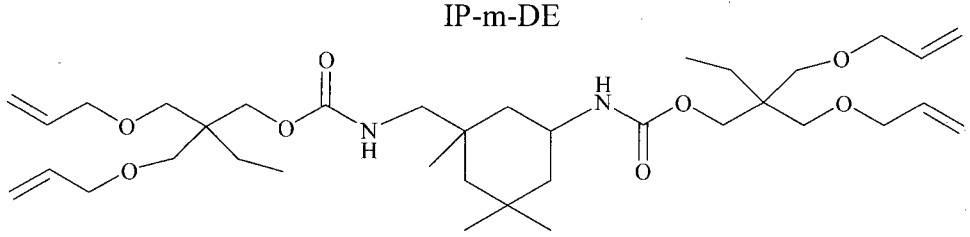

IP-m-TE

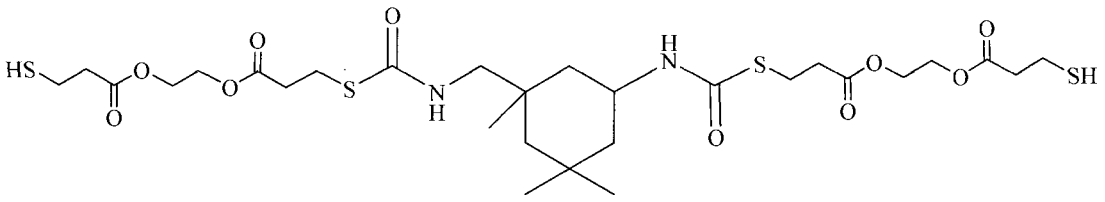

IP-m-DT

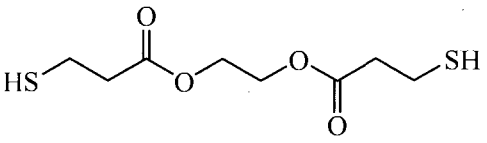

GDMP

Chart B.6. Chemical structures of modified thiol, enes, and GDMP.

Table B.3. Formulation of thiourethane modified thiol – urethane modified ene networks (molar ratio of functional groups)

	Thiol		Ene	
	GDMP	IPDI	IP-m-DE[a]	IP-m-TE[b]
GDIP40-IP2.5E	100	40	45	15
GDIP40-IP3.0E	100	40	30	30
GDIP40-IP3.5E	100	40	15	45
GDIP10-IP2.5E	100	10	67.5	22.5
GDIP20-IP2.5E	100	20	60	20
GDIP30-IP2.5E	100	30	52.5	17.5
GDIP40-IP2.5E	100	40	45	15
GDIP10-IP3.0E	100	10	45	45
GDIP20-IP3.0E	100	20	40	40
GDIP30-IP3.0E	100	30	35	35
GDIP40-IP3.0E	100	40	30	30
GDIP0-IP4.0E	100	0	0	100
GDIP10-IP4.0E	100	10	0	90
GDIP20-IP4.0E	100	20	0	80
GDIP30-IP4.0E	100	30	0	70
GDIP40-IP4.0E	100	40	0	60
GDIP50-IP4.0E	100	50	0	50

[a] urethane modified di-ene (IPDI + BDVE)

[b] urethane modified tetra-ene (IPDI + TMPDAE)

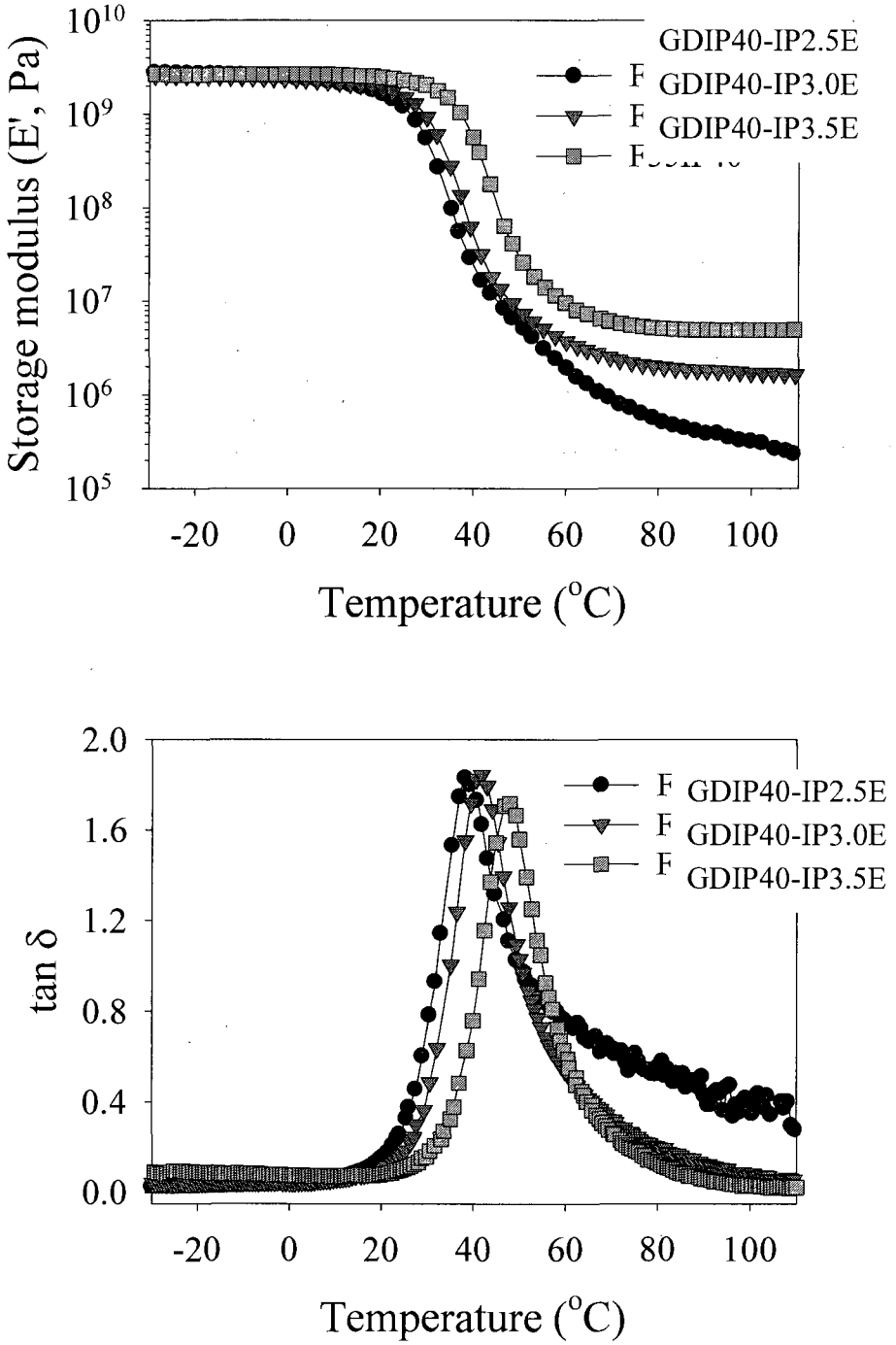

Figure B.3. Dynamic mechanical thermal properties of Urethane Ene (IPDI + BDVE / TMPDAE) + Urethane Thiol (GDMP + IPDI) as a function of ene functionality (IPDI content = 40 mole %).

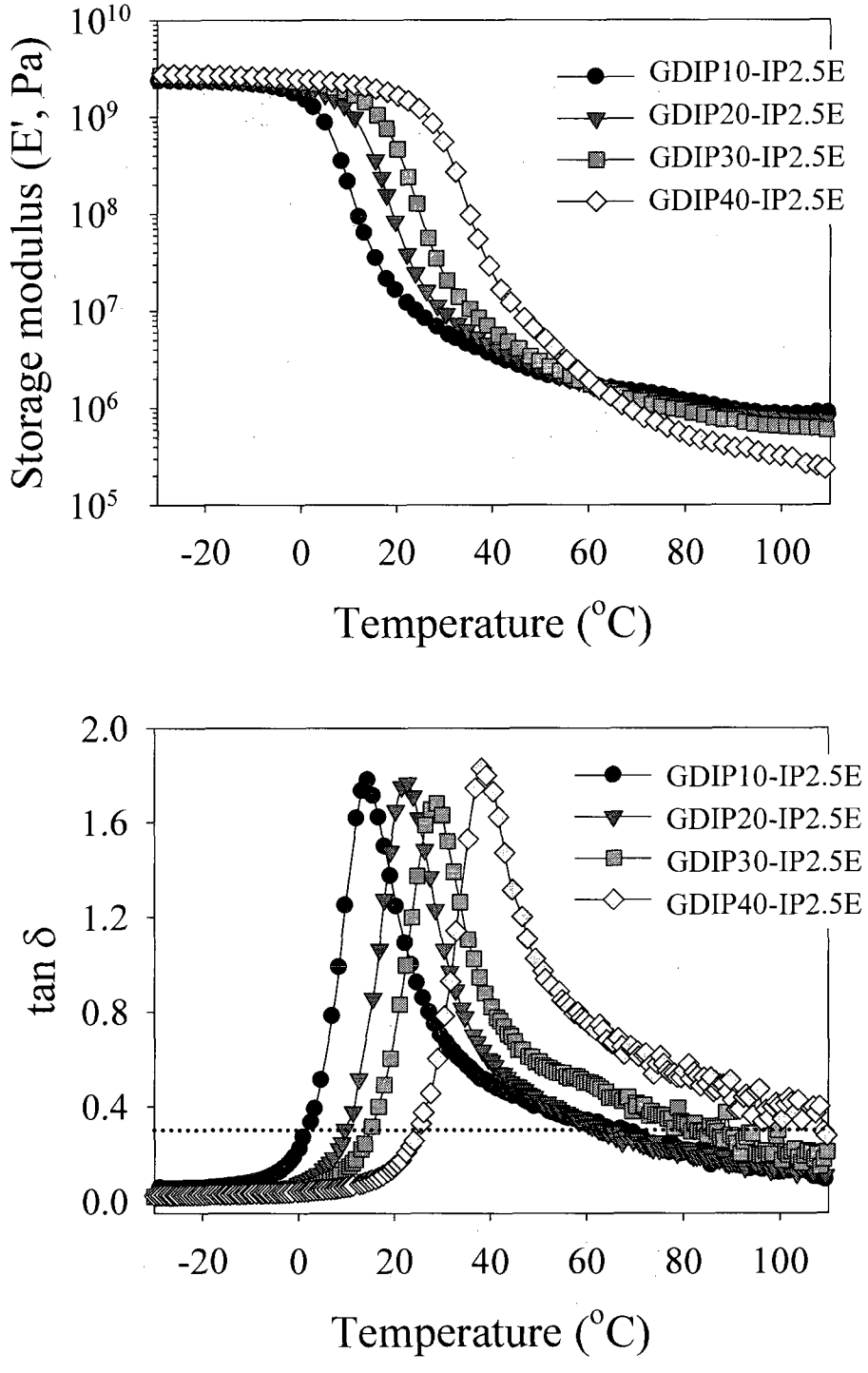

Figure B.4. Dynamic mechanical thermal properties of Urethane Ene (IPDI + BDVE / TMPDAE) + Urethane Thiol (GDMP + IPDI) as a function of IPDI content (F_{avg} of Ene = 2.5).

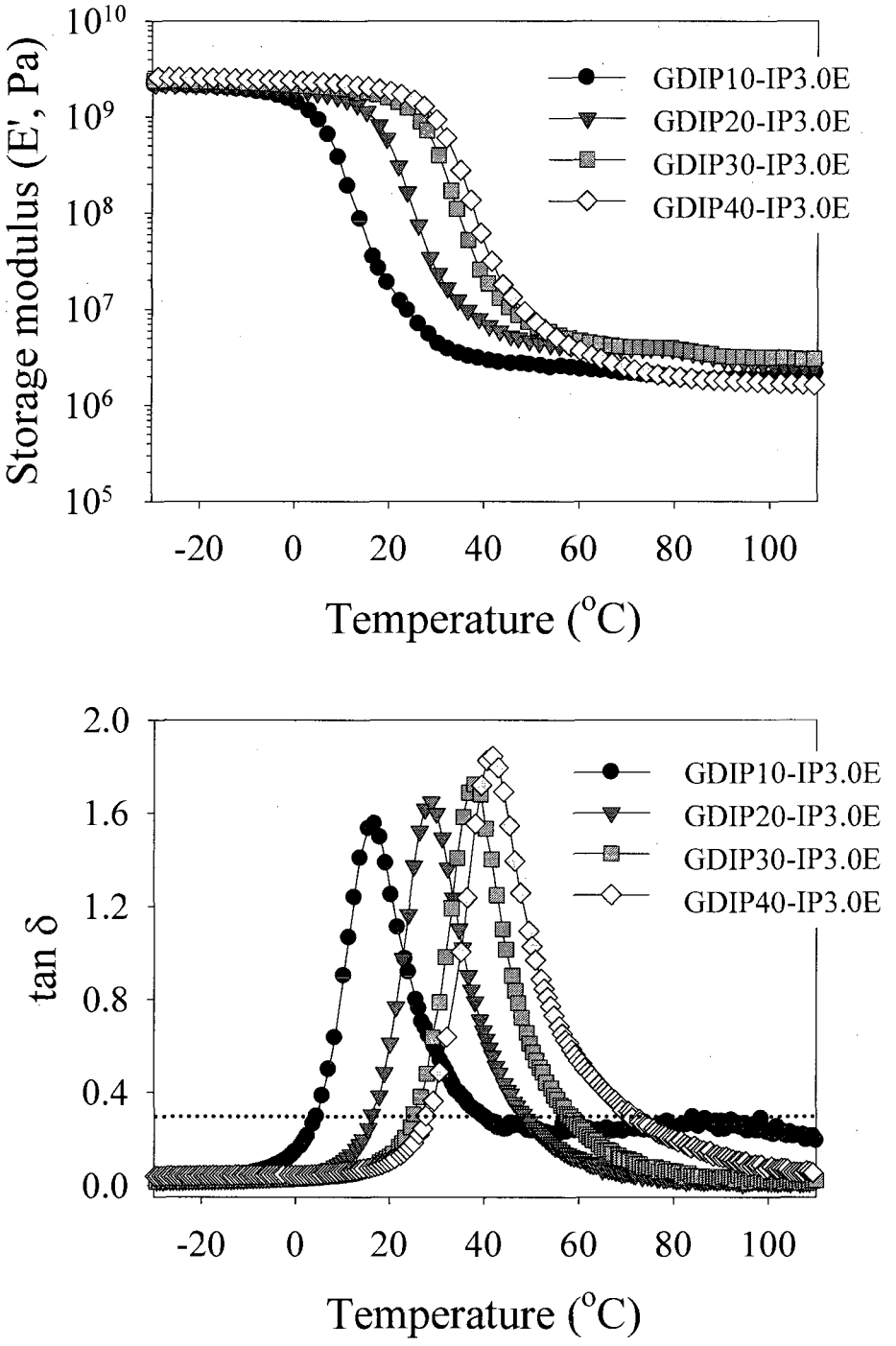

Figure B.5. Dynamic mechanical thermal properties of Urethane Ene (IPDI + BDVE / TMPDAE) + Urethane Thiol (GDMP + IPDI) as a function of IPDI content (F_{avg} of Ene = 3.0).

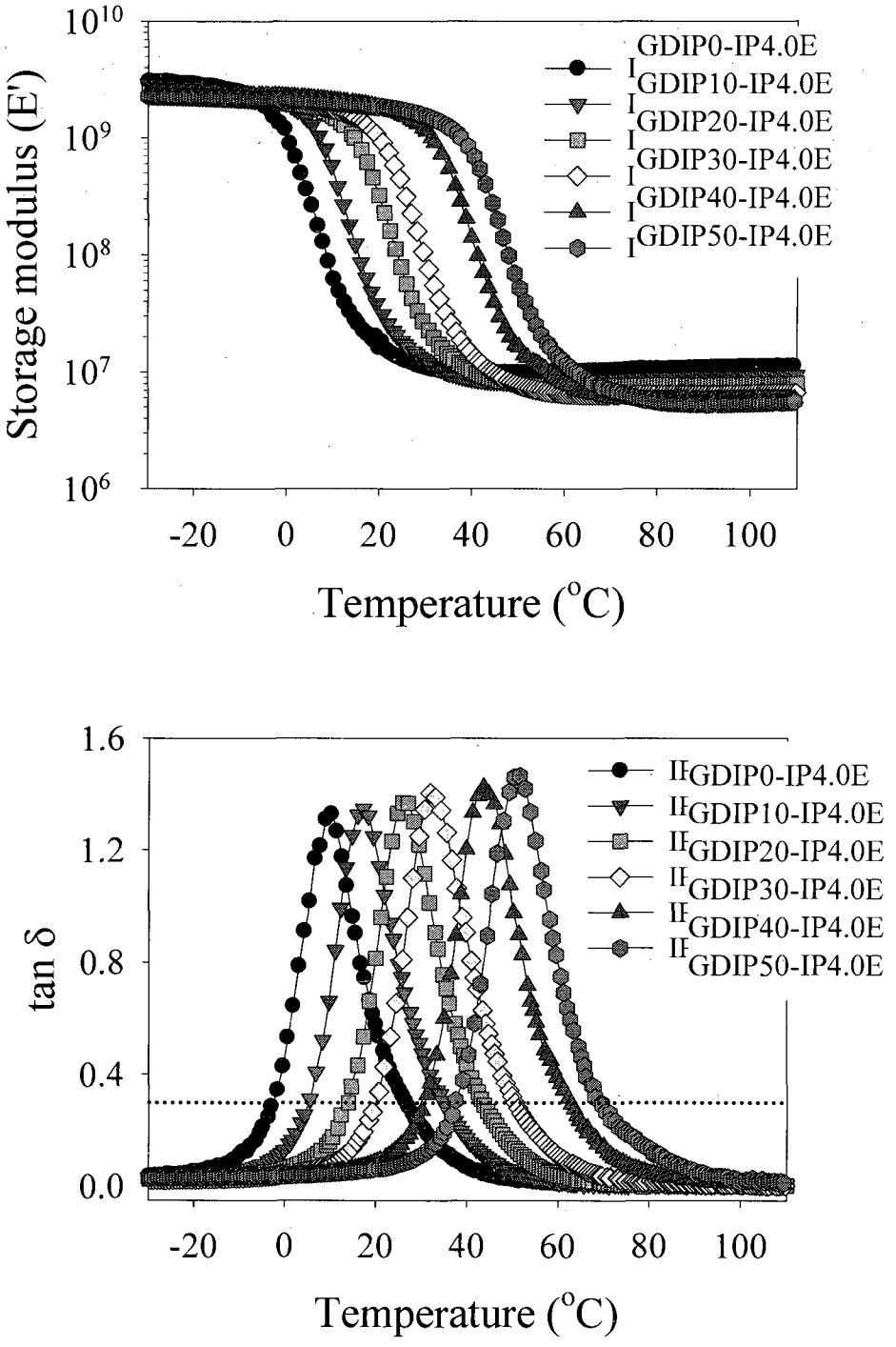

Figure B.6. Dynamic mechanical thermal properties of Urethane Ene (IPDI + BDVE / TMPDAE) + Urethane Thiol (GDMP + IPDI) as a function of IPDI content (F_{avg} of Ene = 4.0).

4. Polyurethane Networks (IPDI + PTMEG + TMP)

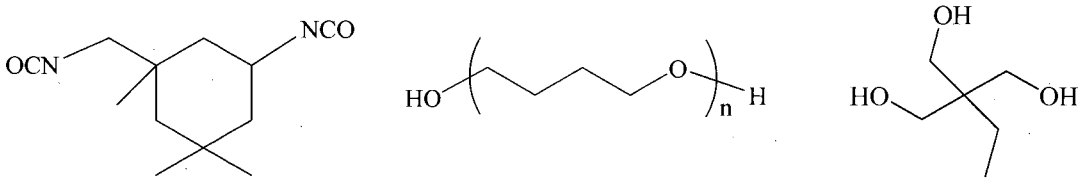

IPDI PTMEG TMP

Chart B.7. Chemical structure of IPDI, PTMEG, and TMP.

Table B.4. Formulation of polyurethane networks (molar ratio of functional groups)

IPDI	PTMEG			TMP
	650	1000	2000	
200	100			100
200		100		100
200			100	100

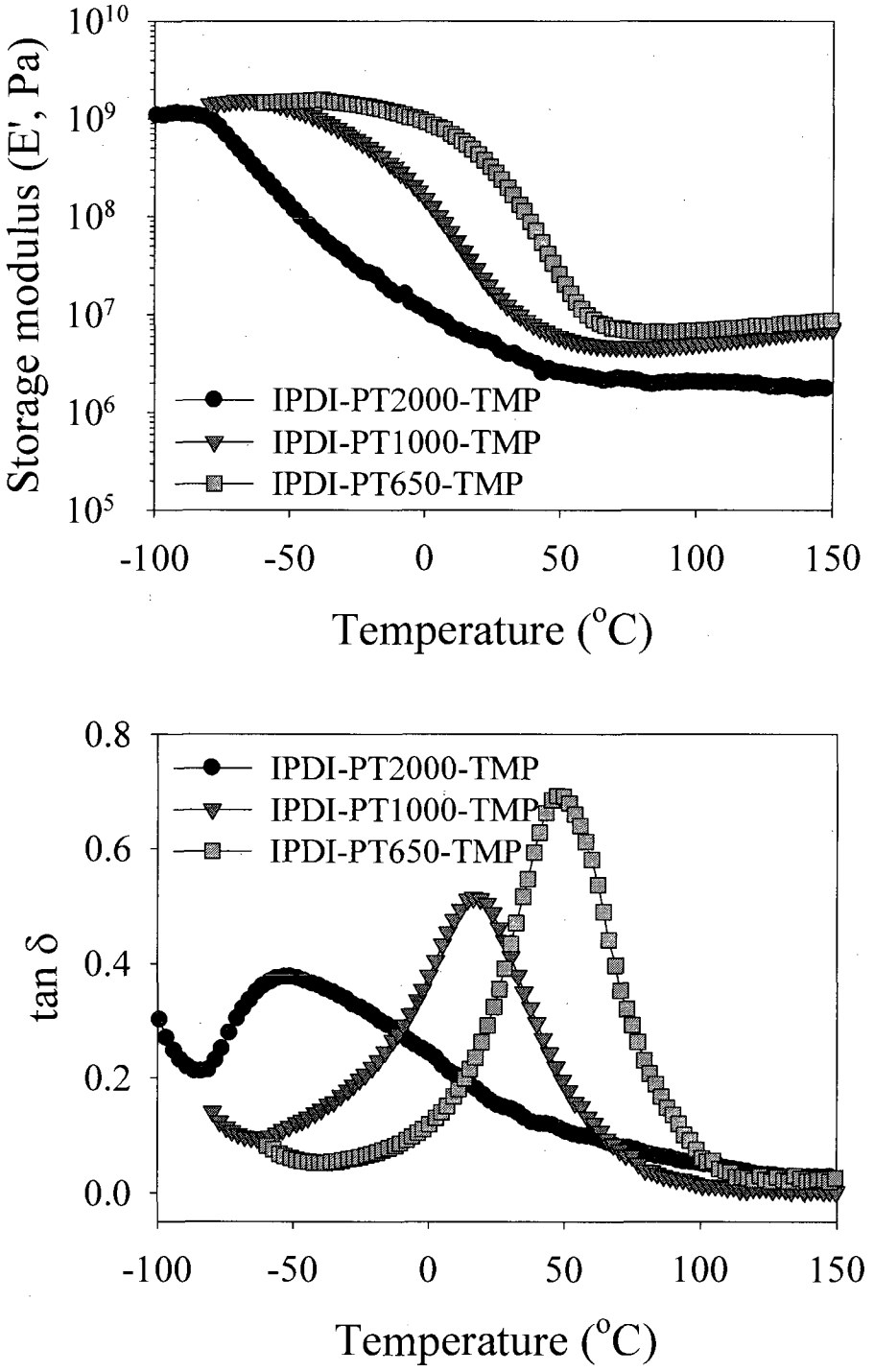

Figure B.7. Dynamic mechanical thermal properties of polyurethane networks as a function of PTMEG molecular weight.

5. Polyurethane (IPDI + PTMEG 1000 + TMP) / Thiol-Ene (TMPMP + TTT) Co-networks

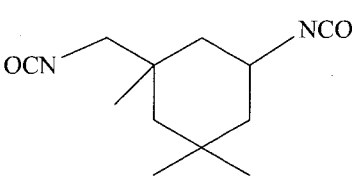

IPDI

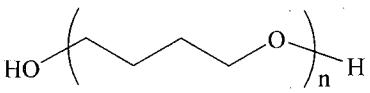

PTMEG

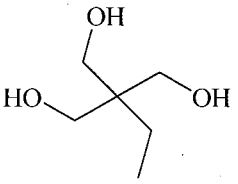

TMP

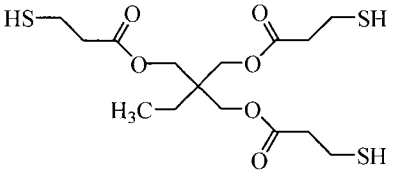

TMPMP

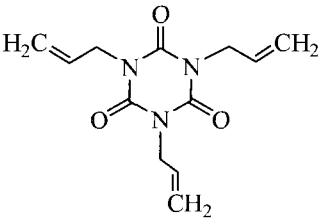

TTT

Chart B.8. Chemical structure of IPDI, PTMEG, TMP, TMPMP, and TTT.

Table B.5. Formulation of polyurethane (PU) / thiol-ene (TE) co-networks

	Polyurethane			Thiol-Ene	
	IPDI	PTMEG*	TMP	TMPMP	TTT
	200 [a]	100 [a]	100 [a]	100 [a]	100 [a]
PU:TE = 8:2 [b]	80 [b]			20 [b]	
PU:TE = 6:4 [b]	60 [b]			40 [b]	

* molecular weight : 1000 g/mole

[a] molar ratio of functional groups

[b] weight ratio of networks

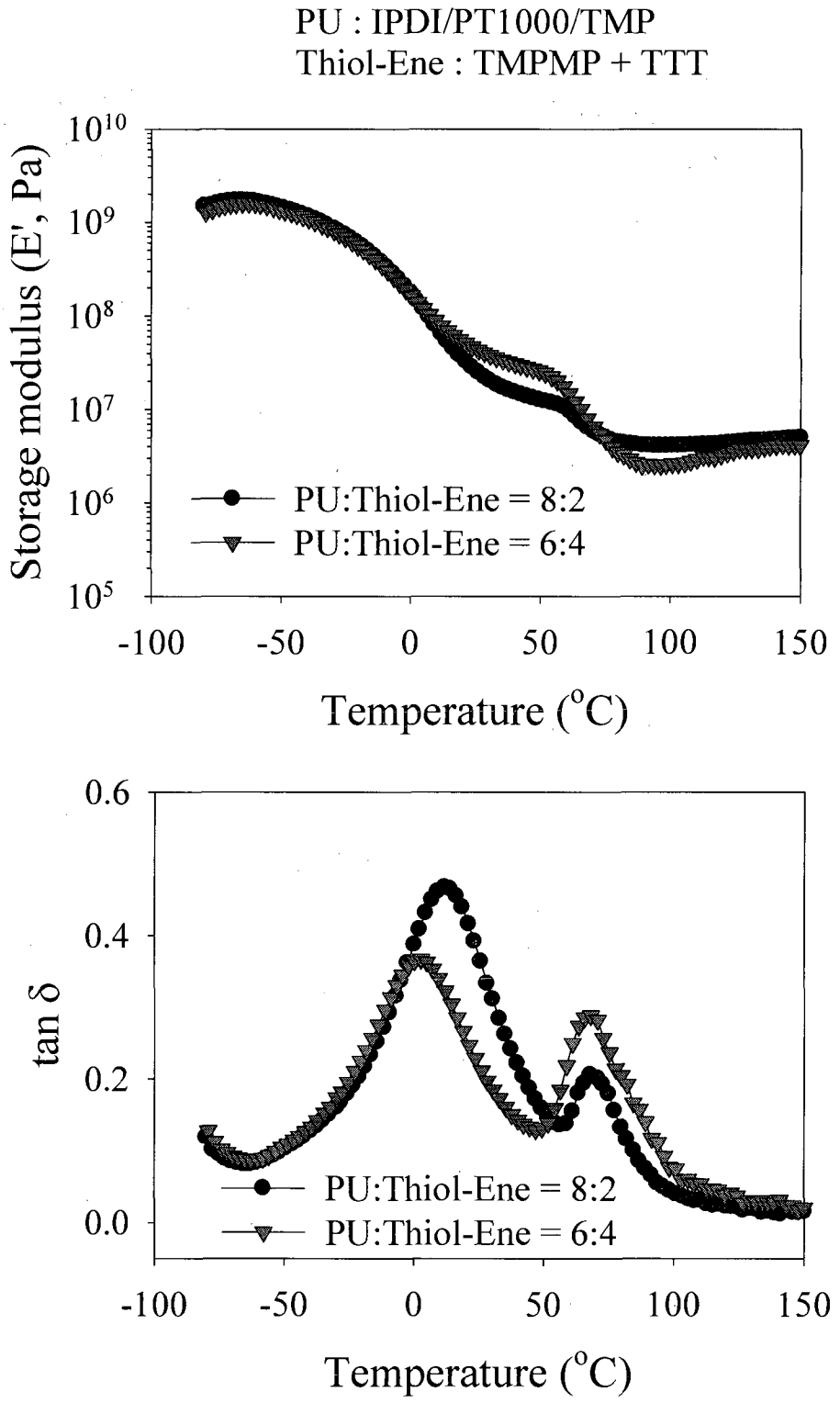

Figure B.8. Dynamic mechanical thermal properties of PU / Thiol-Ene co-networks.

6. Polyurethane (IPDI + PTMEG 1000 + TMP) / Thiol-UrethaneEne (TMPMP + M-m-TE) Co-networks

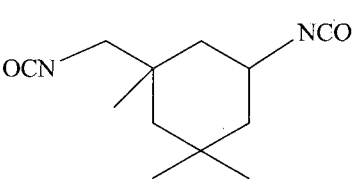

IPDI

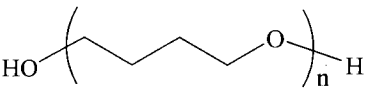

PTMEG

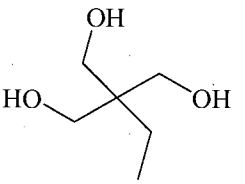

TMP

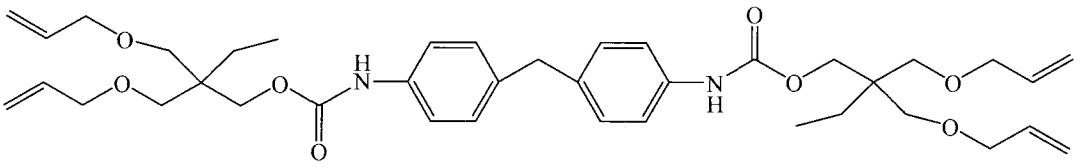

M-m-TE

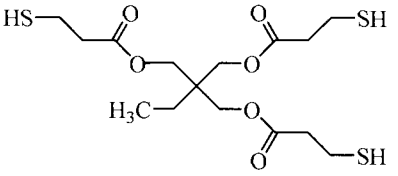

TMPMP

Chart B.9. Chemical structure of IPDI, PTMEG, TMP, M-m-TE, and TMPMP.

Table B.6. Formulation of polyurethane (PU) / thiol-urethane modified ene (PUTE) co-networks

	Polyurethane			Thiol-Ene	
	IPDI	PTMEG*	TMP	TMPMP	M-mTE
	200 [a]	100 [a]	100 [a]	100 [a]	100 [a]
PU:PUTE = 8:2 [b]	80 [b]			20 [b]	
PU:PUTE = 6:4 [b]	60 [b]			40 [b]	

* molecular weight : 1000 g/mole

[a] molar ratio of functional groups

[b] weight ratio of networks

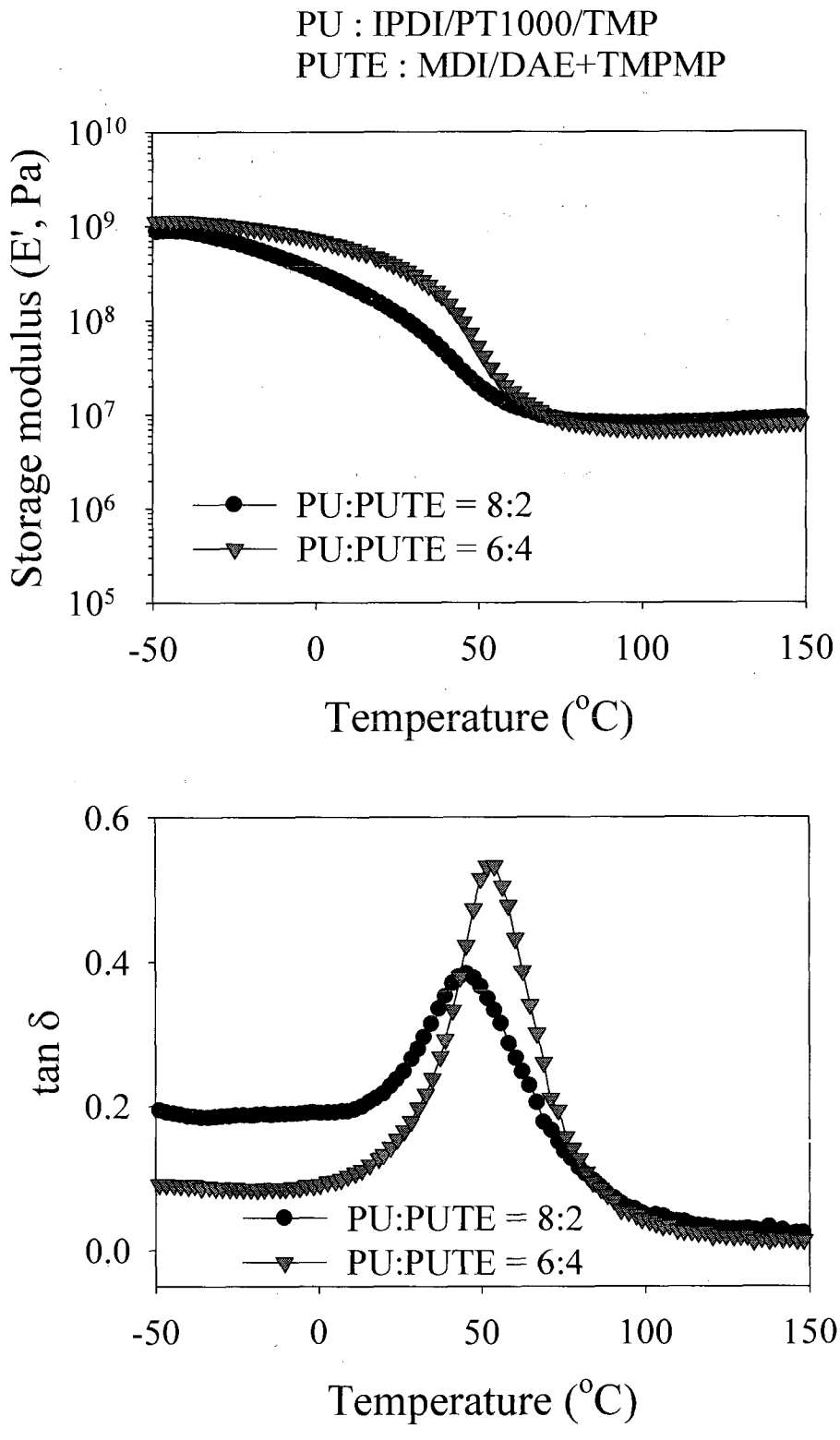

Figure B.9. Dynamic mechanical thermal properties of PU / Thiol-UrethaneEne co-networks.

7. Polythiourethane Networks (IPDI + ETTMP 1300 + PETMP)

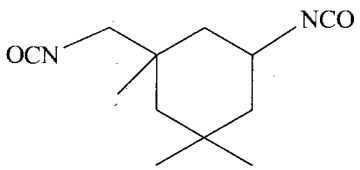

IPDI

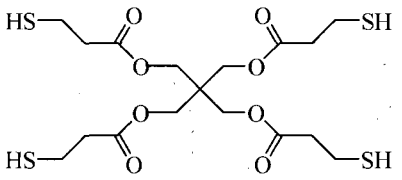

PETMP

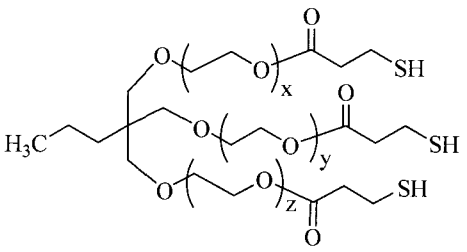

ETTMP 1300

Chart B.10. Chemical structure of IPDI, PETMP, and ETTMP 1300.

Table B.7. Formulation of polythiourethane networks (molar ratio of functional groups)

Isocyanate	Thiols	
IPDI	ETTMP 1300	PETMP
100	100	0
100	80	20
100	60	40
100	40	60
100	20	80
100	0	100

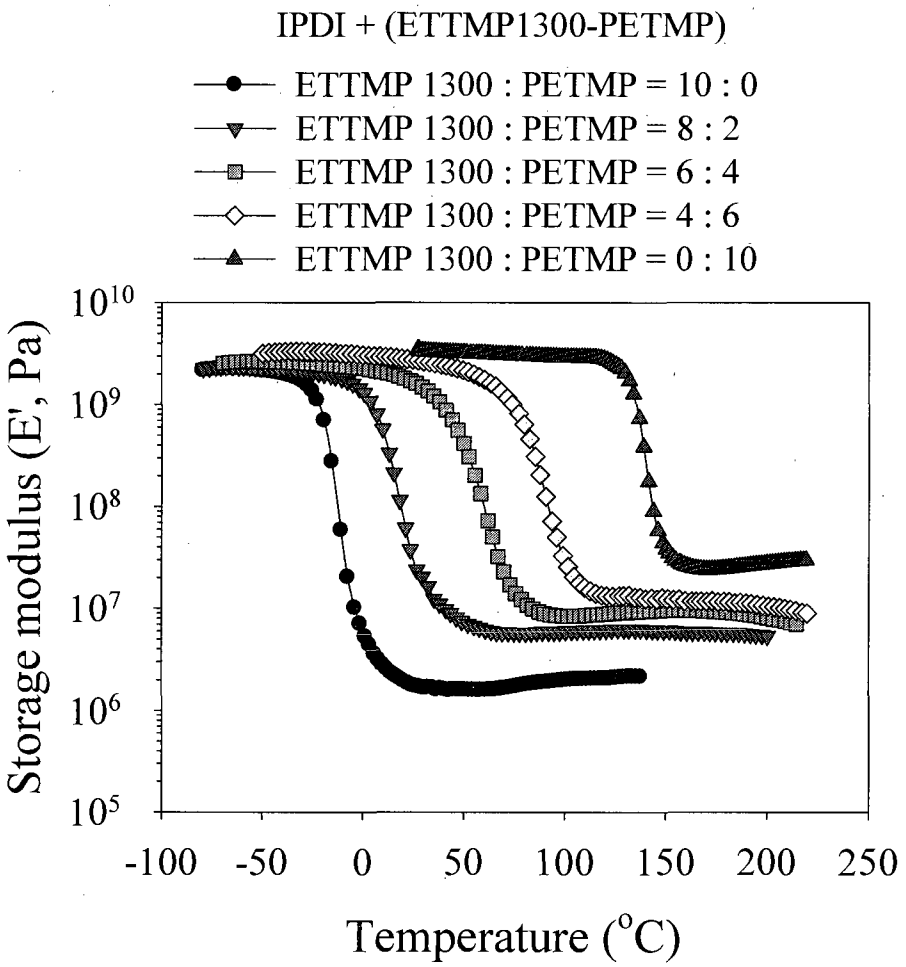

Figure B.10 (a). Dynamic mechanical thermal property (storage modulus) of polythiourethanes networks.

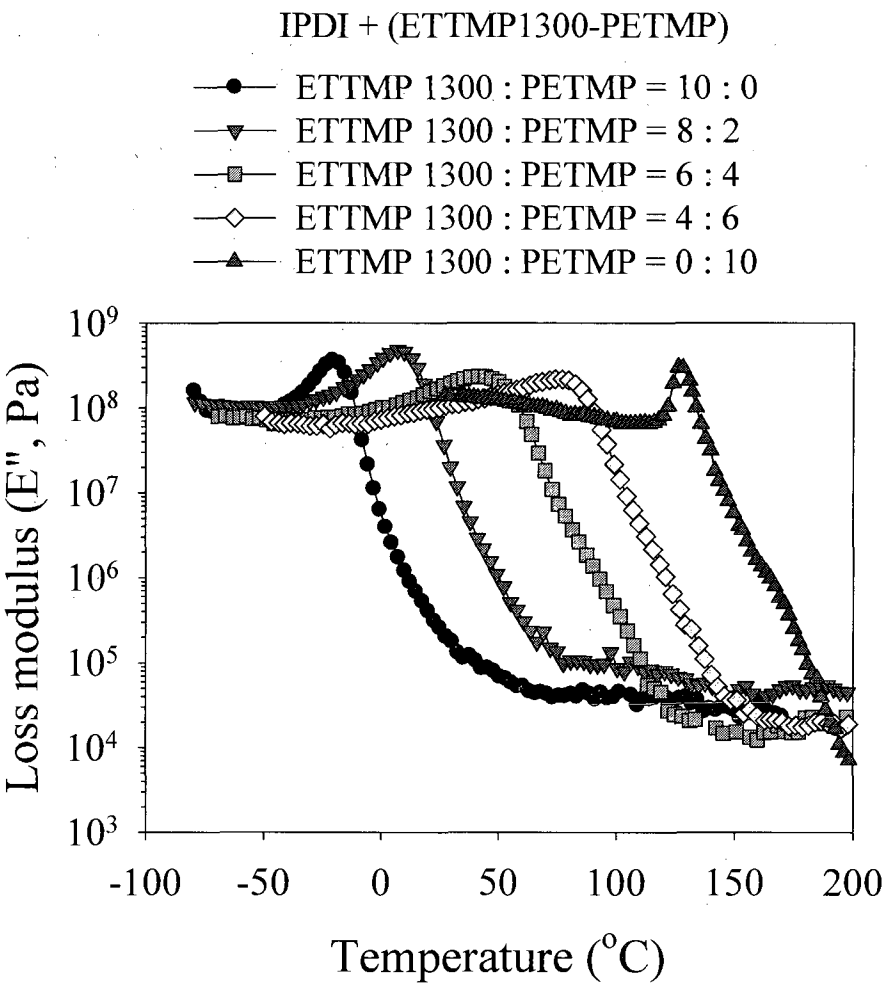

Figure B.10 (b). Dynamic mechanical thermal property (loss modulus) of polythiourethanes networks.

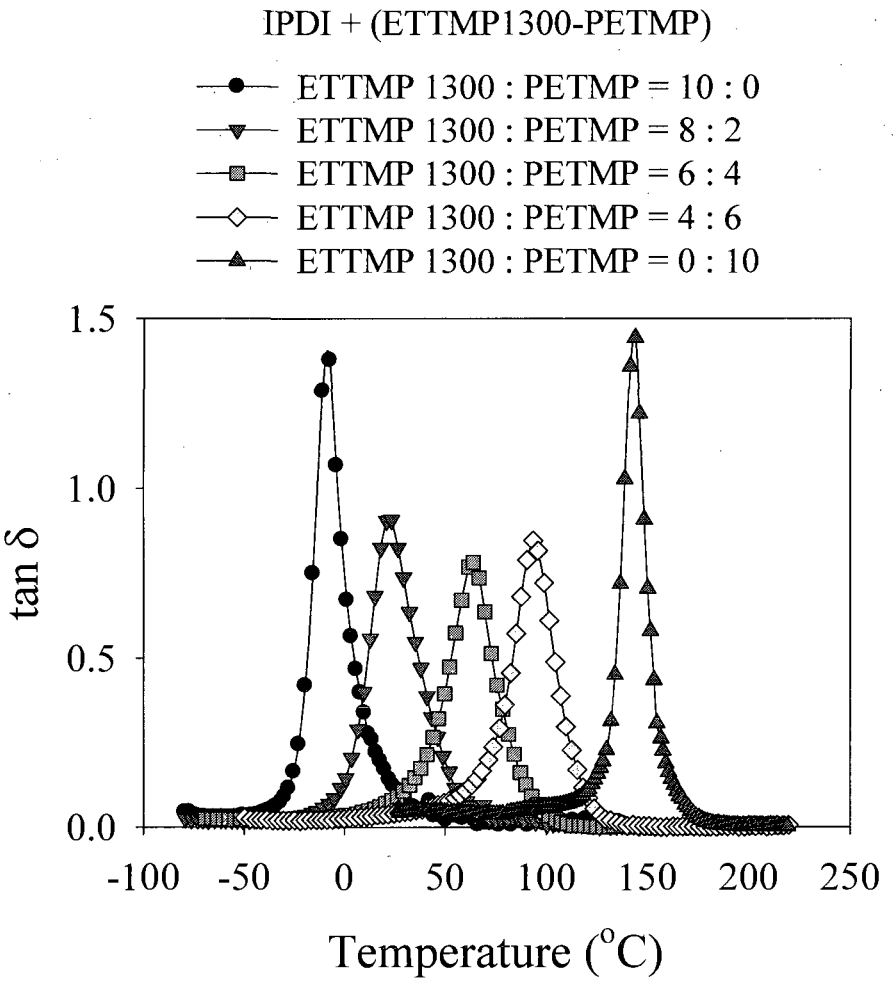

Figure B.10 (c). Dynamic mechanical thermal property (tan δ) of polythiourethanes networks.

8. Polythiourethane networks (IPDI + ETTMP 1300 + PETMP + m-PPGMP 3800)

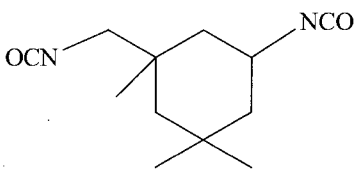

IPDI

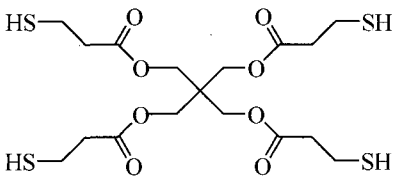

PETMP

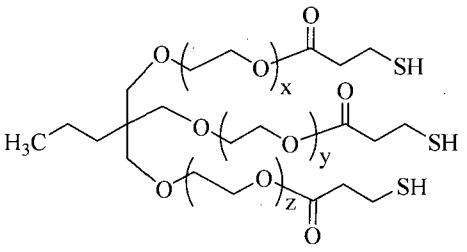

x + y + z = 20

ETTMP 1300

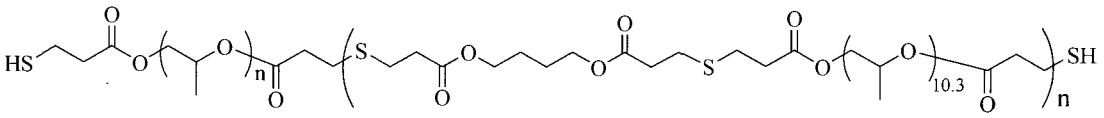

m-PPGMP 3800

Chart B.11. Chemical structure of IPDI, PETMP, ETTMP 1300, and m-PPGMP 3800.

Table B.8. Formulation of polythiourethane networks (molar ratio of functional groups)

Isocyanate	Thiols		
IPDI	ETTMP 1300	PETMP	PPGMP 3800
100	60	40	0
110	60	40	10
120	60	40	20
140	60	40	40
180	60	40	80

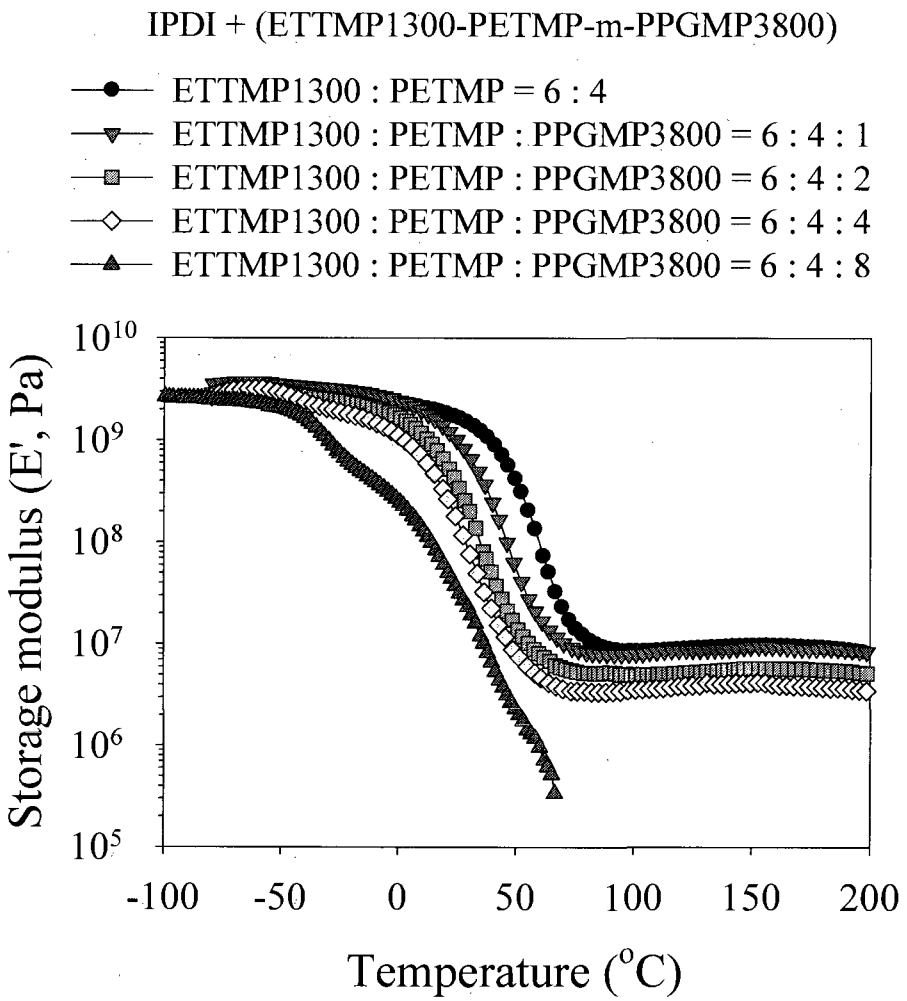

Figure B.11 (a). Dynamic mechanical thermal property (storage modulus) of polythiourethanes networks.

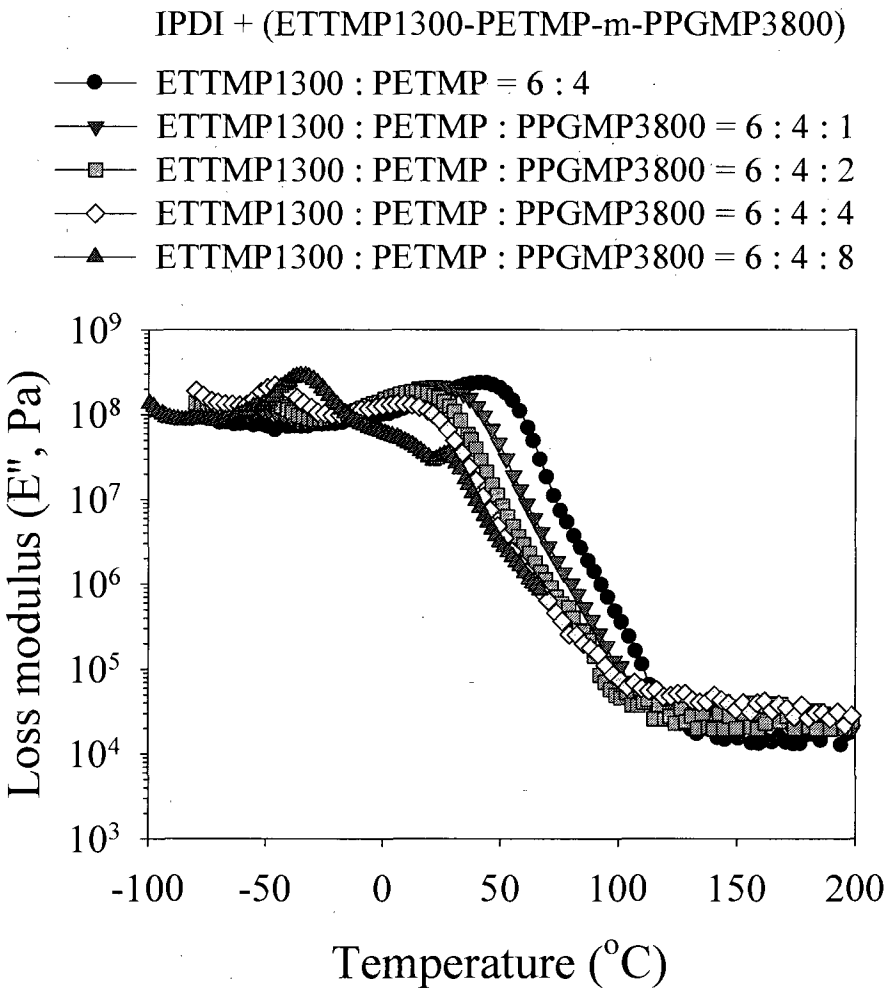

Figure B.11 (b). Dynamic mechanical thermal property (loss modulus) of polythiourethanes networks.

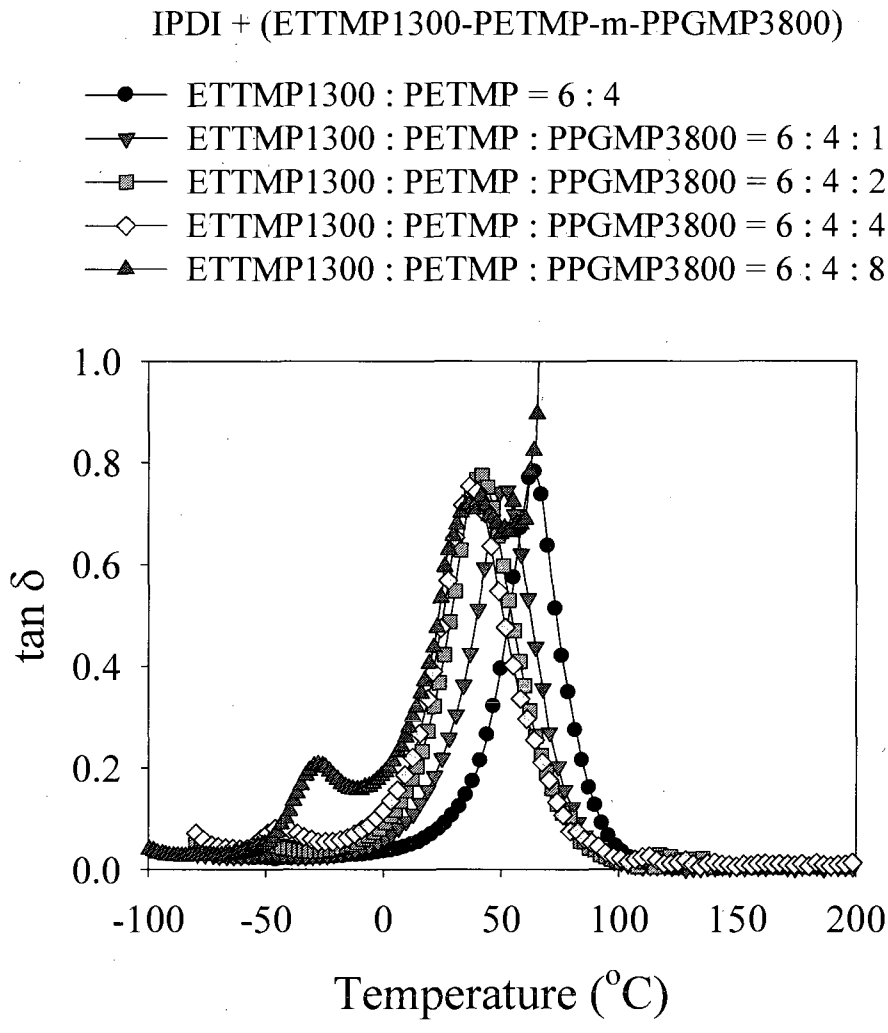

Figure B.11 (c). Dynamic mechanical thermal property (tan δ) of polythiourethanes networks.

9. Polythiourethane networks (IPDI + ETTMP 1300 + TMPMP + m-PPGMP 3800 + PPGMP 800)

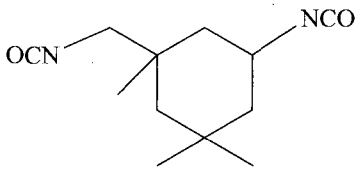

IPDI

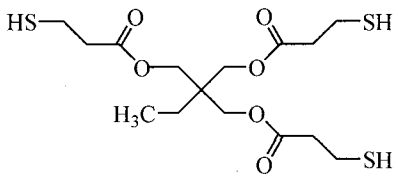

TMPMP

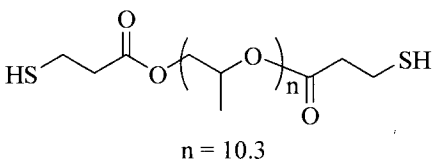

PPGMP 800

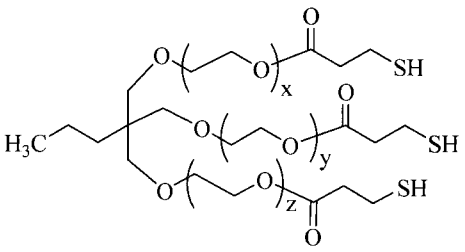

ETTMP

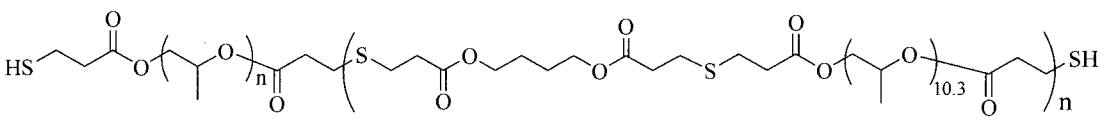

m-PPGMP 3800

Chart B.12. Chemical structure of IPDI, ETTMP 1300, TMPMP, m-PPGMP 3800, and PPGMP 800.

Table B.9. Formulation of polythiourethane networks (molar ratio of functional groups)

Isocyanate	Thiols			
IPDI	ETTMP 1300	PETMP	PPGMP 3800	PPGMP 800
100	25	25	25	25
100		25	25	25
100		25	50	25
100		25	25	50
100		25	50	50

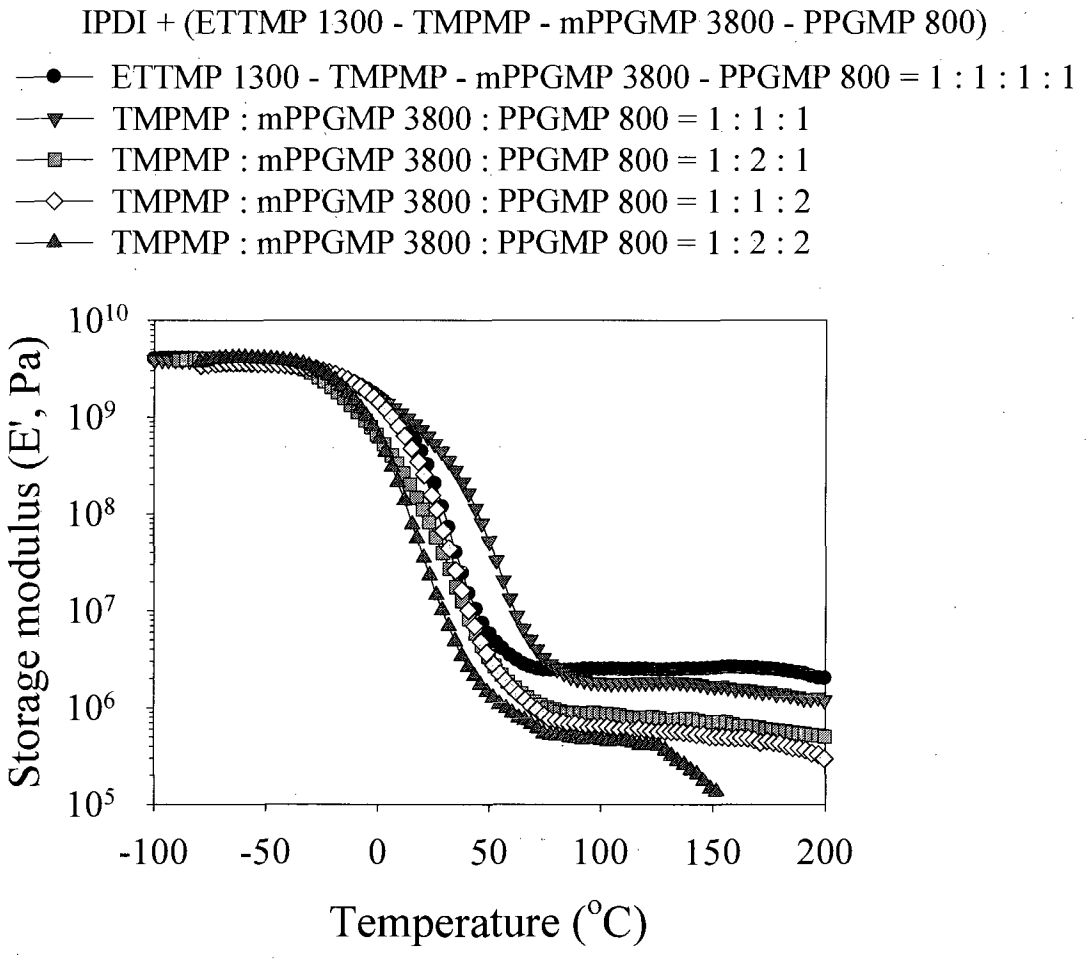

Figure B.12 (a). Dynamic mechanical thermal property (storage modulus) of polythiourethanes networks.

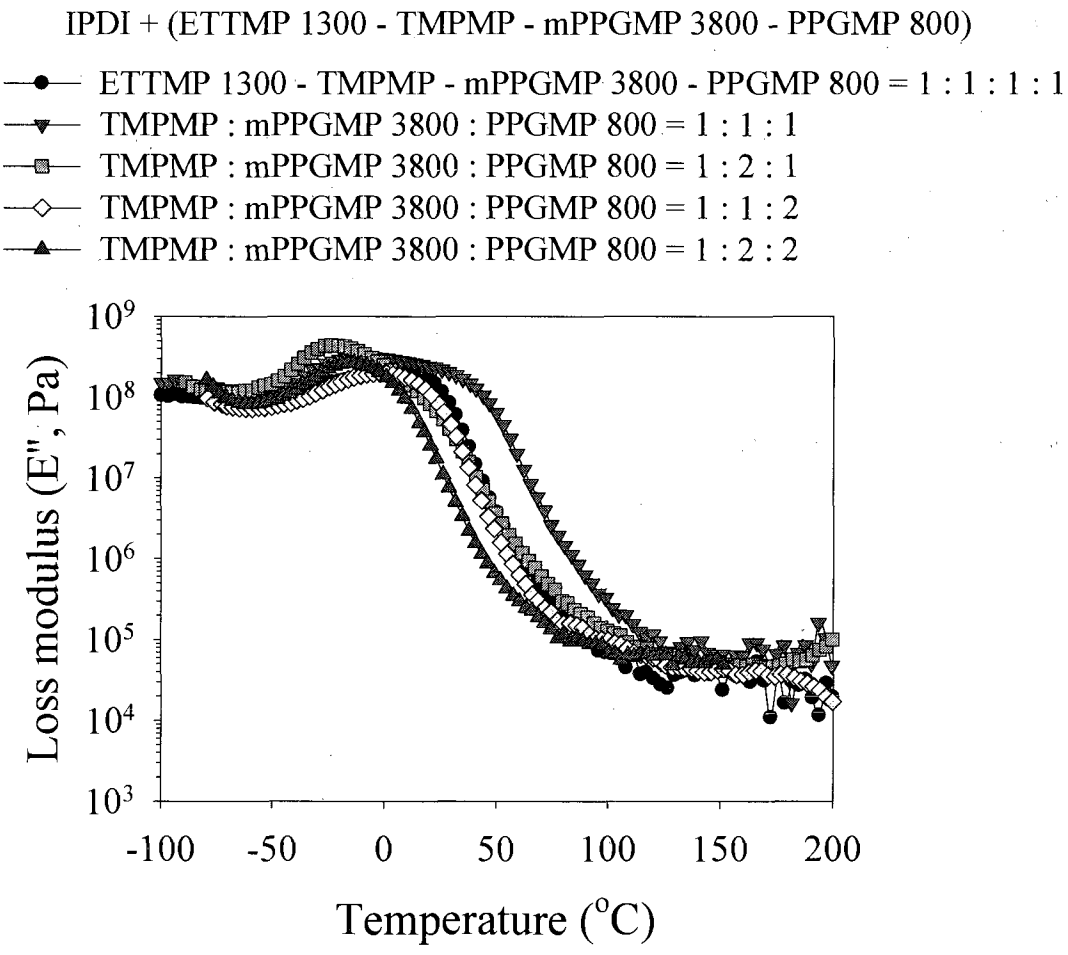

Figure B.12 (b). Dynamic mechanical thermal property (loss) of polythiourethanes networks.

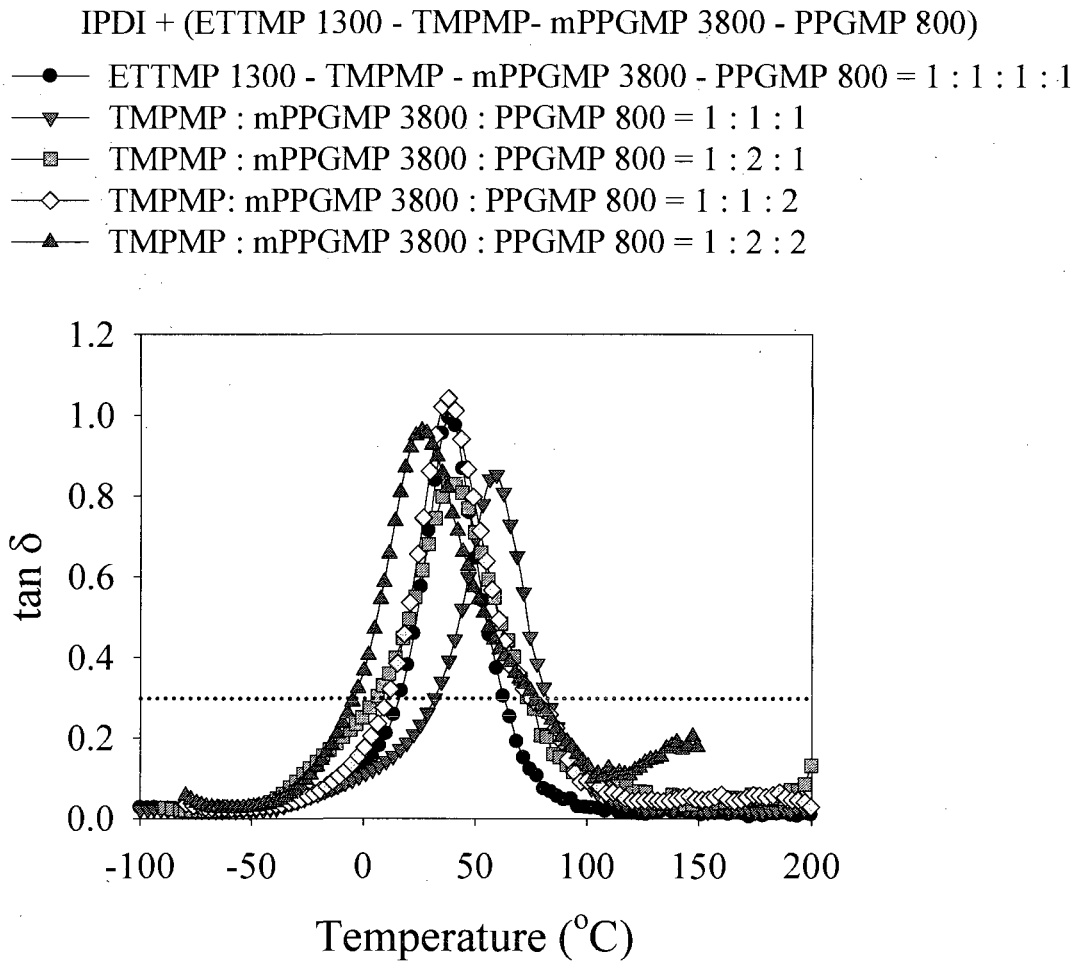

Figure B.12 (c). Dynamic mechanical thermal property (tan δ) of polythiourethanes networks.